Type I PKA as a co-incidence detector
Integration of cAMP and oxidant signals

Oviosu, Olujimi Adeyemi

Awarding institution:
King's College London

Type Iα PKA as a co-incidence detector: Integration of cAMP and oxidant signals

Olujimi A. Oviosu

King's College London
Cardiovascular Division
Rayne Institute, BHF Centre
4th Floor Lambeth Wing
St Thomas' Hospital
London, SE1 7EH

Thesis undertaken for the degree of
Doctor of Philosophy
2015

Abstract

Protein kinase A (PKA) is activated by elevated intracellular cAMP downstream of β-adrenergic signalling. PKA's subcellular localisation is determined by its affinity for A-kinase anchoring proteins (AKAPs), scaffolds that sequester PKA proximal to its substrates. The regulatory RIα subunits present in type I PKA can form two intermolecular disulphide bonds, each flanking its AKAP-binding domain, in response to oxidants. Rationally this change in the redox state of PKARIα may alter its affinity for AKAP, with potential for consequential regulation of substrate phosphorylation.

I made the novel observation that co-treatment of cells with H_2O_2 and cAMP caused increased global PKA substrate phosphorylation compared to cAMP or H_2O_2 alone in HEK 293 cells. This suggested RIα serves as a co-incidence detector that integrates the two signals to synergistically enhance PKA substrate phosphorylation. Chronic cAMP treatment increased PKARIα expression in HEK 293 cells and PKARIα was also upregulated in a mouse model of hypertrophy, whilst PKARIIα was downregulated. This may represent a switch to an oxidant sensitive PKA signalling phenotype during chronic β-adrenergic stimulation.

AKAP7 was identified as a potential redox-dependent PKARIα AKAP. Examination of the AKAP7 crystal structure revealed putative redox sensitive cysteines adjacent to its A-kinase binding domain, leading to the hypothesis that the redox state of this AKAP may alter its affinity for PKARIα. I developed and validated the 'PEG-maleimide switch assay', a method used to identify proteins that are susceptible to reversible oxidative modification. Using the PEG-maleimide switch assay I found AKAP7 to be insensitive to oxidation. Furthermore, I demonstrated that PKARIIα, but not PKARIα, is a binding partner for AKAP7δ and this interaction was redox modulated.

I described, for the first time, that cAMP can modulate PKARIα disulphide dimer levels. DTT-dependent PKARIα reduction was potentiated by cAMP, and cAMP-agarose induced PKARIα reduction. Furthermore, a mutant PKARIα that could not bind cAMP formed disulphide-linked complexes under oxidative conditions. These complexes may be cAMP-regulated intermediates that form during a novel oxidant-dependent mechanism of PKARIα targeting to AKAPs. LC-MS/MS identified the novel AKAP tubulin as part of a disulphide linked complex with PKARIα. Consistent with the hypothesis that oxidants target PKARIα to tubulin, phosphorylation of the microtubule associated protein GEF-H1 was enhanced after co-treatment with cAMP and H_2O_2 compared to cAMP alone. Thus PKARIα is a co-incidence detector at the interface of cAMP and oxidant signalling that is able to integrate both modalities to fine-tune phosphorylation events.

Acknowledgments

I would like to thank my supervisor Prof. Philip Eaton, for his guidance, support and patience throughout my degree. He has imparted to me the foundations to think critically in a scientific context (which may be just a synonym for cynically or sceptically) for which I will be forever grateful.

All the members of the Eaton lab and the wider King's intellectual community have been wonderful. Advice, encouragement and knowledge have been forthcoming from every direction. A special mention must go to Dr. Joseph Burgoyne, who was happy to explain everything to me 7 times when I was green behind the ears. I am grateful to Dr. Andrii Boguslavskyi for providing cardiac hypertrophy samples and Miss Alisa Kamynina for her help with the aortic excision and the CLP model.

I thank all the folks in the mezzanine, you have made the longer days seem shorter (not that we could see when the sun went down). For all the scientific debate and mostly the non-scientific debate you have made my experience richer, fuller and brighter. Thank you for tolerating my 'only-child' moments of which I'm sure there were many. It has been a tough road but it was fun in the end wasn't it?

I'm grateful to my friends for their unwavering belief. You have been present in moments of triumph and despair equally. Your personal achievements over the years and your collective desire to 'keep it pushing' have been a source of constant inspiration. I am simply riding on your coattails.

Lastly I would like to thank my family, and especially, my beautiful mother. Although you will probably never read it, this is a monument constructed in your honour. Our journey has been a long one; and we were driven here by your hope, and your selflessness, and your unconditional love. I am eternally grateful, and I owe you the world.

Table of Contents

List of Figures

List of Tables

List of Abbreviations

2-AHA-cAMP	2-(6-aminohexylamino)-adenosine- 3', 5'- cyclic monophosphate
5'AMP	5' adenosine monophosphate
5-HT	serotonin
8-AEA-cAMP	8-(2-aminoethylamino)-adenosine- 3', 5'- cyclic monophosphate
8-AHA-cAMP	8-(6-aminohexylamino)-adenosine- 3', 5'- cyclic monophosphate
8-CPT-cAMP	8-(4-Chlorophenylthio)-adenosine 3', 5'-cyclic monophosphate
A	adrenaline
AC	adenylate cyclase
AKAP	A-kinase anchoring proteins
AKB	A-kinase binding domain
ARVM	adult rat ventricular myocyte
ATP	adenosine triphosphate
BAEC	bovine aortic endothelial cells
BK	Ca^{2+}-activated K^{+} channels
Ca^{2+}	calcium
CaMKII	Ca^{2+}/calmodulin-dependent kinase II
cAMP	cyclic adenosine monophosphate
$Ca_V1.2$	calcium channel, voltage-dependent, L type, α 1C subunit
CCCA	Caprotec™ capture compound Assay
cGMP	cyclic guanosine monophosphate
ChChd3	coiled-coil-helix-coiled-coil-helix domain containing 3
CLP	cecal ligation puncture

CNBA	cyclic nucleotide binding site A
CNBB	cyclic nucleotide binding site B
CREB	cAMP response element binding
C-terminal	carboxy-terminal
CysNO	S-nitrosocysteine
DAKAP1	dual AKAP1
DAKAP2	dual AKAP2
D/D	dimerisation/docking domain
DH	Dbl homology domain
Drp1	dynamin-related protein 1
DTT	dithiothreitol
e^-	electron
eNOS	endothelial nitric oxide synthase
Epac 1/2	exchange proteins activated by cAMP 1/2
ERK 1/2	extracellular signal-regulated kinase 1/2
Fe^{2+}/ Fe^{3+}	iron ion
FRET	Föster resonance energy transfer
GAPDH	glyceraldehyde-3-phosphate dehydrogenase
GCL	glutamate cysteine ligase
GCLC	glutamate cysteine ligase catalytic
GCLM	glutamate cysteine ligase modifier
GDP	guanosine diphosphate
GEF	guanine exchange factors
GEF-H1	Rho guanine nucleotide exchange factor

GPCR	G-protein coupled receptor
Gpx1	glutathione peroxidase
Grx	glutaredoxin
GSH	glutathione
Gsr	glutathione reductase
GSSG	oxidised glutathione
GTP	guanosine triphosphate
H^+	hydrogen ion
H_2O_2	hydrogen peroxide
HEK 293	human embryonic kidney 293 cells
$HOO^{\cdot -}$	hydroperoxyl radical
I-1	inhibitor-1
ICAM-1	intercellular adhesion molecule 1
IL-1	interleukin-1β
IS	inhibitory site
Iso	isoprenaline
K^+	potassium
Keap1	kelch-like ECH-associated protein 1
KI	knock-in
KO	knock-out
LC-MS/MS	liquid chromatography-mass spectrometry/mass spectrometry
LPS	lipopolysaccharide
MAO	monoamine oxidase
MAP	microtubule associated protein

min	minutes
MLC_{20}	myosin light chain 20
MLCK	myosin light chain kinase
Na^+	sodium
NA	noradrenaline
NADPH	nicotinamide adenine dinucleotide phosphate
NOX	NADPH oxidase
Nrf2	nuclear factor-erythroid-2-related factor 2
N-terminal	amino-terminal
N_2O_3	dinitrogen trioxide
NO	nitric oxide
NO·	nitroxyl radical
NO^-	nitroxyl ion
NO^+	nitrosonium ion
NO_2^-	nitrite ion
NO_2^+	nitronium ion
NO_3^-	nitrate ion
O_2	molecular oxygen
$O_2\cdot^-$	superoxide
OCl^-	hypochlorite ion
OH^-	hydroxyl ion
OH·	hydroxyl radical
$ONOO^-$	peroxynitrite
ox-LDL	oxidised- low density lipoproteins

P/S	penicillin/streptomycin
PDE	phosphodiesterase
PDGF	platelet-derived growth factor
PGE_1	prostaglandin E1
PH	pleckstrin homology domain
PKACα	cAMP-dependent protein kinase A catalytic subunitα
PKARIα	cAMP-dependent protein kinase A RIα
$PKARI\alpha^{-cAMP}$	cAMP-dependent protein kinase A RIα with mutated cAMP site (Gly200Glu)
PKARIIα	cAMP-dependent protein kinase A RIIα
PKC	protein kinase C
PKGIα	cGMP- dependent protein kinase G Iα
pK_a	acid dissociation constant
PLB	phospholamban
PP1	protein phosphatase 1
PP2B	protein phosphatase 2B
Prx	peroxiredoxin
PTP	protein tyrosine phosphatases
PVDF	polyvinylidene fluoride
R-S-Cys	S-cysteinylation
R-S-SG	S-glutathionylation
Rac 1/2	ras-related C3 botulinum toxin substrate 1/2
RNS	reactive nitrogen species
ROCK1/2	Rho-associated protein kinase 1/2
ROO·	peroxyl radical

ROS	reactive oxygen species
RyR_2	ryanodine receptor 2
S^-	thiolate anion
S-S	disulfide bond
SDS-PAGE	sodium dodecyl sulphate polyacrylamide gel electrophoresis
SEM	standard error of the mean
SERCA2a	sarco/endoplasmic reticulum Ca^{2+}-ATPase 2a
sGC	soluble guanylate cyclase
SKIP	sphingosine kinase interacting protein
sMAF	small Maf
SNO	nitrosothiols
SOD	superoxide dismutase
SOH	sulfenic acid
SO_2H	sulfinic acid
SO_3H	sulfonic acid
TNFα	tumour necrosis factor α
TR	thioredoxin reductase
Trx	thioredoxin
VASP	vasodilator-stimulated phosphoprotein
VCAM-1	vascular cell adhesion protein 1
VEGF	vascular endothelial growth factor
VSMC	vascular smooth muscle cells
WAVE1	WASP-family verprolin-homologous protein 1

1 General Introduction

1.1 Reactive oxygen species

Historically oxidants were implicated primarily as perpetrators of cellular dysfunction and pathologies including cancer, neurodegenerative and cardiovascular diseases[1-5]. The traditional view asserted that oxidants, produced largely by unregulated processes, indiscriminately and detrimentally 'attacked' biological molecules[6]. Antioxidant treatment ameliorated disease progression in a great many pre-clinical animal models, and therefore it was anticipated that these positive outcomes would translate to human patients[7-10]. However antioxidant therapy has not been efficacious with respect to reducing disease risk or progression in large scale human clinical trials, with some studies showing the intervention was in fact detrimental[9,11,12]. Whilst the unselective and damaging aspect of oxidants persists, it is now generally accepted that they also play a crucial homeostatic role as signalling molecules in the maintenance of normal cellular function[13]. Within the cardiovascular system, oxidants have been implicated in numerous physiological processes including, excitation-contraction coupling, the regulation of vascular tone, stress responses to hypoxia, ischemia, angiogenesis, and inflammation[4,14].

Reactive oxygen species (ROS) is a term used to collectively describe free radicals (a species with an unpaired electron in its outer shell) and non-radical derivatives of molecular oxygen (O_2) also termed oxidants. ROS are generally unstable molecules that react with and alter the structure of organic substances including proteins, lipids and DNA[15]. ROS can be generated from enzymatic activity or by electrons that leak from the electron transport chain and are transferred to O_2 to form the superoxide radical ($O_2{\cdot}^-$) ($O_2 + e^- \rightarrow O_2{\cdot}^-$)[16] . Addition of a second electron to $O_2{\cdot}^-$ can occur spontaneously or can be catalysed by superoxide dismutase (SOD) to yield the more stable, and less reactive, signalling molecule hydrogen peroxide (H_2O_2) ($2\ H^+ + 2\ O_2{\cdot}^- \rightarrow H_2O_2 + O_2$) . Further electron addition to H_2O_2 via the Fenton reaction, where Fe^{2+} donates an electron to become Fe^{3+}, produces the hydroxyl radical ($OH{\cdot}$), a strongly oxidising molecule which is highly reactive and is consequently not considered to be a viable signalling molecule[17]. There are many different ROS, including the peroxyl radical ($ROO{\cdot}$), hydroperoxyl radical ($HOO{\cdot}^-$), hydroxyl ion (OH^-) and the hypochlorite ion (OCl^-). Oxidative signalling molecules also involve reactive nitrogen species (RNS) including the nitroxyl ion (NO^-), peroxynitrite ($ONOO^-$), dinitrogen trioxide (N_2O_3), nitroxyl radical ($NO{\cdot}$), nitrosonium ion (NO^+), nitronium ion (NO_2^+), nitrite ion (NO_2^-), nitrate ion (NO_3^-). All of these molecules vary in their abundance, stability, reactivity and selectivity with protein thiols[18].

Redox signalling can be defined as a specific, usually reversible, modification of cellular signalling pathway components by a reactive species[19]. As discussed in more detail below, oxidant signal transduction can be mediated by ROS-induced modifications of protein structure resulting in alterations to protein function. This thesis focuses on cAMP-dependent protein kinase A RIα (PKARIα), which forms disulfide bonds in the presence of oxidants and this is associated with its activation.

Protein cysteine thiols serve as a major class of ROS sensors. The reactivity of a cysteine thiol depends on the surrounding tertiary structure of the protein and its solvent environment, which will govern access by oxidants. Most intracellular cysteine thiols have a high acid dissociation constant (pK_a) of ~8.5 and are therefore relatively unreactive and unlikely to undergo oxidation at physiological pH of ~7.1. Reactive cysteine thiols tend to have a low pK_a, meaning that they exist within the cell primarily as the deprotonated thiolate anion (-RS^-) at physiological pH and as such have enhanced reactivity to oxidants. Basic amino acid residues such as arginine, histidine or lysine in close proximity to cysteines can lower the pK_a of the thiol as the amino group can accept protons and stabilise the thiolate ion. Only a small proportion of the total cellular proteins contain thiolates, and this provides a basis for selectivity in thiol-mediated redox signalling. Further selectivity is mediated through co-localisation of the sensor thiol to the oxidant source[20,21].

Reactive cysteines can undergo numerous post-translational modifications (Figure 1.1). H_2O_2 reversibly reacts with a thiol to produce sulfenic acid (R-SOH). When large amounts of oxidants are present the sulfenic acid can be further oxidised to sulfinic acid (R-SO_2H) and sulfonic acid (R-SO_3H), which are usually considered to be biologically irreversible events termed hyperoxidation. Under mild oxidising conditions the sulfenic acid intermediate can rapidly react with thiol reducing equivalents to form disulfide bonds (R-S-S-R), before being recycled back to the reduced state by intracellular antioxidants, discussed in more detail below. The location of the reducing thiol determines whether the protein forms an intramolecular disulfide or an intermolecular disulfide with an adjacent protein. Certain cysteines can also form mixed disulfides with low molecular weight thiols such as free cysteine or glutathione, termed S-cysteinylation (-R-S-Cys) or S-glutathionylation (R-S-SG) respectively. As well as oxidant signal transduction, disulfide bond formation has been considered as an important form of protection against irreversible thiol hyperoxidation mentioned above[13,16].

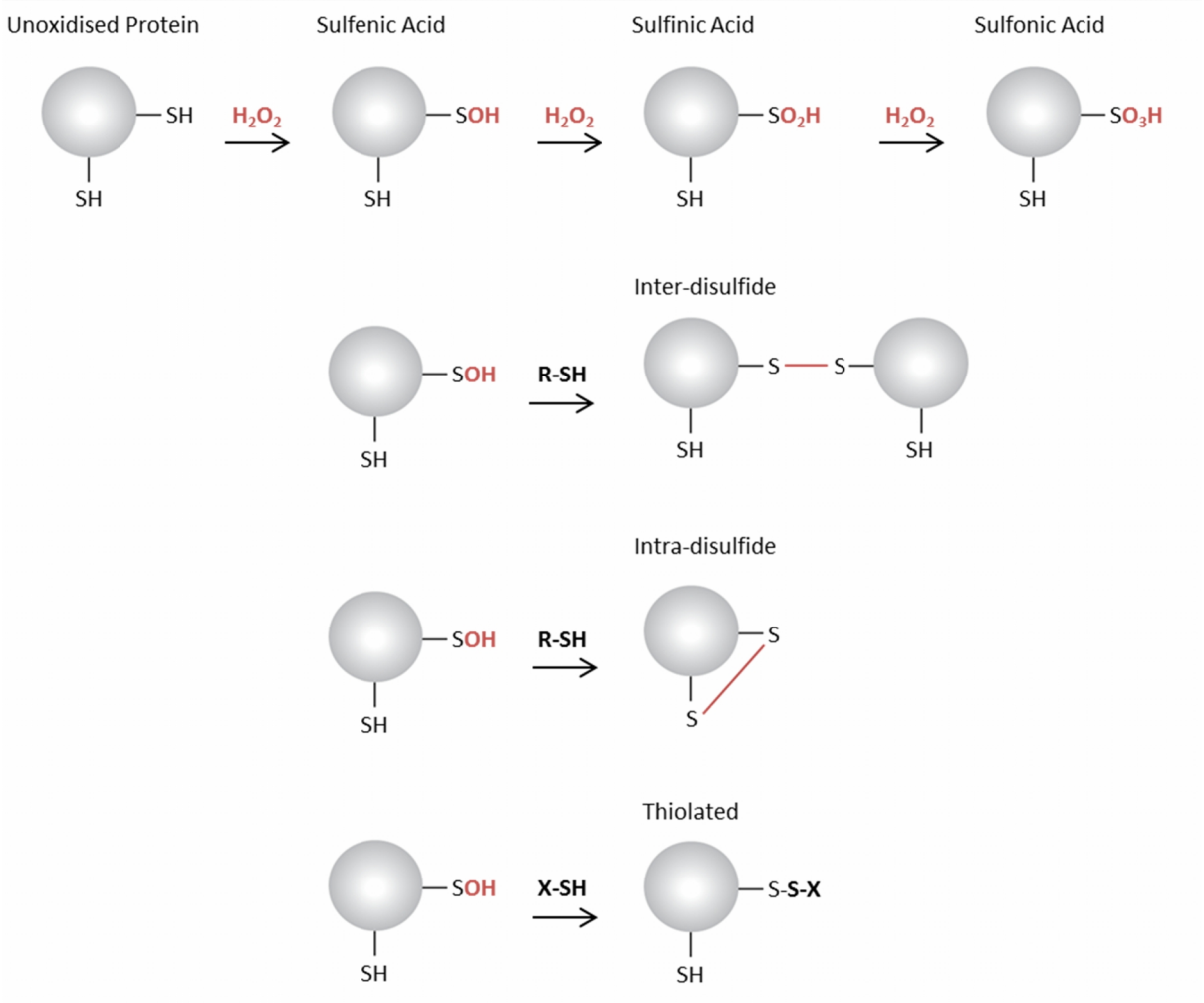

Figure 1.1 Summary of post-translation modifications of reactive cysteine thiols induced by H_2O_2.

1.2 Sources of reactive oxygen species

The mitochondria are a primary source of cellular ROS. Under normal circumstances O_2 is the terminal electron acceptor at complex IV of the electron transport chain where it is reduced to form H_2O. However electrons can 'leak' at complexes I and III where they can be transferred to O_2 to generate $O_2\cdot^{-}$[22]. Although these mitochondrial-derived ROS can be detrimental, they can also contribute to homeostatic redox signalling[27]. Located on the outer membrane of the mitochondria is the ubiquitous enzyme monoamine oxidase (MAO) which catalyses the oxidative deamination of adrenaline (A), noradrenaline (NA), serotonin (5-HT) and other related monoamines. Here, H_2O_2 is produced as a by-product of monoamine catabolism to an aldehyde intermediate[23]. MAO-dependent ROS production has been confirmed in the cardiovascular system, for example there is elevated O_2^{-} in homogenates of cardiac valves or blood vessels after incubation with serotonin, which can be blocked by the MAO inhibitor clorgyline[24]. Furthermore pharmacological inhibition of MAO has demonstrated a role for MAO-dependent ROS production in both 5-HT and NA-induced cardiac hypertrophy[25].

ROS is not simply generated as a by-product of metabolism. For example, NADPH oxidases (NOX) are a family of enzymes which generate $O_2\cdot^{-}$ as a primary outcome by transferring electrons from NADPH to flavin and then on to molecular O_2 to form $O_2\cdot^{-}$ ($2O_2 + NADPH \rightarrow 2O_2\cdot^{-} + H^{+} + NADP^{+}$)[14]. The NOX enzyme is a complex of several protein components including the membrane spanning flavocytochrome b_{558} (composed of flavin, the haem-binding (gp91phox) and p22phox), the cytosolic regulators (p47phox, p67phox, p40phox) as well as the small GTPase, Rac 1 or 2. Upon stimulation, the four cytosolic proteins translocate to the membrane and assemble with flavocytochrome b_{558} to enhance $O_2\cdot^{-}$ production[26]. ROS derived from NOX enzymes have been extensively studied as part of the innate immune system. For over 80 years professional phagocytes such as macrophages and neutrophils have been known to utilise ROS upon activation, known as the 'respiratory burst', to destroy invading microorganisms[27]. The importance of physiological ROS generation as part of the innate host defence is highlighted in patients afflicted with chronic granulomatous disease whom lack a functional NOX and suffer from microbial infections more frequently as a consequence[28]. The death of the pathogens also highlights the destructive capacity of indiscriminate ROS, and why oxidants were consistently associated with detrimental effects on biological molecules by the scientific community[29]. However there is now a greater appreciation for the role of NOX enzymes in a broad range of cell types and various physiological processes including apoptosis, cell proliferation, angiogenesis, and fibrosis[29,30] (Table 1.1).

Within the cardiovascular system the NOX isoforms are expressed differentially. Both the endothelium and cardiomyocytes contain NOX2 and NOX4 whereas vascular smooth muscle cells also additionally express NOX1[31]. NOX2 is found on the plasma membrane and its activation appears to be directly linked to acute receptor agonism by hormones, growth factors and cytokines including angiotensin II, insulin, platelet-derived growth factor (PDGF) and tumour necrosis factor α (TNFα). The constitutively active NOX4 is located intracellularly and its activity appears to be directly related to its abundance[32]. Physiologically, the targeting of NOX to specific subcellular compartments may serve to ensure specificity and selectivity of the oxidant signal within the microenvironment that it is generated in[16]. Despite this physiological role, NOX4 is upregulated and is associated with pathogenesis in the cardiovascular system, including ischemic injury, hypoxia, reperfusion, atherosclerosis, hypertrophy and hypertension[33].

The effectiveness of $O_2\cdot^-$ as a signalling molecule may be limited by its inability to penetrate cellular membranes and its rapid conversion into H_2O_2. There are three mammalian isoforms of SOD; copper-zinc SOD (SOD1) located in the cytosol, manganese SOD (SOD2) located in the mitochondria, and copper-zinc SOD (SOD3) located in the extracellular space[34]. SOD catalysed dismutation of $O_2\cdot^-$ occurs at a near diffusion limited rate, and the high concentration of SOD in the cytosol and the mitochondria is such that the probability of $O_2\cdot^-$ undergoing a reaction other than dismutation is unlikely. The exceptions occur when a reaction with $O_2\cdot^-$ has a rate constant that is comparable to its dismutation by SOD, such as the reaction between $O_2\cdot^-$ and NO to form $OONO^-$. Further exceptions occur in subcellular compartments where SOD is low or absent, or when a reactive molecule is within one molecular diameter of where $O_2\cdot^-$ is produced[35].

NOX isoform	Tissue/Cell Expression	Type of ROS Release
NOX1	colon epithelium, smooth muscle, endothelium, osteoclasts, retinal pericytes, CNS	$O_2^{\cdot -}$
NOX2	cardiomyocytes, endothelium, phagocytes, fibroblasts	$O_2^{\cdot -}$
NOX3	inner ear, liver, lung, spleen, kidney	$O_2^{\cdot -}$
NOX4	liver, smooth muscle cells, osteoclasts, endothelium, fibroblasts, keratinocytes, neurons	H_2O_2
NOX5	Spleen, testis, mammary glands, heart, kidney, lung, liver, endothelium, smooth muscle cells	$O_2^{\cdot -}$
Duox1	Thyroid, airway epithelia prostate, endothelium	H_2O_2
Duox2	Thyroid, salivary gland, rectal mucosa, gastrointestinal tract, prostate, pancreas, endothelium	H_2O_2

Table 1.1 Overview of NOX isoforms. *Table adapted from Bedard and Krause 2007[36], Santillo et al. 2015[37] and Panday et al. 2015[38].*

1.3 Overview of biological antioxidants

H_2O_2 has the advantage of being a small and neutral molecule, making it highly diffusible and able to cross cellular membranes. It is also less reactive than $O_2^{\cdot -}$ and therefore considered by some to be a more important redox signalling second messenger[16]. H_2O_2 has multiple physiological roles within the cell but given its cytotoxic effect at high concentrations its abundance must be tightly regulated. Oxidative stress can be defined as an imbalance between endogenous oxidants and antioxidants in favour of the former thus ROS and RNS are counterbalanced by antioxidant systems to maintain the redox homeostasis in the cell[39]. Furthermore for H_2O_2 to be considered as a signalling molecule, cysteine modifications should be reversible, as occurs for other regulatory posttranslational modifications such as phosphorylation.

H_2O_2 concentration is controlled non-enzymatically by intracellular antioxidants such as glutathione (GSH) or the antioxidant vitamins C and E[40-42]. GSH, with a cellular concentration in the millimolar range, is the most abundant non-protein thiol in cell and thus has key role in the adaptive response to oxidative stress. However its concentration is depleted in response to oxidative insults[43]. Biosynthesis of GSH is dependent upon the availability of intracellular cysteine and the rate-limiting enzyme, glutamate cysteine ligase (GCL), a heterodimer comprising a catalytic (GCLC) and a modifier (GCLM) subunit[44]. Elevated cellular oxidants lead to increased Nrf2 transcriptional activity (discussed below in more detail) and consequently increased downstream expression of GCLC and GCLM. The result is a 'rebound' effect post-oxidative insult whereby the intracellular concentration of GSH exceeds initial levels after oxidant-induced depletion. This 'rebound' effect is lost in cells lacking Nrf2, highlighting the importance of the transcription factor for adaptive GSH-dependent cytoprotection[45]. Throughout this thesis, H_2O_2 is routinely used to acutely induce oxidative stress (10 mins) in various cell types; therefore the rebound increase in glutathione concentrations will only play a potential role in conditions of chronic oxidative stress.

Enzymatic regulation of H_2O_2 concentration is primarily mediated by peroxidases, which include catalase, glutathione peroxidase (Gpx1), and peroxiredoxin (Prx) that can neutralise the oxidant signal. The tetrameric enzyme catalase exists predominantly within cytosolic peroxisomes. High concentrations of H_2O_2 undergo catalase-dependent decomposition into H_2O and O_2. Gpx1, a key antioxidant enzyme localised in the cytosol, is a H_2O_2 scavenger that utilises GSH as a reductant and generates oxidised glutathione (GSSG) as a metabolic product, whilst glutathione reductase (Gsr) uses NADPH as source of reducing power to regenerate GSH from GSSG. Prxs make up around 1% of total cellular protein content. All 6 members of the Prx family contain a peroxidatic cysteinyl thiol which has a very low pK_a (~5.5) in comparison to those in other proteins, thus making them highly reactive oxidant scavengers. 2-Cys Prxs react with H_2O_2 to form intermediate sulfenic acids before transitioning to intermolecular disulfides by reacting with thiols on a neighbouring Prx molecule[46]. Oxidised Prx then is reduced by thioredoxin (Trx) via thiol disulfide exchange (R-S-S-R + R'-S^- → R'-S-S-R + R-S^-) to restore the catalytic activity of Prx. The nucleophilic N-terminal Trx catalytic thiolate attacks a disulfide thiol in Prx which breaks the bond and creates a new mixed disulfide between Trx and Prx. The second Trx catalytic thiol attacks the thiol in the newly formed mixed disulfide, resulting in an internal disulfide bond in Trx as well as restoring reduced Prx which is now available again to react with another H_2O_2 molecule[47]. Trx is a universal disulfide reductase that can also directly reduce oxidised substrates to reverse the oxidative modifications induced by H_2O_2, again resulting in the formation of an intramolecular disulfide bond via thiol disulfide exchange. The

catalytic activity of oxidised Trx is restored by thioredoxin reductase (TR) which utilises NADPH and FAD as reducing power[48]. Glutaredoxin (Grx) is another enzyme capable of reducing disulfide containing substrates via thiol disulfide exchange, and is reduced and restored non-enzymatically by GSH.

As Prx is such an effective antioxidant it is difficult to reconcile how H_2O_2 could effectively oxidise target substrates before being scavenged. One explanation, the floodgate hypothesis, is that oxidation occurs only after the local 2-Cys Prxs have been inactivated[49]. A burst of local H_2O_2 would lead to sulfination and consequent inhibition of the local peroxiredoxin 'gatekeepers' permitting substrates in close proximity to the be oxidised. The activity of sulfiredoxin, an antioxidant enzyme that utilises ATP to reduce sulfinated Prx, would restore the catalytic activity of Prx thus closing the 'floodgates', but in the interim less reactive local substrates can become oxidised. A complimentary hypothesis is that Prx enzymes are initially oxidised to sulfenates or disulfides which can then react with less reactive substrates as a potential mechanism of oxidant signal transduction[14,50]. For example, oxidised Prx 4 in the endoplasmic reticulum can pass on its redox state to protein disulfide isomerase via thiol-disulfide exchange[51].

1.4 Biological roles of oxidants

Oxidants play a role in a diverse range of physiological and pathophysiological effects that depends on the abundance, duration, location and of the composition of the oxidant signal. Susceptible proteins to oxidation include receptors, ion transporters, transcription factors and kinases which are structurally modified to produce specific functional outputs[20]. How H_2O_2 can transduce signals through modification of proteins to alter function is a major focus of this thesis.

1.4.1 Pathophysiological roles of oxidants

Apoptosis: Dysregulated and/or excessive concentrations of H_2O_2 can accelerate cell death through activation of apoptosis signal-regulating kinase 1 (ASK1). This mechanism contributes to ischemia/reperfusion injury and heart failure. In adult cardiomyocytes, β-adrenoceptor–induced apoptosis leads to oxidant-dependent activation of c-Jun N-terminal kinase (JNK) and the programmed mitochondrial death downstream of ASK1[52]. Under basal conditions reduced Trx is negative regulator of ASK1 activity and the two proteins exist together in complex. H_2O_2 leads to the formation of an intra-molecular disulfide bond in Trx. This oxidation event disrupts the complex and permits autophosphorylation of ASK1 Thr838 leading to its activation and

downstream phosphorylation of JNK to induce apoptosis[53]. The importance of this pathway is demonstrated in ASK-1$^{-/-}$ mice which exhibit attenuated ventricular remodelling in a model of cardiac hypertrophy as a consequence of decreased apoptosis[54].

Arrhythmias and cardiac hypertrophy: Oxidative signalling has been shown to be pro-arrhythmic and pro-hypertrophic via the redox activation of Ca^{2+}/calmodulin-dependent kinase II (CaMKII). CaMKII is a ubiquitously expressed multimeric serine/threonine kinase responsible for the phosphorylation of key excitation-contraction coupling proteins as well as regulating genes associated with pathological cardiac hypertrophy. CaMKII phosphorylates key Ca^{2+} handling proteins the net effect of which is diastolic accumulation of arrhythmogenic Ca^{2+} and Na^{+}[55]. Each monomer of the dodecameric CaMKII multimer associates via its C-terminal domain to form a double-ringed hexameric complex[55]. The catalytic N-terminal of the kinase is responsible for substrate phosphorylation but under basal conditions is inhibited by the C-terminal regulatory domain[56]. The activation of CaMKII is mediated by binding of Ca^{2+}-calmodulin to the regulatory domain. This induces a conformational change in the kinase structure which disrupts the association between the regulatory and catalytic domains and permits substrate phosphorylation. CaMKII can also be activated via oxidative modification of methionine (Met281 and Met282) residues on the regulatory subunit which maintains the kinase in the active conformation. Angiotensin II-dependent activation of NOX2, *in vitro* and *in vivo*, increased M281/282 oxidation and induced apoptosis, which was lost in M281/282V CaMKII knock-in (KI) mice[55,57]. Furthermore treatment of cardiomyocytes with H_2O_2 increases the incidence of pro-arrhythmic Ca^{2+} sparks and pro-hypertrophic Ca^{2+} overload downstream of CaMKII activation[58].

Atherosclerosis: Atherosclerosis is a disease of the arterial blood vessels that is characterised by the formation of a complex fatty plaque surrounded by a fibrous cap. Loss of fibrous cap integrity leads to thrombus formation, and consequently impinged blood flow and oxygen delivery to the affected tissue[59]. Rupture of the fibrous cap is intrinsically linked to macrophage activity as they express matrix degrading enzymes such as matrix metalloproteinases and cathepsins that degrade the fibrous cap and reduce the stability of the plaque[60]. ROS derived from a variety of systems including NOX enzymes, lipooxygenases and cycloxogenases contributes to the oxidation of low density lipoproteins (ox-LDL) within the atheroma. Ox-LDL induces the expression of adhesion molecules VCAM-1 and ICAM-1 on endothelial cells; serves as a chemoattractant for circulating monocytes; promotes differentiation and activation macrophages; and induces the production of pro-inflammatory cytokines (TNFα, interleukin-1β)[61-63]. The detrimental role of H_2O_2 in disease progression is

further highlighted as atherogenic ApoE$^{-/-}$ mice crossed with mice over-expressing both SOD1 and catalase had markedly reduced atherosclerosis[64].

Vascular permeability: Numerous *in vitro* and *in vivo* studies have demonstrated that oxidants can induce endothelial permeability[65,66]. Elevated vascular permeability is associated with various pathologies such as atherosclerosis, diabetes, ischemia/reperfusion injury and sepsis[65]. The perfusion of H_2O_2 into isolated lungs of guinea pigs or rabbits increased their capillary filtration coefficient, leading to pulmonary oedema[65]. Treatment of endothelial cells with H_2O_2 increased albumin flux through their monolayer and decreased transendothelial electrical resistance in a dose-dependent manner[67]. Disruption of VE-cadherin at cell-cell junctions and increased junctional protein phosphorylation, often associated with increased permeability, has been observed downstream of vascular endothelial growth factor (VEGF)-dependent ROS generation[66]. This may further be perpetuated by the ability of H_2O_2 to upregulate VEGF expression[68]. Oxidants can also regulate endothelial cell activation and junctional permeability through the re-organisation of the actin cytoskeleton upregulate on[69]. $O_2^{\cdot -}$ is generated downstream of oedemagenic TNFα and IL-1, cytokines that are d during sepsis. This contributes to actin stress fibre formation which is thought to drive endothelial contraction and thus increases permeability[70]. In Chapter 6 I explore the role of oxidant-dependent activation of PKARIα on actin stress fibre formation in the pathogenesis of sepsis.

1.4.2 Physiological roles of oxidants

Gene transcription: Cells have evolved mechanisms that sense high concentrations of ROS and upregulate the expression of antioxidant enzymes accordingly. This stress response is exemplified by the transcription factor OxyR in bacteria. H_2O_2 induces oxidation of OxyR Cys199 to a sulfenic acid intermediate which then reacts with Cys208 to form an intramolecular disulfide bond. This activates OxyR to increase transcription of antioxidant enzymes including catalase and SOD[71,72]. In eukaryotic cells the transcription factor nuclear factor-erythroid-2-related factor 2 (Nrf2) is sequestered to the cytoplasm in an inactive complex with Kelch-like ECH-associated protein 1 (Keap1). Here Nrf2 is ubiquitinated, signalling it for its proteasomal degradation. Keap1 contains reactive cysteines that sense cellular oxidants[73]. Oxidation of these critical cysteine residues leads to a change in Keap1 conformation, thus stabilising Nrf2 and facilitating translocation of *de novo* synthesised Nrf2 to the nucleus[74]. Here, it binds to the antioxidant response element (ARE) located in the promoter region of genes to upregulate transcription of various cytoprotective proteins including but not limited to sulfiredoxin, Prx1 and TR (Figure 1.2)[75,76]. APE1 is a dual function protein involved with the base excision repair pathway of DNA damage by oxidative stress[77]. If

these lesions are not adequately repaired they may promote a variety of diseases such as cancer. Independent of the DNA repair action of APE1 is its co-transcriptional activity, modulating gene expression directly regulated by various transcription factors, including AP-1, CREB, NF-κB, p53 and HIF[77]. APE1 maintains such transcription factors in their active, reduced state, to enhance their DNA binding, providing another link between oxidative signals and gene expression[78]. Cys65 of APE1 is critical for its redox control and is thought to be responsible for the nucleophilic attack of oxidised transcription factor thiols[79]. Interestingly, Cys65 is not a solvent accessible residue and therefore APE1 must undergo a conformational change for it to serve as a nucleophilic cysteine[80]. In Chapter 5, I propose a model whereby the novel AKAP tubulin similarly undergoes a conformational change that reveals a cysteine residue capable of reducing disulfide PKARIα.

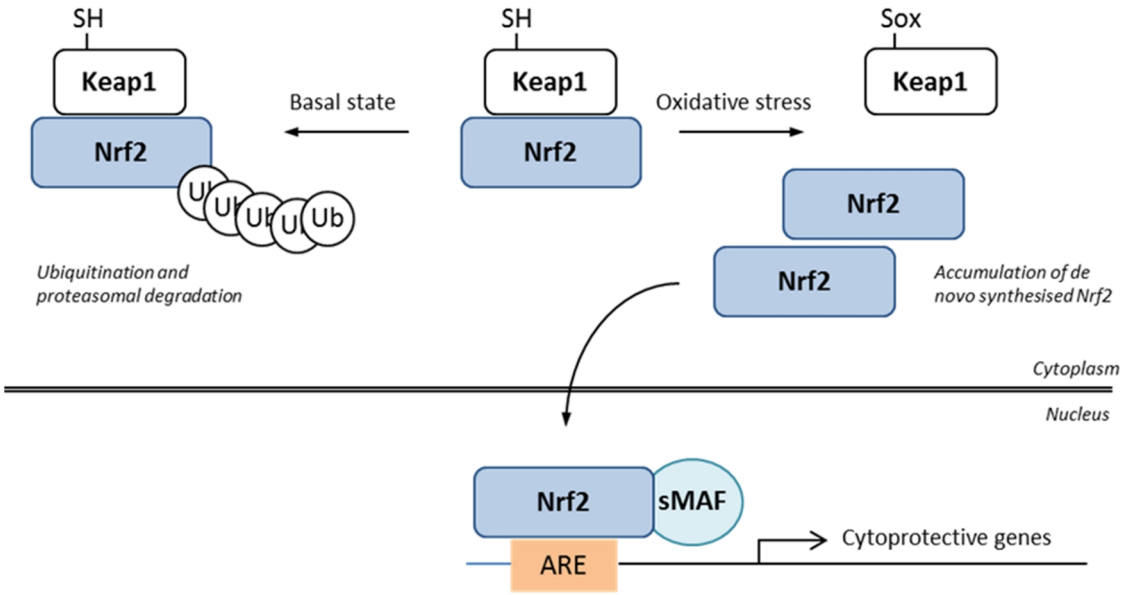

Figure 1.2 Effect of oxidative stress on Nrf2 activation. Keap1 is bound to Nrf2 under basal, unstressed conditions thus facilitating the degradation of Nrf2 via the ubiquitin-proteasome pathway. Oxidative stress leads to modification of Keap1 cysteine residues thus stabilizing Nrf2 whilst allowing *de novo* synthesised Nrf2 to translocate to the nucleus. Expression of cytoprotective genes is mediated via heterodimerisation with small Maf (sMAF) proteins and binding to the antioxidant response element (ARE).

Blood pressure: NO is a well characterised mediator of vascular tone and is produced by plasma membrane endothelial nitric oxide synthase (eNOS), through the oxidation of L-arginine. NO diffuses into smooth muscle cells binding to and activating soluble guanylate cyclase (sGC), which produces cyclic guanosine monophosphate (cGMP) that activates protein kinase G Iα (PKGIα) to decrease contractility (Figure 1.3)[81]. Cellular oxidants can influence this signalling cascade to further regulate vascular tone and consequently blood pressure. Cellular NO can be lost by reacting with $O_2\cdot^-$, forming the highly reactive $OONO^-$. Such reductions in NO bioavailability, as well as $OONO^-$-mediated protein nitration, may contribute to disease pathogenesis[18,33]. eNOS can itself produce $O_2\cdot^-$ when it becomes uncoupled. For example, if the concentration of the co-factor tetrahydrobiopterin (BH_4) is depleted it is unable to accept an electron leading to the generation of $O_2\cdot^-$ instead of NO[82]. ROS generation and the depletion of NO caused by eNOS uncoupling is strongly associated with the endothelial dysfunction associated with atherosclerosis and hypertension[83]. S-glutathionylation of two highly conserved cysteine residues in eNOS reversibly decreases NO and increases $O_2\cdot^-$ generation which is also associated with impaired endothelium-dependent vasodilation[84]. Furthermore NO species can modify reactive cysteines to generate nitrosothiols (-R-SNO) in a reaction termed S-nitrosation. There is controversy about whether this is a stable oxidative signalling modification in its own right, or whether it is a transitory intermediate prior to more stable disulfide bond formation[85,86]. Nevertheless, this laboratory identified PKGIα as being sensitive to oxidation by either H_2O_2 or the NO derivative nitrosocysteine (CysNO) that directly leads to its activation[81,85]. Exogenously applied H_2O_2 caused the formation of an interprotein disulfide bond between the two Cys42 residues in the PKGIα homodimers whilst simultaneously decreasing coronary perfusion pressure in a correlative manner. This led to the hypothesis that PKGIα disulfide formation may activate the kinase independently of the classical NO-cGMP pathway. Indeed, pharmacological inhibition of sGC with 1H-[1,2,4]oxadiazolo[4,3-*a*]quinoxalin-1-one (ODQ) did not attenuate H_2O_2-induced vasorelaxation of isolated thoracic aorta rings and *in vitro* experiments. Furthermore, recombinant PKG showed it was directly activated by oxidation, which was abrogated when Cys42 was mutated to a serine[81]. Cys42, which is unique to the Iα isoform, oxidation to disulfide induced by H_2O_2 is likely to initially be 'primed' by means of sulfenation of one monomer thiol. The Cys42 sulfenate is subsequently reduced by the Cys42 residue on the adjacent subunit to yield an interprotein disulfide. The susceptibility of Cys42 to oxidation can be explained by the surrounding basic residues and the proximity of the thiol residues (~8 Å)[81]. Finally KI mice expressing only a C42S 'redox-dead' version of PKGIα are not susceptible to the vasodilatory action of H_2O_2 on resistance vessels and are consequently basally hypertensive *in vivo*[87].

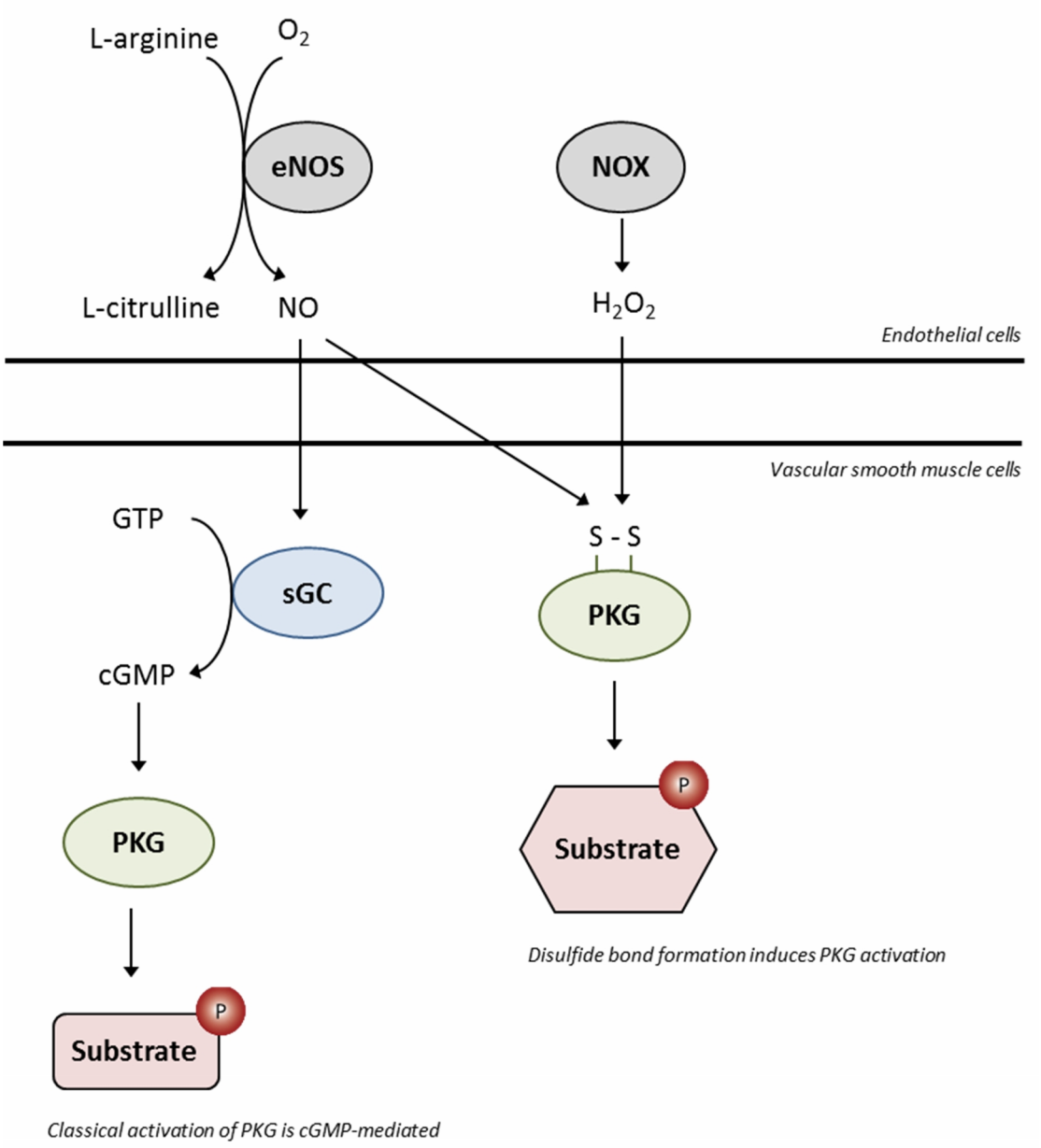

Figure 1.3 Classical-NO and oxidative-dependent activation of PKGIα. NO derived from eNOS activity diffuses from endothelial cells into smooth muscle cells where it binds to the haem-centre of sGC, leading to the catalysis of GTP to cGMP. The binding of four cGMP molecules to PKG is for classical activation of the kinase, and subsequently leads to downstream substrate phosphorylation. The oxidative activation of PKG is caused by reactive nitrogen/oxygen species inducing disulfide bond formation between the two subunits of the PKG homodimer which enhances kinase activity in the absence of cGMP, and is thought to lead to differential substrate phosphorylation in vivo.

Growth factor signalling: Growth factor receptor stimulation is commonly coupled to NOX activation which elicits an increase in cellular ROS. Enzymes that contain a catalytic thiol in their active site such as protein tyrosine phosphatases (PTP) can be inactivated by oxidation and are a potential target for NOX-derived oxidants downstream growth factor signalling. Inactivation of PTPs allows propagation of the extracellular growth factor signal downstream[88,89]. H_2O_2 signalling is important for vascular endothelial cell growth and consequently angiogenesis which is an important process in tissue development and maintenance, as well as wound healing and re-vascularisation of ischemic tissue. Growth factors can stimulate angiogenesis via oxidase-dependent ROS generation. VEGF increases cellular H_2O_2 downstream of vascular endothelial growth factor receptor 2 and NOX4 activation. H_2O_2 directly activates extracellular signal-regulated kinase (ERK1/2), a well-established mediator of growth factor signalling that results in the upregulation of genes involved with endothelial cell proliferation[90]. Recently PKARIα oxidation has also been shown to mediate vessel growth downstream of growth factor receptor activation. A novel Cys17Ser PKARIα 'redox-dead' KI mouse line that cannot undergo oxidant-dependent activation suffered from impaired angiogenesis in models of hind-limb ischaemia and tumour vascularisation. This highlights the importance of oxidant signalling in control of angiogenesis[91]. How the oxidant-induced structural change of PKARIα affects its function is a major focus of these investigations and is discussed in more detail below.

1.5 Overview of PKA

The ubiquitous holoenzyme PKA regulates many cellular processes including cardiac contraction and relaxation[92,93], vascular tone[94,95], vascular permeability[96,97], gene transcription[98,99], cellular proliferation[100-102] and apoptosis[102]. PKA exists as a tetramer comprising of a homodimer of regulatory subunits (R) and two catalytic subunits (C) (R_2C_2)[103]. There are four isoforms of the R subunit that are derived from distinct genes, namely RI (type I PKA) and RII (type II PKA) which can both be further classified into α and β subunits (RIα, RIβ, RIIα, RIIβ)[104]. Each R subunit monomer consists of a disordered linker region that connects the N-terminal dimerisation and docking domain (D/D) to the two 3'-5'- cyclic adenosine monophosphate (cAMP) binding domains (Figure 1.4)[105].

The C subunits, of which there are three isoforms (Cα, Cβ, Cγ), each consists of a small and large lobe with an active site that forms a cleft between the two lobes. The small lobe provides the binding site for adenosine 5-triphosphate (ATP), and the large lobe provides a docking surface for peptide/protein substrates with serine/threonine residues, typically with an -R-R-X-

S/T-X- motif[106]. The activation loop in the large lobe contains a phosphorylation site, Thr197, essential for catalysis[106]. Investigators have demonstrated that the Cys199 in the activation loop can form a disulfide bond with Cys97 of RIIα which inactivates the kinase, although this laboratory has never observed this putative oxidant-dependent interaction[107]. Under basal conditions when cAMP levels are low, the regulatory subunits are bound to and inhibit the catalytic subunits; however when cAMP levels are elevated, two molecules bind to each R subunit to induce dissociation of the catalytic subunits and facilitate substrate phosphorylation (Figure 1.5).

All four R isoforms share a similar domain organization but they are not functionally redundant. For example, RIα is constitutively expressed by all cells whilst RIβ is primarily expressed in neurons and adipose tissue[108]. RIα KO mice are embryonically lethal with notable heart and vasculature deformations, implying that its function is critical for normal development[108]. However whilst the RIIα is also constitutively expressed, RIIα KO mice have no clear phenotype highlighting that the R isoforms have explicit roles within the cell[109]. Dysregulated expression of RIα is suspected to play a role in malignant transformation, and constitutive over-expression of RIα leads to tumour growth in several cancers which is associated with poor patient prognosis[110]. Furthermore mutations in the RIα gene cause familial cardiac myxomas and Carney complex, an autosomal dominant disease where patients suffer from multiple neoplasms including lentiginosis, adrenal hyperplasia, and pituitary tumours that result in endocrine over activity[111]. The R isoforms differ in their subcellular location and substrate phosphorylation profile primarily due to structural differences, as highlighted below. The susceptibility of RIα to oxidants via disulfide bond formation is the key structural difference between the R subunits in the context of these investigations.

A

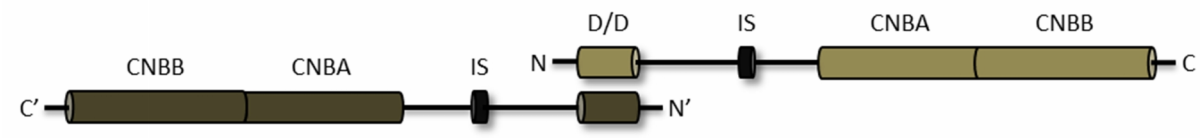

B

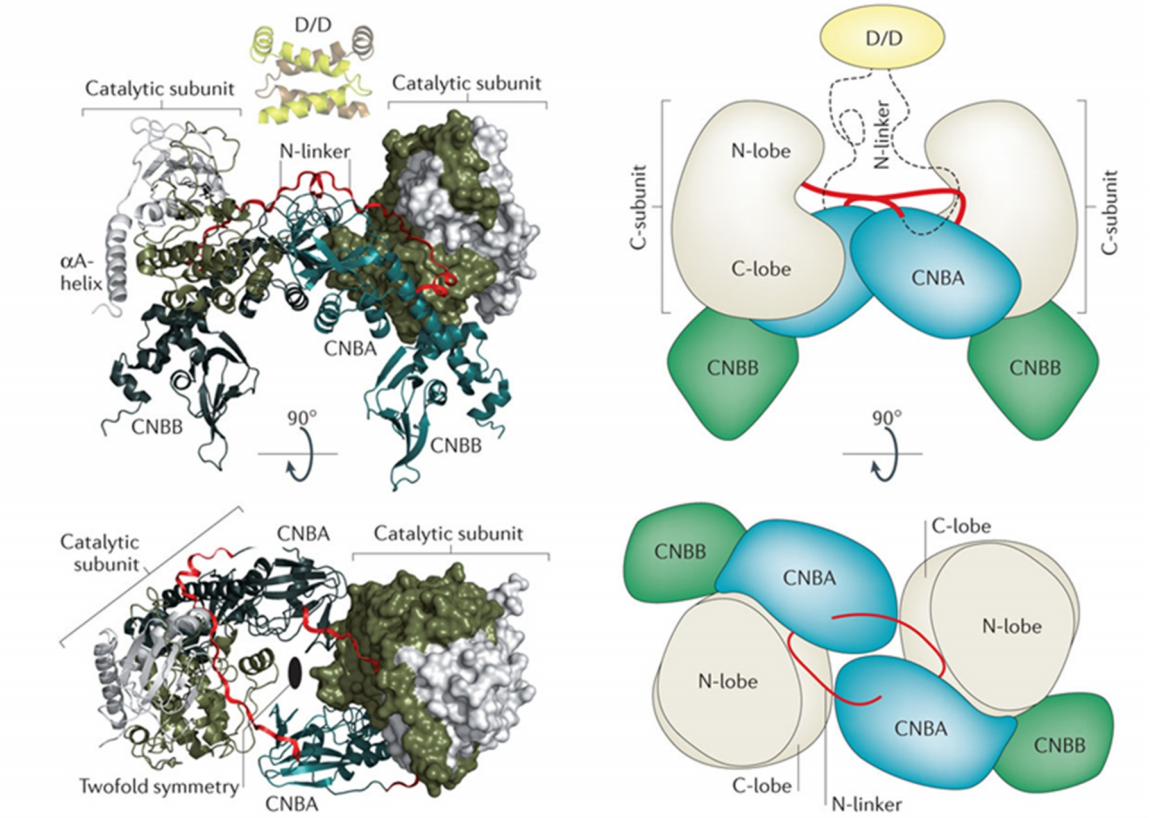

Figure 1.4 PKARIα holoenzyme. (**A**) Schematic representing PKARIα regulatory subunit domain structure. Each subunit contains an N-terminal dimerisation and docking domain (D/D) which is the point of contact for the adjacent R subunit and A-kinase anchoring proteins (AKAPs); an inhibitor site (IS) that sequesters the PKA catalytic subunits and two C-terminal cyclic nucleotide binding domains (CNBA and CNBB). (**B**) The crystal structure regulatory subunits (ribbons) complexed with the two catalytic subunits (surfaces) and representative cartoons. *Figure adapted from Taylor et al. 2012*[112]

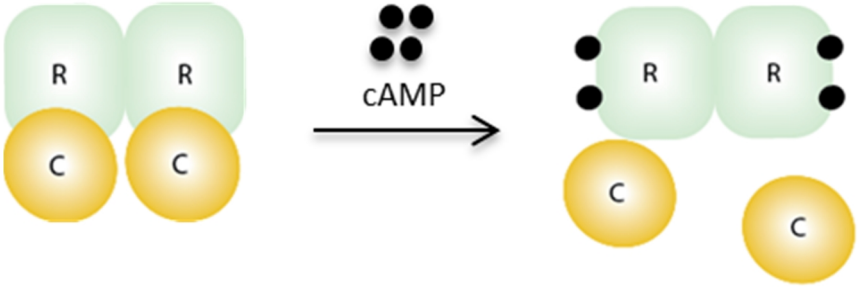

Figure 1.5 Classical activation of PKA. Cartoon depicting PKA in its inactive conformation before four molecules of cAMP (black circles) induce a conformational change in the regulatory (R) subunits (green) to facilitate the release of the catalytic (C) subunits (yellow) and permit phosphorylate substrates.

1.5.1 PKA structure

The co-discoverer of cAMP, Ted Rall, expressed his dissatisfaction at the idea of the "…catalytic subunit of protein kinase swimming about, happily phosphorylating a variety of cellular constituents whether they need to or not"[113]. Our current understanding of the structure of the R subunits confirms his assertions. The D/D at the N-terminal of the R subunits provides the interface for R subunit homodimerisation, and is also the point of contact between PKA and A-kinase anchoring proteins (AKAPs), scaffold proteins that tether PKA to specific subcellular locations to regulate substrate phosphorylation (discussed in more detail below)[114]. The two R subunits of PKA assemble in an "X-type, anti-parallel four helix bundle" which forms a binding pocket for the helical amphipathic A-kinase binding domain (AKB) of the AKAP to bind (Figure 1.6)[103]. Nuclear magnetic resonance and X-ray crystallography experiments demonstrate that the dimer interface of the D/D domain is formed predominantly from hydrophobic side chains. This critical cluster of hydrophobic residues provides a surface for the complimentary hydrophobic residues on the exterior of the AKAP helix to interact with[115,116].

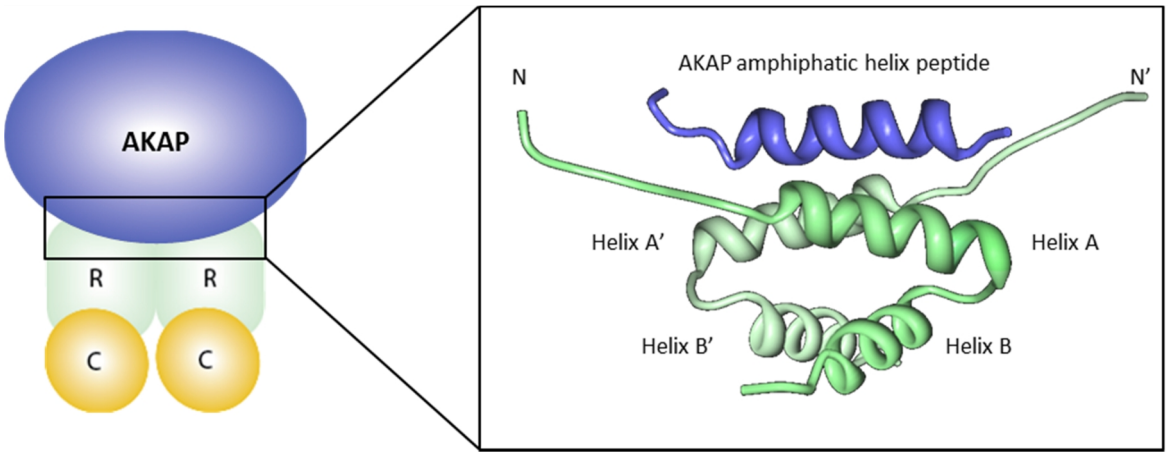

Figure 1.6 The D/D domain of PKA binds to an AKAP amphipathic helix. Cartoon depicting the PKA holoenzyme with an AKAP. Ribbon diagram of the RIIα subunit dimer (1–43, green) which forms an X-type, anti-parallel four helix bundle to create a binding pocket for the AKAP helix peptide (blue). *Figure adapted from Newlon et al. 2001*[114]

Fundamentally the R subunits bind the catalytic subunits to render them inactive and unable to phosphorylate target substrates. The inhibitory site (IS) that binds to the catalytic subunits in type II PKA is a bona fide phosphorylation site (Arg-Arg-Val-Ser(P)-Val), whilst in type I PKA it is a pseudosubstrate that contains a non-phosphorylatable alanine in place of the serine[117]. Both R subunits of the holoenzyme contain two carboxyl-terminal cyclic nucleotide binding domains. The binding of two cAMP molecules per R subunit is necessary to induce dissociation of the catalytic subunits and facilitate substrate phosphorylation. cAMP binds cooperatively to the A and B sites as occupation of one site alone (i.e. low intracellular cAMP concentrations) is insufficient to activate PKA. A conformational change upon cAMP binding to the B site is required to increase accessibility of the A site. Consequently co-operative binding to both sites causes a profound change in conformation that permits the release of the catalytic subunits and leads to substrate phosphorylation[118].

1.5.2 Classical PKA activation in the cardiovascular system

Activation of β-adrenergic receptors by catecholamines is the primary mechanism by which cAMP is generated and contraction of the heart is modulated[119]. Binding of agonists such as noradrenaline or adrenaline causes a conformational change in the receptor and leads to dissociation of the $G\alpha_s$ subunit from the heterotrimeric G protein. $G\alpha_s$ then activates adenylate cyclase (AC) which catalyses the conversion of ATP to cAMP, a ubiquitous second messenger that has three downstream effectors[120,121]. cAMP interacts with cyclic-nucleotide gated ion channels to regulate their open probability[122]. cAMP also targets exchange protein directly activated by cAMP 1/2 (Epac1/2), which function as guanine nucleotide exchange factors for

the G proteins Ras-related protein 1 and 2[123]. The principal target of cAMP is PKA which is well known for phosphorylating key regulators of excitation-contraction coupling that govern the inotropic (force of contraction), lusitropic (rate of relaxation) and chronotropic (rate of contraction) effects associated with β-adrenergic receptor activation[124,125] (Figure 1.7).

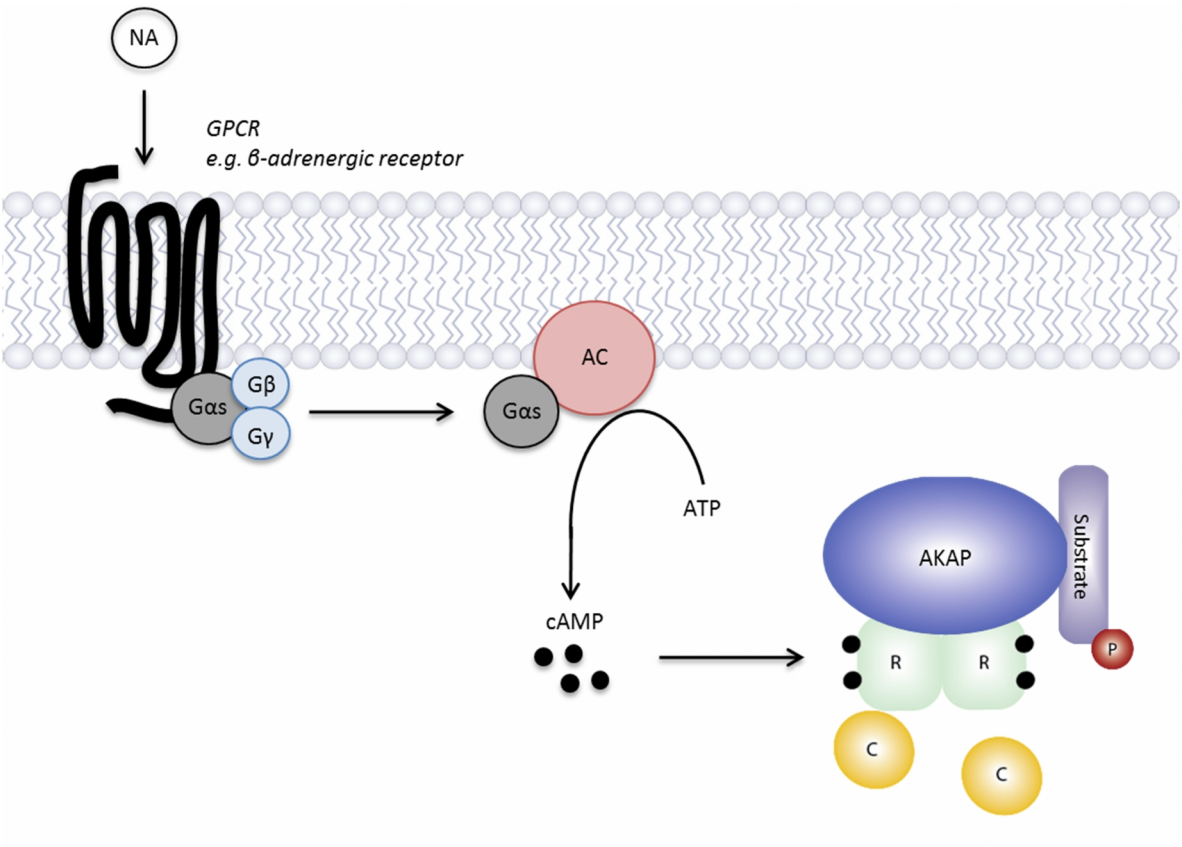

Figure 1.7 Classical activation of PKA. GPCR activation leads to translocation of Gαs to bind and activate adenylate cyclase (AC). AC converts ATP to cAMP which binds and activates PKA and leads to substrate phosphorylation.

An elevation of cytosolic Ca^{2+} is essential for coupling cardiomyocyte excitation to contraction. Ca^{2+} induces a conformational change in the troponin complex to expose the myosin binding site of actin and facilitate their interaction to generate force and initiate contraction[118]. PKA phosphorylates the L-type calcium channel at Ser1928 on α_{1c} and Ser478 and 479 on β_{2a} to increase channel open probability, allowing more Ca^{2+} into the cytosol upon arrival of an action potential to increase cardiac contractility[118,126]. Phosphorylation of the ryanodine receptor 2 (RyR_2) at Ser-2030 or Ser-2808 sensitises it and causes increased calcium release from the sarcoplasmic reticulum (SR) during excitation-contraction coupling which consequently increases inotropy. Whilst phosphorylation of Ser-16 on PLB enhances the active transport of Ca^{2+} back into SR via sarco/endoplasmic reticulum Ca^{2+}-ATPase 2a (SERCA2a) to reduce intracellular Ca^{2+} levels and consequently increases the rate of myocyte relaxation (Figure 1.8)[127]. Regulation of PKA substrate phosphorylation is mediated by phosphodiesterases (PDEs) that hydrolyse cAMP to an inactive it, therefore PDEs can determine the duration and amplitude of the cyclic nucleotide signal. Furthermore, phosphatases directly oppose the action of kinases to dephosphorylate proteins and return them to their basal state[128].

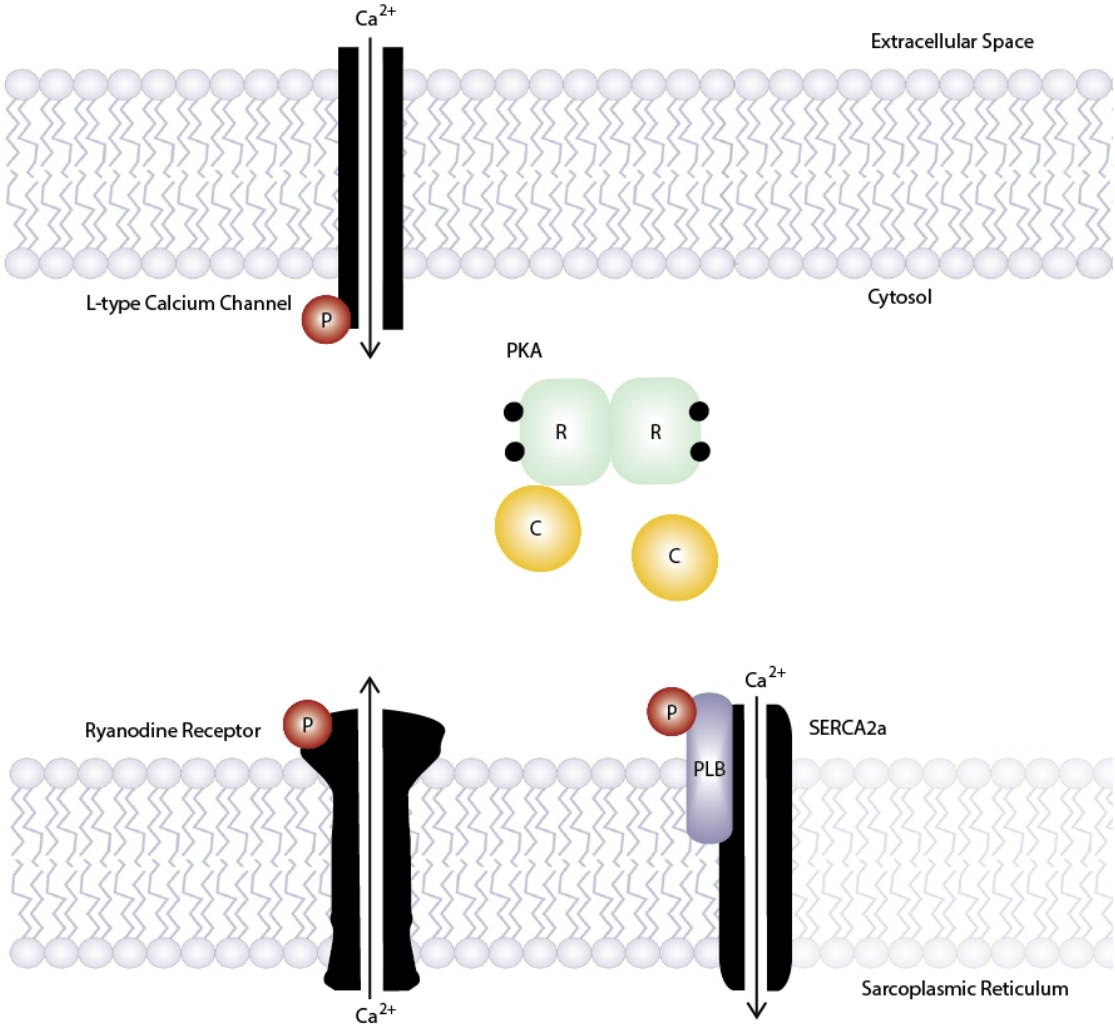

Figure 1.8 Classical cAMP-dependent activation of PKA leads to phosphorylation of ion translocators involved with excitation-contraction coupling. cAMP (black circles) binding to the regulatory subunits (R) causes the dissociation of the catalytic subunits (C) to permit phosphorylation.

PKA has other roles beyond excitation-contraction coupling in the cardiovascular system. For example, PKA phosphorylates the transcription factor cAMP response element binding protein (CREB) at Ser133 to modify gene expression profile of its downstream targets[129]. Cardiac myocyte-specific expression of dominant negative CREB revealed atrophic and hypertrophied muscle fibres, as well as significant interstitial fibrosis emphasising the importance of CREB activity regulation for normal cardiac function[130] In the vasculature PKA regulates smooth muscle tone, impairment of which can contribute to the pathophysiology of vascular diseases including hypertension[94,95]. Ca^{2+}-activated K^+ channels (BK) are activated by changes in membrane potential and increases in intracellular Ca^{2+} to passively allow K^+ efflux from the cytoplasm down its electrochemical gradient and induce hyperpolarisation and reduce cell excitability[131]. PKA phosphorylates BK channels to increase open channel probability further

decreasing the excitability of the cell to favour vasorelaxation[132]. In vascular smooth muscle cells myosin light chain (MLC_{20}) phosphorylation at Ser19 by myosin light chain kinase (MLCK) is necessary for actin activation of myosin ATPase and subsequent crossbridge cycling[133]. cAMP production downstream of β_2 adrenergic receptors activates PKA which phosphorylates MLCK, decreasing its activity and consequently inducing vasorelaxation. Furthermore PKA phosphorylates a 20 kDa heat shock-related protein HSP20 at Ser16 which can modulate the contractile apparatus to also induce vasorelaxation[134]. PKA also has a prominent role in endothelial cells where it is able to influence actin filament dynamics which dictate cell shape and consequently impact on vascular permeability[96,97]. The role of PKA on vascular permeability is discussed in more depth in Chapter 6. The numerous roles of PKA highlight its importance within the cardiovascular system.

1.6 Overview of AKAPs

Given the diversity of roles PKA has within the cell its localisation and activity has to be tightly regulated to ensure specific and appropriate intracellular responses. This is mediated through the interaction between PKA and AKAPs; scaffold proteins that typically have no intrinsic enzymatic activity but assemble spatially discrete signalling complexes comprised of effectors of the cAMP signalling cascade and tether them to a specific subcellular compartment. These effectors certainly include PKA, PKA substrates and PDEs, and may also include phosphatases, ACs and G-protein coupled receptors (GPCRs)[135,136].

1.6.1 Structural features of AKAPs

AKAPs are a large family of scaffold proteins that are structurally diverse but functionally similar. The first AKAPs were detected as contaminants that were co-captured with R subunits on cAMP-agarose affinity columns[137]. Since then over 50 human genes that encode AKAPs have been identified, this number increases when considering the tendency for AKAP genes to undergo alternative splicing[138]. For example the AKAP9 gene has at least four known splice variants including yotiao, AKAP350, AKAP450, and centrosome- and golgi- localised PKN-associated protein[139]. Some AKAPs are ubiquitously expressed whereas others have niche roles in a specialised cell type, for example AKAP7γ/δ is thought to specifically co-ordinate excitation and contraction coupling in cardiomyocytes[140]. AKAPs bind the D/D on the R subunits of PKA via the hydrophobic face of an amphipathic helix approximately 14-20 residues in length, which can be categorised depending on the PKA isoform they bind, denoted RI-specific, RII-specific or dual-specific accordingly[103]. Most known AKAPs are RII specific or bind RI subunits with significantly less affinity (25-500 fold) *in vitro*[141]. This may explain why PKARII is basally

localised to discrete parts of the cell (i.e. pre-targeted), whereas RI subunits tend to be distributed diffusely in the cell (principally in the cytosol) before being dynamically recruited to discrete sites such as the cap site of activated lymphocytes[142,143]. Many type II specific AKAPs have been identified using blot overlays (or Far Westerns), however this approach to identify RI-binding proteins has been unsuccessful for technical reasons that are unknown but may be specifically characteristic of PKARI/AKAP interaction[144,145]. For example, Herberg *et al.* demonstrate that the dissociation rate constant of PKARIα with Dual-AKAP 1 (DAKAP1) is 100-fold accelerated compared to the RIIα subunit[146].

The differences in AKAP affinity between RI and RII can be accounted for by structural differences between the D/D domain and the amino acids presented on the surface that make contact with the AKAP helix[147]. The AKAP helix lies diagonally in the D/D domain and its importance has been demonstrated with proline mutations that disrupt the conformation and consequently ablate PKA anchoring[148]. The RIIα D/D domain is non-polar, flat and rigid and devoid of any bulky aromatic residues to form a shallow groove that compliments the hydrophobic AKAP helix[147]. In contrast RIα forms a rugged, deep binding groove that is lined with more basic and acidic residues that contact the AKAP helix. For example RIα contains Gln26 in place of Ile17, suggesting that it forms larger more hydrophilic pockets capable of accommodating the larger and polar amino acids but reduces its capacity to bind natural AKAPs (Figure 1.9). Such larger pockets have been exploited to design AKAP-PKARI inhibitor peptides that specifically disrupt RI from AKAPs[147]. Furthermore Ile3 and Ile5 in RIIα exist within a short β-strand prior to the Helix A of the four helix bundle that makes up the D/D and are available to make critical contacts with the AKAP helix to stabilise the interaction. In contrast, RIα contains a small N-terminal helix before the D/D domain which incorporate these residues, thus rendering them unavailable and reducing the affinity between RIα and the AKAP[103,141].

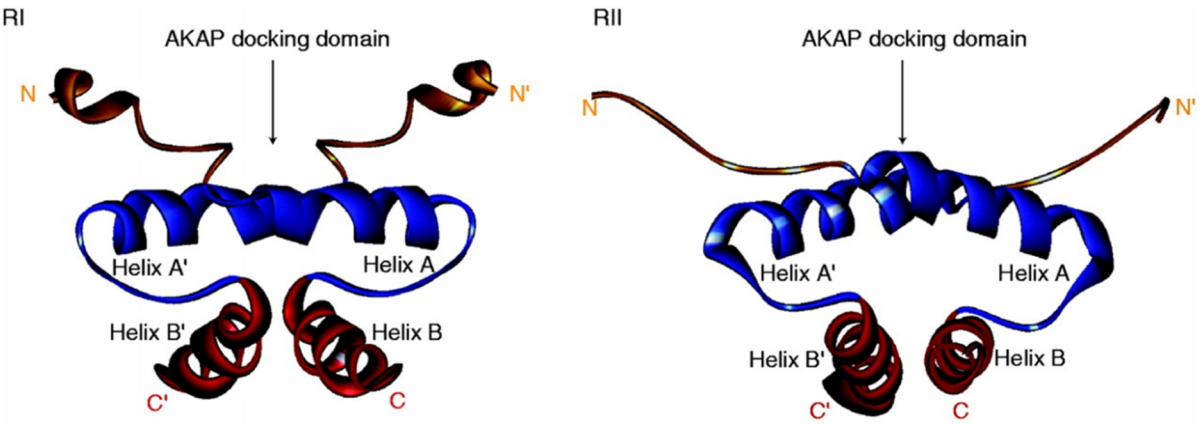

Figure 1.9 Comparison of RIα and RIIα D/D domains. The RIα D/D domain (12–61) forms a deep groove with N-terminal helices which restricts binding AKAP helix binding whilst the RIIα D/D domain (1-44) forms a shallow hydrophobic pocket. *Figure adapted from Pidoux et al. 2010*[128]

AKAPs contain motifs that target them to specific subcellular locations via protein–lipid or protein–protein interaction to facilitate recruitment of PKA to a particular site or to a given organelle[135]. AKAPs have been identified in numerous cellular compartments, including but not limited to the centrosomes, the Golgi apparatus, mitochondria, microtubules, cell and nuclear membranes, and the cytoskeleton[142]. Interestingly different AKAPs can target PKA to the same organelle, indicating that the assembly of signalling complexes with specific substrates even within a subcellular compartment is necessary for appropriate integration of cAMP signals. At least four anchoring proteins (D-AKAP1, D-AKAP2, PAP7, and Rab32) anchor PKA to the mitochondria[128]. Furthermore, splice variants and isoforms of an AKAP may be diversely targeted. The different isoforms of AKAP7 have distinct subcellular localisation in polarized epithelial cells. AKAP7α is located at the lateral membrane whereas AKAP7β isoform is located at the apical membrane, whilst AKAP7γ is predominantly cytoplasmic[149]. Some proteins function as AKAPs although this is not classically considered to be their primary function. For example membrane-bound proteins α4-integrin and ezrin are important for T-cell motility and cell shape respectively, but have recently been found to also function as AKAPs[150-152]. Similarly in Chapter 5 I propose that tubulin, a major component of the microtubules, is a redox-dependent PKARIα AKAP. WAVE1 has previously been identified as PKARIIα-specific AKAP at the actin cytoskeleton and is thought to regulate dorsal ruffle formation but little is known about the role of PKARIα at this subcellular localisation[153].

1.6.2 AKAP functions

AKAPs bind to PKA substrates and effectors of the cAMP signalling pathway such as phosphatases and PDEs. Assembling such enzymes in close proximity allows integration and termination of cAMP signals that govern phosphorylation and dephosphorylation events, thus the amplitude and duration of signal transduction is tightly controlled (Figure 1.10)[128].

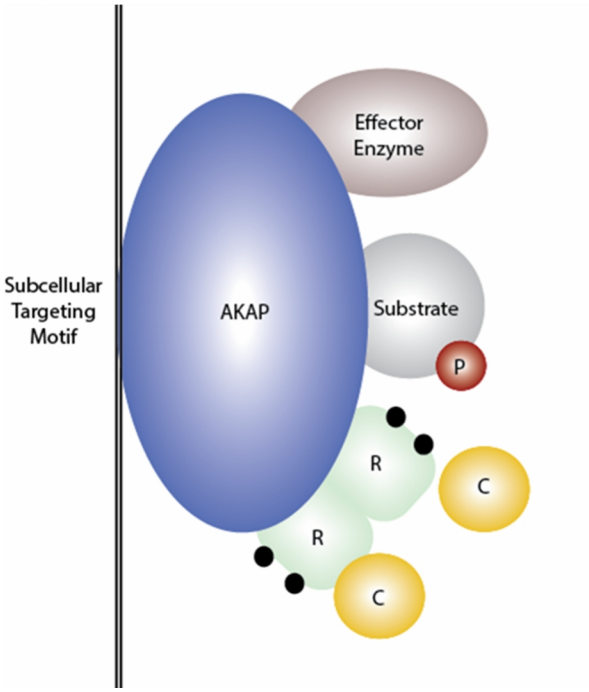

Figure 1.10 AKAPs assemble multienzyme signalling complexes. AKAPs tether PKA, PKA substrates and effectors of the cAMP signalling pathway, such as phosphatases and PDEs, to specific subcellular locations and thus regulate cAMP dependent phosphorylation events.

Disruption of the complexes has deleterious effects on PKA-dependent physiological functions. The Ht31 peptide is a 24 amino acid α-helix derived from the AKAP-Lbc AKB domain that directly competes with PKA to displace it from binding sites[48]. One of the first experiments with Ht31 uncoupled PKA from AMPA type glutamate receptor ion channels in hippocampal neurons leading to dysregulated synaptic transmission, whilst perfusion into pancreatic beta-cells resulted in insulin secretion uncoupling[139]. At least 13 AKAPs have been found in the cardiovascular system[139]. Delivery of Ht31 to cardiomyocytes decreased PKA-dependent phosphorylation of RyR2, PLB, troponin I and myosin binding protein C. As such the peptide attenuated the enhanced contractility normally induced by β adrenergic stimulation reinforcing the functional significance of PKA localisation for cAMP signal transduction[154]. AKAP-Lbc itself is thought to be a mediator of the pathological response associated with angiotensin II type 1 receptor activation, and mitogenic signals through RAF/MEF/ERK1/2 kinase pathway[155]. Knockdown of AKAP-Lbc expression in rat neonatal ventricular cardiomyocytes significantly reduced the ability of angiotensin II to induce RhoA activation and transcription of pro-hypertrophic genes[156]. Furthermore, AKAP-Lbc mRNA is upregulated in patients with cardiac hypertrophy, whilst AKAP-Lbc knockout mice die in utero due to defective heart tube development, highlighting the importance of AKAP scaffolding complexes in the functioning heart[135].

Characterization of these complexes is critical to better understanding the cAMP signalling pathway[157]. PKA-dependent phosphorylation of the KCNQ1 subunit of the slowly activating delayed rectifier potassium channel (I_{Ks}) is necessary for sympathetic regulation of the cardiac action potential[158]. The AKAP yotiao complexes PKARIIα, protein phosphatase 1 (PP1), PDE4D3 and AC to KCNQ1, a component of I_{Ks}. PKA dependent phosphorylation enhances channel open probability whilst PP1 dependent dephosphorylation supresses I_{Ks} currents[139]. The importance of the yotiao in assembling this complex is highlighted by familial mutations in the AKAP, which can lead to the potentially lethal type 1 long QT arrhythmia syndrome. These mutations lead to dysregulation of KCNQ1 phosphorylation, loss of control of the cAMP signal and membrane repolarisation[139]. Certain AKAPs potentially permit the integration of inputs from other second messenger systems such as Ca^{2+} by acting as scaffold for protein kinase C (PKC) and protein kinase D. AKAP79, a product of the AKAP5 gene, tethers PKARIIα, PKC and protein phosphatase 2B (PP2B) to integrate cAMP and Ca^{2+} signals and as such has been implicated in persistent Ca^{2+} signals (sparklets) that increase vascular tone[159]. In ventricular cardiomyocytes AKAP79 has been demonstrated to form a supramolecular complex containing a β-adrenergic receptor, AC5/6, RIIα and PP2B tethered to a caveolin 3-associated complex containing L-type calcium channel[160]. Thus AKAPs act as signalling nodes that are able to integrate signals from multiple

inputs. A primary aim of the present study is to determine whether AKAPs and PKARIα can integrate concomitant cAMP and oxidant signals.

Using a cAMP affinity-based chemical proteomics strategy a novel AKAP in the human heart has recently been uncovered termed small membrane smAKAP. It is specifically localised at the plasma membrane via potential myristoylation/palmitoylation anchors. *in vitro* binding assays revealed that smAKAP has an approximate 8 fold nM specificity for PKARIα over PKA-RII making it a dual-specific AKAP, but as yet the PKARIα substrate associated with this complex is unknown[116]. In contrast, sphingosine kinase interacting protein (SKIP) has been described as the first truly RI-specific mammalian AKAP. Interestingly it contains two AKB sites and is therefore able to sequester two molecules PKARI of to the inner mitochondrial membrane where it associates with the PKA substrate ChChd3, a coiled-coil helix protein[161].

DAKAP1 is a regulator of mitochondrial dynamics identified in a wide range of tissues including heart, liver, kidney, skeletal muscle and brain, and is so-named “dual” because it binds to both type I and type II PKA. The N-terminal mitochondrial targeting sequence localises the protein to the outer mitochondrial membrane where it has been reported to bind to several proteins including various isoforms of PP1, RSK1, PDE4 and calcineurin[162]. The best characterised effector associated with DAKAP1 is the PKA target dynamin-related protein 1 (Drp1). Drp1 is a large GTPase that oligomerises to physically constrict mitochondria and induce fission. PKA phosphorylates Ser637 resulting in Drp1 inhibition[163]. DAKAP1 promotes PKA-dependent phosphorylation of Ser637 whilst the calcium-dependent phosphatase calcineurin dephosphorylates Ser637, to relieve Drp1 inhibition[163]. In hippocampal neurons, DAKAP1 knockdown induces mitochondrial fragmentation and apoptosis presumably due to inefficient targeting of PKA to Drp1. Conversely, over-expression of DAKAP1 and consequent Ser637 phosphorylation of Drp1 are neuroprotective, promoting mitochondrial elongation. Expression of mutant DAKAP1 that cannot bind to PKA is ineffective at promoting neuronal survival, indicating that appropriate PKA targeting to the mitochondrial membrane is essential for mitochondrial integrity and neuronal survival[163,164].

Genetic polymorphisms and AKAP knockout mice that exhibit symptoms similar to human diseases reinforce that dysfunction of these scaffold proteins and inappropriate PKA targeting can result in cardiovascular pathologies (Table 1.2). Thus appropriate targeting of PKA to specific subcellular compartments to respond to cAMP signals is critical for regulation of many physiological functions.

AKAP	Modification/Intervention	Disease outcome
DAKAP2	Genetic polymorphism Ile646Val	Increased basal heart rate, reduced heart rate variability[165]
AKAP-Lbc	Down-regulation by shRNA	α1-adrenergic receptor-induced cardiac hypertrophy[156]
	Knockout mice	Defective cardiac development, death by cardiac arrest[166]
mAKAP	Down-regulation by shRNA	Cytokine-and GPCR-induced cardiac hypertrophy[167]
Yotiao	Genetic polymorphism Ser1570Lys	Long Q-T syndrome, cardiac arrhythmias[168]

Table 1.2 Dysfunction or deletion of AKAPs in humans or animal models leads to cardiac pathologies

1.7 PKARIα as an integrator of cAMP and oxidant signals

As previously mentioned the primary focus of this thesis is the redox sensitive RIα isoform of PKA. PKARIα was first identified as susceptible to disulfide dimer formation in response to oxidants via diagonal gel electrophoresis followed by proteomic analysis[169,170]. Conventional lysate preparation means proteins can be artificially oxidised by oxygen in the air, explaining why RIα homodimers were previously considered to exist constitutively as a disulfide dimer. However these disulfide bonds between the two RIα subunits were in fact inducible in response to exogenously applied H_2O_2[170]. Preparation of the lysates in the presence of an alkylating agent such as maleimide prevented artificial air oxidation, enabling the authors to conclude that the disulfide bonds were inducible. Treatment with the NO donor CysNO has also been shown to induce PKARIα disulfide dimer via a transient S-nitrosation intermediate[85]. Remarkably stimulating cardiomyocytes with H_2O_2 caused simultaneous phosphorylation of known PKA substrates without elevating cAMP implying that PKA disulfide dimer formation was a novel mechanism of kinase activation[170]. It remained unclear if the disulfide bonds directly activated the kinase as is the case with PKGIα. Furthermore the PKA inhibitor H89 did not completely attenuate the oxidant-dependent phosphorylation of PKA substrates. Therefore further work, as presented here, is required to understand the mechanism of oxidant-dependent PKARIα activation.

Endogenous mediators of oxidant production have been demonstrated to induce PKARIα disulfide formation and consequent PKA substrate phosphorylation. Members of this laboratory have demonstrated that very high (0.1-1 mM) concentrations of monoamines such as NA and 5-HT are capable of inducing PKARIα oxidation through the oxidative deamination activity of MAO[171]. PDGF-BB induced PKARIα disulfide dimer and concomitant phosphorylation of vasodilator-stimulated phosphoprotein (VASP) that was abrogated when rat glomerular mesangial cells were pre-treated with the antioxidant diphenylene iodonium[172]. The authors proposed the increased intracellular oxidants were NOX1 dependent[172]. Furthermore Beck *et al.* induced PKARIα disulfide formation and consequent increase in VASP phosphorylation with a cytokine mix of TNFα and IL-1β in rat mesangial cells[173]. The authors speculate that this may be due to increased expression of iNOS and consequent $OONO^-$ formation rather than growth factor-mediated oxidation[173]. Interestingly, the concentration of cAMP was not elevated in either study highlighting a role for oxidant-dependant PKARIα activation.

A principal aim of this thesis is to determine how formation of disulfide bonds in PKARIα can result in increased substrate phosphorylation. I hypothesise that the interaction between PKARIα and AKAPs is critical for redox-dependent substrate phosphorylation. The crystal structure of the bovine PKARIα D/D domain shows the alignment of Cys16 with Cys37 on adjacent RIα subunits (17 and 38 respectively in human and mouse), creating the possibility of two disulfide bonds existing simultaneously under conditions of oxidative stress (Figure 1.11)[103]. The PKARIα disulfide bonds directly flank the D/D domain and due to their proximity to the AKAP α-helix, it is reasonable to suggest that the presence or absence of these bonds may regulate the affinity for which PKARIα binds to AKAPs. This is based on structural data produced by Sarma *et al.,* who systematically mutated PKARIα Cys-16 and Cys-37 to alanine residues to prevent disulfide bond formation[103]. The authors observed a 3-fold and 16-fold decrease in nanomolar affinity to DAKAP2 respectively compared to wild-type PKARIα. They reported that disulfide bond formation decreases the flexibility of the overall structure of the molecule, enabling the assembly of binding pockets for the AKB, whilst simultaneously bringing critical residues into close contact with the AKAP to improve binding (Figure 1.12). Thus the observation that oxidants increase phosphorylation of specific PKA substrates can potentially be explained by increased affinity to its associated AKAP. Investigating the potential oxidant-dependent PKARIα-AKAP interaction is justified given their importance in governing physiological responses. Furthermore oxidant-dependent interactions between PKARIα and AKAPs would create a new paradigm, whereby PKARIα integrates cAMP and oxidant signals to fine tune substrate phosphorylation and downstream functions (Figure 1.13).

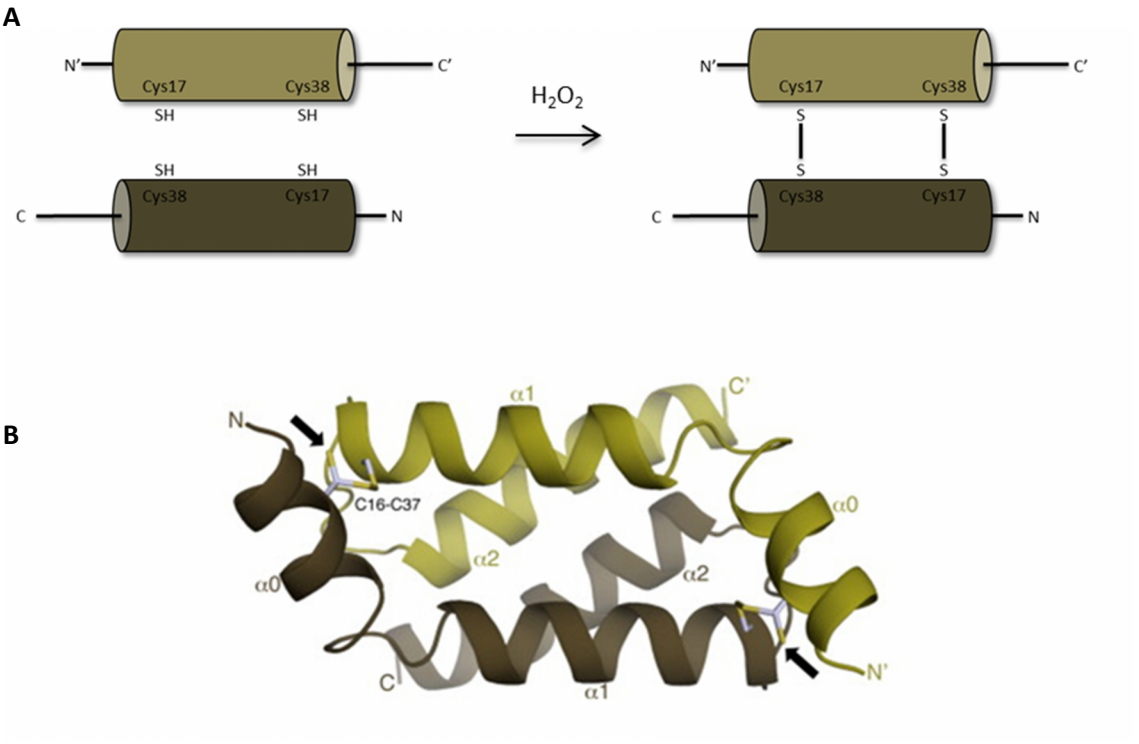

Figure 1.11 PKARIα forms inducible disulfide dimer. (**A**) Schematic of the PKARIα D/D domain. Cys17 and Cys38 face each other on opposing RIα subunits. Interprotein disulfide bond formation is inducible in the presence of an oxidant such as H_2O_2. (**B**) Crystal structure of RIα D/D (gold and grey). Ball and stick model of disulfide bonds formed between Cys16 and Cys37 (bovine residues) on opposing RIα subunits are indicated with black arrows. *Figure adapted from Sarma et al. 2010*[103]

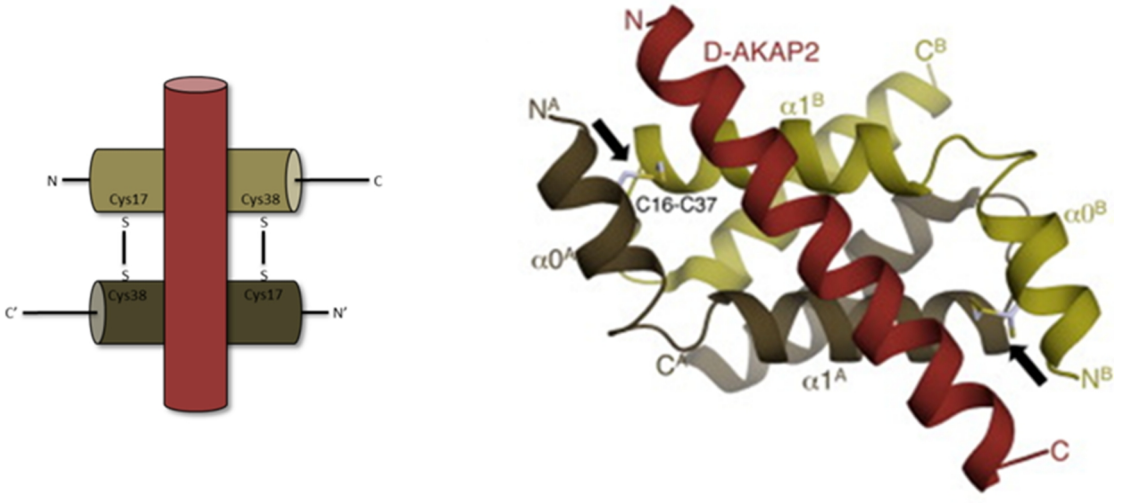

Figure 1.12 PKARIα disulfide bonds directly flank the AKAP helix. Cartoon and crystal structure of the RIα D/D domain (grey and gold) bound to DAKAP2 helix (red). Mutation of the Cys16-Cys37 disulfide bonds of RIα that directly flank the AKAP helix have been shown to decrease RIα and DAKAP2 affinity. *Figure adapted from Sarma et al. 2010*[103]

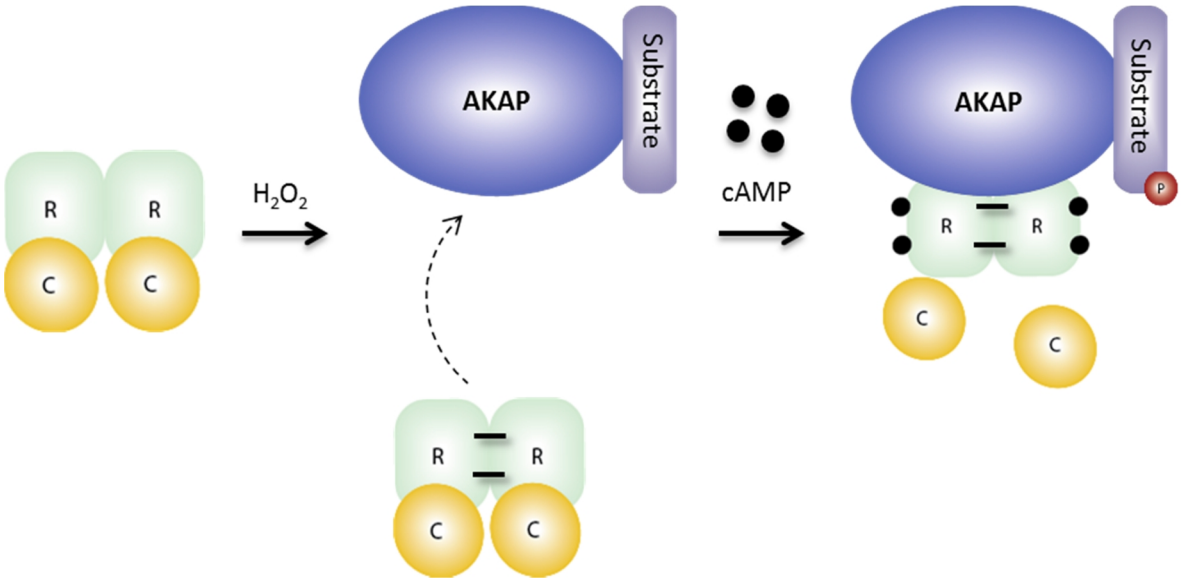

Figure 1.13 Increased PKARIα disulfide dimer affinity for AKAP may lead to elevated substrate phosphorylation.

1.8 Aims of the thesis

The primary effector of cAMP, PKA, is an enzyme involved in a wide variety of cellular processes within the cardiovascular system. The PKARIα isoenzyme forms a disulfide dimer in response to oxidants but the physiological consequences of this 'redox switch' are unknown. I hypothesise that the disulfide dimer increases affinity for AKAPs which consequently leads to enhanced phosphorylation of any associated substrates. This thesis is an attempt to ascertain the biochemical and functional effects of concomitant cAMP and oxidant signals on PKARIα disulfide and activity.

The following will be investigated:

- To determine whether cAMP can promote or inhibit PKARIα disulfide bond formation
- To determine whether PKARIα can synergise cAMP and oxidant signals to enhance substrate phosphorylation
- To determine whether PKARIα disulfide dimer has increased affinity for AKAPs
- To identify potential substrates in AKAP complexes that are differentially phosphorylated by PKARIα disulfide dimer, and subsequently investigate the functional effects of this interaction

Chapter 3 documents that co-treatment of HEK 293 cells with cAMP and H_2O_2 leads to enhanced PKA substrate phosphorylation compared to cAMP or H_2O_2 alone, hypothetically due to enhanced PKARIα interaction with AKAPs. Chapter 4 describes the development and optimisation of the PEG-maleimide switch assay, a novel method that can be used to determine if a candidate protein is susceptible to reversible oxidative modifications. Chapter 4 also attempts to interrogate whether PKARIα disulfide dimer has enhanced affinity for AKAPs using cAMP tethered to agarose beads as bait. Whilst this method yielded inconclusive results, it led to the unexpected observation that cAMP can induce the reduction of PKARIα. Chapter 5 explores this observation of cAMP-mediated reduction of disulfide PKARIα further, which led to the identification of tubulin as a redox sensitive AKAP. Tubulin forms a transient disulfide with PKARIα in the presence of oxidants that enhances the interaction between the two proteins. Chapter 6 investigates the consequences of this redox-dependent PKARIα-tubulin interaction and identifies the microtubule associated protein, Rho guanine nucleotide exchange factor (GEF-H1), as a PKARIα substrate. Interestingly, H_2O_2 potentiates GEF-H1 phosphorylation in a PKARIα disulfide dimer dependent manner, which may have physiological implications is pathologies such as sepsis. Thus PKARIα is a co-incidence detector that is capable of integrating concomitant cAMP and oxidant signals to fine-tune phosphorylation events.

2 General Methods

2.1 Materials

All materials used throughout this thesis were purchased from Sigma-Aldrich (St. Louis, MO) unless otherwise stated.

2.2 Molecular Biology

2.2.1 Polymerase chain reaction

DNA fragments were amplified with Phusion® High-Fidelity DNA polymerase (New England Biolabs) according to standard protocols[174]. Agarose gel (1% agarose in tris acetate ethylenediaminetetraacetic acid (TAE) buffer) electrophoresis was conducted accordingly. 0.01 % of GelRed Nucleic Acid Gel Stain (Biotium) was added to allow visualisation of DNA. 15 µl of PCR products were loaded and run until the samples had run to the bottom of the gel, DNA fragments were subsequently visualised using UV light, excised and extracted with the gel extraction kit (Qiagen) according to the manufacturer's protocol.

2.2.2 Bacterial transformations

For cloning and plasmid amplification transformation of *E.coli* DH5-α (Invitrogen) was conducted according to standard protocols[174]. Briefly, DH5-α cells were allowed to thaw on ice and incubated for 30 min with 1-10 µg of the appropriate DNA plasmid. Cells were subsequently subjected to heat shock for 45 seconds at 42°C and incubated on ice for a further 2 min. Cells were then diluted in 10x S.O.C medium (2% tryptone, 0.5% yeast extract, 10 mM NaCl, 2.5 mM KCl, 10 mM $MgCl_2$, 10 mM $MgSO_4$, and 20 mM glucose) (Invitrogen) and incubated on a shaker for 1 hour at 37°C. Cells were then spread on agar plates (prepared with 50-100 µg of the appropriate antibiotic from a x1000 stock) and incubated overnight at 37°C. The next day, one colony was scraped using a sterile pipette tip, added to 5 ml of *E.coli* LB broth (with the appropriate antibiotic) and incubated overnight at 37°C ready for plasmid purification by mini-preparation (Qiagen) according to the manufacturer's protocols. For maxi-preparation (Qiagen), 5 ml culture was added to 250 ml LB broth (with the appropriate antibiotic) and incubated overnight before using the plasmid purification kit. The sequences of purified plasmids were verified by the sequencing service at Eurofins MWG Operon (Ebersberg).

2.3 Cell culture

The high sequence identity of PKARIα across species meant experiments concerning disulfide formation or reversal could be investigated in numerous cell types without expectation that the species type would influence the outcome (Table 2.1). Myocytes, aortic vascular smooth muscle cells and endothelial cells are all relevant cell types to study in the context of cardiovascular physiology. HEK 293 cells are a useful to study protein-protein interactions due to the ease of which they can be transfected. In experiments where cells were treated, treatments were for conducted for 10 min unless otherwise stated.

```
Human       mesgstaaseearslrecelyvqkhniqallkdsivqlctarperpmaflreyferleke
Bovine      mesgstaaseearslrecelyvqkhniqallkdsivqlctarperpmaflreyferleke
Rat         masgsmaaseeerslrecelyvqkhniqallkdsivqlctarperpmaflreyferleke
Mouse       masgsmatseeerslrecelyvqkhniqallkdsivqlcttrperpmaflreyferleke
            * *** *:*** ****************************:******************

Human       eakqiqnlqkagtrtdsredeisppppnpvvkgrrrrgaisaevyteedaasyvrkvipk
Bovine      eakqiqnlqkagtrtdsredeisppppnpvvkgrrrrgaisaevyteedaasyvrkvipk
Rat         earqiqslqksgirtdsredeisppppnpvvkgrrrrgaisaevyteedaasyvrkvipk
Mouse       earqiqclqktgirtdsredeisppppnpvvkgrrrrgaisaevyteedaasyvrkvipk
            **:*** ***:* ************************************************

Human       dyktmaalakaieknvlfshlddnersdifdamfsvsfiagetviqqgdegdnfyvidqg
Bovine      dyktmaalakaieknvlfshlddnersdifdamfsvsfiagetviqqgdegdnfyvidqg
Rat         dyktmaalakaieknvlfshlddnersdifdamfpvsfiagetviqqgdegdnfyvidqg
Mouse       dyktmaalakaieknvlfshlddnersdifdamfpvsfiagetviqqgdegdnfyvidqg
            ********************************* ************************

Human       etdvyvnnewatsvgeggsfgelaliygtpraatvkaktnvklwgidrdsyrrilmgstl
Bovine      etdvyvnnewatsvgeggsfgelaliygtpraatvkaktnvklwgidrdsyrrilmgstl
Rat         emdvyvnnewatsvgeggsfgelaliygtpraatvkaktnvklwgidrdsyrrilmgstl
Mouse       emdvyvnnewatsvgeggsfgelaliygtpraatvkaktnvklwgidrdsyrrilmgstl
            * ************************************************************

Human       rkrkmyeeflskvsilesldkwerltvadalepvqfedgqkivvqgepgdeffiilegsa
Bovine      rkrkmyeeflskvsilesldkwerltvadalepvqfedgqkivvqgepgdeffiilegsa
Rat         rkrkmyeeflskvsilesldkwerltvadalepvqfedgqkivvqgepgdeffiilegta
Mouse       rkrkmyeeflskvsilesldkwerltvadalepvqfedgqkivvqgepgdeffiilegta
            ************************************************************:*

Human       avlqrrseneefvevgrlgpsdyfgeiallmnrpraatvvargplkcvkldrprfervlg
Bovine      avlqrrseneefvevgrlgpsdyfgeiallmnrpraatvvargplkcvkldrprfervlg
Rat         avlqrrseneefvevgrlgpsdyfgeiallmnrpraatvvargplkcvkldrprfervlg
Mouse       avlqrrseneefvevgrlgpsdyfgeiallmnrpraatvvargplkcvkldrprfervlg
            ************************************************************

Human       pcsdilkrniqqynsfvslsv
Bovine      pcsdilkrniqqynsfvslsv
Rat         pcsdilkrniqqynsfvslsv
Mouse       pcsdilkrniqqynsfvslsv
            ********************
```

Table 2.1 Sequence alignment of PKARIα in species used throughout this thesis (cysteines of interest highlighted in red).

2.3.1 Cardiomyocytes

Adult rat ventricular myocytes (ARVM) were isolated from male Wistar rats (250–300 g, Charles River) by collagenase-based enzymatic digestion and was performed by Dr. Shiney Reji

as previously described[175]. After isolation, cardiomyocytes were washed at room temperature with serum-free M199 culture medium (#31150, Invitrogen) modified with 2 mM creatine, 2 mM carnitine and 5 mM taurine and 1% (vol/vol) penicillin/streptomycin (P/S) before plating. 6 well plates were pre-coated with laminin (Sigma) for 2 hours prior to the plating. Once plated cardiomyocytes were then allowed to adhere for 90 min in an incubator (37 °C, 95% air/5% CO_2). At this point, the culture medium was replaced with fresh serum-free modified M199 medium and incubated overnight. The following day cells were treated and harvested in non-reducing SDS-PAGE sample buffer containing 100 mM maleimide.

2.3.2 Vascular smooth muscle cells

Vascular smooth muscle cells (VSMCs) were isolated from the aorta of 8-10 week old mice by dissection from connective tissue and collagenase-based enzymatic digestion. Cells were washed at room temperature with Gibco® DMEM (#31966-047, Invitrogen) and 10% vol/vol foetal calf serum (Invitrogen) and stored in liquid nitrogen until ready for use. In preparation for experimental interventions cells were thawed and maintained in Gibco® DMEM supplemented with 10% vol/vol foetal calf serine and 1% vol/vol P/S. Cells were subsequently seeded onto 12-well plates to ~80% confluency and incubated overnight. The following day cells were treated and subsequently harvested directly into SDS-PAGE sample buffer containing 100 mM maleimide. Cells were used between passage 3-7.

2.3.3 Human embryonic kidney 293 cell culture and transfections

Human embryonic kidney 293 cells (HEK 293) obtained from American Type Culture Collection, (Manassas, VA, USA) were maintained in Gibco® DMEM (#31966-047, Invitrogen) supplemented with 10% vol/vol foetal calf serum and 1% vol/vol P/S. In preparation for experimental interventions HEK 293 were seeded onto 12-well plates or T75 flasks. The following day DNA was transfected into cells that were ~80% confluent using Lipofectamine® 2000 (Invitrogen) according to the manufacturer's protocol. Cells were treated and harvested between 24-72 hours depending on the experiment. Cells were used between passage 3-20.

2.3.4 Bovine aortic endothelial cells

Bovine aortic endothelial cells (BAECs) (Cell Applications, B304K-05) were maintained in Gibco® DMEM supplemented with 10% (vol/vol) foetal calf serum and 1% (vol/vol) P/S. For experimental treatments, BAECs were grown until 80% confluent before being starved overnight in DMEM containing 1% (vol/vol) P/S without FBS. The following day cells were treated and subsequently harvested directly into SDS-PAGE sample buffer containing 100 mM maleimide. Cells were used between passage 3-10.

2.3.5 Serum starvation

Unless indicated, all cells were cultured and treated in full media. In some indicated experiments cells were serum starved. For this, cell culture was replaced with the equivalent media that was free of serum, 24 hours prior to treatment.

2.4 Langendorff perfusion

Langendorff perfusions throughout this thesis were performed by various members of the Eaton lab, and are described in full here[176]. Briefly, hearts were excised from anesthetised rats, cannulated and perfused with Krebs buffer (118 mmol/L NaCl, 4.75 mmol/L KCl, 1.18 mmol/L KH_2PO_4, 25 mmol/L $NaHCO_3$, 1.19 mmol/L $MgSO_4$ and 11 mmol/L glucose) under constant pressure. Each heart was aerobically perfused for 20 min before treatment. Hearts were then perfused for an additional 10 min with Krebs buffer alone (control) or H_2O_2. Hearts were snap frozen in liquid nitrogen and homogenised in 100 mM Tris pH 7.4 and protease inhibitor cocktail (Roche) to make a 10% weight to volume homogenate.

2.5 SDS-polyacrylamide electrophoresis and immunoblotting

Sodium dodecyl sulphate polyacrylamide gel electrophoresis (SDS-PAGE) was performed using BioRad Protean system. 5-15 µl of sample was loaded into the wells of each gel which were made according to Table 2.2.

	Resolving					**Stacking**
	8%	**10%**	**12%**	**12.5%**	**15%**	**-**
1M Tris-HCl pH8.8 (ml)	3.8	3.8	3.8	3.8	3.8	-
Water (ml)	3.3	2.7	2.04	1.85	1	2.8
Acrylamide solution (ml)	2.7	3.3	3.96	4.15	5	0.6
10% SDS (µl)	100	100	100	100	100	40
TEMED (µl)	10	10	10	10	10	7
10% APS (µl)	90	90	90	90	90	75
1M Tris-HCl pH6.8 (ml)	-	-	-	-	-	0.48

Table 2.2 Composition of different percentage gels used throughout this thesis

Proteins were separated by one-dimensional SDS-PAGE and then transferred onto polyvinylidene fluoride (PVDF) membranes (GE Healthcare, UK) using a semi-dry transfer blotter. All gels were run under non-reducing conditions unless otherwise stated. Blocking of PVDF membranes were performed using PBS-Tween-20 containing 10% (wt/vol) non-fat milk (Premier International Foods, UK) powder. The membranes were incubated with agitation for 3 hours at room temperature or overnight at 4 °C with a primary antibody diluted in PBS-

Tween-20 containing 2% (wt/vol) non-fat milk. Membranes were subsequently washed for 1 hour, changing the PBS-Tween buffer regularly and then incubated with a HRP-conjugated secondary antibody for 1 hour at room temperature (Table 2.3). After washing the membrane with PBS-Tween, changing the buffer regularly, the membrane was subjected to chemiluminescence detection according to the manufacturers protocol (ECL, Thermo Scientific Pierce, Illinois, US) and blots were developed onto autoradiographic film (GE healthcare, UK) using a film developer (Fuji, JPN). Digitised immunoblots were quantitatively analysed using Gel-Pro Analyzer 3.1.

Antibody	Company	Dilution
Anti-mouse IgG HRP	Cell Signaling	1:1000
Anti-goat IgG HRP	Dako	1:1000
Anti-rabbit IgG HRP	Cell Signaling	1:1000

Table 2.3 Secondary antibodies used in throughout this thesis

2.5.1 Immunoblot controls

It was established that acute treatment of cells (10 min) with an agent that elevates cAMP, H_2O_2, or co-treatment with both, did not cause any cell/protein loss as determined by a marker protein. Figure 2.1 is a representative immunoblot from HEK 293 cells that demonstrates this, with anti-tubulin being used to detect the marker protein. Furthermore, immunoblots that were probed with PKARIα do not necessarily require loading controls, as they are quantified as percentage of dimer relative to the total amount of PKARIα in the sample, thus in this sense, PKARIα acts as its own control. As such it was not always necessary to run a loading control. Loading controls were run as standard for all experiments conducted with animals due to the increased chance of variability from organ harvest and processing.

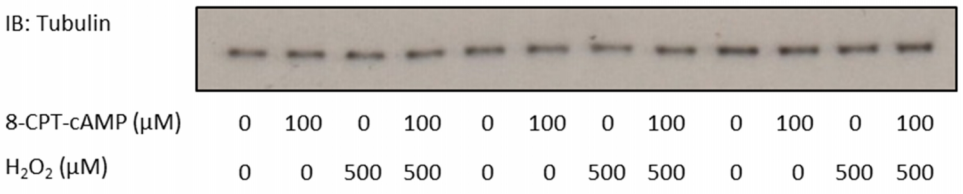

Figure 2.1 Representative tubulin immunoblot demonstrating equal sample loading in HEK 293 cells. 8-CPT-cAMP and H_2O_2 for 10 minutes were standard treatments used throughout the thesis. Tubulin is a standard protein used as a loading control and remains unchanged indicating no cell/protein loss and equal loading of gels.

2.6 Immunofluorescence

HEK 293 cells or VSMCs were fixed with 4 % paraformaldehyde in PBS for 10 min at room temperature, washed in PBS and permeabilised with 0.2% Triton X-100 in PBS for 5 min . To avoid non-specific antibody binding the cells were incubated with blocking buffer (5% non-specific goat serum diluted in 1 % bovine serum albumin, Tris-base 20 mmol/L, NaCl 155 mmol/L, EGTA 2 mmol/L, MgCl2 2 mmol/L, pH 7.5) for 1 hour at room temperature. Cells were incubated in primary antibodies diluted (1:100) in blocking buffer overnight at 4 °C and washed with PBS the next day. Cy3-conjugated anti-rabbit (Jackson ImmunoResearch) and Cy5-conjugated anti-mouse (Jackson ImmunoResearch) secondary antibodies were used in a 1:100 dilution for 1 hour at room temperature. Diamidine-2-phenylindole dihydrochloride (D8417, Sigma) was added with the secondary antibodies to stain the nucleus. Slides were viewed using a laser scanning confocal microscope (Zeiss LSM510).

2.7 Animals

Animals received humane care in compliance with the Principles of Laboratory Animal Care formulated by the National Society for Medical Research and the Guide for the Care and Use of Laboratory Animals prepared by the National Academy of Sciences and published by the National Institutes of Health.

2.8 Statistical Analysis

Quantitative data are presented as mean ± standard error of the mean (SEM). In cell experiments, n= replicate measurements in n different cultures. Statistical analysis was conducted with Students' *t*-tests, one-way or two-way analysis of variance (ANOVA), followed by *post hoc* Tukey corrections where applicable. Statistical analysis was carried out using GraphPad Prism (GraphPad Software, Inc). *p*-values of <0.05 were considered significant.

3 Assessing the effect of concomitant cAMP and H_2O_2 signals on PKARIα disulfide and PKA phosphorylation events

3.1 Introduction

3.1.1 Compartmentalised cAMP signalling

How can a cell produce a specific response when a single molecule is responsible for transducing multiple input signals? This question, which is especially pertinent to cAMP signalling, is important to address. Numerous factors contribute to the localisation and duration of a cAMP signal, for example, the isoform of adenylate cyclase and the type of GPCR can be constrained to distinct locations within the plasma membrane and determine precisely where the cAMP is generated[177]. Historically it was confounding that prostaglandins could activate $G_{\alpha s}$-coupled EP_2 and EP_4 receptors to elevate intracellular cAMP levels but did not produce the same functional effects as β-adrenoceptor activation. Heyes *et al.* first demonstrated that both isoprenaline and prostaglandin E1 (PGE_1) were capable of increasing cAMP content in mammalian hearts to similar levels but only isoprenaline activated glycogen phosphorylase and enhanced ventricular pressure development[178]. Furthermore PGE_1 appeared to activate PKA in the soluble fraction of hearts but not in the particulate fraction, whilst isoprenaline induced cAMP elevation primarily in the particulate. This evidence lead to the postulation of "hormonally specific compartmentation of cyclic AMP and cAMP-dependent protein kinase"[179].

The physiochemical properties of cAMP mean that it is free to rapidly diffuse throughout the aqueous cellular environment[102]. This would ostensibly contradict any perceived notion of compartmentalised cAMP signalling. Föster resonance energy transfer (FRET), a phenomenon whereby the excited state energy of a donor fluorophore is transferred to a nearby acceptor fluorophore, which then emits its own characteristic fluorescence, has been utilised to visually detect changes in subcellular cAMP concentrations in real time[180]. These FRET probes are constructed from cyclic nucleotide binding domains and upon cAMP binding the transfer of energy significantly increased, providing biosensors that allow cAMP compartmentalisation to be monitored[181,182]. Such probes have confirmed that upon hormonal stimulation cAMP is elevated in discrete microdomains within the cell rather than increasing globally[182,183].

Inhibition of PDEs abolishes these microdomains leading to 'leakage' of cAMP across subcellular compartments. Thus PDEs ensure compartmentalisation of cAMP and prevents its unabated cell-wide diffusion[184,185]. Isoform-specific PDE inhibitors demonstrated that PDE3 or PDE4 are responsible for degrading β-adrenergic-derived cAMP signals whilst PDE4 subtypes B and D are responsible for degrading those triggered by PGE_1[181,185]. This suggests that the cell is organised to convey precise messages and cAMP is generated and terminated in distinct subcellular locations, by specific mediators, to ensure explicit control of the hormonal input. The formation of these cAMP microdomains has been attributed to AKAPs that bind to PDEs and assemble the signalling complexes. As such, AKAPs co-ordinate and regulate the location and duration of the cAMP signal and consequently the extent of PKA substrate phosphorylation[186].

3.1.2 PGE_1 elevates cAMP in type I PKA domains

Activation of different GPCRs leads to elevation of cAMP in specific subcellular microdomains[181]. Furthermore, all four PKA isozymes expressed in cardiomyocytes demonstrate distinct subcellular localisation. Type I PKA, which this thesis focuses on, is associated with the cytosol whereas Type II PKA is purified in the particulate fraction of cell lysates[187]. Differential cAMP production in these locations where the expression of the PKA isozymes differs provides a further level of regulation to cAMP signalling. FRET sensors linked to the AKAP binding regions of RI and RII have been used to monitor cAMP concentration in their respective specific subcellular regions after myocytes were challenged with a GPCR agonist. The RI sensor, but not the RII sensor, detected an elevation in cAMP after cells were challenged with PGE_1. In contrast, isoprenaline caused an elevation in cAMP that was selectively detected by the RII-based sensor. The authors conclude that PGE_1 predominately activates type I PKA[188]. This suggests I may be able to use the propensity for PGE_1 to elevate cAMP in RI domains to identify potential PKARIα-specific substrates.

3.1.3 Substrate-induced dissociation of PKARIα

Central to this thesis is investigating how formation of PKARIα disulfide bonds results in increased phosphorylation of the kinases substrates? As highlighted in Chapter 1.7, I hypothesise that the interaction between PKARIα and AKAPs is necessary for its redox-dependent substrate phosphorylation. Cys16Ala mutation of PKARIα decreased its affinity for DAKAP2[103] and due to the proximity of the disulfide bonds to the D/D domain, it is reasonable to suggest that the presence these bonds may increase the affinity between PKARIα and AKAPs, and lead to enhanced substrate phosphorylation (Figure 1.10 and 1.11).

Our understanding that cAMP leads to the physical dissociation of the catalytic subunits is supported by *in vitro* ion exchange chromatography, gel filtration and ultracentrifugation experiments that demonstrated high concentrations of cAMP were necessary to induce dissociation from the regulatory subunits[189]. However these methods exert artificial forces upon the molecules that are not present in cells. As such there is also contradictory evidence to suggest that PKA can remain associated even in the presence of high cAMP concentrations[189-191]. Kopperud *et al.* acutely observed that addition of substrate could destabilise the type I holoenzyme[192]. Small angle x-ray scattering revealed PKA type I, but not type II, was sensitised to cAMP by the presence of PKA substrate. They found a higher concentration of PKARIα was necessary to inhibit kinase activity at a given cAMP concentration if substrate was present[189,193]. In other words, cAMP induces partial dissociation of the holoenzyme whilst cAMP and substrate together leads to full dissociation of PKARIα but not PKARII (Figure 3.1).

This substrate-induced dissociation may be a physiological means to enhance substrate phosphorylation at a given concentration of cAMP. It is particularly interesting given that the phenomenon is restricted to PKARIα, the only PKA isoform that forms disulfide bonds. Taken together, the hypothesised increase in affinity between PKARIα disulfide dimer and AKAPs could be a means to localise PKARIα to its substrates within an assembled complex and consequently undergo substrate-induced dissociation to enhance phosphorylation.

3.1.4 cAMP-dependent modulation of PKARIα disulfide dimer

As previously mentioned our laboratory also identified PKG, another AGC kinase, as being modified by oxidants to form a disulfide bond dimer. Interestingly binding of PKGIα to cGMP, its associated nucleotide, precludes its ability to form a disulfide dimer[194]. Although there is no complete crystal structure available for PKGIα, cGMP blockade of the interprotein disulfide is likely due to the conformational change induced by nucleotide binding that increases the distance between the two cysteines involved in disulfide formation[194]. Whether cAMP can also prevent PKARIα disulfide bond formation is still uncertain, but if so, this would likely regulate PKARIα mediated oxidant-dependent substrate phosphorylation. In fact, agents capable of simultaneously elevating intracellular cAMP and also inducing disulfide dimer formation would be interesting in the context of PKARIα oxidant activation. Monoamines, including noradrenaline and serotonin, are capable of increasing cAMP concentration via β-adrenoceptor and serotonin receptor agonism respectively. In addition, members of this laboratory demonstrated that these monoamines, albeit at millimolar concentrations, are capable of inducing PKARIα oxidation through the oxidative deamination activity of MAO

which generates H_2O_2. Furthermore pharmacological inhibition of MAO ablated the increase in PKARIα disulfide dimer formation[171]. PKARIα potentially represents a point of convergence between oxidant and cAMP signals and may be able to conflate them to dictate specific phosphorylation events.

The primary aim of this chapter was to characterise the effects of cAMP on oxidant-induced PKARIα disulfide dimer formation. A key finding is that cAMP and oxidants act synergistically to enhance PKA substrate phosphorylation. I also present evidence that cAMP can modulate PKARIα expression, providing another mechanism, in addition to alterations to redox state, by which the amount of disulfide kinase may be modulated by the cell.

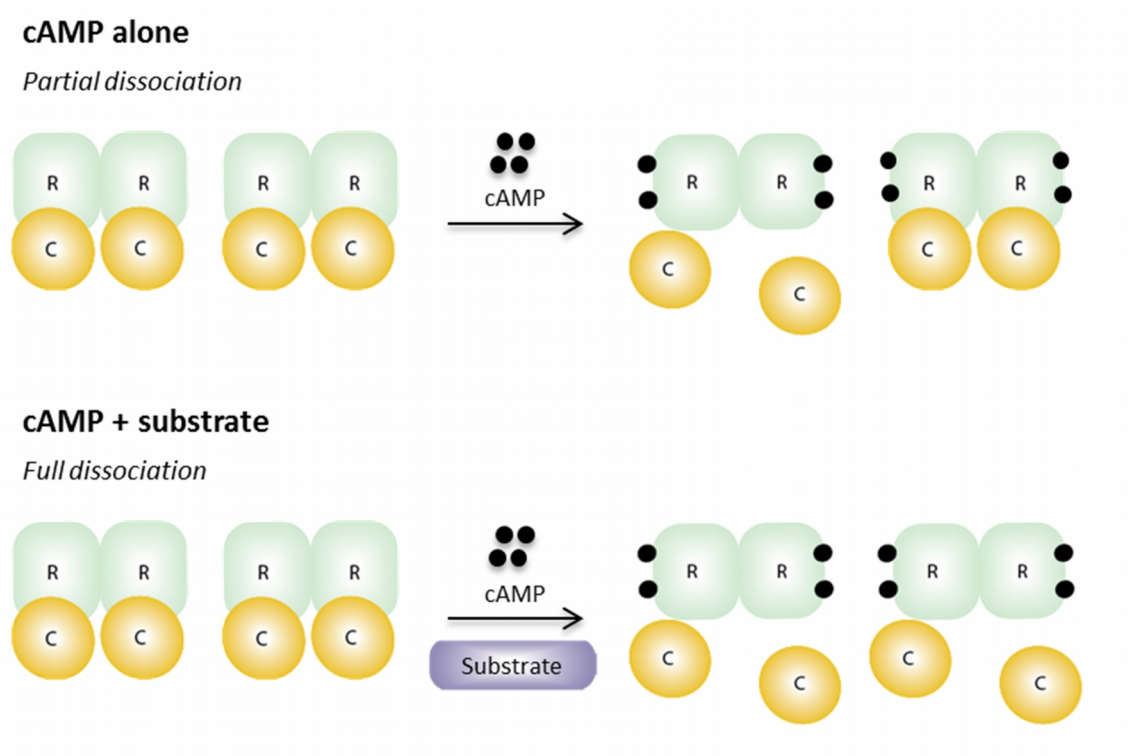

Figure 3.1 Substrate-induced dissociation of PKARIα holoenzyme. Substrates sensitise the PKARIα to cAMP; a feature that is specific to this isoform.

3.2 Specific methods

3.2.1 Antibodies

Antibody	Purchase Code	Company	Species	Dilution
PKARIα	610165	BD Transduction Laboratories	Mouse	1:1000
Phospho-PKA Substrate	9624	Cell Signaling Technology	Rabbit	1:1000
PKARIIα	612242	BD Transduction Laboratories	Mouse	1:1000
PKACα	610980	BD Transduction Laboratories	Mouse	1:1000
Calsequestrin	PA1	Thermo Scientific	Rabbit	1:1000

Table 3.1 Antibodies used in Chapter 3

3.2.2 Cardiac hypertrophy by suprarenal aortic constriction

Myocardial hypertrophy induced by pressure overload following suprarenal aortic constriction was performed by Dr. Andrii Boguslavskyi and is described in full here[195]. Briefly, 6-week-old C57BL/6J mice (20-22 g) were anesthetized by inhalation of isoflurane/O2 mixture (2/98%) and aortic constriction was performed by placing a suture around the abdominal aorta and a 28-gauge blunted needle stent, which was subsequently removed. Sham surgery was an identical procedure with the exception of band placement. After 3 or 14 days hearts were harvested, dissected and left ventricles were frozen and stored at -80°C. Left ventricle homogenates (10% w/v) were re-suspended in reducing SDS-PAGE buffer (5% 2-mercaptoethanol).

3.3 Results

3.3.1 H_2O_2 induces PKARIα dimerisation

Increasing concentrations of H_2O_2 (50-500 μM) induced PKARIα disulfide dimer formation in adult rat ventricular myocytes (ARVM) and HEK 293 cells in a dose-dependent manner (Figure 3.2A). The disulfide dimer was fully reducible upon the addition of 2-mercaptoethanol confirming the observation that had been previously described by the group (Figure 3.2B).

Due to their inherent relevance in the cardiovascular system it could be argued that cultured ARVMs should be the cell type of choice when characterising PKARIα dimerisation. However ARVMs tended to have a high basal rate of kinase oxidation likely induced by to the stress of the isolation. This was a problem when attempting to detect differences in PKARIα oxidation after treatments in this cell type. Furthermore, the basal dimerisation between isolations was more widely varied than HEK 293 cells (Figure 3.3). This meant that comparing results between different experiments was extremely challenging. Therefore in many of the following characterisation experiments other cells lines including HEK 293 cells, VSMCs or BAECs were used. Whilst there was still some baseline variability in the percentage of PKARIα disulfide dimer these preparations were acceptably consistent and are also pertinent models.

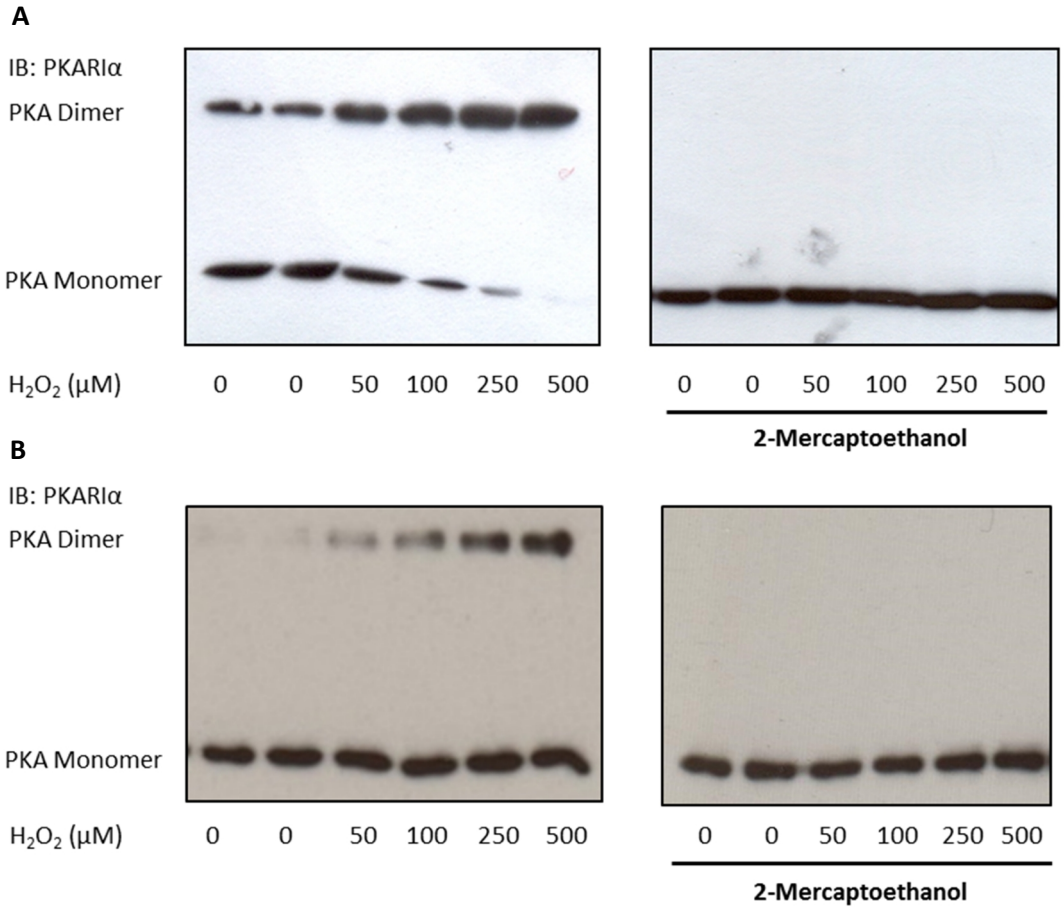

Figure 3.2 H_2O_2 induces disulfide bond dimerisation in PKARIα. Treatment of cells with H_2O_2 (50-500 μM) caused dose-dependent disulfide bond formation which was fully reducible upon supplementation with 2-mercaptoethanol (5%) in (**A**) ARVM (**B**) HEK293 cells as detected with anti-PKARIα by immunoblotting.

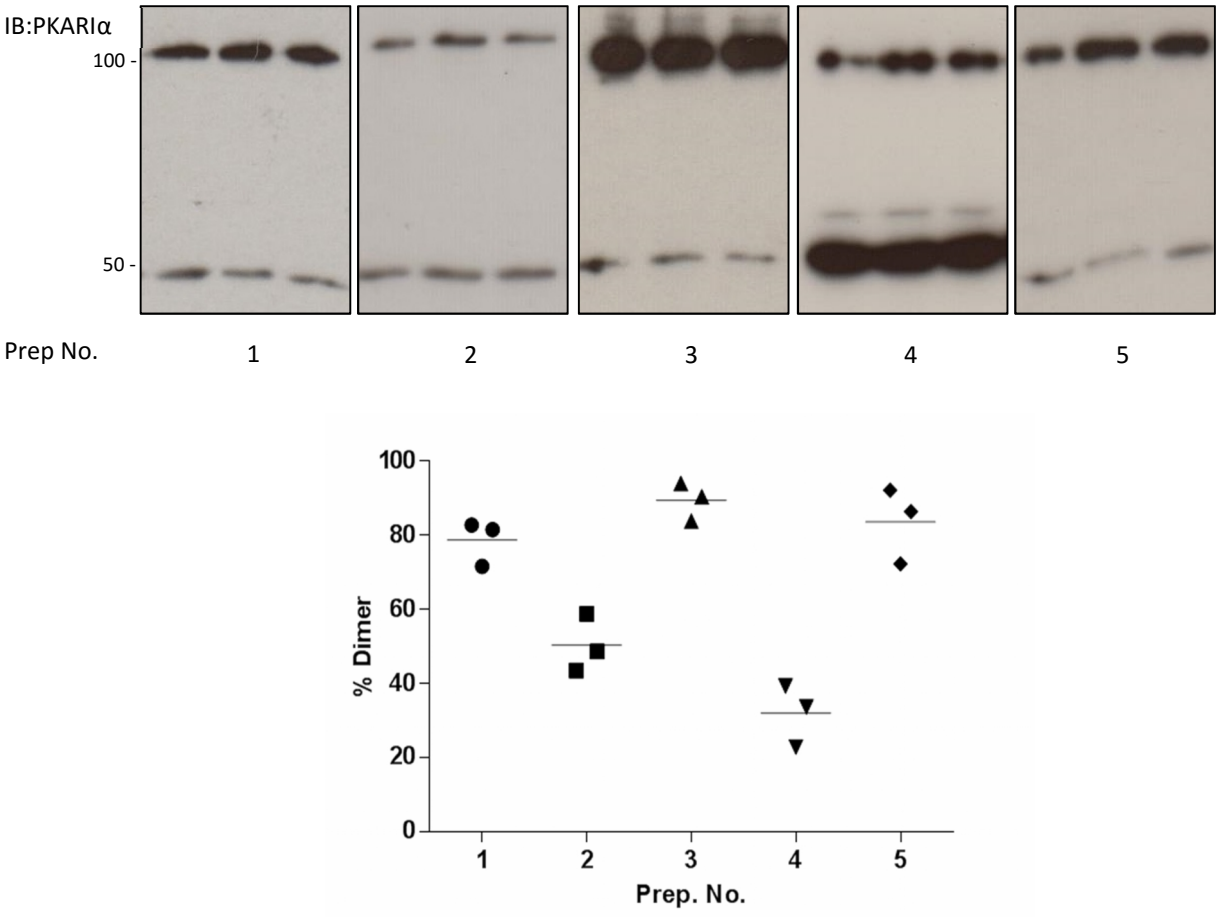

Figure 3.3 Preparations of adult rat ventricular myocytes had variable baseline PKARIα disulfide dimer. 5 separate isolations of adult rat ventricular myocytes were cultured overnight and PKARIα was detected by immunoblotting. The percentage PKARIα dimer of each preparation is plotted in the graph below.

3.3.2 Investigating the role of agents that elevate cAMP on PKARIα dimerisation

Since PKARIα is able to sense the oxidative state of the cell through disulfide dimer formation and is a kinase that is activated by elevated levels of intracellular cAMP, an agonist that could produce both effects concomitantly would be interesting for further investigation. Monoamine deamination via MAO in freshly isolated and cultured cardiomyocytes induces PKARIα disulfide[171], however there was no indication of whether this mechanism of PKARIα oxidation was present in HEK 293 cells. To determine if the catalysis of monoamines by MAO induced PKARIα oxidation in HEK 293 cells, cells were treated with increasing concentrations of noradrenaline or serotonin (1 nM – 1 mM) for 30 min, however there was no evidence of PKARIα oxidation post treatment (Figure 3.4).

Another elevator of intracellular cAMP in the cardiovascular system is PGE_1-dependent activation of EP receptors. Receptor-mediated oxidation of proteins via NOX is a phenomenon that has been attributed to the angiotensin II receptor and a subset of receptor tyrosine kinases including the insulin receptor. I could find no evidence in the literature to suggest that EP receptors are coupled to NOX enzymes, but investigating the possibility that PGE_1 could induce PKARIα dimerisation was still considered worthwhile. AVRMs, HEK 293 or BAEC cells were treated with 10 μM PGE_1 for 30 min to assess the formation of PKARIα dimerisation post treatment via immunoblotting but kinase oxidation was not observed in any of the cell types (Figure 3.5).

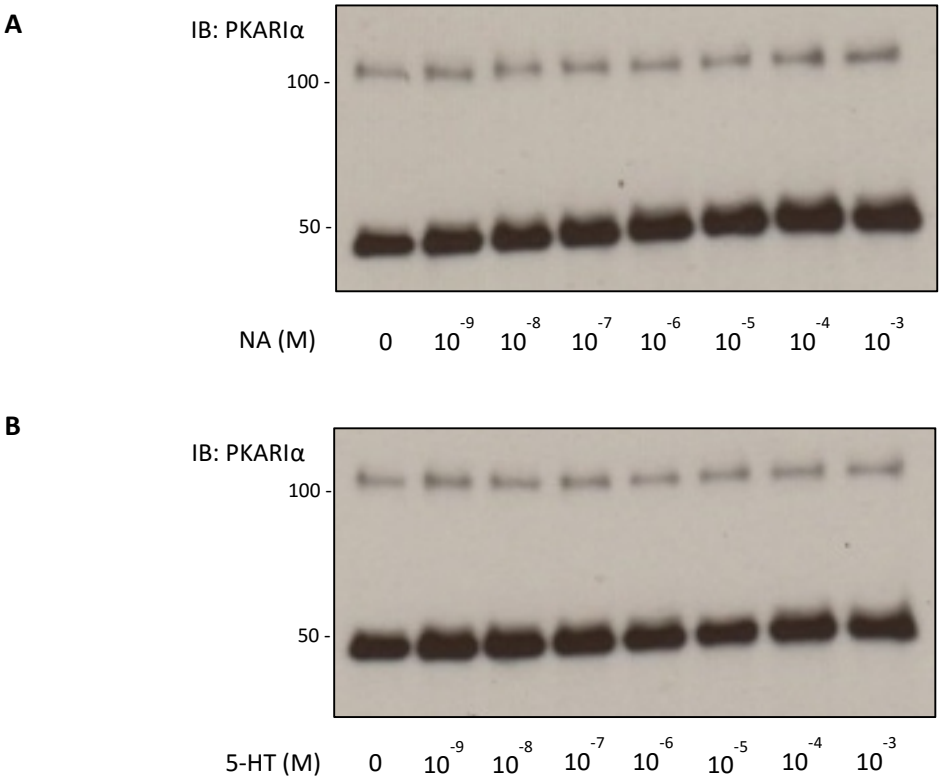

Figure 3.4 Monoamines do not induce PKARIα disulfide dimerisation in HEK 293 cells. Serum starved HEK 293 cells were treated with either (**A**) noradrenaline or (**B**) serotonin (1nM- 1 mM) for 30 min prior to detection of PKARIα by immunoblotting.

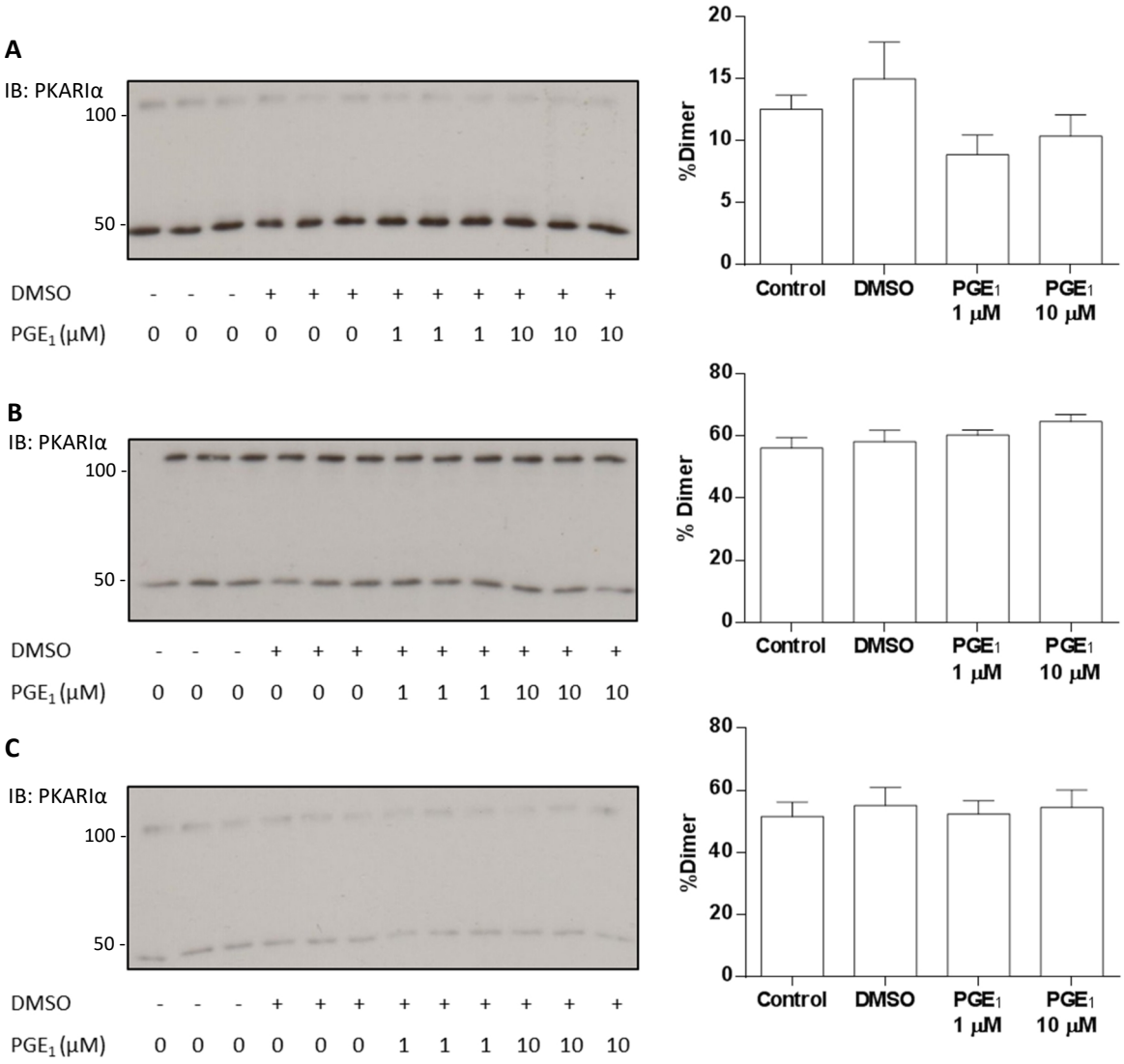

Figure 3.5 PGE_1 does not induce PKARIα disulfide dimerisation. (**A**) Serum starved HEK 293 cells (**B**) ARVMs (**C**) BAECs were treated with PGE_1 (1 or 10 μM) for 30 min. The percentage of PKARIα disulfide dimer was analysed after detection of PKARIα by immunoblotting and is represented graphically for each cell type (n=3 ± SEM).

3.3.3 Investigating the role of cAMP in PKARIα disulfide dimer formation

The conformational change induced in PKARIα upon cAMP binding may prevent the formation of the PKARIα disulfide bonds in a similar way that cGMP binding to PKGIα precludes its dimerisation[194]. Conversely, the conformational change upon cAMP binding may enhance PKARIα disulfide dimer formation. In order to determine the effect of cAMP on PKARIα disulfide bond formation HEK 293 cells were pre-treated with the β-adrenergic receptor agonist isoprenaline, which leads to increased intracellular cAMP, and subsequently treated with 50 µM or 500 µM H_2O_2. Isoprenaline treatment did not significantly modulate PKARIα disulfide dimerisation at either of the H_2O_2 concentrations used (Figure 3.6).

Receptor-mediated cAMP elevation will increase cAMP only in specific subcellular compartments. Compartmentalisation of cAMP production may limit its binding to subtypes of PKA other than PKARIα, and therefore limit the potential to detect any effect it may have on disulfide dimerisation. To overcome this potential issue that may occur due to compartmentalisation of cAMP using receptor mediated cAMP elevation, cells were treated with a stable, cell-permeable form of cAMP, 8-CPT-cAMP. Treatment of cells with 100 µM 8-CPT-cAMP either prior to, or post-application of 500 µM H_2O_2 did not significantly alter the formation of the PKA disulfide bond (Figure 3.7).

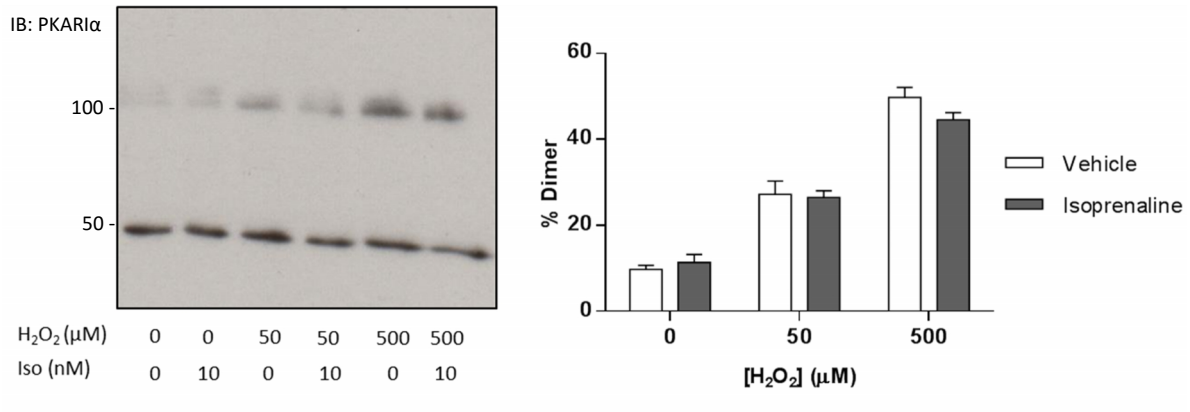

Figure 3.6 Isoprenaline does not modulate PKARIα disulfide dimerisation. HEK 293 cells were treated with isoprenaline (10 nM) for 10 min and subsequently treated with H_2O_2 (50 or 500 µM) for 10 min. The percentage of PKARIα disulfide dimer was analysed after detection of PKARIα by immunoblotting and is represented in the graph (n=6 ± SEM).

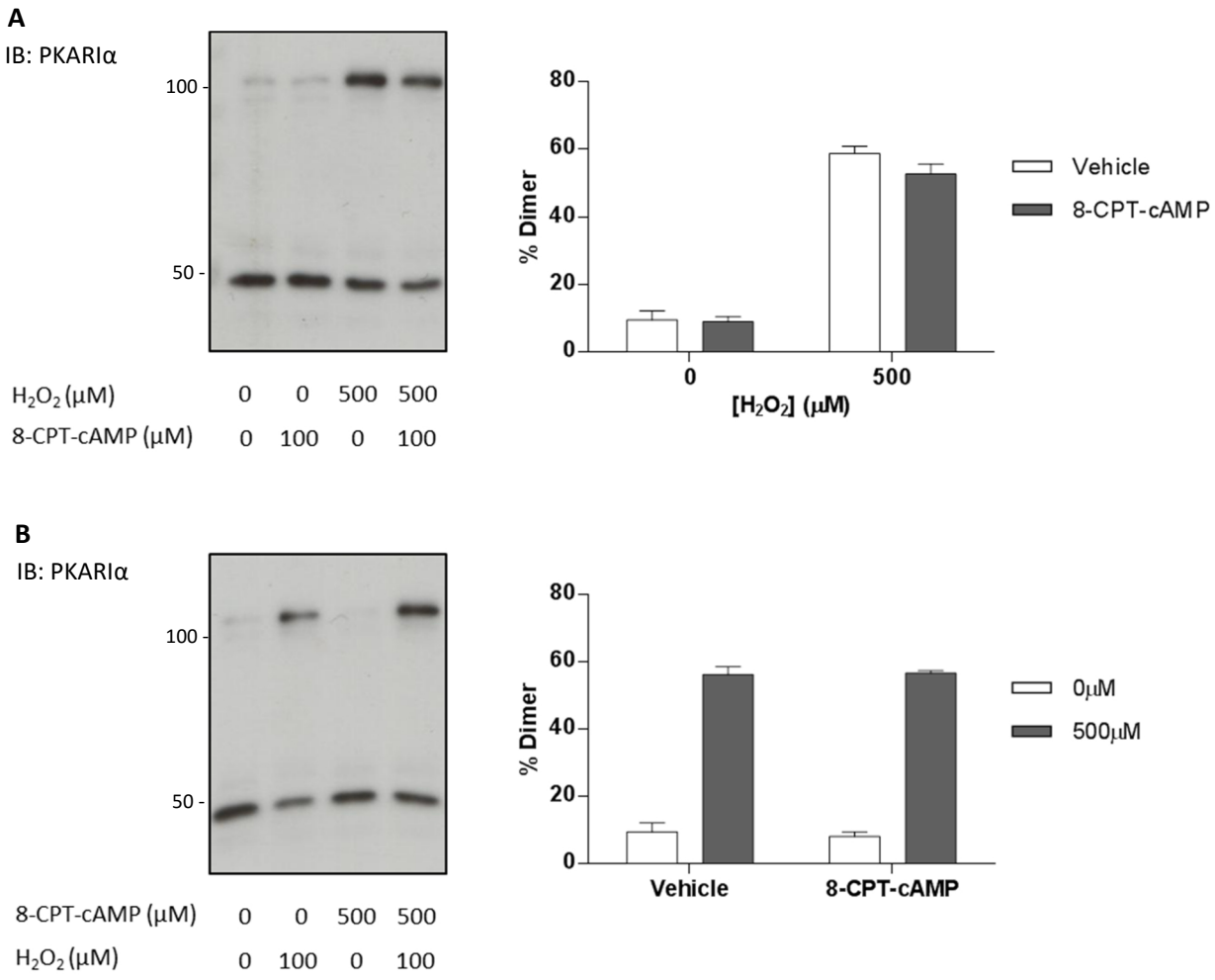

Figure 3.7 8-CPT-cAMP does not inhibit or reverse PKARIα dimerisation in rat vascular smooth muscle cells. (**A**) VSMCs were treated with 8-CPT-cAMP (100 μM) for 10 min and subsequently treated with H_2O_2 (500 μM) for 10 min or, (**B**) treated with H_2O_2 (500 μM) for 10 min and then 8-CPT-cAMP (100 μM) for 10 min. The percentage of PKARIα disulfide dimer was analysed after detection of PKARIα by immunoblotting and is represented in graphically (n=3-6 ± SEM).

The inability to detect any significant changes in PKARIα monomer/dimer ratio after cAMP elevation may be due to the length of time cells were exposed to cAMP or H_2O_2. Given more time cAMP may occupy more PKARIα binding sites, and as such the duration of 8-CPT-cAMP pre-treatment was extended to investigate whether this would alter the PKARIα disulfide formation in HEK 293 cells after H_2O_2 treatment. Figure 3.8 shows the revised experimental plan. However even with this expanded protocol where HEK 293 cells were pre-treated with 8-CPT-cAMP for between 0.5 and 30 min prior to treatment with H_2O_2 (50 or 500 µM), there were no significant differences in PKARIα disulfide formation at any time point (Figure3.9).

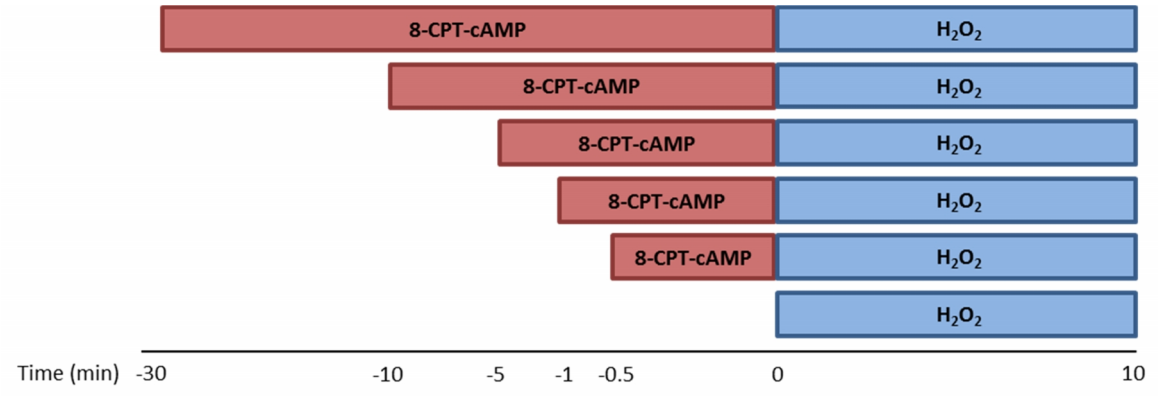

Figure 3.8 Revised experimental protocol to investigate potential for 8-CPT-cAMP to modulate PKARIα disulfide dimer.

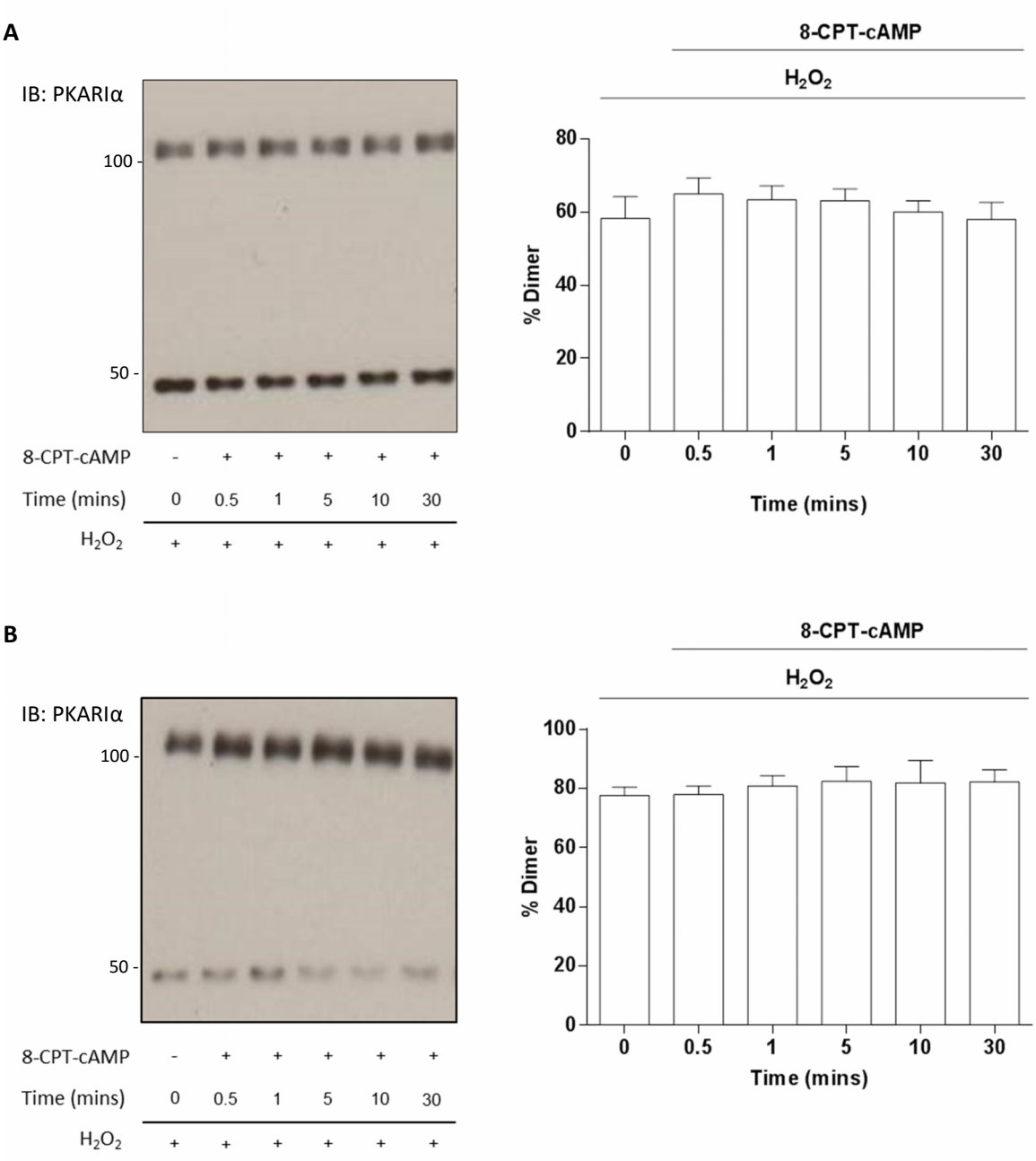

Figure 3.9 8-CPT-cAMP does not modulate PKARIα disulfide dimerisation in HEK 293 cells. HEK 293 cells were treated with 8-CPT-cAMP (100 µM) for 0-30 min and subsequently treated with (**A**) 500 µM H_2O_2 or (**B**) 50 µM H_2O_2 for 10 min. The percentage of PKARIα disulfide dimer was analysed after detection of PKARIα by immunoblotting and is represented in the graphically (n=4-10 ± SEM).

Further experiments were conducted to elucidate whether cAMP could modulate the PKARIα disulfide dimer. In the following studies cells were pre-treated with H_2O_2 and subsequently treated with 8-CPT-cAMP to determine if cAMP could regulate PKARIα disulfide as indicated in the experimental protocol (Figure 3.10). Treatment of cells with 8-CPT-cAMP did not significantly alter PKARIα disulfide dimer regardless of the length of time cells were exposed to H_2O_2 at either high or low concentrations (Figure 3.11). In another experiment to investigate whether cAMP could reverse PKARIα disulfide dimerisation HEK 293 cells were pre-treated with H_2O_2 (400 µM) to induce the disulfide, the culture media was subsequently removed and cells were then treated with 8-CPT-cAMP or vehicle in fresh media. PKARIα disulfide dimer was monitored over 6 hours. There was no difference in the rate of PKARIα disulfide reduction between vehicle and 8-CPT-cAMP treated cells (Figure 3.12). Taken together these experiments suggest that pre-treatment with cAMP does not inhibit or reverse PKARIα dimerisation, although this will be explored further in Chapter 5.

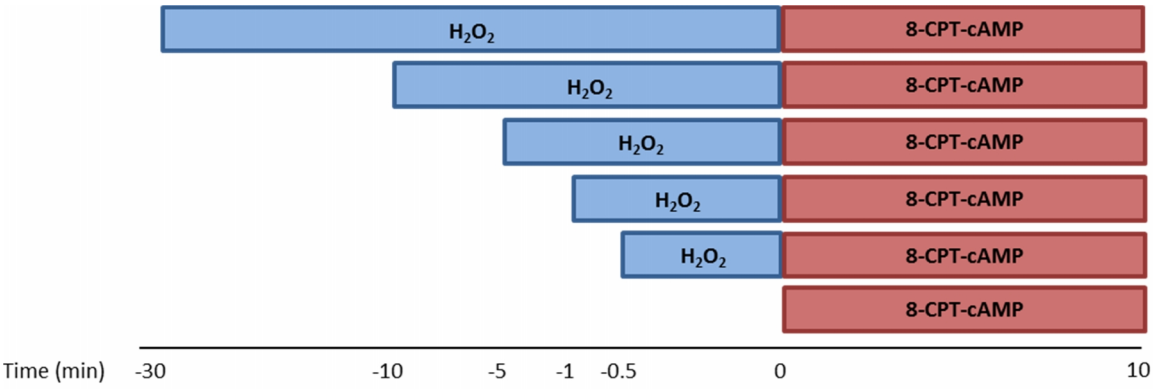

Figure 3.10 Experimental protocol to investigate 8-CPT-cAMP modulation of PKARIα disulfide dimer.

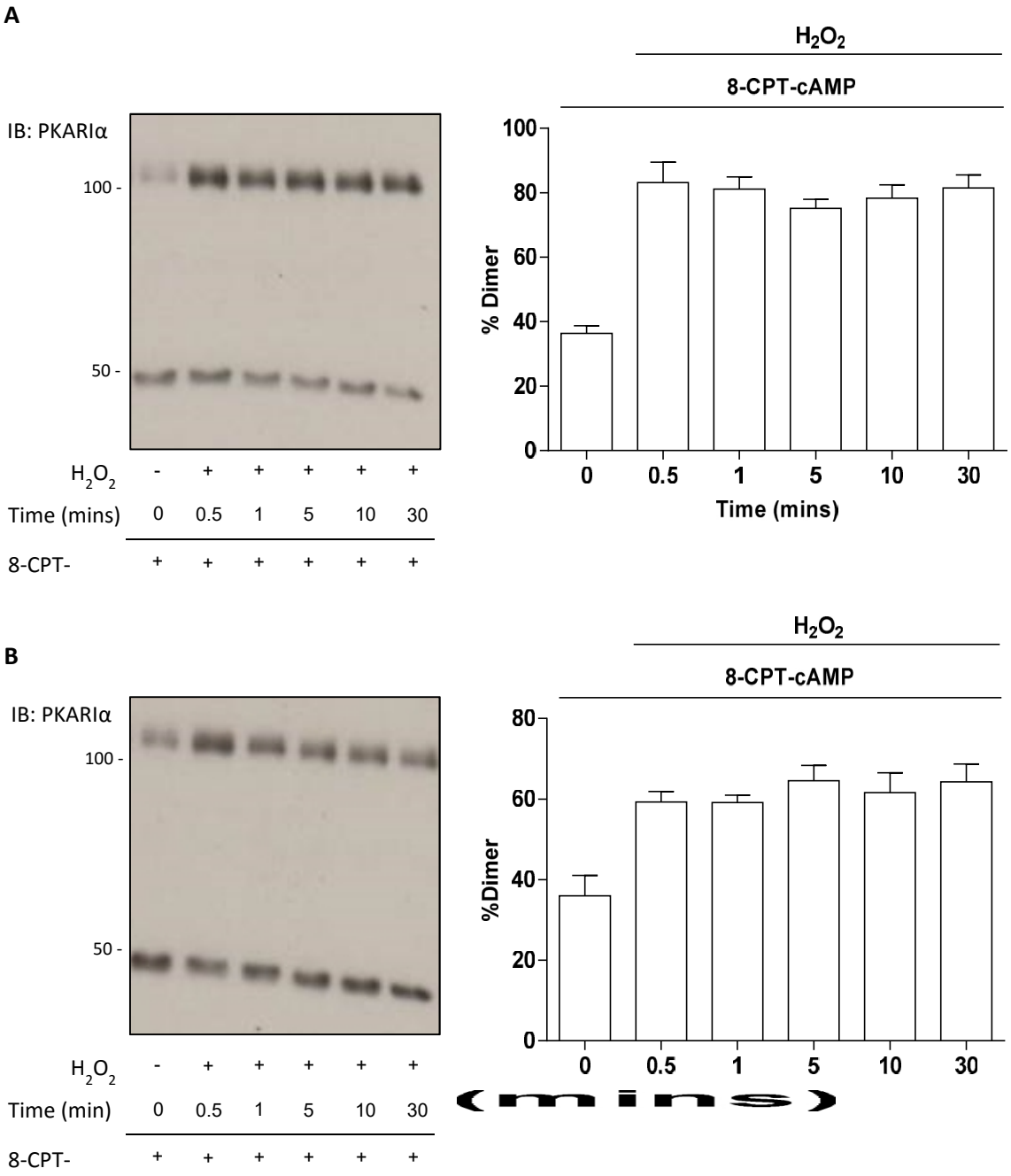

Figure 3.11 8-CPT-cAMP does not reverse PKARIα disulfide dimerisation in HEK 293 cells. HEK 293 cells were treated with (**A**) 500 µM H_2O_2 or (**B**) 50 µM H_2O_2 for 0-30 min and subsequently treated 8-CPT-cAMP (100 µM) for 10 min. The percentage of PKARIα disulfide dimer was analysed after detection of PKARIα by immunoblotting and is represented graphically (n=4-10 ± SEM).

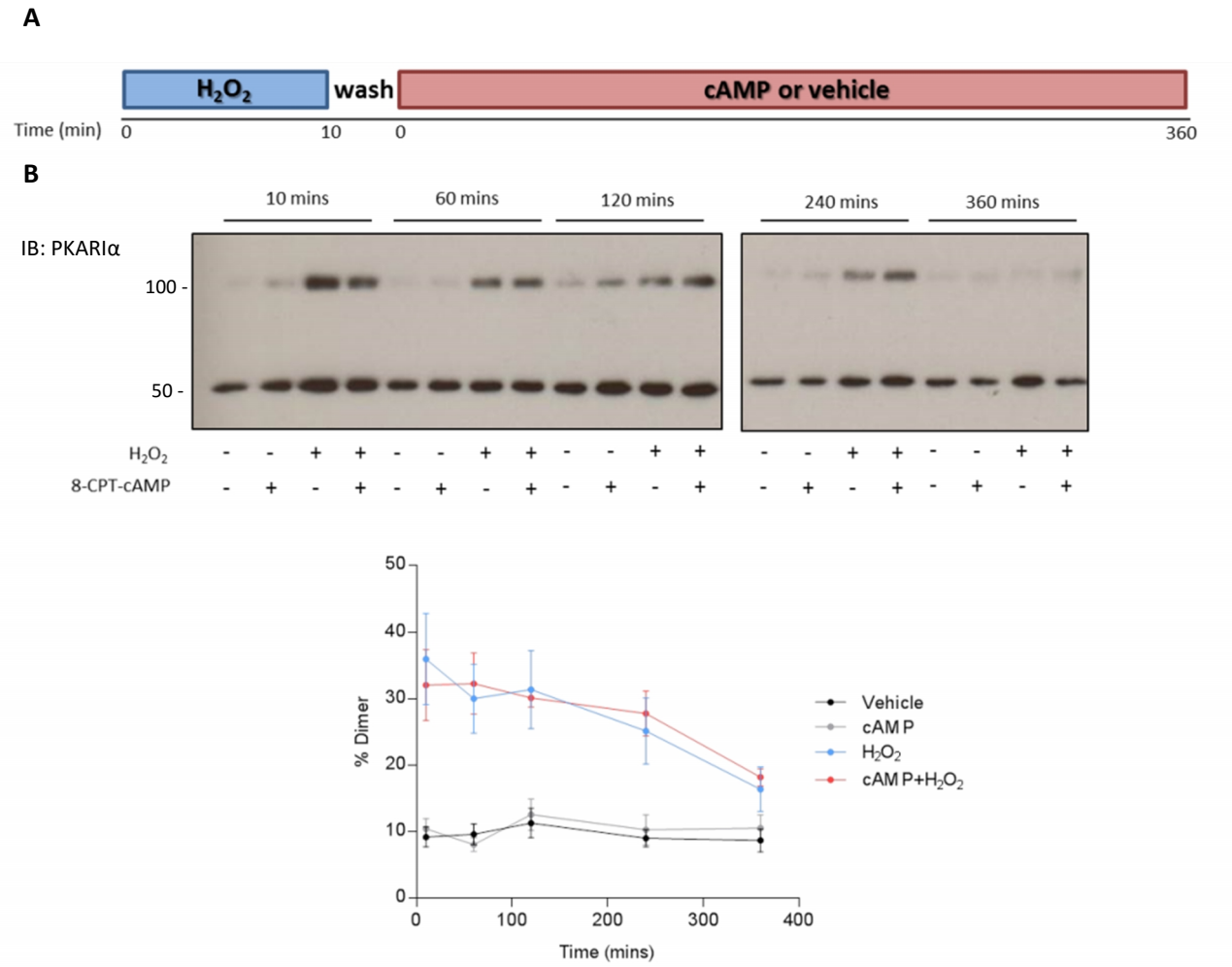

Figure 3.12 8-CPT-cAMP does not increase the rate of PKARIα disulfide reduction. (**A**) Experimental protocol for monitoring 8-CPT-cAMP reduction of PKARIα disulfide. (**B**) HEK 293 cells were treated with 400 µM H_2O_2 10 min and subsequently treated with 8-CPT-cAMP (100 µM) in fresh culture media for between 10-360 min. The percentage of PKARIα disulfide dimer at each time point was analysed after detection of PKARIα by immunoblotting and is represented graphically (n=4 ± SEM).

3.3.4 Investigating the role of PGE_1 and isoprenaline on PKA substrate phosphorylation

Activation of β-adrenergic receptors or EP receptors leads to cAMP elevation in distinct subcellular locations leading to specific functional effects. Furthermore PGE_1-dependent EP receptor activation leads to elevated cAMP in subcellular compartments specific to type I PKA. Therefore substrates that are phosphorylated after PGE_1 treatment but not isoprenaline could potentially be type I PKA-specific substrates.

PKA phosphorylation events can be monitored using immunoblotting with an antibody that pan-specifically recognises the PKA phosphorylation consensus motif Arg-Arg-X-pSer/pThr. To investigate potential type I PKA specific substrates ARVMs were treated with PGE_1 or isoprenaline for 10 min. The PKA substrate antibody detected bands at various molecular weights which represented distinct PKA substrates. In AVRMs numerous proteins were basally phosphorylated as demonstrated by the presence of bands in the absence of any intervention. After treatment with 10 nM isoprenaline the signal from some bands became more intense, and additional bands were detected indicating increased β-adrenergic receptor-dependent phosphorylation of these substrates. H_2O_2 treatment also induced PKA substrate phosphorylation as has been previously described[170]. However treatment with PGE_1 (1 or 10 µM) did not appear to cause any additional phosphorylation of proteins above basal levels, nor did it cause the appearance of additional bands (Figure 3.13).

The ability of PGE_1 to induce substrate phosphorylation was also assessed in other cell types in order to determine if the lack of detectable phosphorylation was specific to ARVMs. ARVMs, HEK 293 cells and bovine aorta endothelial cells (BAECs) were treated with either 1 or 10 µM PGE_1. The pan-specific PKA substrate antibody detected an increase in PGE_1-induced protein phosphorylation in HEK 293 cells only, and therefore HEK 293 cells were selected as the cell type of choice to investigate potential differences between PGE_1- and isoprenaline-induced phosphorylation (Figure 3.14).

HEK 293 cells were then treated with either PGE_1 or isoprenaline to determine if there was differential substrate phosphorylation, as monitored by immunoblotting with the pan-specific PKA substrate antibody. There was no difference in the banding pattern between isoprenaline- or PGE_1-treated cells, and therefore this approach using was considered not viable for identifying type I PKA-specific substrates (Figure 3.15).

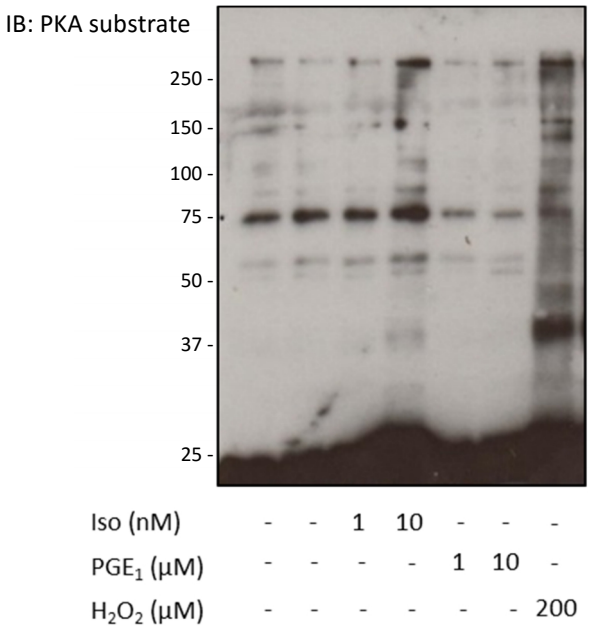

Figure 3.13 Isoprenaline or H_2O_2 but not PGE_1 induces PKA-dependent substrate phosphorylation in adult rat ventricular myocytes. ARVMs were treated with isoprenaline (1 or 10 nM), PGE_1 (1 or 10 µM) or H_2O_2 (200 µM) for 10 min. PKA substrate phosphorylation was assessed with a pan specific PKA substrate antibody (R-R-X-pS/pT) by immunoblotting.

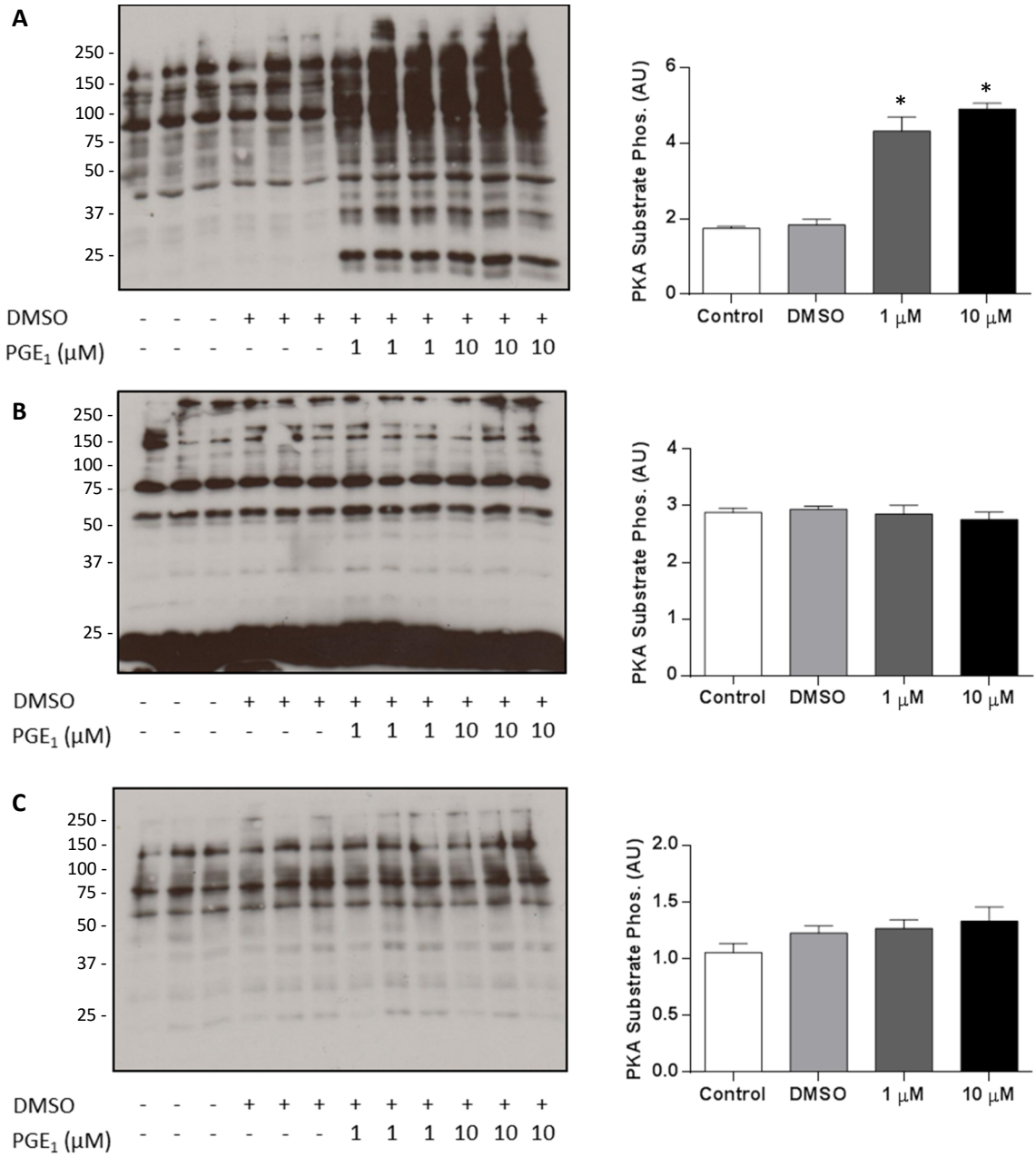

Figure 3.14 PGE_1 induces PKA-dependent substrate phosphorylation in HEK 293 cells but not ARVMs or BAECs. (**A**) HEK 293 (**B**) ARVM (**C**) BAEC cells were treated with PGE_1 (1 or 10 μM) for 10 min. PKA substrate phosphorylation was assessed with a pan specific PKA substrate antibody by immunoblotting (n=3 ± SEM, * $p<0.05$).

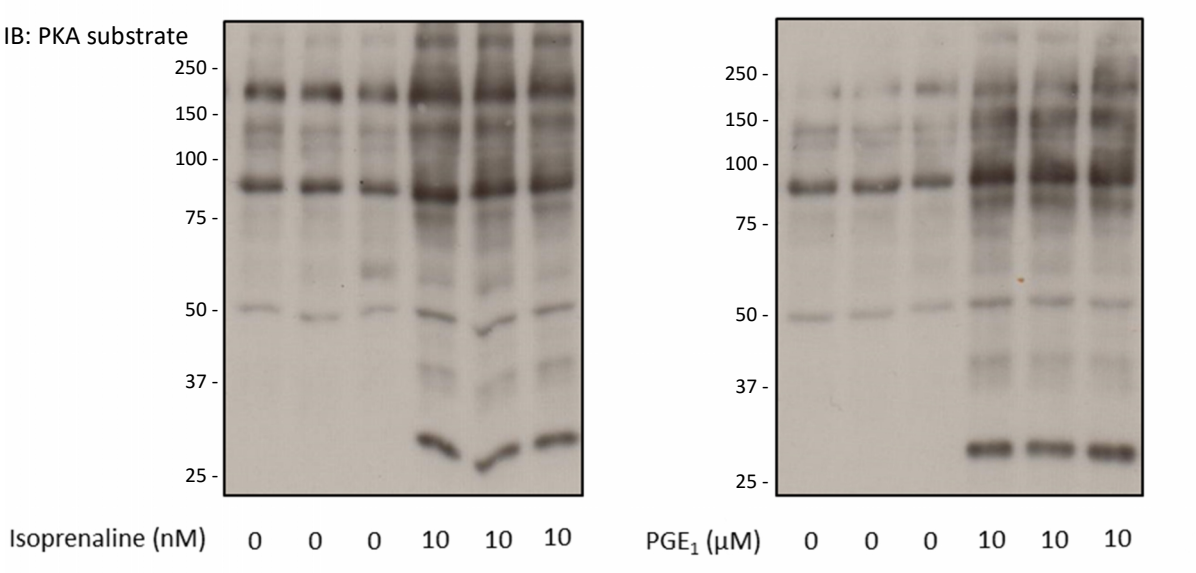

Figure 3.15 Isoprenaline or PGE_1 induce the phosphorylation of the same substrates in HEK 293 cells. HEK 293 cells were treated with either isoprenaline (10 nM) or PGE_1 (10 µM) for 10 min. PKA substrate phosphorylation was assessed with a pan specific PKA substrate antibody by immunoblotting.

3.3.5 The acute effects of cAMP and H_2O_2 co-treatment on PKA-dependent substrate phosphorylation

Elevated levels of both cAMP and oxidants together may occur simultaneously in physiological or pathophysiological conditions in cells. As outlined above, I hypothesise that disulfide formation in PKARIα increases its affinity for certain AKAP proteins. These AKAPs have specific substrates they co-localise with, which would then be phosphorylated as a result of this oxidant-induced complex formation. If this hypothesis is correct, one might predict that treating cells with H_2O_2 to induce disulfide PKARIα and then consecutively or simultaneously treating them with an agent that elevates intracellular cAMP would cause substrate phosphorylation to a greater extent than cAMP alone. It was therefore important to investigate cAMP elevating agents applied simultaneously with exogenously applied H_2O_2 and attempt to model PKA substrate phosphorylation in this setting.

Initially VSMCs were used to try and model the effect of cAMP and H_2O_2 co-treatment on PKA substrate phosphorylation due to their relevance in the cardiovascular system. Cells were pre-treated with H_2O_2 for 10 min and then isoprenaline or PGE_1 for a further 10 min and compared against H_2O_2 or isoprenaline or PGE_1 alone, as outlined in the experimental protocol (Figure 3.16).

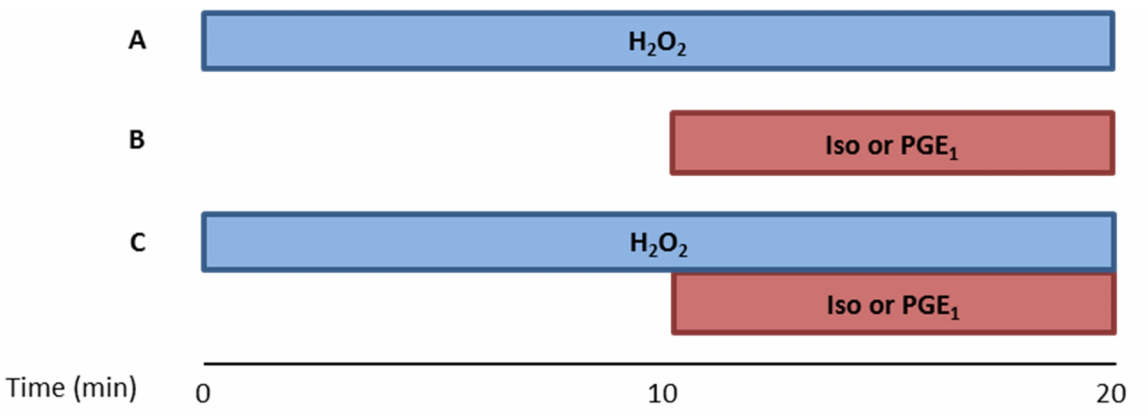

Figure 3.16 Experimental protocol to investigate co-treatment of isoprenaline or PGE_1 and H_2O_2 on PKA substrate phosphorylation

Various substrates were more phosphorylated after co-treatment compared to PGE_1 or isoprenaline or H_2O_2 alone, whilst others appeared to decrease (Figure 3.17). Due to the more robust phosphorylation profile observed in HEK 293 cells, especially with PGE_1 treatment, the experiment was repeated using this cell line. When the total signal corresponding to PKA phosphorylation events were summated, there was approximately a 2-fold increase in total phosphorylation between vehicle treated cells and cells treated with either isoprenaline or PGE_1 (Figure 3.18). There was a slight trend towards increased substrate phosphorylation when cells were treated with H_2O_2 alone, although this was not statistically significantly different from control. There was also a trend towards increased phosphorylation of cells that had been co-treated with H_2O_2 and a cAMP elevating agent compared to cells that had been treated solely with isoprenaline or PGE_1 alone (Figure 3.18).

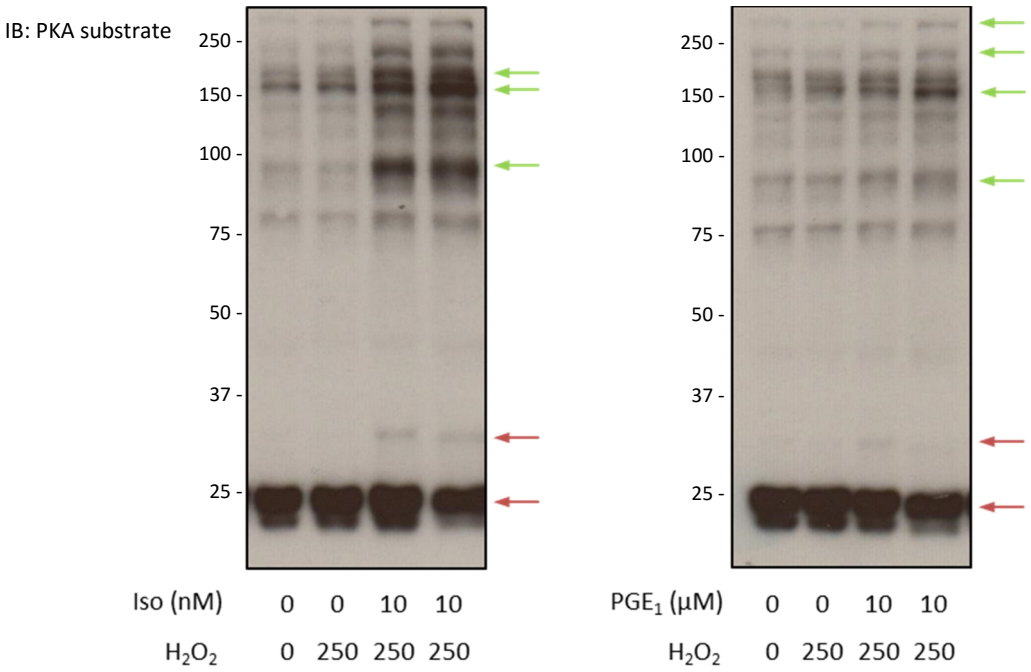

Figure 3.17 Co-treatment with H_2O_2 together with isoprenaline or PGE_1 potentiates phosphorylation of specific PKA substrates. VSMCs were treated with H_2O_2 (250 µM) for 20 min, either isoprenaline (10 nM) or PGE_1 (10 µM) for 10 min, or pre-treated with H_2O_2 for 10 min before subsequent treatment with either isoprenaline (10 nM) or PGE_1 (10 µM). PKA substrate phosphorylation was assessed with a pan specific PKA substrate antibody by immunoblotting. Green arrows indicate substrates that have elevated phosphorylation relative to agonist alone whilst red arrows indicate substrates that have decreased phosphorylation.

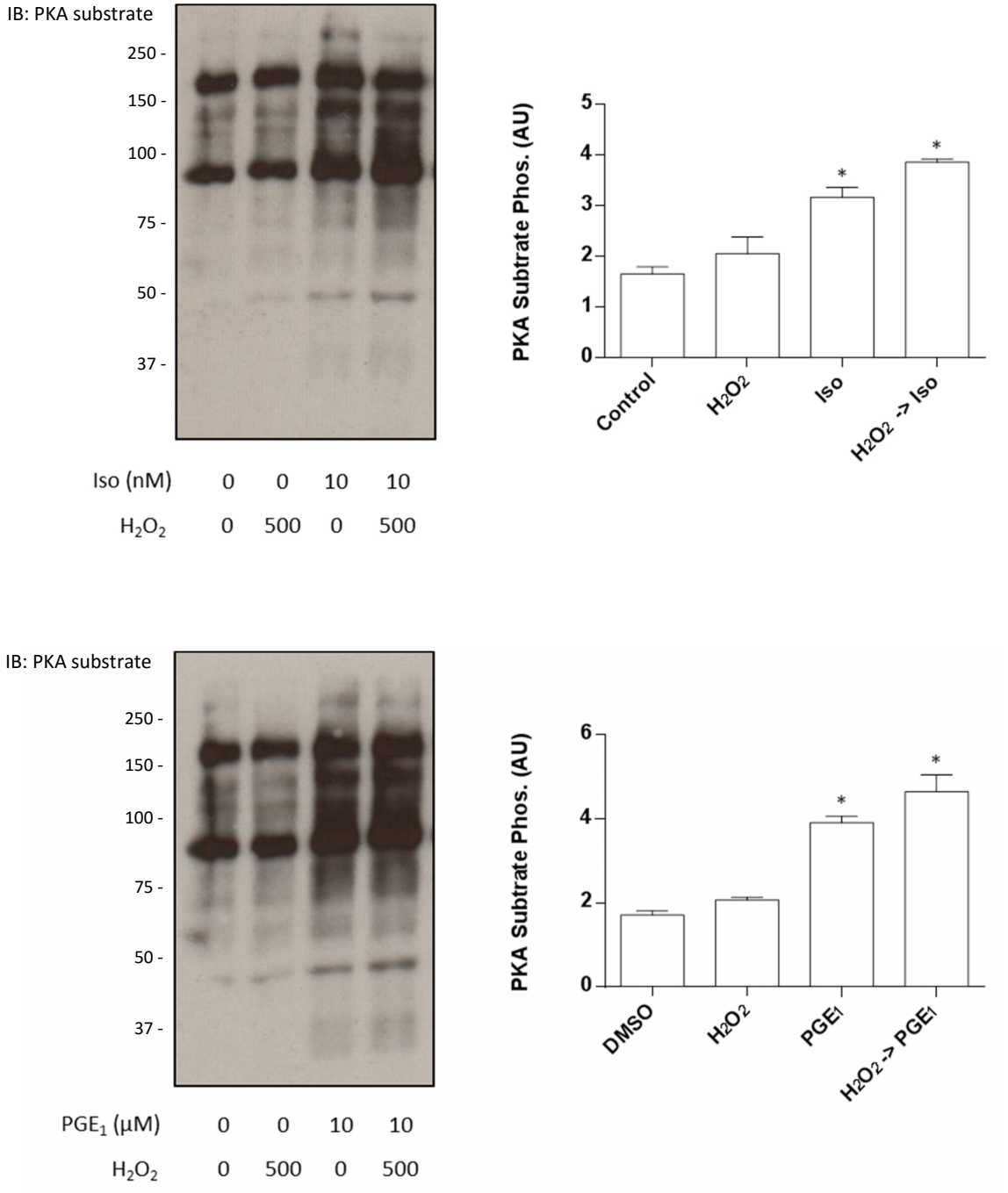

Figure 3.18 Co-treatment with H_2O_2 and isoprenaline or PGE_1 leads to increased 'total' phosphorylation of substrates in HEK 293 cells. HEK 293 cells were treated with H_2O_2 (500 µM) for 20 min, either isoprenaline (10 nM) or PGE_1 (10 µM) for 10 min, or pre-treated with H_2O_2 for 10 min before subsequent treatment with either isoprenaline (10 nM) or PGE_1 (10 µM). PKA substrate phosphorylation was assessed with a pan specific PKA substrate antibody by Western blotting. All phosphorylation events are summated and represented graphically for both isoprenaline and PGE_1 (n=3 ± SEM, * $p<0.05$).

3.3.6 Modelling the chronic effects of cAMP and H_2O_2 co-treatment on PKA dependent phosphorylation and PKARIα expression

So far the experiments have focused on acute activation of the cAMP signalling pathway and likewise the application of exogenous ROS over a short time period. Pathologies, such as heart failure, manifest over sustained period of time and therefore it was also important to determine if chronic cAMP treatment impacts on PKARIα disulfide levels, PKA substrate phosphorylation and PKARIα expression. To model a chronic response to cAMP, HEK 293 cells were treated with vehicle or 8-CPT-cAMP for 6 or 24 hours. At the end of the 8-CPT-cAMP treatment some cells were then treated with H_2O_2 to then compare their PKARIα disulfide dimer and PKA-dependent phosphorylation in response to oxidants. To directly compare the chronic response with the acute response some cells were also treated with 8-CPT-cAMP, H_2O_2 or co-treated with both for 10 min. The experimental protocol is outlined in Figure 3.19.

Acute treatment of HEK 293 cells with 8-CPT-cAMP (10 min) lead to an increase in total PKA substrate phosphorylation. Treatment with 8-CPT-cAMP for 6 or 24 hours also induced PKA substrate phosphorylation, which was comparable to acute treatment (Figure 3.20). 10 min of 8-CPT-cAMP and H_2O_2 co-treatment tended towards an increase in total phosphorylation but this was not was not statistically significant compared to 8-CPT-cAMP treatment alone. There was also a trend towards increased phosphorylation after 8-CPT-cAMP and H_2O_2 co-treatment at both 6 or 24 hours, but again this was not statistically significant (Figure 3.20). Interestingly, treatment of HEK 293 cells for 24 hours with 8-CPT-cAMP caused an approximate 2-fold increase in PKARIα expression compared to vehicle treated controls. This increased expression was detected at the both monomeric and dimeric levels (Figure 3.21). The relative increased levels of PKARIα disulfide dimer was maintained even after cells had been subsequently treated with H_2O_2 (Figure 3.21).

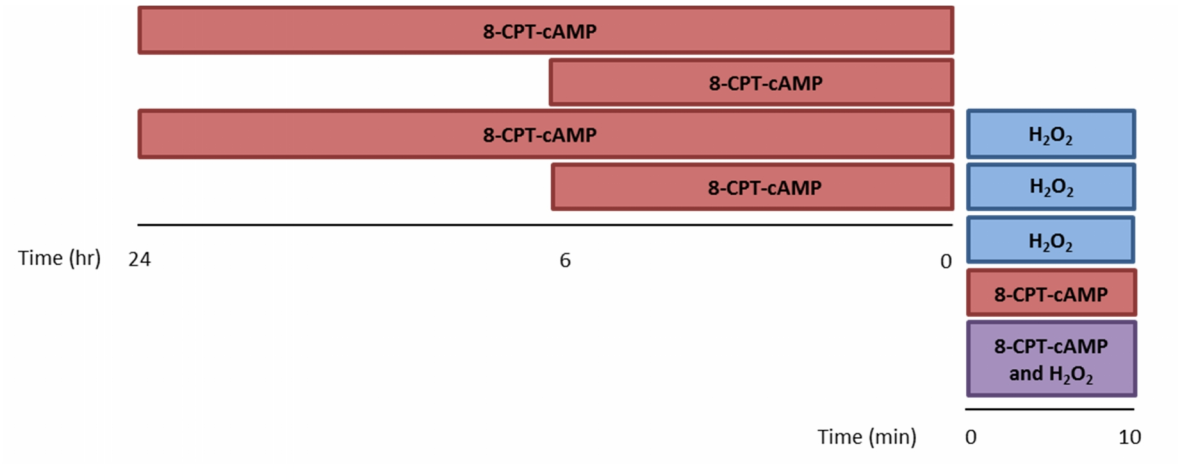

Figure 3.19 Experimental protocol for investigating the responses of PKARIα following chronic or acute exposure to 8-CPT-cAMP.

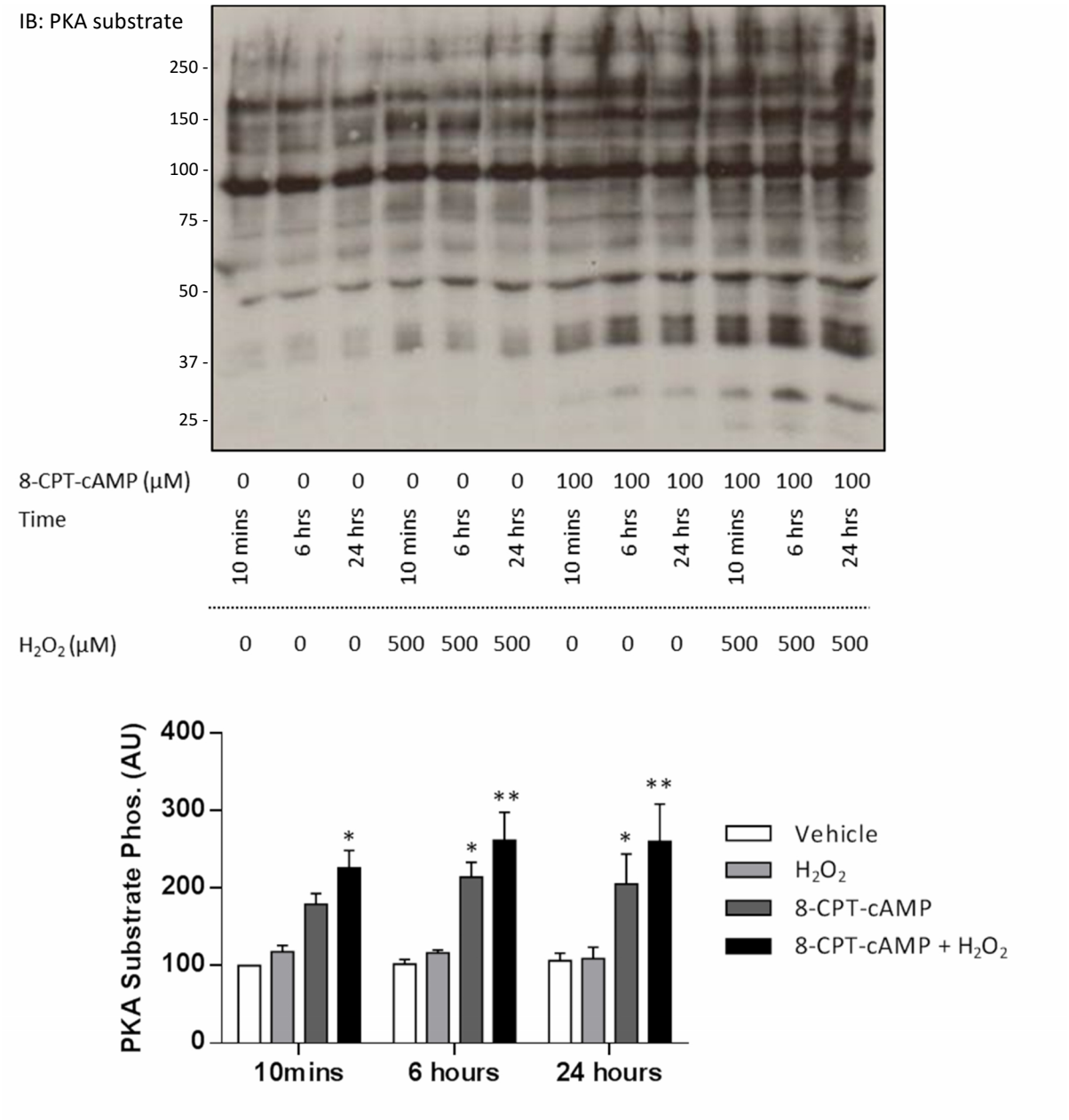

Figure 3.20 Co-treatment of HEK 293 cells with H_2O_2 and 8-CPT-cAMP leads to increased 'total' phosphorylation of substrates after 10 min, 6 hours and 24 hours. HEK 293 cells were treated with vehicle or 8-CPT-cAMP (100 µM) for 10 min, 6 hours or 24 hours. Some cells were then treated with H_2O_2 (500 µM) for 10 min. PKA substrate phosphorylation was assessed with a pan specific PKA substrate antibody by immunoblotting. All phosphorylation events are summated and represented graphically for each time point (n=4 ± SEM, * $p<0.05$, ** $p<0.001$ vs. vehicle).

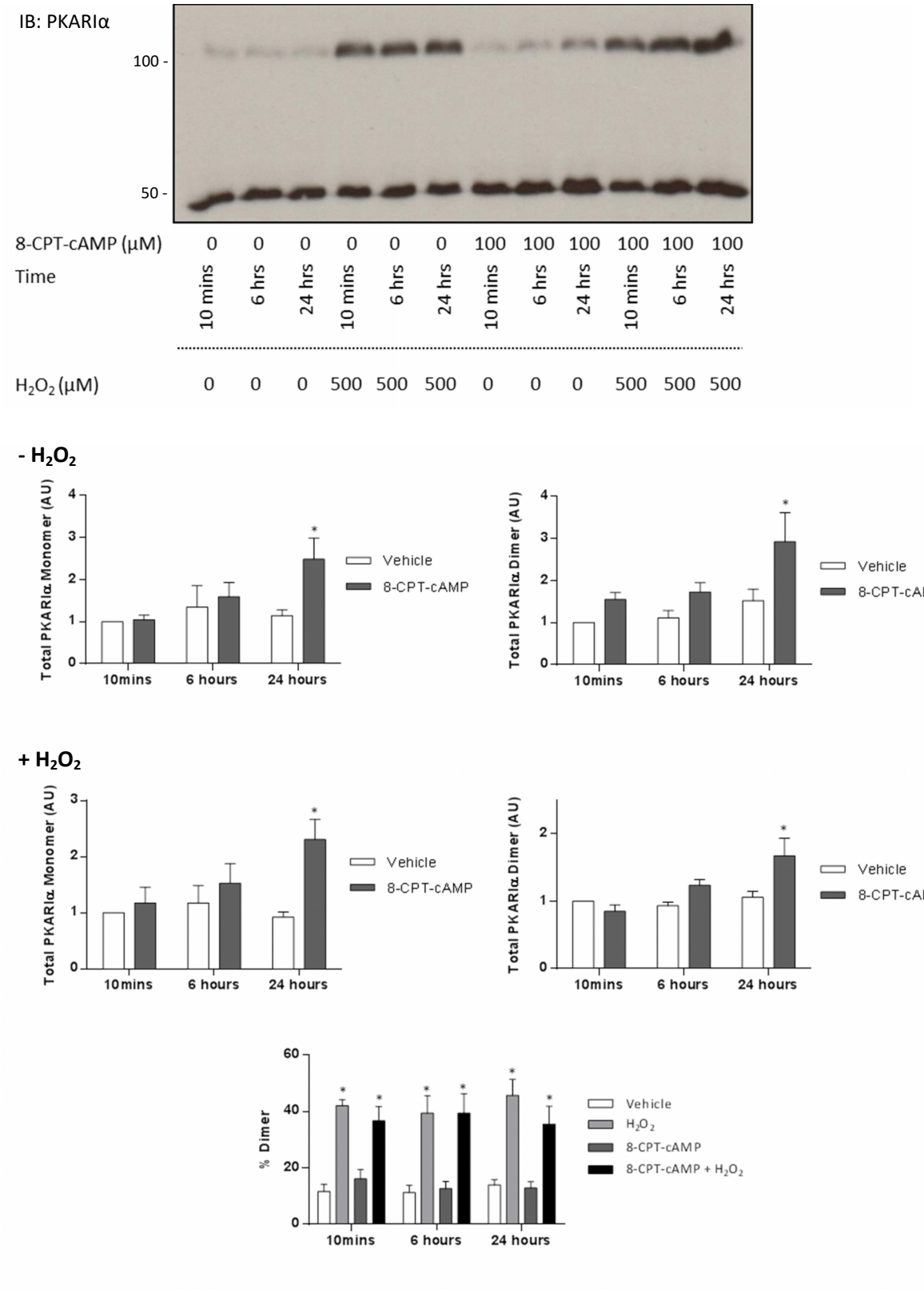

Figure 3.21 Treatment of 8-CPT-cAMP leads to increased expression of PKARIα and increased PKARIα disulfide dimer after 24 hours. HEK 293 cells were treated with vehicle or 8-CPT-cAMP (100 μM) for 10 min, 6 hours or 24 hours. Some cells were then treated with H_2O_2 (500 μM) for 10 min. Expression of PKARIα monomer and dimer were evaluated with a PKARIα antibody by immunoblotting (n=4 ± SEM, * $p<0.05$, vs. vehicle).

3.3.7 Investigating PKARIα expression in a cardiac hypertrophy mouse model

It was tempting to conclude that increased cAMP concentrations caused increased expression of PKARIα. Suprarenal aortic constriction is an animal model that mimics chronic pressure overload-induced cardiac hypertrophy. Ligation of the aorta leads to compensatory elevated levels of circulating catecholamines and consequently elevated cardiac cAMP to promote positive inotropy and chronotropy[196]. Therefore this was an ideal model to investigate whether cAMP could increase PKARIα expression *in vivo*. Male C57BL/6J mice (6 weeks, 20-22g) were subjected to either sham surgery or aortic banding and protein expression was measured by immunoblotting on Day 3 or 14 post-surgery. Banded animals had a 3-fold increase in PKARIα expression on both Day 3 and 14 which was significantly different compared to sham animals. PKARIIα expression levels were significantly reduced by approximately 20% on Day 3 compared to sham animals. By Day 14 the deficit in PKARIIα protein concentration was not significantly different from sham animals. The expression levels of the catalytic subunit of PKA (PKACα) and calsequestrin remained unchanged at both time points (Figure 3.22).

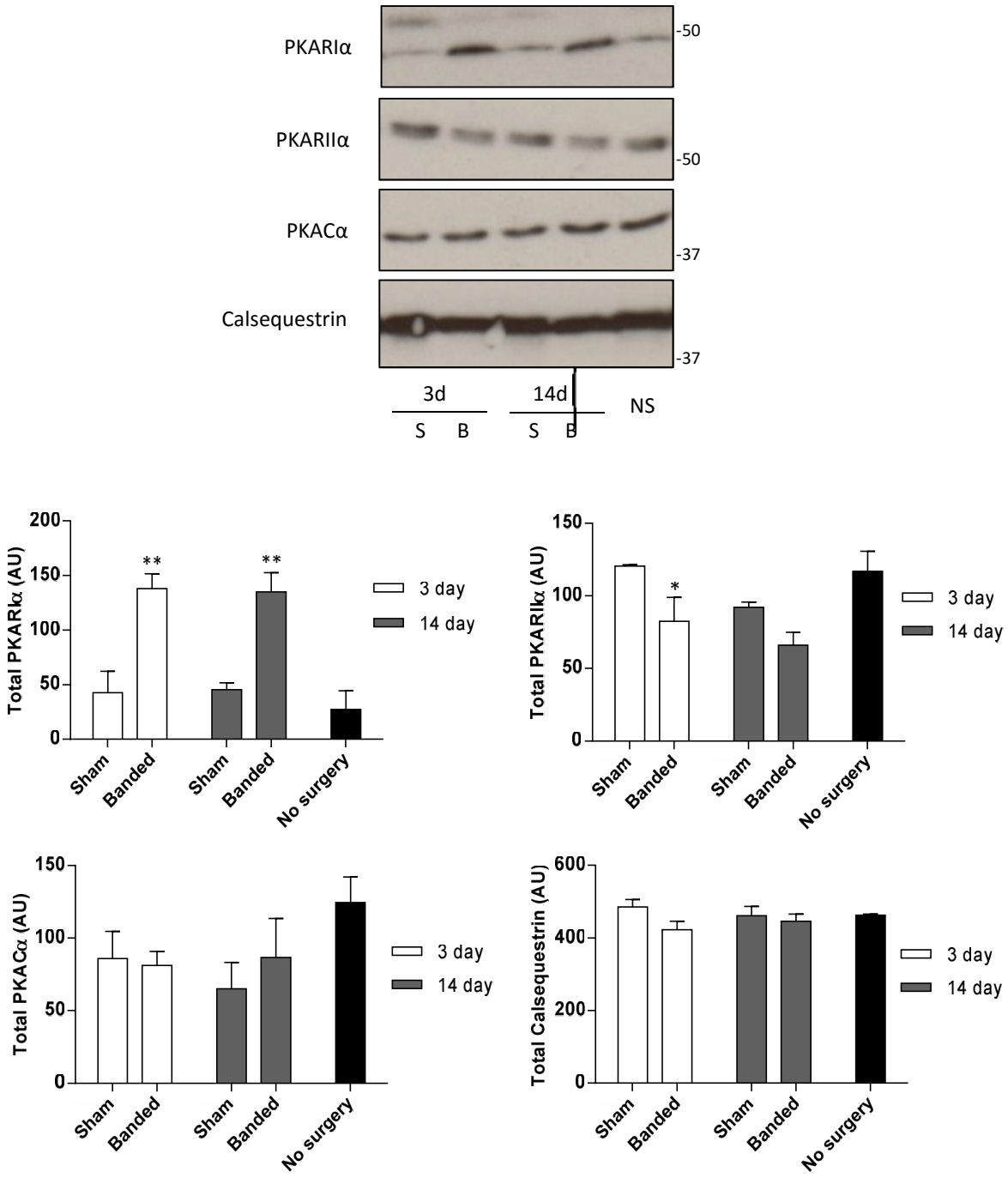

Figure 3.22 Aortic banding leads to increased expression of PKARIα and decreased expression of PKARIIα. C57BL/6J mice underwent sham or aortic banding surgical procedure and allowed to recover whilst others did not undergo any surgery as an additional control (NS). Mice were sacrificed on Day 3 or Day 14, hearts were excised and homogenised for analysis by Western blotting under reducing conditions. Anti-PKARIα, anti-PKARIIα, anti-PKACα and anti-calsequestrin were developed on separate gels and used to assess protein expression which is represented graphically (n=3 ± SEM, *p<0.05. **p<0.01 vs. sham).

3.4 Discussion

The studies in this chapter were focused on assessing the effects of cAMP on PKARIα dimer formation and understanding the effects of cAMP and H_2O_2 on PKA phosphorylation events. PKARIα potentially lies at the axis of cAMP and ROS signalling; here I attempted to ascertain the biochemical consequence of these signal inputs occurring concomitantly. Interestingly, as hypothesised, there was a trend towards increased global PKA substrate phosphorylation when cells were co-treated with 8-CPT-cAMP and H_2O_2.

3.4.1 cAMP modulation of PKARIα disulfide dimer

PKARIα disulfide dimer is induced in a concentration-dependent manner after oxidant treatment in ARVMs, HEK 293 cells, VSMCs and BAECs. Historically this disulfide was already known to exist but was previously considered to be constitutive structural bonds[197,198]. Furthermore SDS-PAGE is routinely carried out under reducing conditions which prevents visualisation of disulfide complexes[199-201]. The oxidant-dependent modification can be detected because samples are lysed and prepared in the presence of the alkylating agent maleimide. Alkylation of free thiols prevents artificial oxidation which occurs during lysis when proteins are removed from the reduced cellular environment and exposed to molecular oxygen in the air. This intervention is crucial to ensure the oxidative modification that is being detected is due to experimental intervention.

MAO has been proposed as a potential mediator of PKARIα oxidation due to ROS generation during oxidative deamination of monoamines[25,202]. NA or 5-HT are capable of inducing PKARIα oxidation in cardiomyocytes[171] however I was unable to replicate this in HEK 293 cells. MAO-dependent oxidant generation in HEK 293 cells has been described when the enzyme has been over-expressed[203,204]. The lack of endogenous MAO expression or lack of monoamine uptake in HEK 293 cells may be why PKARIα oxidation was not observed.

Treatment of cells with isoprenaline or PGE_1 did not modulate PKARIα disulfide dimer. Agonism of receptors such as the insulin receptor and the angiotensin II receptor have been linked to NOX activation and consequent oxidant production[205,206]. There is a limited literature that suggests activation of EP receptors is associated with decreased intracellular ROS in cellular models of Alzheimer's and oxidative renal medulla injury[207,208], however neither EP nor β-adrenergic receptor agonism modulated PKARIα disulfide dimer in the models used.

As previously discussed cGMP binding to PKGIα precludes the kinase from forming a disulfide and it was anticipated that cAMP may have an effect on PKARIα via a similar mechanism[194].

However modulation of PKARIα disulfide dimer was not observed in cells treated with 8-CPT-cAMP. Increasing the amount of time the cells were incubated with 8-CPT-cAMP, or modifying the concentration of H_2O_2, did not alter the ability for 8-CPT-cAMP to regulate PKARIα disulfide dimer formation. There is a considerable distance between the cyclic nucleotide binding domains of PKARIα and the cysteines necessary for disulfide bond formation, whereas the cysteines in PKGIα lie closer to the nucleotide binding domain, perhaps explaining why cyclic nucleotide binding has an effect on disulfide dimerisation of PKGIα, but not PKARIα[194]. Given the properties of cAMP it is unsurprising that there was no significant decrease in PKARIα disulfide dimer as it has no intrinsic reducing capacity. Whilst the experiments thus far do not indicate a role for cAMP in modulating PKARIα disulfide, I will present other lines of evidence in Chapter 5 that suggests that cAMP can indeed regulate the redox state of PKARIα. Any effects of cAMP on PKARIα disulfide may have potentially been missed as immunoblotting may not be a suitable method to detect subtle changes in disulfide dimer formation that may occur only in specific subcellular compartments.

3.4.2 Analysis of PKA substrate phosphorylation

PGE_1 leads to elevation of cAMP in type I PKA domains[188]. Therefore substrates phosphorylated by PGE_1 could potentially be RIα specific substrates. Contrary to the literature I did not detect PKA-substrate phosphorylation with the PKA-substrate antibody in cardiomyocytes when cells were challenged with PGE_1. This was surprising given that various groups have reported increases in cAMP using radioimmunoassays or fluorescent microscopy methods in cardiomyocytes after treatment with PGE_1[181,185,209]. The PKA substrate antibody might be limiting as it may only detect a certain cohort of substrates. Furthermore there is a paucity of evidence in the literature regarding specific PKA-dependent substrates downstream of PGE_1 in the heart or in cardiomyocytes. EP receptor downregulation after isolation is a speculative reason for the lack of detectable substrate phosphorylation. In contrast robust PKA-substrate phosphorylation was observed in HEK 293 cells treated with PGE_1. Several studies report that PGE_1 and isoprenaline cause cAMP elevation in distinct microdomains[188,210,211]. FRET phosphorylation reporter probes directed to these distinct microdomains reveal agonist-dependent phosphorylation[211], and therefore it was reasonable to assume that the profile of PKA phosphorylation events as detected by the PKA-substrate phosphorylation antibody may differ between the two agonists. Surprisingly, the pattern of substrate phosphorylation was similar for both PGE_1 and isoprenaline in HEK 293 cells. This may be because the pan-specific antibody is not as sensitive to changes in protein phosphorylation as FRET reporter probes. Ultimately RIα specific substrates could not be detected using this method.

Whereas Brennan *et al.* monitered the phosphorylation of specific substrates using the pan-specific antibody, I used 'whole lane intensity' to monitor global substrate phosphorylation. Due to monitoring 'total' phosphorylation, I was unable to detect a significant difference between control and H_2O_2 in contrast to the Brennan study, as only a few phosphorylation events increased upon exposure to H_2O_2. Furthermore, Brennan *et al.*, H_2O_2 caused the phosphorylation of PKA substrates as detected by the pan-specific PKA substrate antibody in ARVMs[170]. However in VSMCs or HEK 293 cells H_2O_2 alone induced only a minimal increase in substrate phosphorylation. de Pina *et al.* suggest that H_2O_2 results in catalytic subunit inhibition which would consequently decrease phosphorylation of PKA substrates, however a decrease in basal phosphorylation was not observed in any cell type[107]. It has been argued that the positive effect of oxidants on PKA phosphorylation events is due to inhibition of Ser/Thr phosphatases rather than PKA activation[212]. The above experiments do not preclude this possibility, but the differences in H_2O_2-dependent phosphorylation events observed in cell types makes this unlikely. Rather several studies have suggested that the degradation of cAMP by PDEs, and not phosphatase activity, is the main regulator of PKA phosphorylation events[213,214]. In fact, the key factor in oxidant-dependent PKA phosphorylation may be the concentration of endogenous intracellular cAMP in the different cell types. Basal cAMP levels in cardiomyocytes are approximately 1.25 µM whilst in HEK 293 cells the concentration is below 100 nM[215]. This suggests that oxidant-dependent PKA substrate phosphorylation is contingent on the presence of cAMP rather than the activity of phosphatases. Since PKARIα is the only isoform that can sense and transduce both oxidant and cAMP signals, it is reasonable to suggest that is responsible for integrating the inputs to enhance substrate phosphorylation in cardiomyocytes. Furthermore when HEK 293 cells and VSMCs were challenged with a cAMP elevating agent and H_2O_2 together, there was a trend towards increased PKA substrate phosphorylation compared to when cells were challenged with each agent alone. This again suggests that PKARIα can transduce both cAMP and oxidant inputs to regulate substrate phosphorylation, and that oxidants leads to potentiation of PKA-dependent substrate phosphorylation. cAMP has been reported to only induce partial dissociation of the PKARIα isoform from the catalytic subunits whereas substrate and cAMP together leads to full dissociation[189,193]. I hypothesise that the enhanced substrate phosphorylation in the presence of H_2O_2 and cAMP is due to increased affinity PKARIα disulfide dimer to an associated AKAPs and therefore targeted to within close proximity of its substrates. The affinity between PKARIα disulfide dimer and AKAPs will be explored further in Chapter 4.

3.4.3 Increased Expression of PKARIα after chronic treatment with 8-CPT-cAMP

Interestingly HEK 293 cells exposed to 8-CPT-cAMP for 24 hours had increased expression of PKARIα, some of which was in the disulfide state, which increased after the application of H_2O_2. Pathological hypertrophy induced by aortic constriction is associated with elevated concentrations of cAMP due to increased circulating catecholamines[216,217], and therefore provided a more relevant setting to investigate chronic cAMP on PKARIα expression. PKARIα expression was upregulated in the *in vivo* cardiac hypertrophy model, an observation that is also confirmed by Han *et al.* whilst PKACα expression remained constant and PKARIIα expression was downregulated[218]. Interestingly, pathological hypertrophy has been associated with a switch to foetal gene expression and PKARIα KO mice die during embryonic development, thus this 'PKA switch' may be representative of a change in cardiovascular R subunit phenotype[219]. It is likely that RIα expression is upregulated to compensate for the over activity of the C subunits that would occur when cAMP levels are elevated. However it is curious that RIα expression is increased given that it is the only isoform able to detect oxidative inputs. It is therefore tempting to suggest that the increased expression of PKARIα is not only to inhibit catalytic activity, but also to perhaps direct the cAMP signal to oxidant-dependent PKA targets thus integrating the two signalling modalities. Although this cAMP-dependent upregulation of PKARIα would be an interesting subject to pursue, it was deemed to be outside the remit of this thesis.

3.4.4 Examination of PKARIα disulfide in different cell types

The susceptibility of PKARIα to disulfide dimerisation varied depending on the type of cell that was being challenged with the oxidative stimulus. For example, cardiomyocytes were more sensitive to 500 μM H_2O_2 treatment than HEK 293 cells. This concentration of H_2O_2 induced almost complete dimerisation of PKARIα in this cardiomyocytes but only approximately half in HEK 293 cells. This may be because the endogenous antioxidant system in HEK 293 cells has a greater capacity to offset the increases in ROS. GSH is a vital antioxidant thiol for protection against oxidative stress. Indeed, rat cardiomyocytes reportedly have a GSH concentration of ~11 nmol/mg concentration[220] compared to HEK 293 cells which have a GSH concentration of ~30- 45 nmol/mg[221-223], 3-4 times greater than myocytes. This difference in GSH concentration between cell types is perhaps reflected in the sensitivity of PKARIα in cardiomyocytes to form a disulfide dimer in response to acute H_2O_2 treatment, in comparison to PKARIα in HEK 293 cells. Given this, throughout this thesis the concentration of oxidant used to treat cells has varied depending on the cell type, with lower concentrations required to induce PKARIα disulfide dimer in ARVMs and VSMCs compared to HEK 293 cells.

In the absence of any exogenous oxidants cardiomyocytes tended to have a basal PKARIα disulfide dimer of at least 50% which was very variable between isolations. This made it very difficult to obtain consistent results when attempting to characterise PKARIα disulfide response in this cell type. It is unknown whether this high level of oxidation is due to some intrinsic characteristic of cardiomyocytes; if the cells are particularly sensitive to stress that occurs during the isolation; or if the plating procedure causes them to produce oxidants. As such, HEK 293 cells were used for many of the experiments as I was able to obtain a more consistent level of PKARIα disulfide between experiments.

There is criticism that surrounds the use of exogenously applied H_2O_2, as its physiological production would be tightly regulated in discrete subcellular compartments[224,225]. Moreover the physiological and pathophysiogical concentrations of H_2O_2 *in vivo* has not been well defined[226]. Throughout this report H_2O_2 concentrations from 50-500 µM have been used which is within the range that has been routinely used in the literature[227]. Physiological and pathophysiological concentrations have been recorded between 1-1000 µM[227]. It is important to consider that exogenous H_2O_2 concentration is not the same as in the intracellular environment, due to impedance by the cell membrane, and is estimated to be approximately 10% of the concentration applied[228]. Furthermore due to the activity of endogenous antioxidant proteins it can be difficult to trap proteins in their oxidised form because they are constantly being redox-cycled to their reduced form. Therefore it is often necessary to use higher than may be physiologically-relevant concentrations of oxidising agent in order to compromise the reducing system and allow detection or visualisation of the oxidative modification being investigated.

3.4.5 Notes on anti-PKARIα from BD Transduction Laboratories

A range of PKARIα antibodies had been screened previously to determine which could most reliably detect the PKARIα disulfide dimer. The BD Transduction Laboratories PKARIα antibody was the only antibody that detected an increase in PKARIα disulfide dimer with increasing concentrations of H_2O_2[171]. In some tissues such as cardiomyocytes there is a clear reciprocal decrease in PKARIα monomer and increase in PKARIα disulfide dimer. However in H_2O_2 treated HEK 293 cells the reciprocal decrease of PKARIα monomer is not very obvious despite a clear and corresponding increase in the disulfide dimer. This has led to the conclusion that the antibody has a higher affinity for the disulfide dimer than for the monomeric form of PKARIα. It was important to bear this in mind when considering data obtained using this antibody as presented throughout this thesis.

3.4.6 Biological significance

PKA is an important mediator of cAMP signalling and regulates numerous cellular functions. The RIα isoform can sense the redox potential of the cell via the formation of a disulfide bond between the two regulatory subunits. Evidence suggests that PKARIα can integrate oxidant and cAMP signals to enhance substrate phosphorylation and potentially fine tune functional effects, but the exact mechanism remains to be elucidated[170]. In the next chapter I will investigate whether the oxidant-potentiated PKA substrate phosphorylation is due to increased affinity between PKARIα disulfide dimer and AKAPs.

4 Assessing AKAP7 as a redox-dependent target for PKARIα

4.1 Introduction

In the previous chapter it was shown that H_2O_2 potentiated cAMP-induced phosphorylation of PKA substrates. The primary focus of this chapter is to investigate whether this is due to an increased affinity between PKARIα disulfide dimer and AKAPs, thus leading to increased phosphorylation of associated substrates. In addition to the findings of the previous chapter, this hypothesis is also significantly based on evidence that a Cys17Ala PKARIα mutant had decreased affinity for DAKAP2 compared to WT PKARIα (Figure 1.10)[103].

A "redox dead" mutant Cys17Ser PKARIα knock-in (C17S PKARα KI) mouse that cannot form a disulfide bond between the two regulatory subunits has been generated to study the effects of PKARIα disulfide dimer on physiological responses. If the hypothesis is correct we might expect these mice to have functional deficiencies due to a failure in AKAP targeting usually facilitated by PKARIα disulfide during oxidant signalling (Figure 4.1). Indeed electrically stimulated isolated ventricular myocytes from PKARα KI mice exhibit delayed decay of their calcium transients compared to WT myocytes (Figure 4.2). This means in PKARα KI mice it takes a greater length of time for SERCA2a to actively pump Ca^{2+} back into the SR. SERCA2a underactivity could potentially be explained by decreased phosphorylation of the PKA substrate phospholamban (PLB), perhaps caused by deficient targeting of C17SPKARIα to an AKAP in the PKA/PLB/SERCA2a signalling complex. The AKAP that is thought to assemble this complex is AKAP7γ/δ as considered in more detail below.

4.1.1 AKAP7

The AKAP7 gene is located on chromosome 6 6q23 encodes for four splice variants α, β, γ and δ that range from 81 to 353 amino acids in length, each targeted to a specific subcellular location with differing functional roles[229]. AKAP7α/β are known as the short isoforms due to truncations at the 5' end compared to the large isoforms AKAP7γ/δ, but all four have a conserved 64 amino acid sequence at the C-terminus that contains the A-kinase binding (AKB) domain and a leucine zipper (Figure 4.3)[230].

The α and β isoforms both contain membrane-targeting motifs located at their N-terminus through myristoylation and dual palmitoylation of one glycine and two cysteine residues

respectively, confirmed by immunofluorescence studies with constructs containing mutations of these critical amino acids (Figure 4.3)[231]. Whilst relatively little is known about AKAP7β, AKAP7α has been shown to co-immunoprecipitate with $Ca_V1.2$ channels isolated from rat heart membrane extracts and skeletal muscle[232,233]. The C-terminus of $Ca_V1.2$ channels interacts with the N-terminal AKAP7 leucine zipper mutation which results in a loss of co-purification and inhibition β-adrenergic regulation of I_{Ca} in rat ventricular myocytes. Similarly, the use of AKB domain peptides disrupted the PKA regulation of $Ca_V1.2$ currents in ventricular myocytes as PKA-dependent phosphorylation of $Ca_V1.2$ channels is necessary to increase open channel probability[232]. However the importance of AKAP7α mediated regulation of $Ca_V1.2$ channels has recently been disputed. It was demonstrated that AKAP7α was not expressed in cardiomyocytes and knockout of AKAP7 had no effect on $Ca_V1.2$ channel phosphorylation after β-adrenergic stimulation[234].

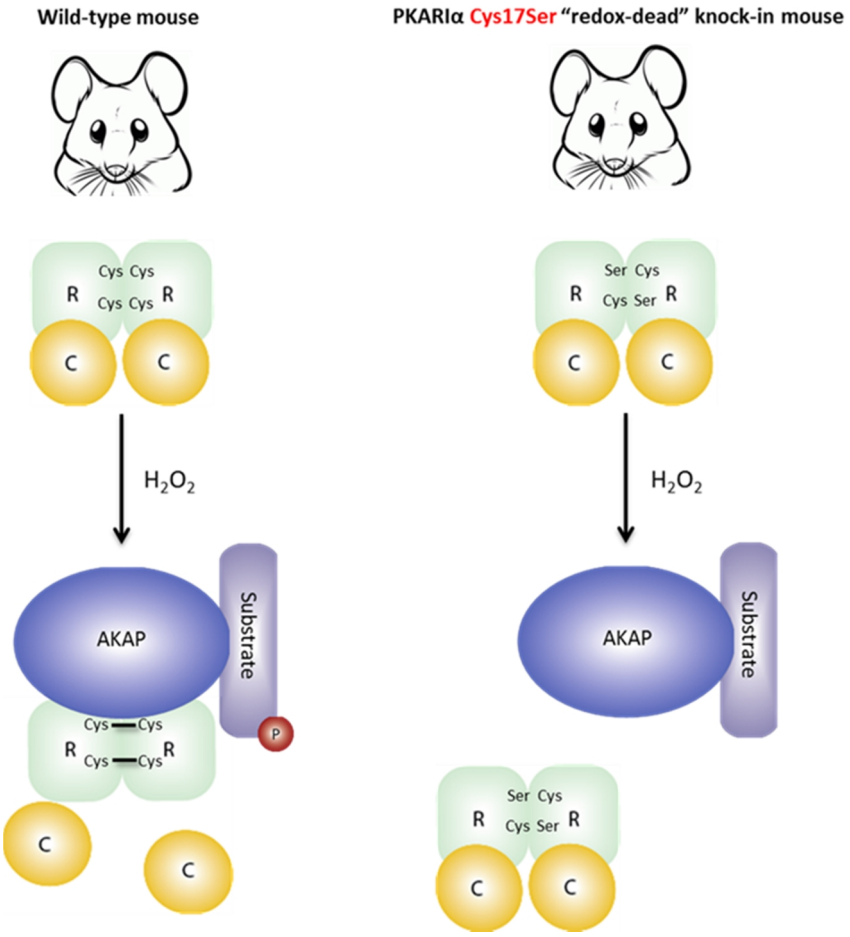

Figure 4.1 Proposed model of PKARIα disulfide dimer in WT vs PKARIα KI mice. Disulfide PKARIα has greater affinity for AKAPs and leads to substrate phosphorylation. PKARIα KI mice would have a lesion in phosphorylation due to aberrant or deficient targeting of Cys17SerPKARIα.

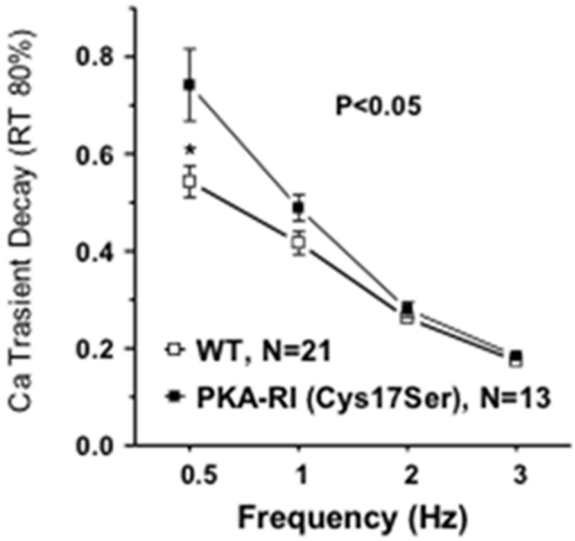

Figure 4.2 Cardiomyocytes from PKARIα KI mice have delayed Ca^{2+} transients. Unpublished data kindly provided by Wagner and Maier (Gottingen University).

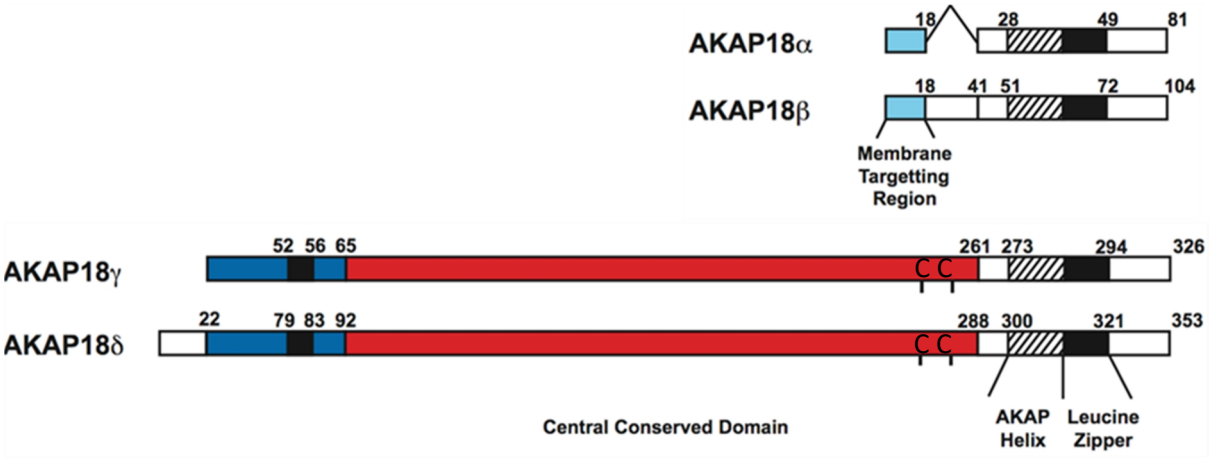

Figure 4.3 Schematic of AKAP7 splice variants α, β, γ, δ. The short isoforms of AKAP7 containing a membrane targeting domain indicated in light blue. Central conserved domain of the large isoforms is highlighted in red. The location of the putative 'redox switch' cysteines are indicated by the black Cs. The dashed lines and adjacent black square is the AKB domain. *Figure adapted from Gold et al. 2008*[229]

4.1.2 Role of AKAP7γ/δ

The long isoforms of AKAP7 have been shown to regulate PLB phosphorylation[140,235], insulin secretion[230,231], and renal homeostasis[236,237]. AKAP7γ has also been shown to bind the lipid-dependent PKC to amplify phosphorylation through this kinase[238,239]. There is conflicting evidence regarding the cellular location of AKAP7γ. Brown *et al.* visualised GFP-AKAP7γ in the nucleus consistent with its N-terminal nuclear localisation signal[240], whilst Trotter *et al.* visualised it diffusely throughout the cytoplasm, but this was likely an artefact due to loss of localisation due to over-expression[149].

The crystal structure of the conserved central domain of both AKAP7γ and δ reveals a bi-lobal and globular α–β-type architecture consisting of four α-helices and eight β-sheets. Each lobe contains four-stranded antiparallel β-sheets, which assemble at the core of the domain (Figure 4.4)[229]. Characterisation of the domain also revealed that AKAP7 interacts with the nucleotide 5'AMP in the physiological micromolar concentrations. 5'AMP is a product of PDE-dependent hydrolysis of cAMP and therefore AKAP7δ may play a role as an AMP sensor, coupling AMP binding to PKA affinity to further regulate cAMP signalling.

There is conflicting evidence as to whether AKAP7 binds to RI and/or RII. The use of cAMP analogues conjugated to agarose beads is an affinity chromatography technique commonly used to enrich PKARI/II, which can also co-capture interacting proteins such as AKAPs. Using this method combined with mass spectrometry-based quantitative proteomics Aye *et al.* described AKAP7 as an RII specific AKAP. The authors used three different immobilized cAMP analogues to enrich for PKAR and its interacting proteins from HEK 293 cells. Stable isotope labelling was used to identify and differentially quantify the four R subunits that were preferentially enriched. This allowed AKAPs that were RI-specific, RII-specific or dual-specific to be determined[121]. In contrast, Brown *et al.* confirmed that AKAP7γ bound RI using a yeast two-hybrid system. The exact region was identified via systematic truncation of AKAP7γ, revealing binding involves the same region previously shown to bind RII. Co-immunoprecipitation using an RI antibody in HEK 293 cells also confirmed the interaction between RI and AKAP7γ[240]. Investigating whether this interaction is influenced by the redox state of RIα is central to the present studies.

The consensus is that AKAP7δ is localised to the SR where it assembles a supramolecular complex of consisting of PKA and PLB in close proximity to SERCA2a, and therefore regulates Ca^{2+} re-uptake back into the SR[140,241,242]. Mutations that disrupt PLB association with AKAP7γ/δ reduced PLB phosphorylation and AKAP7δ siRNA delayed calcium re-uptake in neonatal cardiomyocytes treated with NA. The AKAP7δ binding sequence was mapped to amino acids

13–20 in PLB which overlaps with the PKA phosphorylation site at Ser16[140]. Therefore when phosphorylated PLB does not bind to AKAP7γ/δ which is hypothesised to provide another level of dynamic regulation to facilitate the lowly abundant PKA (100–200 nM) to phosphorylate the relatively highly abundant PLB (50 μM)[235]. AKAP7γ/δ also co-ordinates the dephosphorylation of PLB through interactions with inhibitor-1 (I-1) and protein phosphatase 1 (PP1). PKA phosphorylates I-1 (Ser35) to activate and consequently inhibit PP1, the primary phosphatase responsible for dephosphorylating PLB[241]. This suggests that AKAP7 assembles a signalling complex through binding of activating and deactivating proteins to tightly regulate PLB phosphorylation and therefore SERCA2a activity and the rate of Ca^{2+} re-uptake into the SR. The PKARIα disulfide dimer may further regulate this phosphorylation based on its redox-dependent affinity for AKAP7.

Contrary to this substantive evidence supporting a role for AKAP7γ/δ in cardiomyocytes function, an AKAP7 KO mouse was found to have a normal response to adrenergic stimulation. Both Cav1.2 and PLB were similarly phosphorylated when WT or AKAP7KO mice were compared in response to isoprenaline. Furthermore AKAP7 knock out had no effect on the rate of PLB dephosphorylation[234]. However, the presence of adaptive, compensatory mechanisms in this KO mouse cannot be excluded.

4.1.3 Putative AKAP7γ/δ oxidation

Close examination of the AKAP7δ crystal structure reveals a pair of cysteine residues (Cys268 and Cys 282) on adjacent β-parallel sheets that reside in close proximity to each other (Figure 4.4). The crystal structure also displays Cys282 in two different conformations in space. Therefore it is tempting to speculate that AKAP7δ may exist in a reduced form or an oxidised form involving an intramolecular disulfide bond. Interestingly, these thiol groups are likely to be adjacent to the R binding site (which was not resolved in the crystal structure) and therefore the putative thiol oxidation may alter affinity of the AKB for PKAR, or I speculate may participate in a mixed disulfide AKAP7-PKARIα complex to regulate substrate phosphorylation.

The major aim of this chapter was to establish whether the PKARIα-AKAP interaction is regulated by the redox state of PKARIα. cAMP tethered to agarose beads has been used extensively in the literature to co-purify PKAR subunits with AKAPs and was the primary method used here to investigate the putative redox state-dependent interaction of these proteins. A secondary aim was to determine whether AKAP7 is itself redox regulated, and if so, whether this alters the AKAP's affinity for PKARIα. This led to the development of an assay to determine whether a protein is sensitive to reversible oxidative modifications. The assay requires labelling of reactive thiols with a 5 kDa PEG-maleimide tag which retards protein

migration during SDS-PAGE. The modification can subsequently be visualised by an upward shift of the protein of interest on an immunoblot.

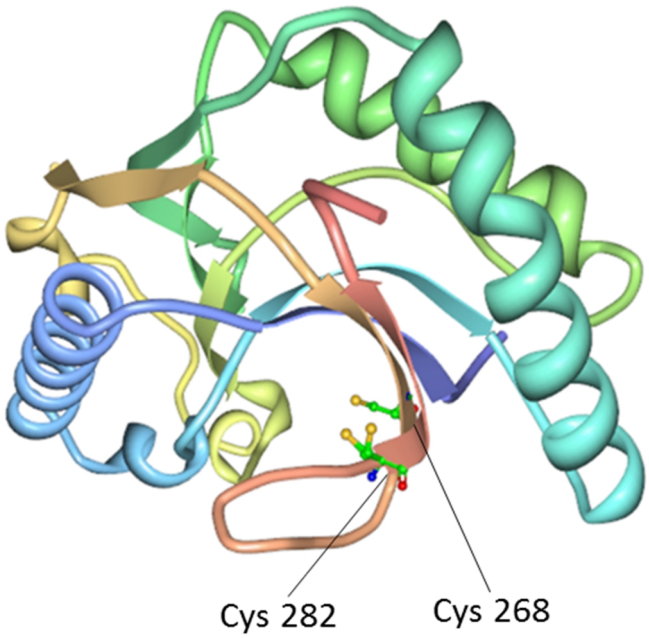

Figure 4.4 Crystal structure of AKAP7δ central domain. The position of the putative 'redox switch' cysteines are shown as ball and stick models. Cys282 is presented in two different conformations. The proximity between the potential disulfide bond in AKAP7δ and the AKB domain in the primary sequence may regulate AKB affinity to PKAR (PDB: 2VFK).

4.2 Specific Methods

4.2.1 Antibodies

Antibody	Purchase Code	Company	Species	Dilution
anti-AKAP7	ab30987	Abcam	Rabbit	1:1000
anti-AKAP7	ARP36331_T100	Aviva Systems Biology	Rabbit	1:1000
anti-AKAP7	ARP36331_T200	Aviva Systems Biology	Rabbit	1:1000
Anti-His	sc-803	Santa Cruz Biotechnology	Rabbit	1:1000
Anti-GFP	11814460001	Roche Applied Science	Mouse	1:1000
anti-DAKAP1	15618-1-AP	Proteintech Europe	Rabbit	1:500
anti-PKGIα	sc-10338, E-17	Santa Cruz Biotechnology	Goat	1:1000
Anti-pDRP1 (ser637)	4867	Cell Signaling Technology	Rabbit	1:500
Anti-SKIP	GTX101952	GeneTex	Rabbit	1:500
Anti-ChChd3	ab99491	Abcam	Goat	1:500
Anti-Strep-HRP	3999	Cell Signaling Technology	-	1:1000

Table 4.1 Antibodies used in Chapter 4

4.2.2 Generation of His-AKAP7δ construct

The cDNA encoding AKAP7δ was amplified by PCR and ligated into a His-TOPO vector to generate His-AKAP7δ. The His-tag was present at the N-terminal end of the AKAP7δ protein. After transformation, DNA was isolated from colonies and the presence of inserts was verified by restriction digestion. Insert DNAs were sequenced to ensure that a particular insert was in-frame with the His-tag.

4.2.3 Generation of GFP-AKAP7γ mutants

GFP-AKAP7γ in pEGFP-C2 was a kind gift from Dr. Carmen Williams (University of Pennsylvania, US). The cysteines residues hypothesised to be susceptible the oxidation in GFP-AKAP7γ were systematically mutated. Amino acid substitutions (C229S), (C243S) and (C229S/C243S) were introduced using the Quik-Change Site-Directed Mutagenesis Kit (Agilent) according to the manufacturer's instructions.

4.2.4 PEG-maleimide switch assay

HEK 293 cells were scraped and harvested in buffer containing 100 mM Tris pH 7.4, 100 mM maleimide and 1% SDS. Each sample was incubated at 50°C for 25 min to increase the efficiency of maleimide-alkylation of free thiols. Excess maleimide was then removed using Zeba^{TM} Spin desalting columns (Thermo Scientific) with elution into fresh tubes. To reduce any oxidant-induced modification, 50 mM DTT was then added to each sample and incubated at room temperature for 20 min. The samples were desalted again to remove the excess DTT and eluted directly into 5 mM PEG-maleimide and 1% SDS. Samples were rotated for 2 hours on a blood wheel at 4 °C. The labelling reaction was quenched with an equal volume of SDS-PAGE sample buffer containing 100 mM maleimide. Samples were run on a non-reducing SDS-PAGE and banding pattern assessed by Western immunoblotting. An overview of the protocol is given in Figure 4.5.

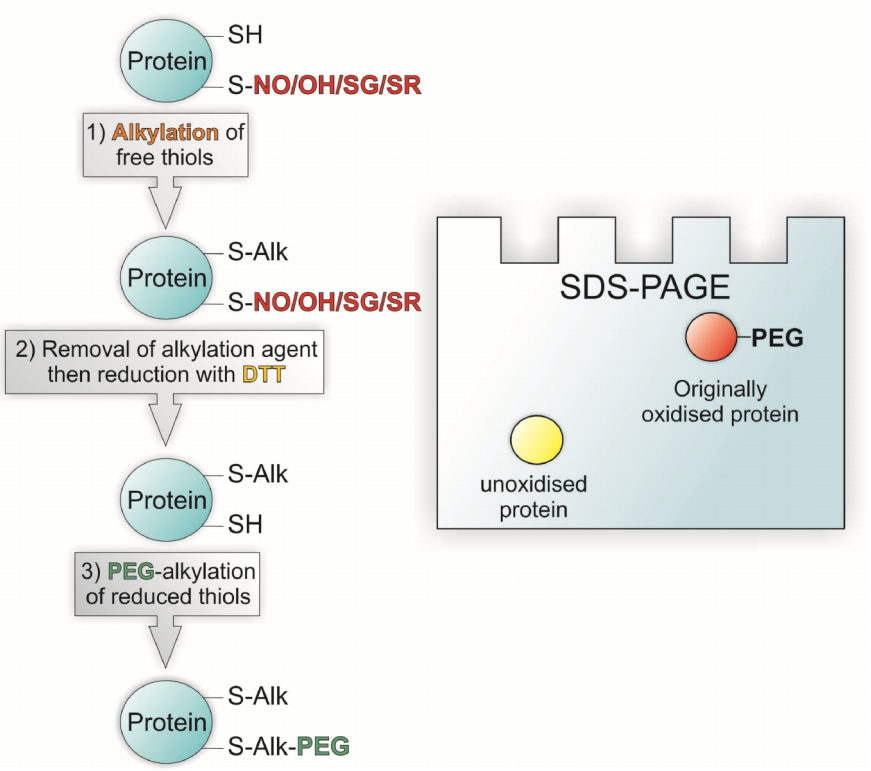

Figure 4.5 Overview of the PEG-maleimide switch method. A target protein containing a thiol residue that has undergone an oxidative modification (-SNO nitrosation, -SOH- sulfenation, -SG- glutathiolation, -SR disulfide bond formation) is shifted on an immunoblot by the PEG-maleimide whilst an unoxidised protein runs at its predicted mass. Cells are lysed in a buffer contain the alkylating agent maleimide. Maleimide irreversibly alkylates free thiol residues leaving any oxidative modification in the protein unaltered. Subsequently DTT is incubated with the lysate to reduce any oxidative modification that was originally present in the protein. These now reduced thiols are free to be alkylated by PEG maleimide. The oxidation state is 'switched' with PEG-maleimide, and therefore only proteins that were originally oxidised should contain the PEG-maleimide, which produces a 5 kDa shift that can be detected on an immunoblot.

4.2.5 Affinity pull down with cAMP-agarose

HEK 293 cells were seeded in 12 well plates to approximately 80% confluent, lysed in ice-cold lysis buffer (100 mM Tris pH 7.4, 100 mM maleimide and 1% Triton X-100) and maintained at 4 °C. Subsequent centrifugation at 15,000 *g* for 15 min in a tabletop Eppendorf centrifuge at 4 °C yielded a soluble supernatant and insoluble fraction. SDS-sample buffer was added to an aliquot of the supernatant and designated as the input. Agarose beads were washed with lysis buffer containing 1% Triton X-100 to minimise non-specific binding. cAMP-agarose beads were then added to the remainder of the soluble fraction and the lysate-bead suspension rotated for 2 hours at 4 °C. Lysates were then centrifuged for 30 seconds at 1500 *g*, SDS-sample buffer was then added to an aliquot of this flow-through and this was designated as the unbound fraction. Subsequently, beads were washed 3 times by centrifugation (1500 *g* for 30 seconds) in wash buffer. Next SDS-PAGE sample buffer was added to the beads for elution. This was the designated as the capture.

Optimisations: The cAMP-agarose experiments were optimised in numerous ways. Initially the dilutions of input, capture, and unbound fractions were kept constant to allow direct comparison of captured proteins across the three fractions. In later experiments, captured proteins were concentrated by eluting in a small volume of SDS-sample buffer (indicated in figure legends) in order to increase the probability of observing co-capture proteins on immunoblots. Numerous cAMP-agarose beads were tested including: 8-(2-aminoethylamino)-adenosine- 3', 5'- cyclic monophosphate (8-AEA-cAMP), 2-(6-aminohexylamino)-adenosine- 3', 5'- cyclic monophosphate (2-AHA-cAMP), 8-(6- aminohexylamino)-adenosine- 3', 5'- cyclic monophosphate (8-AHA-cAMP) (BIOLOG). Furthermore in later experiments HEK 293 cells were seeded in T75 flasks, increasing the concentration of protein in each reaction to ~2 mg/ml. Finally, several buffers were screened to optimise the method and are outlined in section 4.3.5**.**

4.2.6 Affinity pull down with Ni-NTA-agarose

HEK 293 cells seeded in 12 well plates to approximately 80% confluent, lysed in ice-cold lysis buffer (100 mM Tris pH 7.4, 100 mM maleimide and 1% Triton X-100) and the lysate was maintained at 4 °C. Subsequent centrifugation at 15,000 *g* for 15 min yielded a soluble supernatant and insoluble fraction. SDS-sample buffer was added to an aliquot of the supernatant and designated as the input. Ni-NTA-agarose beads were washed with lysis buffer containing 10 mM imidazole to prevent non-specific binding and then incubated with lysates on a blood wheel for 2 hours at 4°C. Beads were subsequently washed three times in lysis

buffer containing 20 mM imidazole, eluted with 250 mM imidazole, before the addition of x2 SDS-PAGE sample buffer.

4.2.7 Caprotec™ capture compound assay

HEK 293 cells were treated as described, washed in ice-cold PBS, lysed (20 mM HEPES pH 7.5, 250 mM sucrose, 150 mM NaCl, 5 mM $MgCl_2$, 0.2% n-dodecyl-β-D-maltoside and protease inhibitor) and underwent freeze-thaw cycles in liquid nitrogen to use the C8-cAMP caproKit™ as per the manufacturer's instructions. Cell lysates were incubated with C8-cAMP capture compound (Figure 4.6) and rotated end-over-end for 30 min at 4°C. Samples were subsequently UV irradiated for 10 min in the caproBox™ (to cross-link C8-cAMP bound PKAR with binding partners) which maintains samples at 4°C. Cross-linked samples were then incubated with streptavidin beads, to capture C8-cAMP bound proteins via the biotin tag, for 30 min at 4°C. Beads were then washed (x5) in the designated wash buffer before the addition of x4 SDS-PAGE sample buffer. Samples were then boiled at 95°C for 5 min to disrupt the streptavidin and biotin interaction.

Optimisation: To increase the efficiency of PKAR capture the concentration of C8-cAMP capture compound was decreased from 10% to 5% (vol/vol).

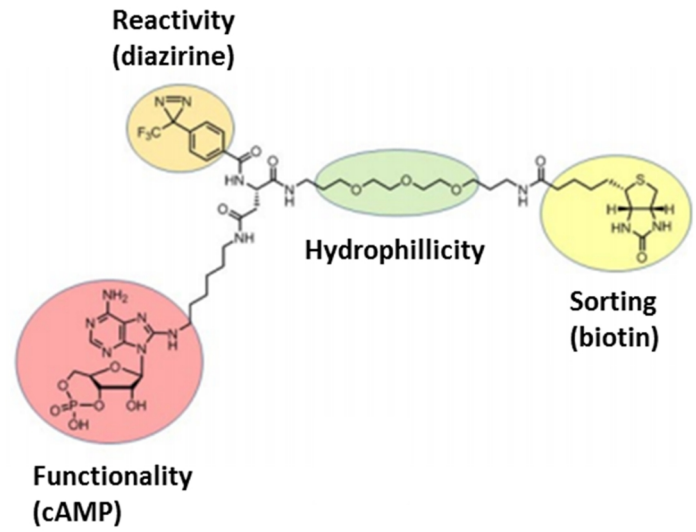

Figure 4.6 Caprotec™ C8-cAMP capture compound used in cross-linking experiments. *Figure adapted from Lou et al. 2009[243].*

4.3 Results

The Cysteine Oxidation Prediction Algorithm (COPA) is able to predict with 80.4% accuracy whether a cysteine is susceptible to reversible oxidation using 11 parameters that include distance to the nearest cysteine sulphur, the solvent-accessible surface area of the target cysteine thiol and distance to the nearest basic amino acid[244]. COPA predicts that by virtue of the proximity between Cys268 and Cys282 in the central conserved domain of AKAP7δ these cysteines are susceptible to oxidation, despite their relatively high pK_a (Table 4.2).

Cysteine Residue	pKa	Oxidation Status	Prediction
268	12.78	RED	SOD
282	8.49	RED	SOD

Table 4.2 Cysteine Oxidation Prediction Program analysis of AKAP7δ cysteines based on crystal structure

4.3.1 Investigating AKAP7 migration on immunoblots

To determine whether AKAP7 was sensitive to oxidative modifications it was necessary to obtain an antibody that could detect AKAP7 in various tissues. Inter- and intramolecular disulfide bonds can potentially be detected by immunoblotting. For example, the migration after SDS-PAGE of oxidised PTEN is subtly altered due to the presence of an intramolecular disulfide bond[245] whilst inter-protein disulfide can be detected by retardations of migration as seen with PKARIα in Chapter 3. It was expected that commercial antibodies would be able to detect both the AKAP7γ and AKAP7δ isoforms due to the similarity between their primary sequences.

Isolated rat hearts and ARVMs were treated with various concentrations of H_2O_2 (0-500 µM) and AKAP7 gel migration was analysed using commercially available AKAP7 antibodies. Figure 4.7 shows a representative blot from rat heart homogenate and ARVMs of one such antibody (ARP36331_T200 from Aviva System Biology) used to detect AKAP7. The profile of all the AKAP7 antibodies used was similar, producing many bands on an immunoblot, the pattern of which changed depending on the tissue, H_2O_2 treatment, the presence of maleimide in the sample buffer and whether the samples had been boiled or not. As such it was difficult to have confidence that any of the bands definitively represented either AKAP7 isoform.

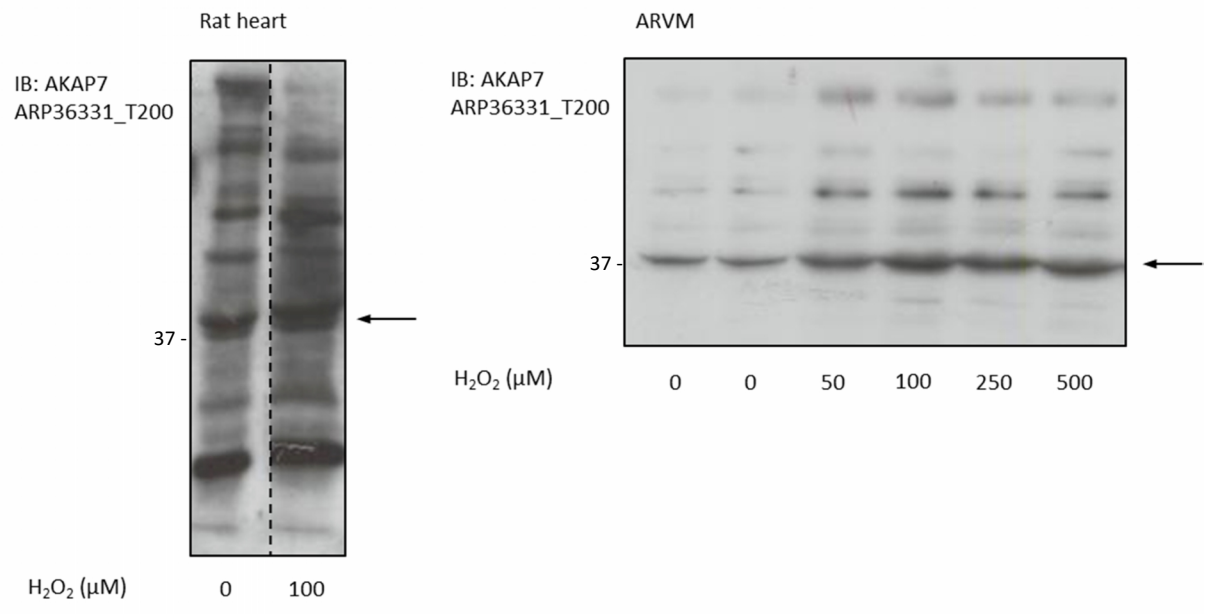

Figure 4.7 Commercial AKAP7 antibodies produce multiple bands in rat heart homogenate and ARVMs. (**A**) Rat heart homogenate was perfused with 100 μM H_2O_2 (**B**) ARVMs were treated with 0-500 μM H_2O_2. Immunoblots probed with anit-AKAP7 (ARP36331_T200). Black arrows indicate expected molecular weight of AKAP7.

Unfortunately, a significant period of time was spent attempting to optimise these immunoblotting conditions and interpret immunoblots using these commercial antibodies to AKAP7. Due to the uncertainty of which, if any, band represented AKAP7 it was decided to switch to an over-expression system to achieve confidence in detection. HEK 293 cells were transfected with titrated concentrations of either His-AKAP7δ or GFP-AKAP7γ DNA to optimise protein expression as monitored by immunoblotting (Figure 4.8A and B). It was decided that 500 ng/ml and 250 ng/ml were an optimal concentrations of His-AKAP7δ and GFP-AKAP7γ DNA to use respectively. It was also salient that the commercial antibodies were unable to detect either of the over-expressed AKAP7 isoforms (Figure 4.8C and D). Thus all subsequent experiments investigating AKAP7 were conducted in transiently transfected HEK 293 cells and protein detection was facilitated by antibodies to their respective affinity tags.

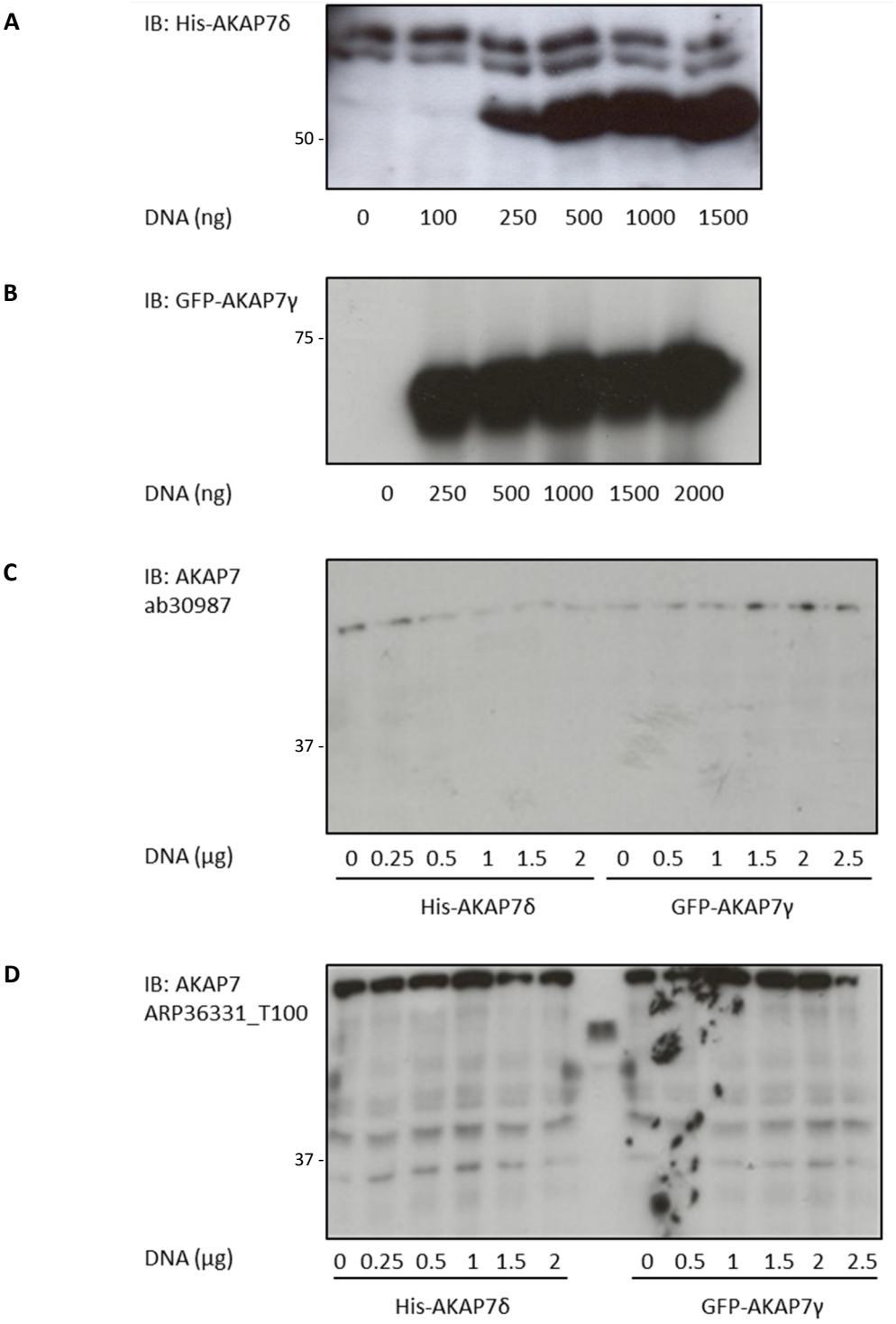

Figure 4.8 AKAP7 commercial antibodies failed to detect His-AKAP7δ or GFP-AKAP7γ. HEK 293 cells were transfected with His-AKAP7δ (0-2000 ng) or GFP-AKAP7γ (0-2500 ng) DNA and were harvested after 24 hours. Immunoblots were probed with anti-His, anti-GFP, anti-AKAP7 (ab30987) or anti-AKAP7 (ARP36331_T100).

The migration of His-AKAP7δ and GFP-AKAP7γ was assessed by SDS-PAGE under non-reducing or reducing conditions after transfected HEK 293 cells were challenged with 0-500 µM H_2O_2. There was no identifiable shift in migration of His-AKAP7δ either with H_2O_2 treatment or after samples were analysed in the presence of the reductant 2-mercaptoethanol (Figure 4.9A). Under control conditions GFP-AKAP7γ ran just below 75 kDa, with a small proportion of the protein possibly aggregating at the top of the above the 200 kDa marker (Figure 4.9B). The putative inter-protein disulfide between AKAP7γ and PKARIα would be expected to form at approximately 125 or 175 kDa depending on whether the two R subunits were disulfide linked too. Thus these ultra-high bands were considered likely to be aggregatory artefacts caused by H_2O_2 treatment.

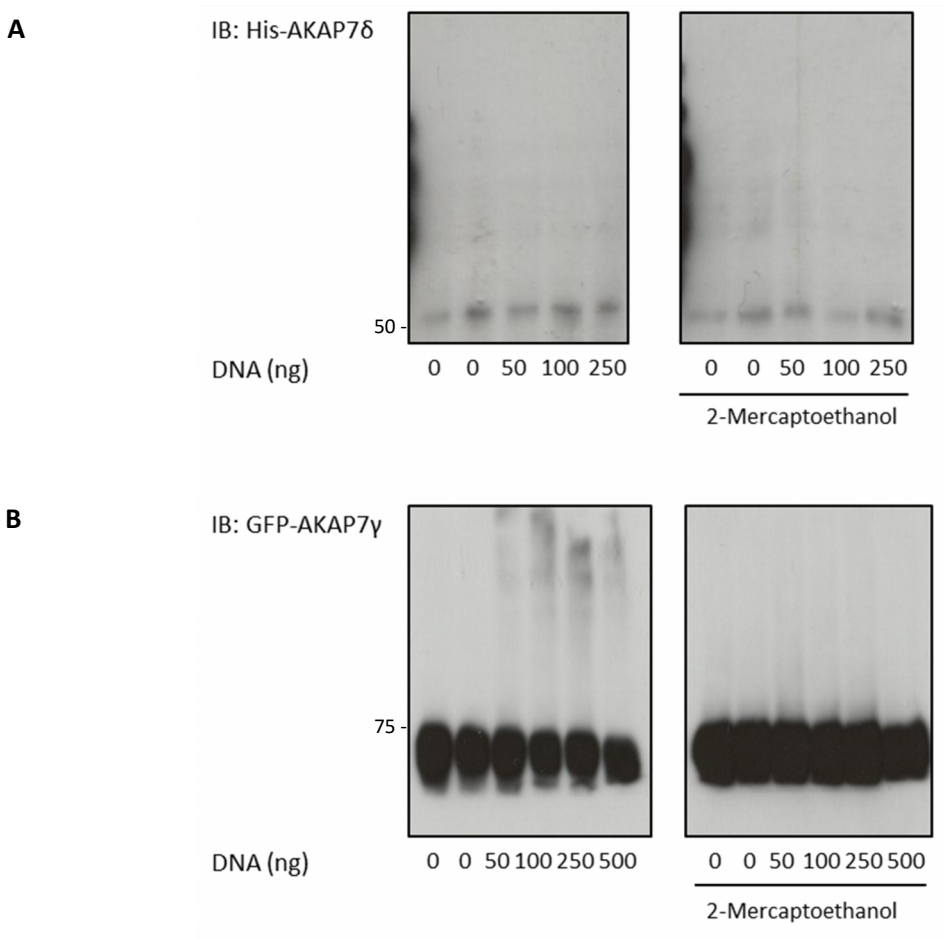

Figure 4.9 AKAP7 migration on SDS-PAGE remains unaltered with H_2O_2 treatment. HEK 293 cells transfected with either (**A**) His-AKAP7δ or (**B**) GFP-AKAP7γ were treated with H_2O_2 (0-500 µM) for 10 min. Samples were run in parallel in the presence of 2-mercaptoethanol (5%) for full reduction. Immunoblots were probed with anti-His or anti-GFP respectively.

4.3.2 Optimisation and validation of PEG-maleimide switch method

The PEG-maleimide switch method was a technique developed during these studies to analyse proteins, such as AKAP7, that may be susceptible to reversible oxidative modifications. The 5kDa PEG-maleimide adducts to thiol residues that are susceptible to oxidation, thus retarding the migration of the protein during SDS-PAGE. Throughout development and validation of this novel method PKARIα and PKGIα were used as readouts as they are known to undergo reversible thiol oxidation.

In HEK 293 cells treated with H_2O_2 (100 μM) PKGIα exhibited PEGylation following processing with PEG-maleimide switch assay (Figure 4.10). The higher 50 mM concentration of DTT used in the reduction step of the assay slightly improved the extent of PEGylation compared to 20 mM, and thus became the standard concentration used in the subsequent experiments. However the addition of SDS during the reduction step was found to be unnecessary. Having successfully applied the protocol to cell models, the method was then assessed for its utility in the analysis of cardiac tissue. Both PKARIα and PKGIα were found to be PEGylated, thus indicating oxidation, in heart exposed to H_2O_2 for 10 min but not in controls (Figure 4.11). To validate the specificity of the method, calsequestrin, a protein not known to be susceptible to thiol redox modifications was assessed using the PEG-maleimide switch method. There was no shift in calsequestrin in heart samples that were assayed, consistent that it is indeed insensitive to reversible oxidative modifications and that the method is able to discriminate between redox sensitive proteins and proteins that are not susceptible to reversible oxidative modifications (Figure 4.11).

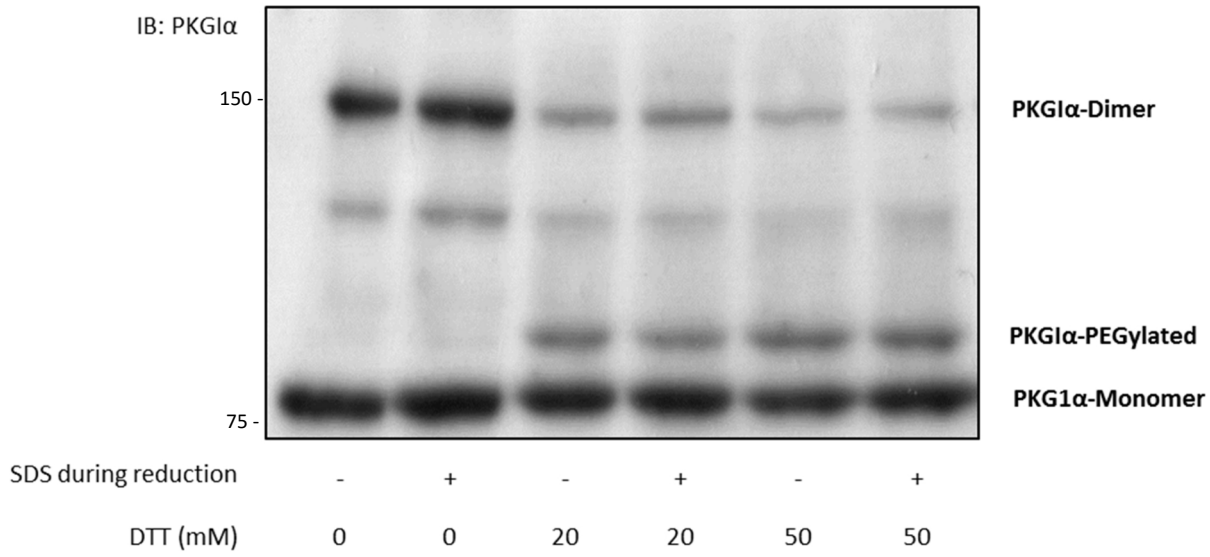

Figure 4.10 Characterisation of the PEG-switch assay in HEK 293 cells. HEK 293 cells were treated with H_2O_2 (100 µM) and lysates underwent PEG-maleimide switch processing. The reduction step of the process was carried out using various concentrations of DTT (0-50 µM) in the absence or presence of 1% SDS. Immunoblot was probed with anti-PKGIα.

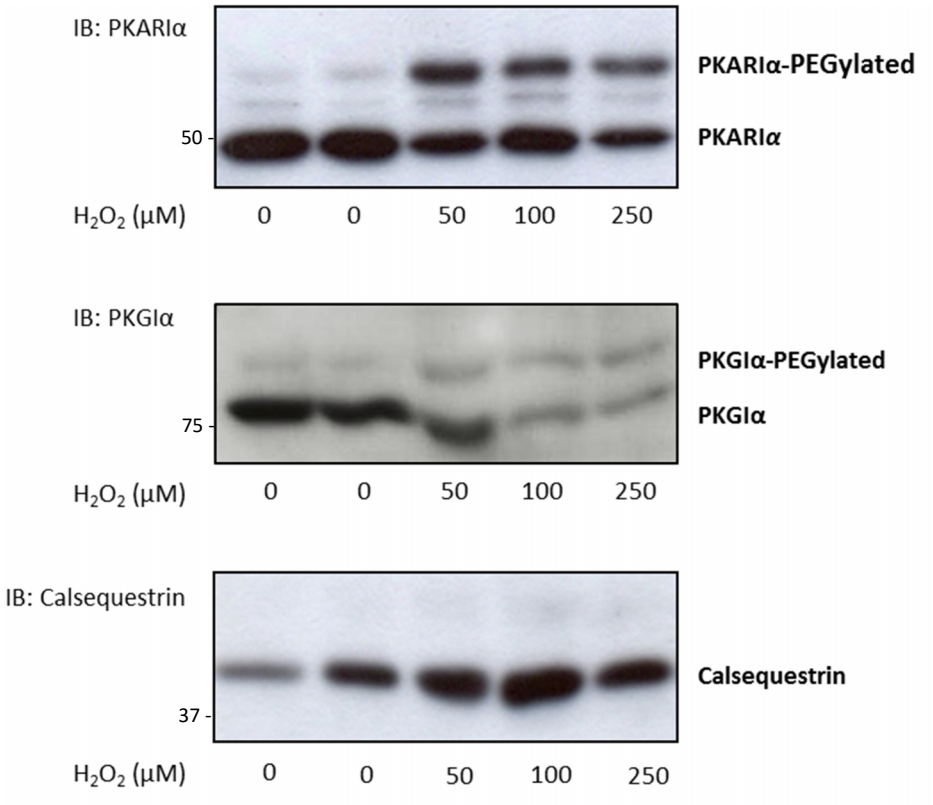

Figure 4.11 PKARIα and PKGIα but not calsequestrin are sensitive to reversible oxidative modification. Rat hearts were perfused with H_2O_2 (0- 250 µM) for 10 min, homogenised and underwent PEG-maleimide switch processing. Immunoblots were probed with anti-PKARIα, anti-PKGIα or anti-calsequestrin.

The method was then applied to HEK 293 cells that had been transfected with GFP-AKAP7γ. GFP-AKAP7γ did not shift in vehicle-treated cells but did demonstrate a H_2O_2 concentration-dependent PEGylation indicating that AKAP7γ may be susceptible to reversible oxidation (Figure 4.12A). As the GFP protein itself contains two cysteine residues it was necessary to confirm that the observed shift in GFP-AKAP7γ was not due to the oxidation of those thiols. Consequently GFP was transfected into HEK 293 cells but was not PEGylated after the samples were processed using the PEG-maleimide switch method, indicating that the oxidation of cysteines in GFP are not responsible for the labelling (Figure 4.12B). To establish which cysteines are responsible for the putative disulfide bond that would explain the reductive-labelling of GFP-AKAP7γ, the cysteine residues were systematically mutated to serine residues to form three new GFP-AKAP7γ constructs. These included GFP-C229SAKAP7γ (C229S), GFP-C243SAKAP7γ (C243S) and the double mutant GFP-C229S/C243SAKAP7γ (C229/C243). Mutations of these cysteines should result in abrogation of the PEGylation. Surprisingly all three constructs exhibited PEG-maleimide shifts that were comparable to wild type GFP-AKAP7γ indicating that these cysteines were not responsible for the previously observed PEGylation (Figure 4.12C). This unexpected observation using the cysteine mutants would appear fully at odds with AKAP7γ being susceptible to disulfide formation. Since the cysteine residues are conserved between AKAP7γ and AKAP7δ it is reasonable to suggest that the two isoforms would demonstrate similar levels of susceptibility to redox modification. Indeed AKAP7δ was not PEGylated after PEG-maleimide switch processing suggesting that it was not susceptible to reversible redox modification (Figure 4.12D).

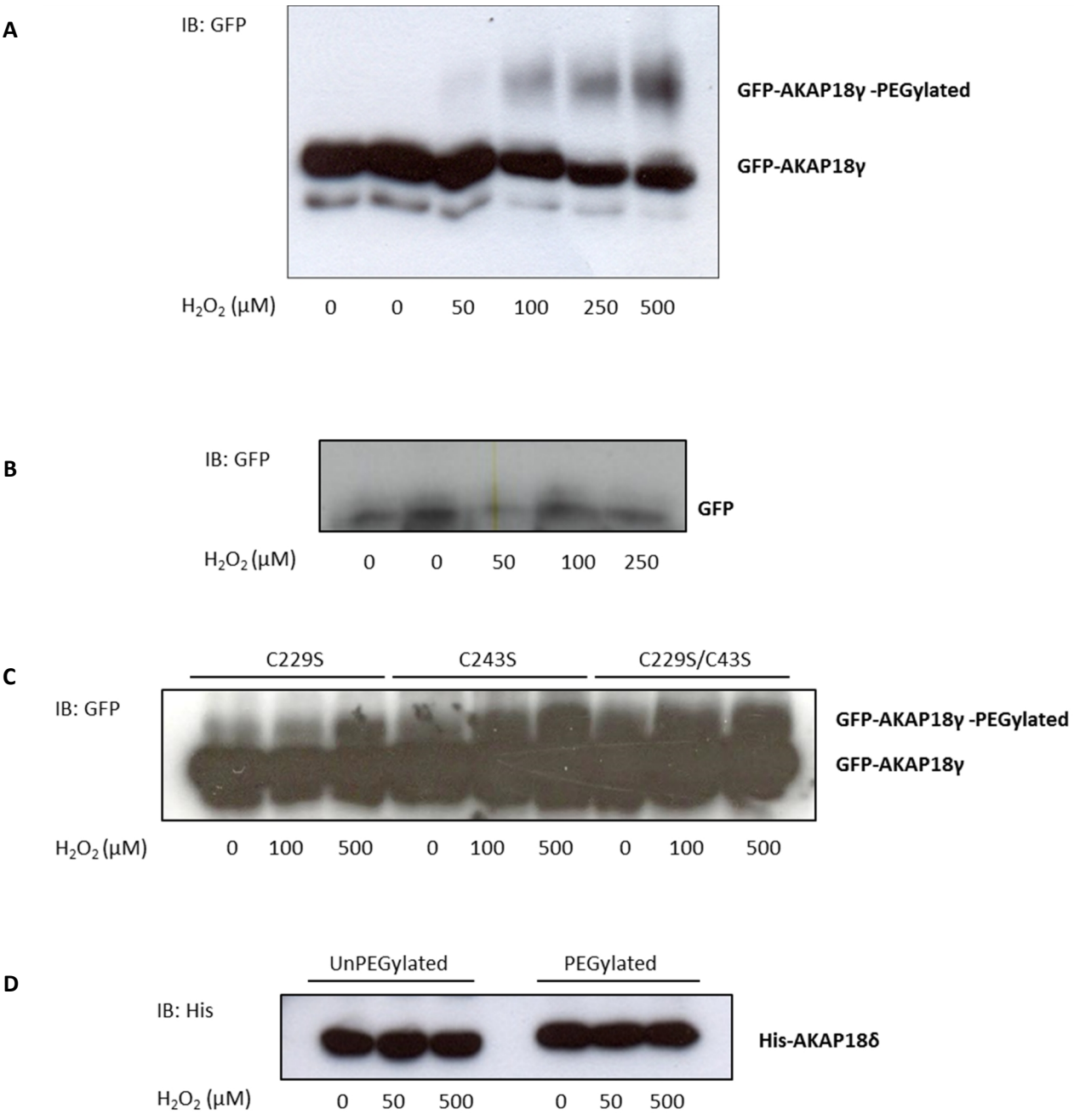

Figure 4.12 PEG-maleimide switch analysis provides evidence that AKAP7 can be reversibly oxidised. HEK 293 cells were transfected with (**A**) GFP-AKAP7γ, (**B**) GFP alone, (**C**) C229S, C243S or C229/C243 or (**D**) His-AKAP7δ. Cells were treated with H_2O_2 (0-500 μM) 24 hours post-transfection, lysed and underwent PEG-maleimide switch processing. Immunoblots were probed with either anti-GFP or anti-His as appropriate.

4.3.3 Investigating the AKAP7 and PKARIα interaction with immunofluorescence

Immunofluorescent imaging allowed visualisation of co-localisation between AKAP7 and PKARIα and determination of whether this interaction was dependent on the redox state of PKARIα. HEK 293 cells were transfected with His-AKAP7δ or GFP-AKAP7γ prior to treatment with vehicle or H_2O_2 (500 μM) and detection was enabled by the His-antibody for AKAP7δ, GFP for AKAP7γ and anti-PKARIα. Transfection efficiency was not determined, but above experiments indicated that both AKAPs were expressed in HEK 293 cells without gross detriment to cell viability. Furthermore cells transfected with GFP-AKAP7γ were visualised using the microscope prior to commencement of the immunofluorescence protocol to ensure protein expression. Both AKAP7 isoforms appeared to accumulate in the nucleus whilst AKAP7δ also appeared in the nuclear membrane (Figure 4.13 and 4.14). In some cells AKAP7 was present diffusely throughout the cytoplasm. PKARIα was consistently found diffusely throughout the cytoplasm and also in the nucleus, but did not appear to co-localise specifically with either AKAP. Additionally there was no detectable change in subcellular location of any of the proteins upon the addition of H_2O_2.

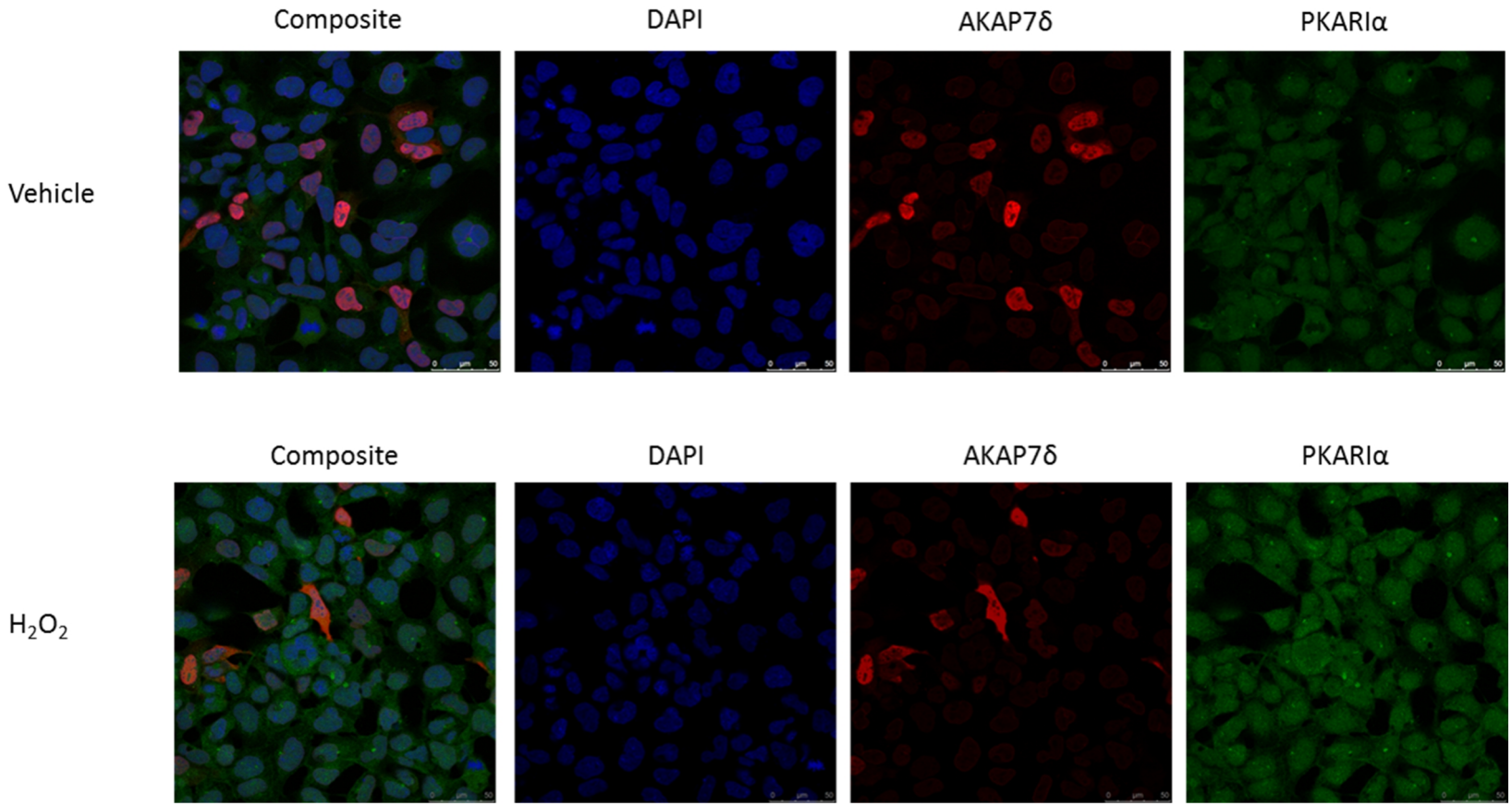

Figure 4.13 AKAP7δ does not co-localise with PKARIα in HEK 293 cells. Representative immunofluorescent image. HEK 293 cells were treated with vehicle or 500 µM H_2O_2 and then stained with AKAPδ (red) and PKARIα (green) antibodies. The nucleus was stained with b4',6-diamidino-2-phenylindole (DAPI, blue).

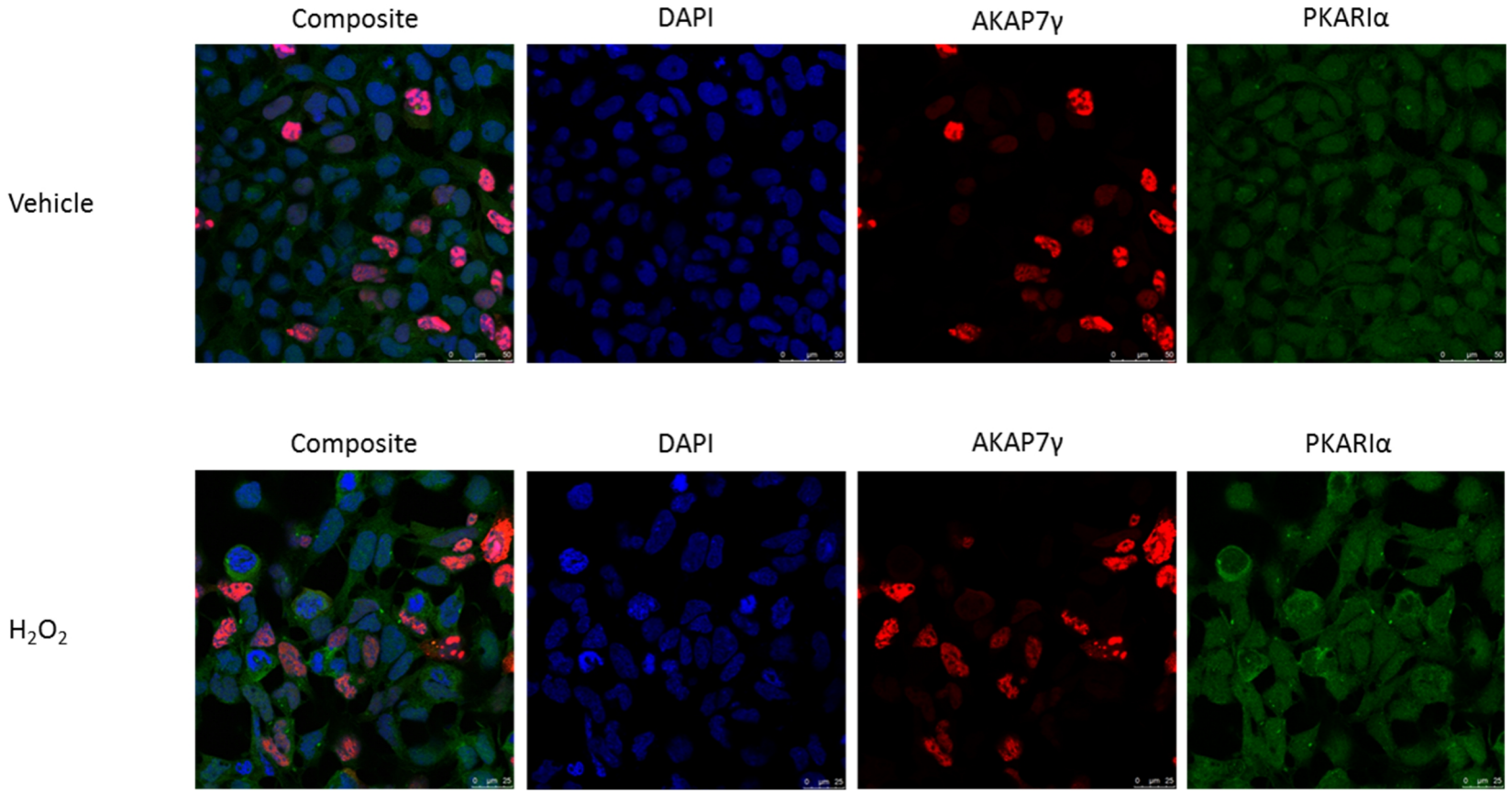

Figure 4.14 AKAP7γ does not co-localise with PKARIα in HEK 293 cells. Representative immunofluorescent image. HEK 293 cells were treated with vehicle or 500 µM H_2O_2 and then stained with the PKARIα (green) antibody whilst GFP-AKAP (red) was visualised using GFP tag. The nucleus was stained with b4',6-diamidino-2-phenylindole (DAPI, blue).

4.3.4 Investigating the His-AKAP7δ interaction with PKARIα and PKARIIα using Ni-NTA-agarose

The working hypothesis being tested was that during oxidative conditions the PKARIα disulfide dimer will bind to His-AKAP7δ with greater affinity than under control conditions when the thiols of RIα are in the reduced state (Figure 1.10). One method to investigate this putative redox-dependent interaction between PKARIα and AKAP7δ was to utilise the affinity His tag on His-AKAP7δ has for nickel ions immobilised on agarose beads, attempting to co-purify PKARIα from HEK 293 cell lysates with it. His-AKAP7δ was successfully purified from lysate in vehicle treated and H_2O_2 (500 µM) treated HEK 293 cells. However, PKARIIα, but not PKARIα, was unexpectedly co-captured with His-AKAP7δ using Ni-NTA-agarose and this association tended to increase with exposure to H_2O_2 (Figure 4.15). The co-capture of PKARIIα was specifically due to its interaction with His-AKAP7δ as PKARIIα was not pulled down in cells that were not transfected with His-AKAP7δ.

Previous experiments using the PEG-maleimide switch method indicated that His-AKAP7δ was not susceptible to reversible oxidative modifications. Therefore it was considered that an oxidative modification on PKARIIα may be responsible for the H_2O_2-dependent increase in affinity between the two proteins. To investigate whether PKARIIα was susceptible to reversible oxidative modifications HEK 293 cells and rat hearts were treated and perfused respectively with various concentrations H_2O_2 (0- 500 µM) and the PEG-maleimide switch assay was performed. Immunoblotting demonstrated that PKARIIα became PEGylated in samples that had been challenged with H_2O_2 suggesting that PKARIIα is susceptible to reversible oxidative modifications (Figure 4.16). Therefore the redox state of PKARIIα may modulate its affinity for His-AKAP7δ.

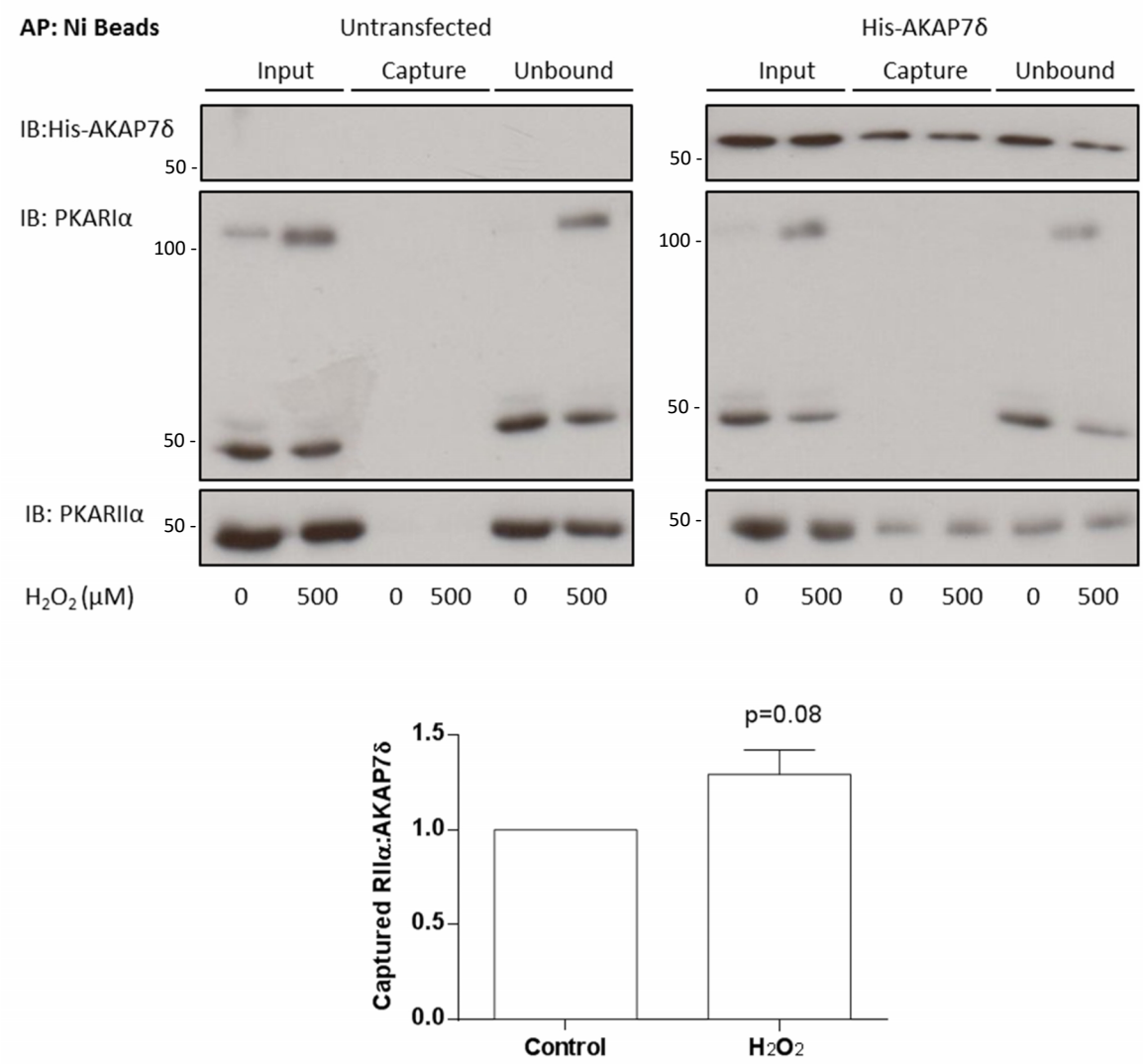

Figure 4.15 AKAP7δ interacts with PKARIIα. Untransfected or His-AKAP7δ transfected HEK 293 cells were treated with H_2O_2 (500 μM) and lysates were incubated with Ni-NTA-agarose. Immunoblots were probed with anti-His, anti-PKARIα or anti-PKARIIα. The extent of PKARIIα capture was is represented graphically (n=5 ± SEM)

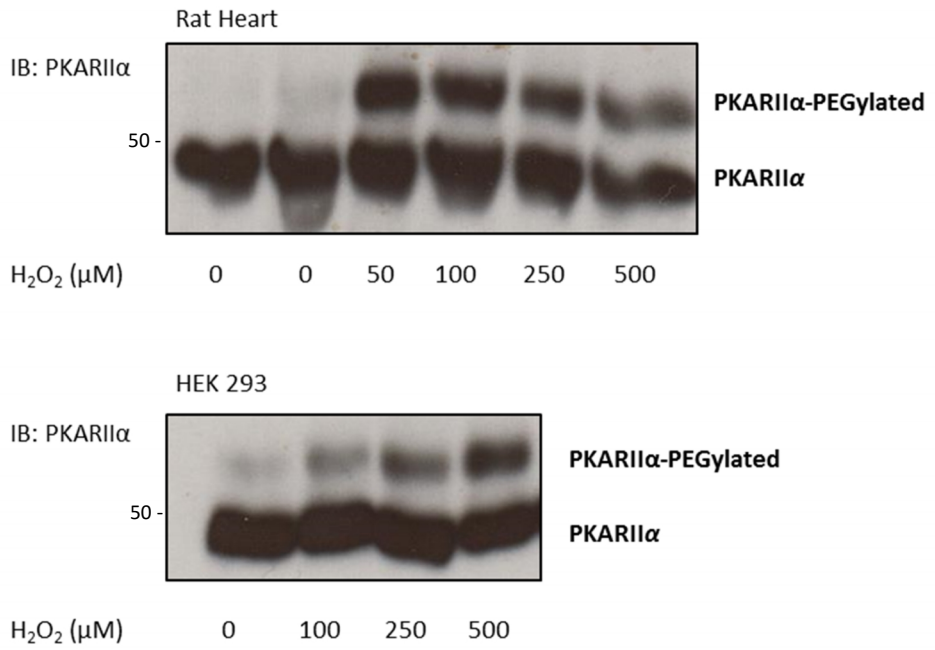

Figure 4.16 PKARIIα is sensitive to reversible oxidative modification. Rat hearts were perfused or HEK 293 cells were treated with H_2O_2 (0- 500 μM) for 10 min, homogenised and underwent PEG-maleimide switch processing. Immunoblots were probed with anti-PKARIIα.

4.3.5 Investigating the interaction between PKAR subunits and AKAP7δ and AKAP7γ using nucleotides immobilised on agarose beads

Experiments were conducted using various analogues of cAMP immobilised on agarose beads via a flexible spacer in the 2'or 8' position on the adenine ring. These serve as bait for PKARIα which may co-purify with AKAP7δ, AKAP7γ or other AKAPs. Again by treating HEK 293 cells with either vehicle or H_2O_2 it may be possible to determine if PKARIα has increased affinity for AKAPs under oxidative conditions compared to controls.

HEK 293 cells were transfected with His-AKAP7δ or GFP-AKAP7γ, treated with H_2O_2 (0- 500 µM) one day post transfection and subsequently harvested. Lysate was incubated with cAMP-agarose for 2 hours, beads were washed and captured proteins were eluted using SDS-sample buffer. PKARIα was present in the capture consistent with the protocol working (Figure 4.17). PKARIα was not present in the unbound fraction which suggests that the capture was efficient, but interestingly and of particular note it was predominantly captured as a monomer despite having initially been oxidised. This observation forms the basis of my investigations documented in Chapter 5 where it is considered in more detail. Unfortunately neither AKAP7 isoform was co-captured with PKARIα (Figure 4.17). Before concluding that the proteins do not interact, I attempted to optimise the experimental conditions to promote likelihood of AKAP7 being co-captured. This is outlined in the methods section; briefly it included using different types and lengths of linker that conjugated cAMP to the agarose, experimenting with different incubation or wash buffer compositions, varying the volume of beads and the volume of HEK 293 cell lysate, and testing different elution protocols. It was not deemed necessary to extensively document all of these optimisations below, but some key steps are included below. However, the essential message was this extensive optimisation unfortunately did not lead to the co-capture of AKAP7 and PKARIα.

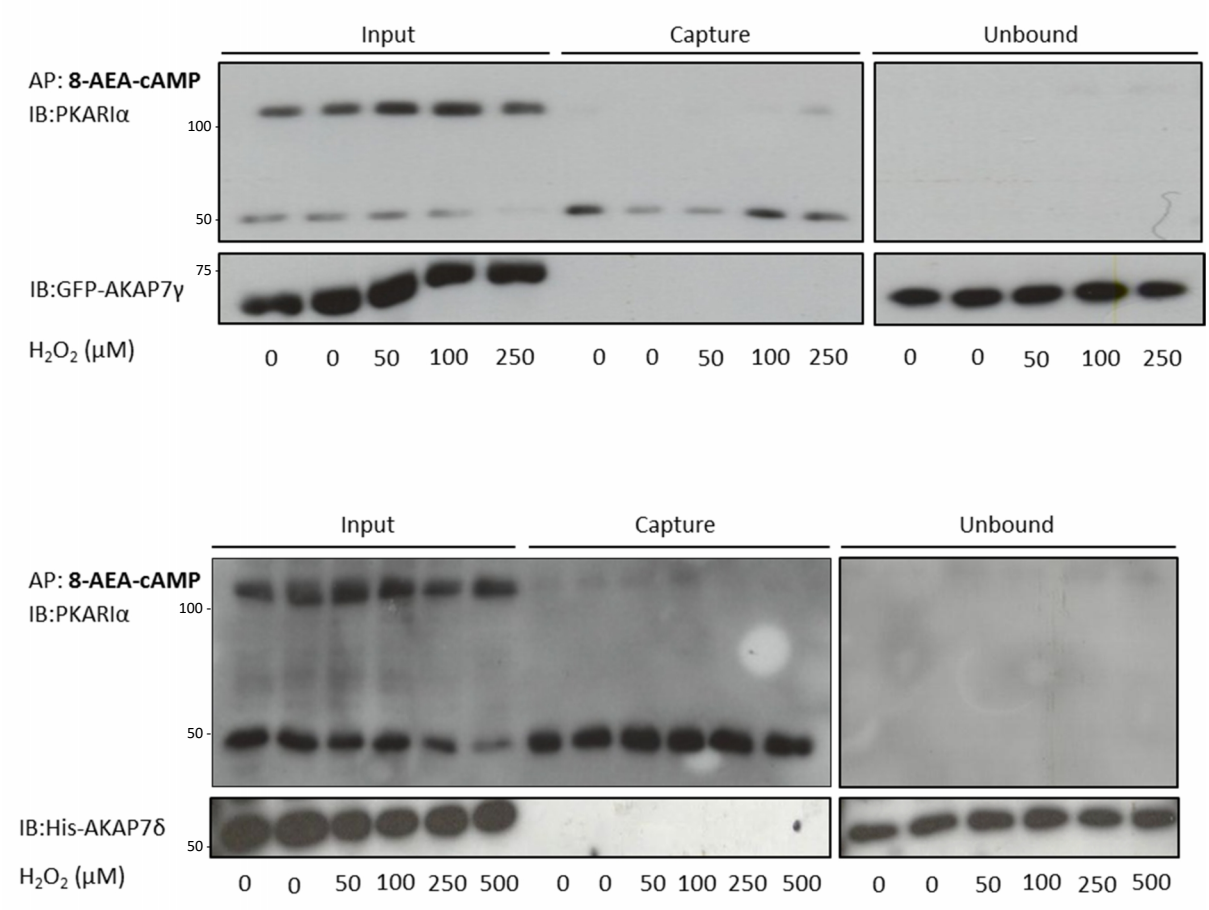

Figure 4.17 AKAP7 is not co-captured with PKARIα. AKAP7δ or AKAP7γ were transfected into HEK 293 cells and treated with H_2O_2 (0-500 μM) and lysates were incubated with 8-AEA-cAMP-agarose. Immunoblots were probed with anti-PKARIα, anti-GFP or anti-His.

cAMP-agarose has been used in many studies to co-capture PKA regulatory subunits with AKAPs. The authors of these articles have used many different buffer compositions and have successfully co-captured AKAPs with PKA. Different buffers were comprehensively screened to determine the best method for AKAP co-capture, with DAKAP-1 being used as a positive control. In these experiments 11 different buffers were used and are outlined in Table 4.3. HEK 293 cells were lysed in the designated buffer, none of which contained maleimide to replicate studies from the literature and PKARIα was captured in all of the experiments and predominantly in the disulfide dimer form (Figure 4.18). DAKAP1 was co-captured only with buffers 3, 7 and 9. A comparison of PKARIα in the input vs. the unbound fraction gave an indication of how efficient the captures were and thus, Buffer 3 was used in subsequent analyses.

Number	Buffer	Detergent	Additional Components	Source
1	100 mM Tris pH 7.4	1% Triton-X100	150 mM NaCl	-
2	100 mM Tris pH 7.4	1% Triton-X100	150 mM NaCl, 1mM EDTA, 1mM EGTA	-
3	100 mM Tris pH 7.4	none	150 mM NaCl	-
4	50 mM Tris pH 7.4	1% NP-40, 0.5% $C_{24}H_{39}NaO_4$, 0.1% SDS	500 mM NaCl	[246]
5	50 mM Tris pH 7.4	0.5% Triton-X100	150 mM NaCl, 1 mM EDTA	[247]
6	20 mM MOPS pH 7.0	1% Triton-X100	150 mM NaCl, 10 mM $MgCl_2$,	[248]
7	20 mM MOPS pH 7.0	none	10 mM NaCl, 2 mM EDTA, 2 mM EGTA	[249]
8	20 mM HEPES pH 7.4	1% Triton-X100	150 mM NaCl, 5 mM EDTA	-
9	50 mM K_2HPO_4 pH 7.0	0.1% Tween-20	150 mM NaCl	[121]
10	10 mM K_2HPO_4 pH 7.0	1% Triton-X100	150 mM NaCl, 5 mM EDTA	[236]
11	20 mM HEPES pH 7.5,	0.1% n-dodecyl-β-D-maltoside	250 mM sucrose, 150 mM NaCl, 5 mM $MgCl_2$	[243]

Table 4.3 Table of buffers screened in cAMP-agarose experiments

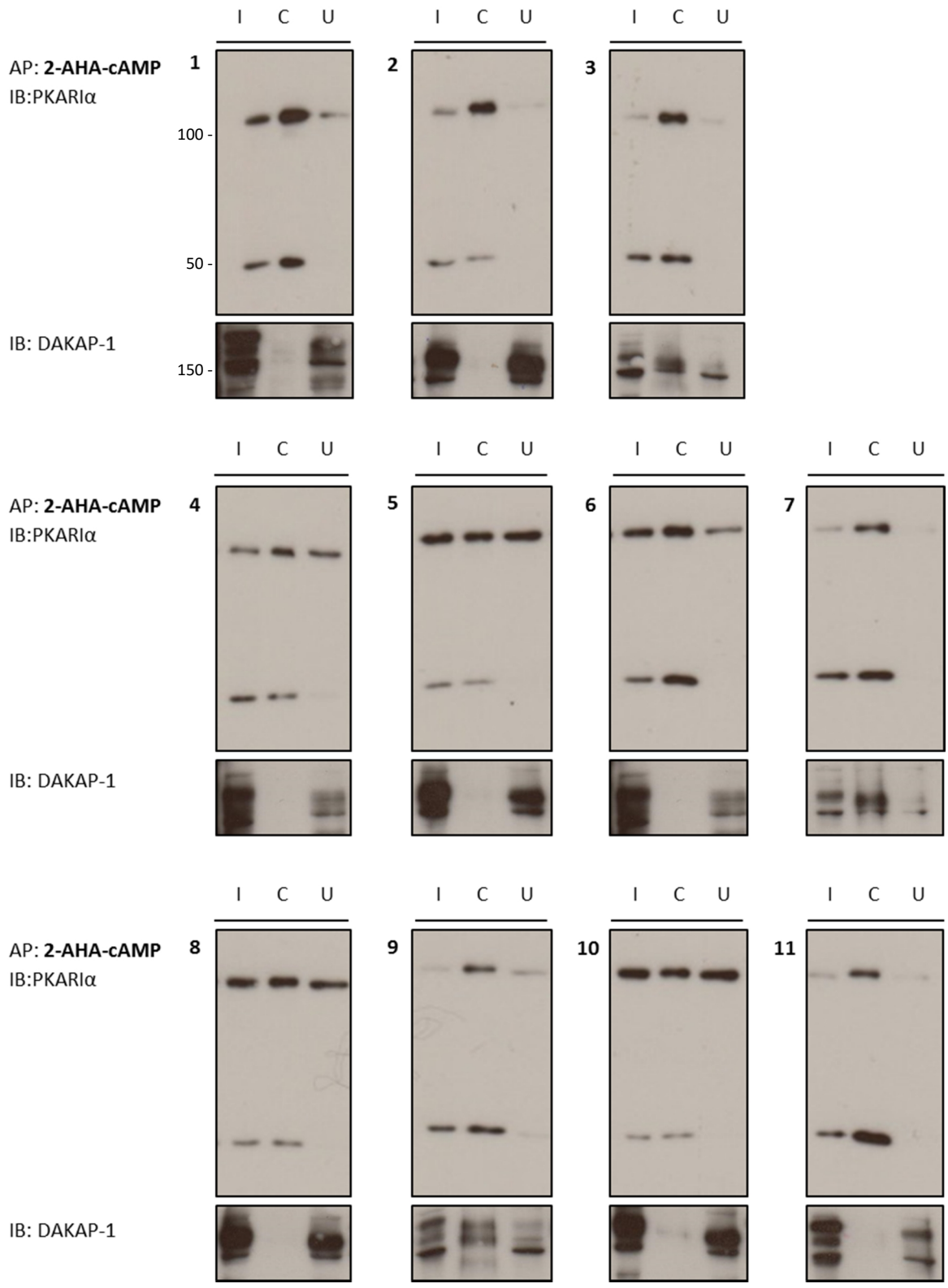

Figure 4.18 Buffer screen for cAMP-agarose capture in HEK 293 cells. 11 different buffers (outlined in Table 4.3) were used in cAMP-agarose experiments to co-capture DAKAP-1. HEK 293 cells were lysed (without maleimide) in the designated buffer and lysates incubated with 2-AHA-cAMP-agarose. I- input, C- capture, U- unbound. Captures were x20 concentrated compared to input. Immunoblots were probed with anti-PKARIα or anti-DAKAP-1.

Capture experiments with Buffer 3 (100 mM Tris-HCl, pH 7.4, 150 mM NaCl, no detergent) were scaled-up to increase the protein in each assay to approximately 2 mg/ml. Maleimide was added to allow comparison of vehicle- and H_2O_2-treated captures. Figure 4.19 shows PKARIα was efficiently captured but neither the established PKARIα-specific AKAP, SKIP, nor its associated PKA substrate, ChCHd3, were co-captured. DAKAP1 was co-captured as previously observed although its known binding partner DRP1 was not. Despite this the phosphorylation of DRP1 appeared to increase with H_2O_2 treatment and this warranted further investigation.

To confirm that the co-capture of DAKAP1 was due specifically to its interaction with PKARIα and not due to non-specific binding to the agarose, HEK 293 cells were treated with H_2O_2 (0-500 μM) and lysed in buffer 3. As a negative control cAMP (1 mM) was added to compete for PKARIα binding during the incubation step. PKARIα and DAKAP1 were captured as previously observed. However in samples that were incubated with cAMP, PKAR binding was significantly abrogated but the extent of DAKAP1 capture remained the same, indicating that it was likely to be bound non-specifically to agarose (Figure 4.20A). Furthermore examination of the phospho-status of DRP1 revealed no significant difference when HEK293 cells were treated with on with H_2O_2, 8-CPT-cAMP alone or H_2O_2 with 8-CPT-cAMP (Figure 4.20B). Given that the interaction between PKARIα and DAKAP1 could not be established it was decided against pursuing further studies using this method to capture PKARIα and AKAPs.

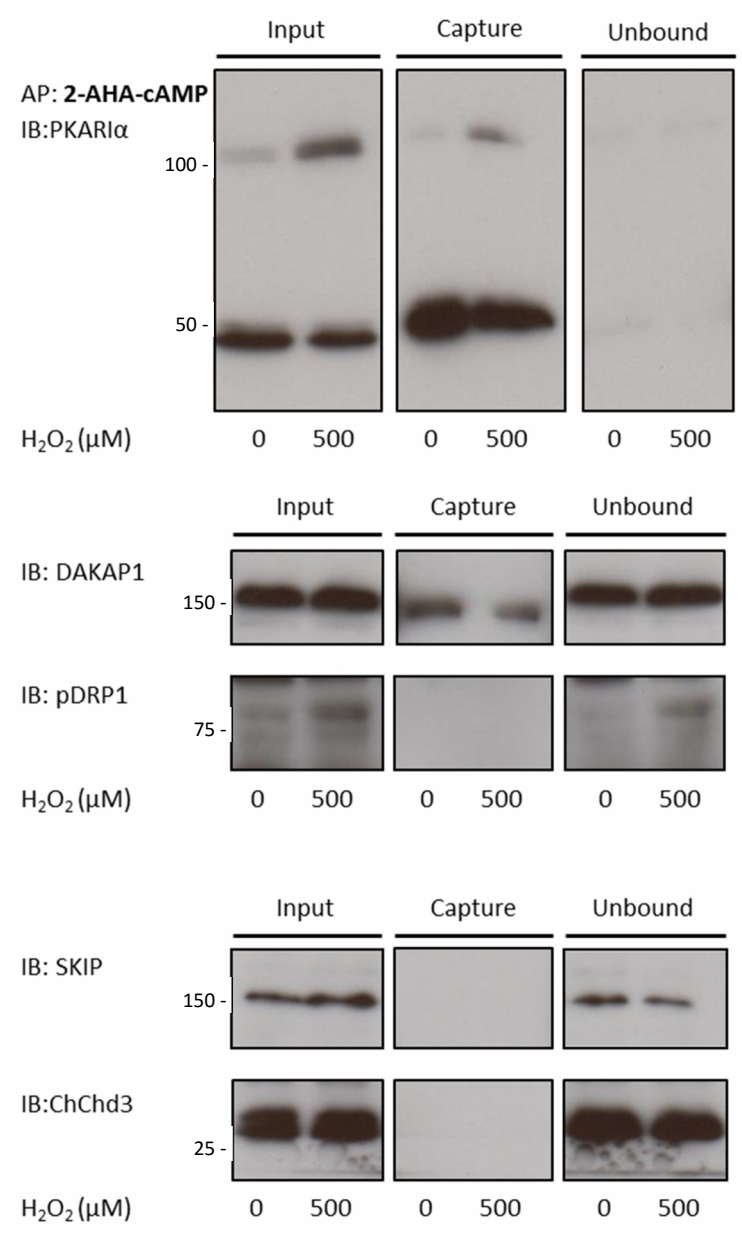

Figure 4.19 2-AHA-cAMP-agarose capture with Buffer 3 in HEK 293 cells. HEK 293 cells were treated with H_2O_2 (500 µM) and lysates were incubated with 2-AHA-cAMP-agarose. Captures were x20 concentrated compared to input. Immunoblots were probed with anti-PKARIα, anti-DAKAP-1, anti-pDRP1, anti-SKIP or anti-ChChd3.

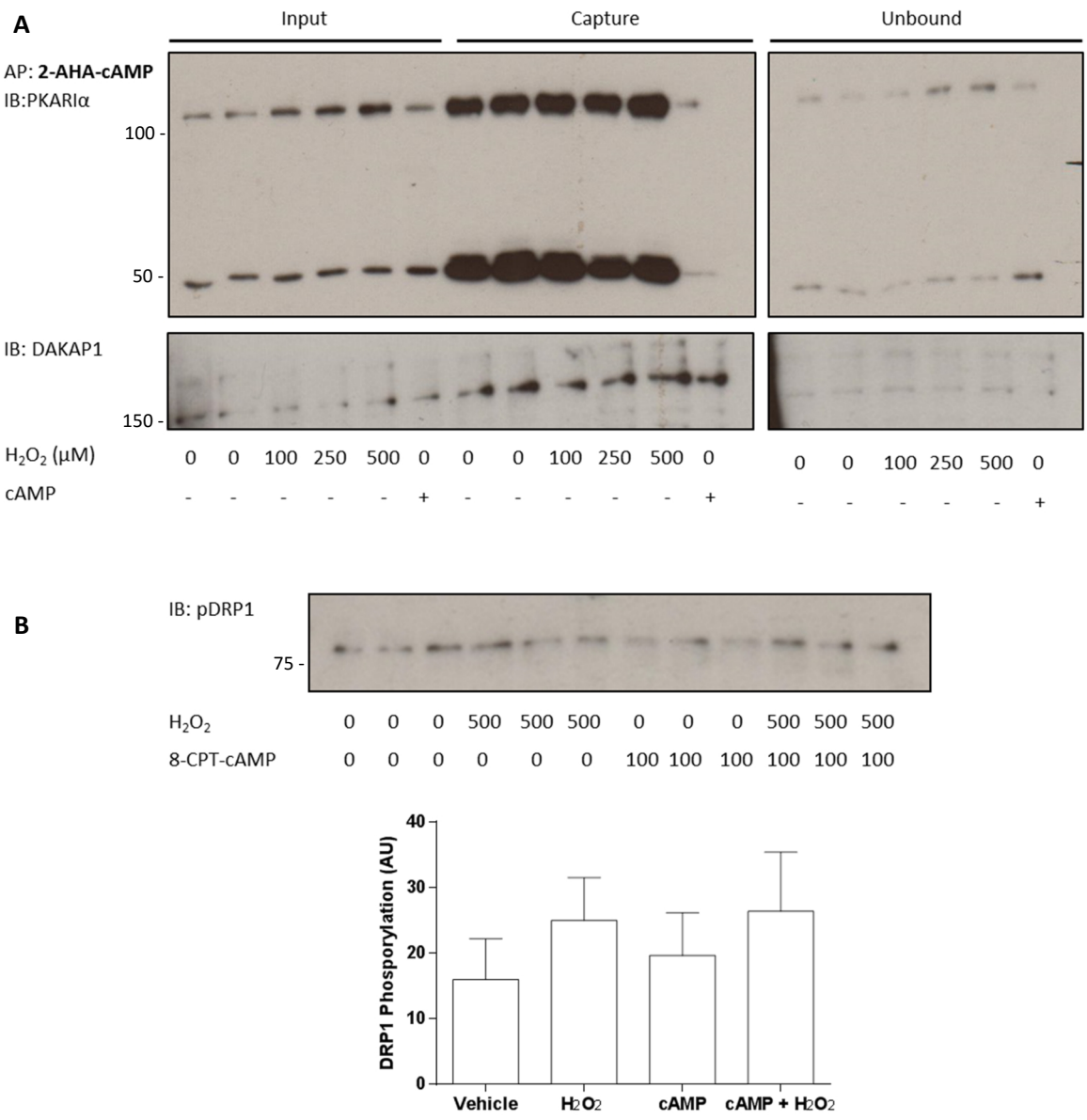

Figure 4.20 2-AHA-cAMP-agarose capture with Buffer 3 and cAMP negative control in HEK 293 cells. (**A**) HEK 293 cells were treated with H_2O_2 (0-500 µM) and lysates were incubated with 2-AHA-cAMP-agarose. cAMP (1 mM) was added to lysate during incubation was used as negative control. Captures were x20 concentrated compared to inputs. Immunoblots were probed with anti-PKARIα or anti-DAKAP1. (**B**) HEK 293 cells were treated with H_2O_2 (500 µM), 8-CPT-CAMP (100 µM) or both for 10 min. Immunoblots were probed with anti-pDRP1 and phosphorylation was summated and represented graphically (n=4)

4.3.6 Investigating the Caprotec™ Capture Compound Assay as a method to capture redox-dependent PKAR binding partners

The Caprotec™ Capture Compound Assay (CCCA) system was another means of potentially identifying oxidant-dependant PKAR binding partners. The design of the capture compound means that it labels proteins associated with PKAR that have been UV-cross-linked to a molecule containing a biotin tag (Figure 4.6). Vehicle or H_2O_2 (500 μM) treated HEK 293 cells were lysed and processed with CCCA. In preliminary experiments PKARIα was not efficiently captured as determined by the relative amount of PKARIα that was present in the unbound fraction (Figure 4.21A). However analysis with streptavidin-HRP antibody revealed a difference in biotin labelled proteins between control- or H_2O_2-treated lysates in the unbound fraction (Figure 4.21B).

In order to capture PKAR and biotin-labelled proteins more efficiently it was necessary to adjust the protein/capture compound ratio and therefore in subsequent experiments the volume of capture compound incubated with HEK 293 cell lysate was halved. The rationale behind this was to decrease the concentration of unbound capture compound after lysate incubation, and therefore decrease the competition between protein-bound capture compound and free capture compound during incubation with streptavidin beads. Decreasing the volume of capture compound increased the efficiency of the capture indicated by the decrease in unbound PKARIα. Again streptavidin-HRP analysis of protein biotinylated during the CCA procedure showed band pattern differences between control, H_2O_2 or isoprenaline (10 nM) treated HEK 293 cells (Figure 4.21B). The bands after H_2O_2 treatment may represent redox-dependent PKAR binding partners.

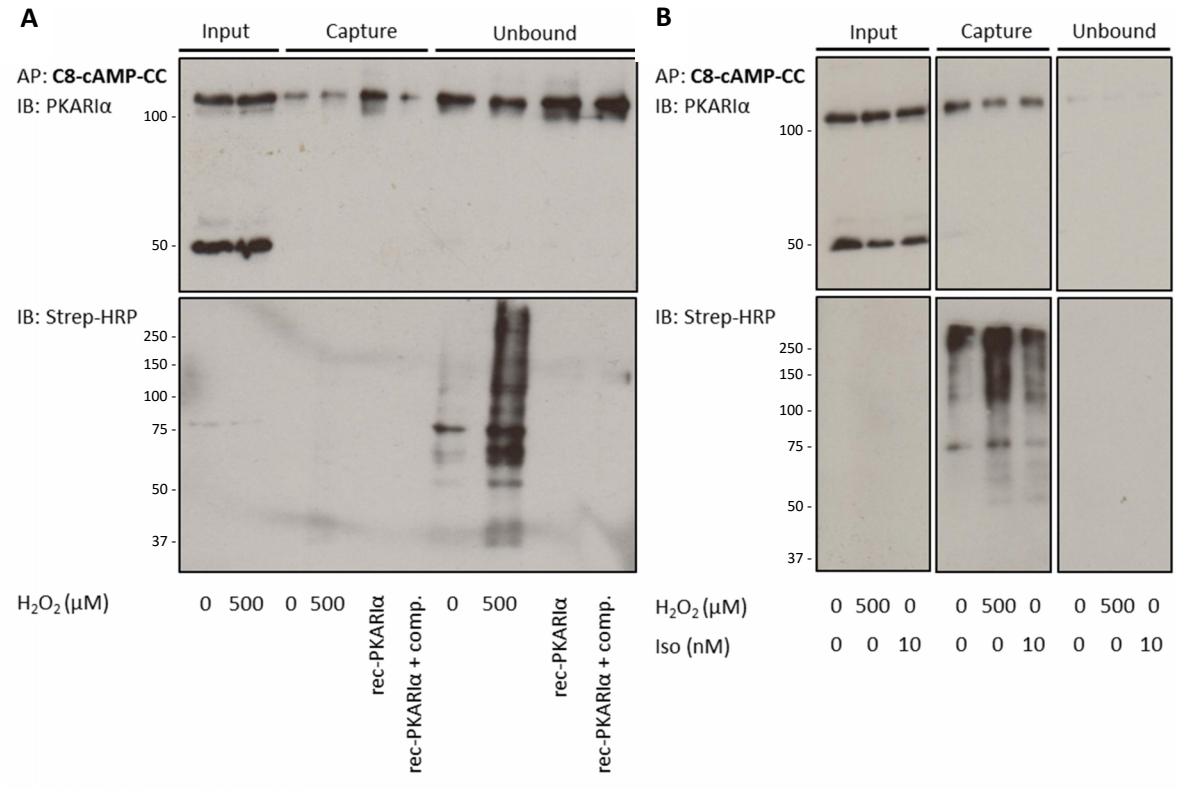

Figure 4.21 Optimisation of Caprotec™ capture with a biotinylated C8-cAMP capture compound. (**A**) HEK 293 cells were treated with H_2O_2 (500 µM) and lysates (without maleimide) were incubated with the C8-cAMP capture compound prior to UV irradiation. Proteins were pulled-down with streptavidin beads. Recombinant-PKARIα and recombinant PKARIα with cAMP analogue were used as a positive control or negative controls respectively. (**B**) To optimise capture, samples were incubated with half the concentration of capture compound. Immunoblots were probed with anti-PKARIα, or anti-streptavidin-HRP to detect PKAR binding partners.

4.4 Discussion

The aim of this chapter was to determine whether PKARIα bound differentially to AKAPs depending on its redox state. The primary approach was to use cAMP-agarose to co-capture AKAPs after H_2O_2 treatment, but this was unsuccessful. AKAP7 has been reported to bind to PKARIα[240], however I was unable to corroborate this. Furthermore, AKAP7 was not found to be sensitive to reversible oxidative modifications using the PEG-maleimide switch method that was successfully developed and validated during these studies. AKAP7δ was found to interact with PKARIIα, but not PKARIα, and this association may be redox-dependent.

4.4.1 AKAP7

The failure of all commercially-available antibodies tested to detect AKAP7 significantly hampered the initial progress of the project. Jones *et al.* used AKAP7 KO animals to highlight that such commercial antibodies for AKAP7 can detect non-specific bands around the expected molecular weight of AKAP7 and lead to misidentification of the protein[234]. The authors reported the loss of bands that represent AKAP7γ/δ at around 37 kDa in their AKAP7 KO animals. In contrast other groups have reported AKAP7 at approximately 50 kDa[140,236]. Furthermore many commercial antibodies for AKAP7 report a band at 50kDa. Therefore there should be an element of caution when considering the established AKAP7 literature. Given this, moving to a cell over-expression system to investigate AKAP7 was justified.

No co-localisation between PKARIα and either AKAP7γ/δ isoform was detected in immunofluorescence studies. Both AKAP7γ/δ localised primarily to the nucleus and in a few cells it was localised in the cytoplasm. Nuclear localisation was unsurprising given that both isoforms contain an N-terminal nuclear localisation signal motif[240,250]. Speculatively the presence of AKAP γ/δ in the cytoplasm could be due to saturation of nuclear binding sites. Electrostatic attraction of positively charged amino acid residues on the exterior of AKAP7δ concentrate in the tertiary structure to form a binding surface for negatively charged lipids in the membrane[250]. This may explain why AKAP7δ was seemingly localised at the nuclear membrane in this study. Despite this, the consensus in the literature is that AKAP7γ/δ binds to the sarcoplasmic reticulum[140,242,251]. However, definitive verification of which would require the expression of AKAP7 in its correct cellular localisation context. This is a disadvantage of over-expression studies in HEK293 cells, but their ease of transfection makes them useful in the study of protein-protein interactions.

4.4.2 Analysis of cAMP-agarose capture experiments

In the present study I was unable to establish an interaction between any AKAP and PKARIα with cAMP-agarose capture experiments, despite its extensive use in the literature for this purpose[246-249]. This was surprising given that these experiments were carried out in accordance with established protocols.

PKARIα and PKARIIα were consistently captured, the former with greater efficiency, however I was unable to co-capture known RIα AKAPs including AKAP7γ/δ, DAKAP1, DAKAP2, SKIP or smAKAP. It was decided to pursue this methodology despite the setbacks because the number of studies in the literature suggests it should be a viable approach. A great deal of time was spent attempting to optimise the method which included: increasing the concentration of protein used in each capture experiment; screening different buffers based on published studies and those routinely used in this laboratory in similar experiments; altering the capture incubation time; changing the stringency of wash buffer, but unfortunately none of these approaches succeeded. The length of the spacer arm is an important consideration as this can influence access to binding sites due to steric hindrance. 8-AEA-cAMP-agarose beads, used routinely in my studies, have a 2 carbon spacer arm which has previously used to capture PKARIα together with AKAPs[249,252,253]. A hydrophilic 19 atom spacer that conjugates cAMP to agarose has recently become available which may improve the ability to co-capture PKARIα binding partners if this method was pursued in future studies.

DAKAP1 was captured on cAMP-agarose even in the presence of a high concentration of competing cAMP meaning that it was bound non-specifically to the agarose. In contrast Jarnaess *et al.* were able to pull down DAKAP1 successfully with PKARIα and these proteins were not captured in the presence of cAMP[246]. Not all examples of cAMP-agarose studies in the literature have used excess cAMP as a negative control; therefore it is possible that some AKAP/PKA interactions reported using this technique may be due to non-specific binding. Some studies have used mass spectrometry to identify AKAPs which can be a beneficial approach because it does not depend on antibodies that are often not fit-for-purpose as outlined in this chapter for AKAP7[254]. To the best of my knowledge no study thus far has utilised excess cAMP in proteomic screens to limit false-positive identification of proteins due to non-specific binding. If this crucial control is included, proteins that are identified in H_2O_2 treated lysates vs. controls can be cross-referenced against a list of proteins from samples that were incubated with an excess of cAMP to ensure that they are bona-fide PKAR binding partners.

AKAP7γ has been shown to bind to both PKARIα[240] and PKARIIα[241], however I was unable to verify this. In the present study using Ni-Ni-NTA-agarose I demonstrated that AKAP7δ bound to PKARIIα but not PKARIα. Evidence of the isoform binding specificity of AKAP7δ is ambiguous. AKAP7δ binding RIIα with high affinity has been demonstrated[121,255] but there is appears to be no information about its interaction with PKARIα. The interaction between AKAP7δ and PKARIIα may be redox-regulated. This may have some biological significance in the kidney where AKAP7δ has been shown to mediate PKA phosphorylation and consequent redistribution of water channel aquaporin-2 to increase water reabsorption in the renal collecting duct[237]. Hypothetically physiological oxidant signalling may regulate this phosphorylation due to PKARIIα targeting to AKAP7δ. The PEG-maleimide switch method showed PKARIIα to be susceptible to a reversible oxidative modification. de Piña *et al.* suggest that ROS induces a disulfide between PKARIIα Cys-97 and the Cys199 in the catalytic subunit thus rendering it inactive[107]. However I found no evidence of mixed disulfide between the two proteins on immunoblots and the catalytic subunits were not co-captured with PKARIIα and His-AKAP7δ after Ni-NTA-agarose pull down (not shown). The redox regulation of PKARIIα and AKAP7δ requires further investigation but was beyond the scope of this study which focuses on PKARIα.

4.4.3 Analysis of PEG-maleimide switch assay

The PEG-maleimide switch method has proved a powerful tool for identifying proteins that are sensitive to reversible oxidative thiol modifications, successfully detecting redox state changes in the established oxidant-sensitive proteins PKARIα and PKGIα. It employs a similar principle to the biotin-switch method, a technique first described by Jaffrey and Snyder that enables detection of proteins that have undergone thiol S-nitrosation[256]. However, the exchange of the modified thiol with PEG-maleimide instead of biotin simplifies the protocol with the benefit that it becomes unnecessary to purify the biotin-labelled samples which is associated with loss of protein and experimental variability. Rather, PEGylated proteins can directly be detected and identified by a shift on an SDS-PAGE gel. Furthermore, the proportion of protein that shifts correlates with an increasing concentration of H_2O_2; providing a semi-quantitative method for indexing a proteins candidate of interest for which there is an antibody available.

There are some potential caveats with the PEG-maleimide switch method. For example, some proteins may lose their immunoreactivity when PEGylated, which seems to have occurred with PEGylated-PKG. This can potentially be addressed by using an antibody that recognises a different region of the protein of interest. In addition, some proteins have been identified as being able to form solvent-inaccessible oxidative modifications that are resistant to reduction

even in the presence of high concentrations of reducing agent[257]. This represents a potential problem with the PEG-maleimide switch because it requires full reduction of the oxidative modification for efficient PEGylating. Such proteins will not be PEGylated during processing and consequently erroneously concluded to be insensitive to oxidative modifications (i.e. generate a false negative). Another potential issue with the PEG-switch assay is that 5 kDa PEG-maleimide may not adequately shift high molecular weight target proteins to allow detection of oxidation using SDS-PAGE. This could be overcome by using higher molecular weight PEG-maleimide variants. However, a larger PEG-tag may affect protein solubility or immunoreactivity. Despite this, the PEG switch is an effective mechanism to rapidly determine whether a protein of interest is sensitive to reversible thiol oxidation.

AKAP7γ, but not AKAP7δ, was PEGylated after H_2O_2 treatment but surprisingly a switch was still observed with the C229S/C243S-AKAP7γ mutant. Mutation of the only other cysteine (Cys12) in AKAP7γ would determine whether it was modified by oxidants, however since this cysteine is also present in AKAP7δ, which was not PEGylated, it is unlikely that it is reversibly oxidised. Instead it is probable that a cysteine in the linker region between GFP and AKAP7γ is responsible for the PEGylation. This could be verified by sub-cloning AKAP7γ into another vector however it was decided not to pursue this due to time constraints and other priorities. Therefore given that there was no evidence of AKAP7 oxidative modification on immunoblots and that the SR associated AKAP7δ didn't switch it was concluded that AKAP7 was not sensitive to reversible oxidation modification.

4.4.4 Analysis of Caprotec™ co-capture assay

cAMP-CCCA was another method explored to try and co-capture redox-dependent PKAR binding partners. S-adenosyl-l-homocysteine and staurosporine have been used to selectively isolate proteome subsets using Caprotec™ technology that utilises UV to crosslink proteins and stabilise protein-protein interactions[258,259]. In this case cAMP bound to the capture compound is able to pull out PKAR before UV irradiation to covalently bind PKAR binding partners, thus purifying the subset of proteins before MS identification. This is an advantageous technique given the difficulty to co-purify partners that have low affinity or low abundance, as may be the case when using cAMP-agarose. The number of PKARIα binding partners increased when cells were challenged with H_2O_2 and optimisation of the method allowed capture of these proteins. These bands potentially represent AKAPs and associated substrates and therefore it is in agreement with the hypothesis that elevated intracellular ROS can target PKARIα to AKAPs. Furthermore artificial PKARIα oxidation that occurs during cell lysis and processing (as these experiments were carried out in the absence of maleimide) does

not lead to additional bands being observed, suggesting PKARIα redox targeting is a co-ordinated intracellular process. Captured proteins can be identified via LC/MS after separation by SDS-PAGE, band excision and tryptic digestion. Preliminary experiments with cAMP-CCCA have yielded promising results but this would have to be scaled up to allow direct comparison of PKAR binding partners from WT or C17S PKARIα KI cardiac tissue with or without H_2O_2 treatment. There is also the limitation that all regulatory subunits of PKA are likely to be captured which may complicate interpretation of any results. Unfortunately Caprotec™ stopped providing support for the technology as they have changed their commercial strategy, as such further studies could not easily be pursued. Nevertheless cAMP-CCCA is potentially an alternative method to cAMP-agarose capture to identify redox PKARIα binding partners.

5 Investigating cAMP-induced reduction of disulfide PKARIα

5.1 Introduction

In the previous chapter I made an unexpected, but intriguing, observation that incubation of HEK 293 cell lysate with cAMP-agarose induced the reduction of disulfide PKARIα. This potentially could be a novel mechanism by which cAMP regulates redox state of PKARIα and therefore oxidant-dependent signalling. Although this is an interesting possibility, a major issue with this being realistic, as expanded on below in detail, is that cAMP itself has no intrinsic chemical reduction capability and so there is significant complexity associated with this observation.

PKARIα is structurally mobile, undergoing large movements as PKARIα toggles between its binding partners, namely cAMP and the catalytic subunits. cAMP first binds to the more accessible phosphate binding cassette in the cAMP B site, as the residues required for stable nucleotide binding in the cAMP A site are masked by the interaction between PKARIα and PKA-C. Upon cAMP binding, the R subunit undergoes a large conformational change in response to the disruption of the salt bridge between Glu261 and Arg366 to allow access of another cAMP molecule to the cAMP A site and facilitate full release of the catalytic subunits (Figure 5.1). In this way there is a communication pathway between the two cAMP-binding domains that provides a mechanism for the cooperative activation of PKA[260].

Hamuro *et al.* utilised amide hydrogen/deuterium exchange measured by mass spectrometry to assess the structural dynamics, protein-protein interactions and protein-ligand interactions of PKARIα[261]. With the exception of the centre of α-helix1 (residues 31-36 involved in PKARIα dimerisation) and the adjacent turn which exchange relatively slowly, deuteration in the D/D domain (residues 1-61) of PKARIα occurs rapidly indicating that it is a dynamic, disordered and solvent exposed region. Interestingly binding of cAMP or the catalytic subunits to PKARIα made no difference to the rate of deuteration in the D/D domain, implying a lack of allosteric communication between the cAMP sites and D/D[261]. Despite this, it is reasonable to suggest that binding of an AKAP to the D/D domain will affect its solvent accessibility, thus regulating the availability of the cysteine residues in this domain to electrophilic attack. The large conformational change that occurs when cAMP binds to PKARIα may lead to steric changes in the AKAP-PKARIα complex that further regulates cysteine accessibility and susceptibility to

attack by oxidants. This would represent a novel method of communication between the cAMP binding sites and the redox cysteines in the D/D domain. I hypothesise that such steric effects that may occur upon cAMP binding may explain the observed cAMP induced reduction of PKARIα.

In this chapter I present evidence to suggest that under certain conditions cAMP can induce the reduction of PKARIα, and that it participates in the resolution of a mixed disulfide complex between PKARIα and tubulin, a novel redox-dependent AKAP.

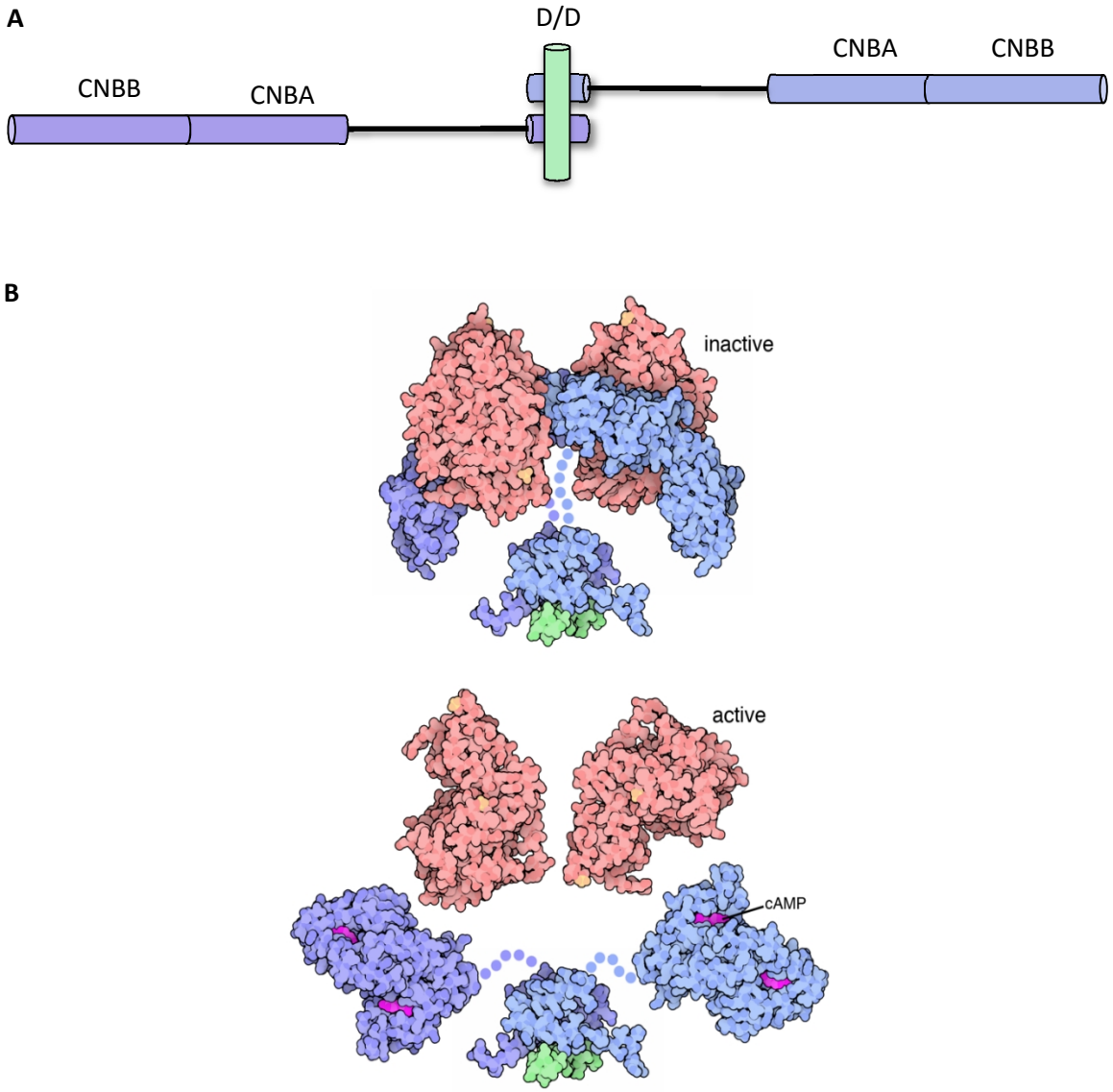

Figure 5.1 PKA undergoes a large conformational change upon cAMP binding. (A) Schematic representing the two regulatory subunits of PKARIα. Shown are the N-terminal dimerisation/docking domain (D/D) complexed with an AKAP helix (AKB), and the C-terminal cyclic nucleotide binding site A and B (CNBA and CNBB). **(B)** Crystal structure of PKARIα (blue) complexed with catalytic subunits (red) when inactive. cAMP (magenta) binding activates PKARIα by inducing conformational change that unleashes catalytic subunits. AKB (green) bound to D/D domain. Movement of cAMP binding domains may alter PKARIα-AKAP complex conformation. *(Figure adapted from Taylor et al. 2012[112] and illustration by David S. Goodsell on behalf of PCSB PDB[262])*

5.2 Specific Methods

5.2.1 Antibodies

Antibody	Purchase Code	Company	Species	Dilution
anti-Gapex-5	SAB4200099	Sigma	Rabbit	1:1000
anti-caprin1	15112-1-AP	Proteintech	Rabbit	1:1000
Anti-α/β-tubulin	2148	Cell Signaling Technology	Rabbit	1:1000

Table 5.1 Antibodies used in Chapter 5

5.2.2 Generation of PKARIα^{-cAMP} and C17SPKARIα^{-cAMP} constructs

The dominant negative mouse PKA plasmid M7 pdnPKA-GFP cDNA (Ungar & Moon, 1996)[263] containing a Gly200Glu mutation in cAMP binding domain A was obtained from (Addgene plasmid # 16716) (PKARIα^{-cAMP}). PKARIα Cys17Ser mutation (C17SPKARIα^{-cAMP}) was introduced using the Quik-Change Site-Directed Mutagenesis Kit (Agilent) according to the manufacturer's instructions by Dr. Joseph Burgoyne.

5.2.3 Generation of V5-PKARIα and V5-C17SPKARIα constructs

Human PRKAR1A was isolated from transformed from DH5-α T1 phage resistant E. coli (DNA Plasmid Repository, HsCD00040733). PKARIα Cys17Ser mutation was introduced using the Quik-Change Site-Directed Mutagenesis Kit (Agilent) according to the manufacturer's instructions. PKARIα-WT and C17SPKARIα entry clones were then transferred to pcDNA ™3.2-DEST Mammalian Expression Vector (C-terminal V5-tag) (Life Technologies) using Gateway® LR Clonase® II Enzyme mix, to generate V5-PKARIα and V5-C17SPKARIα respectively.

5.2.4 HEK 293 cell lysate incubation with cAMP

HEK 293 cells were seeded onto a 12-well plate and incubated overnight. The next day cells were treated with 500 µM H_2O_2 for 10 min, lysed (100mM Tris pH 7.4, 1% Triton, 150 mM NaCl, 100 mM maleimide and protease inhibitor cocktail) and centrifuged at 15,000 *g* for 15 min at 4°C. The soluble fraction was incubated with 0-50 mM cAMP Na^+ and rotated end-over-end for 2 hours at 4°C. The reaction was terminated with x2 SDS-PAGE sample buffer containing 100 mM maleimide.

5.2.5 HEK 293 cell lysate incubation with DTT

HEK 293 cells were seeded onto a 12-well plate and incubated overnight. The next day cells were treated with 500 µM H_2O_2 for 10 min, lysed (100mM Tris pH 7.4, 1% Triton, 150 mM NaCl, 100 mM maleimide and protease inhibitor cocktail) and centrifuged at 15,000 *g* for 15 min at 4°C. Soluble fractions were incubated with 0- 100 mM DTT, and 1 mM cAMP was added to the relevant lysates. Samples were briefly mixed and allowed to stand for 30 min at room temperature. The reaction was terminated with 1 M maleimide before the addition of x4 SDS-PAGE sample buffer.

5.2.6 Affinity Pull Down using cAMP-agarose with biotin maleimide

Samples were prepared as cAMP-agarose experiments, however, pre- and post-incubation with cAMP-agarose an aliquot of lysate was de-salted to remove excess maleimide before incubation with 0.5 µM biotin-maleimide for 1 hour at room temperature. The reaction was terminated with x4 SDS-PAGE sample buffer containing 100 mM maleimide.

5.2.7 Sequential two dimensional non-reducing/reducing SDS-PAGE

Anti-PKARIα immunoprecipitations of PKARIα^{-cAMP} transfected HEK 293 cells that had been treated with vehicle or 500 µM H_2O_2 were resolved on 4-15% SDS-polyacrylamide gels (Bio-Rad mini protean III system). After non-reducing electrophoresis, the entire lane containing the resolved proteins was excised and rotated through 90° and laid horizontally on top of a large format 1.5-mm thick 8% acrylamide gel. The gel slice was incubated in SDS sample buffer containing 100 mM DTT (to reduce any proteins disulfide linked to PKARIα^{-cAMP}) for 10 min. At this stage proteins that were linked by a disulfide bond were separated by DTT treatment and then resolved after SDS-PAGE further down the gel at their true weight in the second reducing dimension. Control or H_2O_2 treated fractions were laid adjacent to each other on the large format gel and run simultaneously to ensure that valid comparisons can be made between treatments. Gels were stained with colloidal Coomassie Blue G stain to visualize the proteins and then destained in 20% methanol. Protein spots that ran off of the diagonal and to the left of the slope represented proteins were disulfide linked to PKARIα. Spots/bands were excised in preparation for identification using liquid chromatography followed by tandem mass spectrometry (LC-MS/MS), which was kindly performed by Dr. Xiaoke Yin.

5.2.8 Immunoprecipitations

HEK 293 cells seeded in T75 flask were lysed in RIPA Buffer (50 mM Tris pH7.4, 500 mM NaCl, 1% NP-40, 0.5% $C_{24}H_{39}NaO_4$, 0.1% Triton X-100, 100 mM maleimide and protease inhibitor cocktail) and centrifuged at 2500 *g* for 5 min at 4°C. The supernatant was used for the immunoprecipitation and the pellet was discarded. An aliquot of the supernatant was taken and added to an equal volume of x2 SDS-sample buffer and this was designated as the input. Lysates were incubated with anti-PKARIα and rotated end-over-end overnight at 4°C. In other experiments lysates from V5-PKARIα transfected HEK 293 cells were incubated with anti-V5 conjugated to agarose beads. Immunoprecipitates were collected using Protein A/G Plus-agarose beads (Santa Cruz Biotechnology, Inc.) that had been washed in RIPA buffer after 3 hours end-to-end rotation at 4°C. Samples were places in spin columns and centrifuged at 1500 g for 30 seconds at 4 °C. Flow through was collected and an equal volume of x2 SDS-sample buffer was added to form the unbound. Samples were washed three times in in RIPA buffer before beads were incubated with x4 SDS-sample buffer for 5 min and eluted as the capture.

5.2.9 *in situ* proximity ligation assay (PLA)

Cells, treated as indicated, were fixed and blocked as per the standard immunofluorescence protocol. The *in situ* PLA experiments were performed using the Duolink® In Situ Red Starter Kit Mouse/Rabbit (Sigma) according the manufacturer's instructions. Cells were incubated with primary antibodies, anti-tubulin and anti-PKARIα, and thereafter incubated with PLA probes, which are secondary antibodies (anti-mouse and anti-rabbit) conjugated to unique oligonucleotides. Circularization and ligation of the oligonucleotides was followed by an amplification step. The products were detected by a complementary fluorescently labelled probe. Slides were mounted in Lisbeth's medium onto microscope slides and were analysed using confocal microscopy on an inverted microscope (Leica SP5 system) equipped with a blue diode and argon and helium neon lasers.

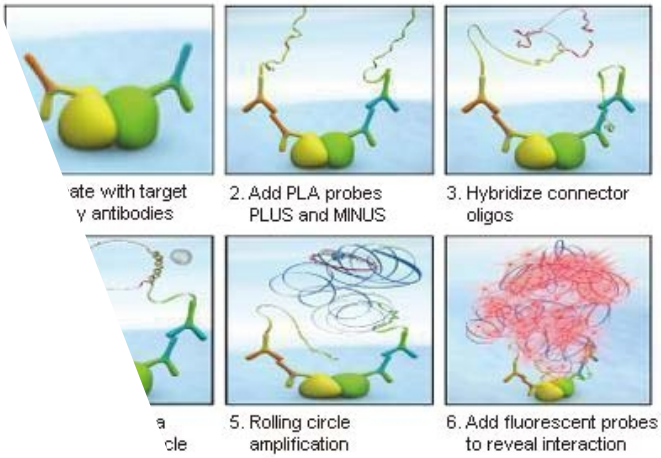

Figure 5.2 Schematic representing *in situ* proximity ligation assay. *Figure adapted from* http://www.olink.com/

5.3 Results

5.3.1 cAMP-agarose induced reduction of PKARIα

Experiments using cAMP-agarose led to the unexpected observation that PKARIα was captured predominantly as a monomer, even after cells had been exposed to H_2O_2 to induce disulfide (Figure 5.3). There was no PKARIα disulfide dimer in the unbound fractions, thus it is tempting to suggest that cAMP binding had induced the reduction of PKARIα. Neither maleimide nor cAMP-agarose altered the pH of the reaction mixture (data not shown) and the reduction was observed regardless of the specific type of cAMP-agarose used. The ability of cAMP to regulate the redox state of PKARIα could be biologically significant and therefore warranted further investigation.

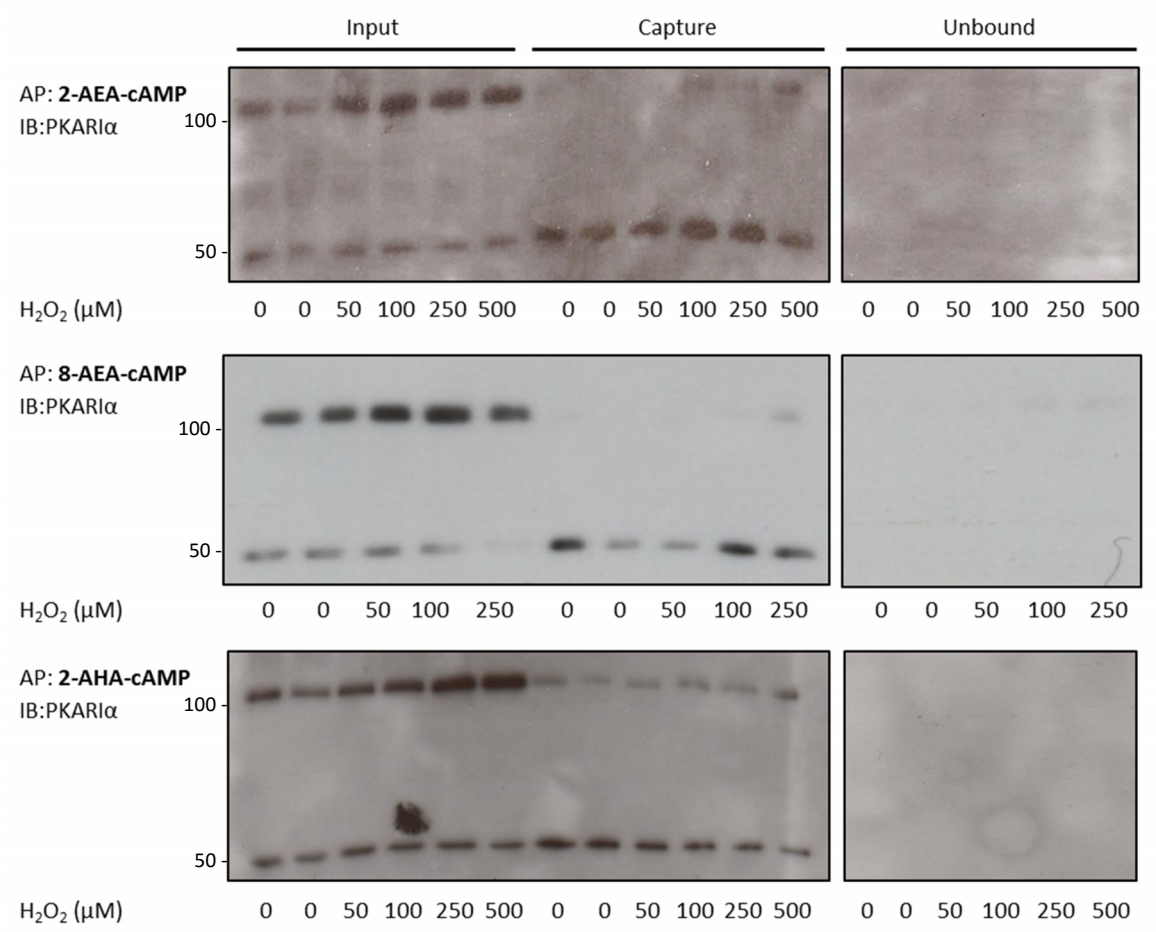

Figure 5.3 PKARIα from HEK 293 cell lysate is reduced after incubation with cAMP-agarose. HEK 293 cells were treated with H_2O_2 (0-500 μM), harvested in buffer containing 100 mM maleimide and subsequently incubated with cAMP-agarose. PKARIα, which was then visualised on non-reducing immunoblots, was captured and observed transitioned predominately to the reduced state when either of 2-AEA-cAMP, 8-AEA-cAMP or 2-AHA-cAMP-agarose were used.

The previous observations were performed with lysis buffer containing maleimide. When cAMP-agarose experiments were performed without maleimide, PKARIα was artificially oxidised in the air during cell lysis and captured predominantly in this dimeric disulfide form (Figure 5.4). Therefore without maleimide PKARIα does not undergo cAMP-induced reduction. To further investigate cAMP-induced reduction of PKARIα, HEK 293 cell lysate pre-treated with H_2O_2 (500 µM) was incubated with various concentrations of authentic cAMP (1-50 mM) instead of cAMP-agarose. Under these conditions cAMP alone was unable to induce the reduction of PKARIα despite the experimental conditions being comparable to those carried out with cAMP-agarose (Figure 5.5).

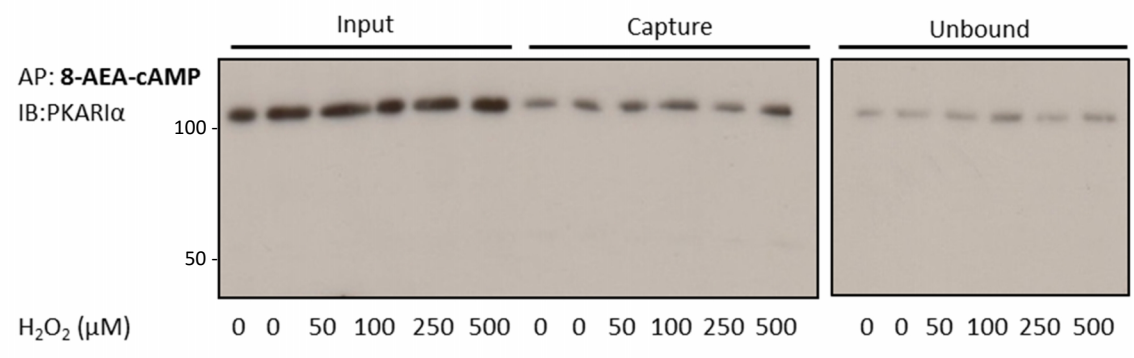

Figure 5.4 PKARIα from HEK 293 cell lysate without maleimide remains oxidised after incubation with cAMP-agarose. HEK 293 cells were treated with H_2O_2 (0-500 µM), lysed and then incubated with 8-AEA-cAMP-agarose. PKARIα detected on a non-reducing immunoblot was captured and observed in the oxidised state.

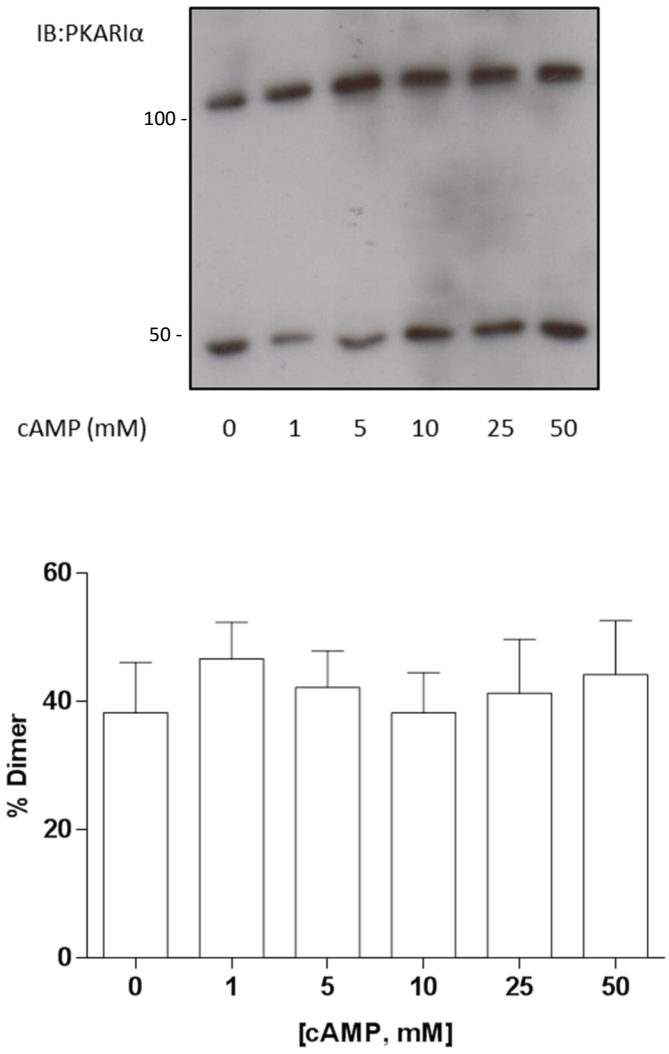

Figure 5.5 PKARIα from HEK 293 cell lysate is not reduced after incubation with authentic cAMP. HEK 293 cells were treated with 500 µM H_2O_2 and lysates (containing maleimide) were subsequently incubated with cAMP (0-50 mM). The proportions of PKARIα in the disulfide dimeric state was then determined using non-reducing immunoblot analysis and is represented graphically (n=6-7 ± SEM).

5.3.2 Investigating effects of time and cAMP-agarose volume on PKARIα disulfide reduction

There was also a lack of evidence supporting PKARIα induced reduction mediated through cAMP in cellular models that modelled global PKARIα monomer and dimer ratios (Chapter 3). Despite this, the initial observation robustly indicated that the nucleotide is capable of inducing PKARIα reduction. I then rationalised that perhaps cAMP reduction may only occur under specific conditions; certainly more complexity is anticipated as cAMP itself is not a reducing agent. Consequently, I decided it was worthwhile to investigate this potentially important observation further as it may have physiological significance.

To further characterise cAMP-induced PKARα reduction, PKARIα capture from H_2O_2 (500 µM) treated HEK 293 cells lysate by cAMP-agarose was monitored over various time points (5-120 min). After 5 min PKARIα monomer and dimer are captured at a ratio matching that in the input. However the concentration of captured PKARIα monomer increases over time to a greater extent than the disulfide dimer (Figure 5.6A). This increased capture of monomer over time relative to disulfide dimer may be accounted for by PKARIα disulfide dimer being reduced to the monomeric form. In a separate experiment the effect of the volume of cAMP-agarose beads on disulfide PKARIα reduction was also investigated. HEK 293 cell lysate was incubated with various amounts of cAMP-agarose (0- 150 µL) and the extent of PKARIα capture was assessed by immunoblotting. In the absence of cAMP-agarose, PKARIα was not captured and the monomer and dimer was comparable between the input and unbound. cAMP-agarose again induced the reduction of PKARIα from disulfide dimer to monomer, regardless of the volume of cAMP-agarose used (Figure 5.6B). This indicates that the capture of disulfide PKARIα by cAMP-agarose is not limited by saturation of “dimer-specific cAMP-agarose binding sites” but rather suggests that cAMP-agarose is able to induce the reduction of PKARIα.

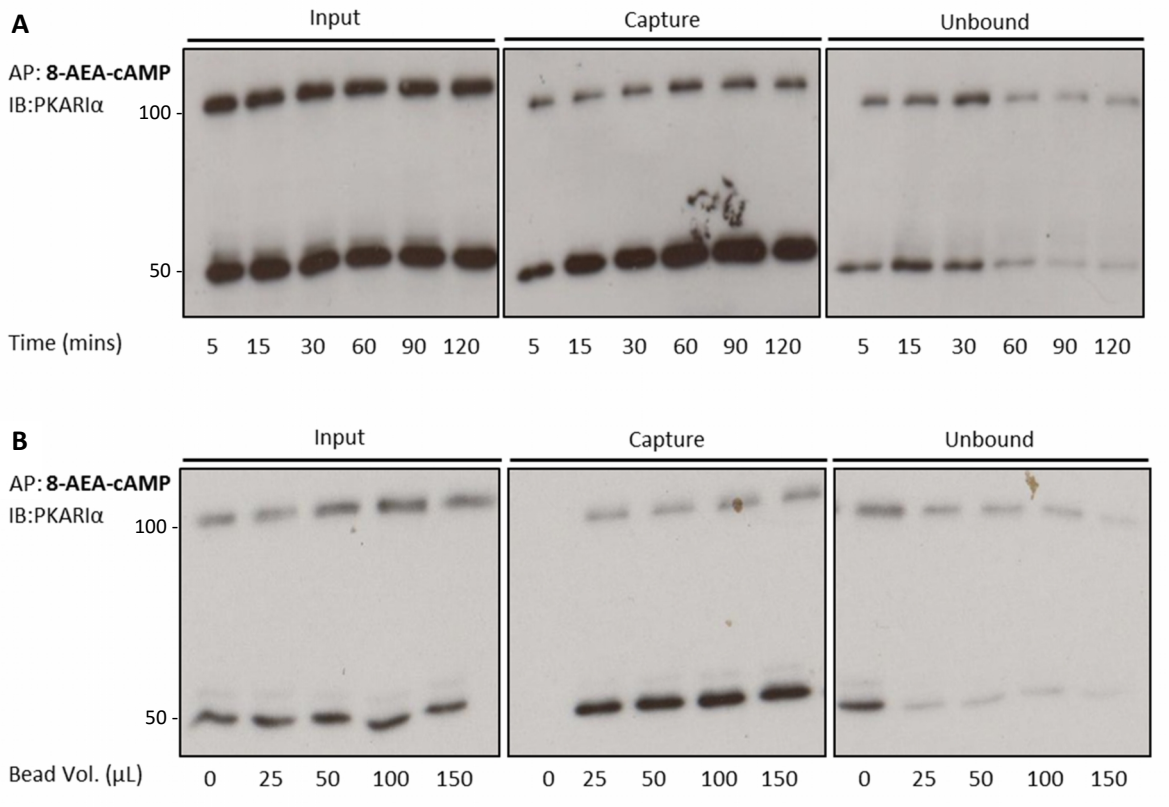

Figure 5.6 cAMP-agarose induced reduction of PKARIα is not limited by time or agarose bead volume. HEK 293 cells were treated with H_2O_2 (500 µM) and lysates were subsequently incubated with 8-AEA-cAMP-agarose (100 µl) for (**A**) 5-120 min. (**B**) Lysates were incubated with various volumes of 8-AEA-cAMP-agarose (0- 150 µL) for 120 min. PKARIα detected on a non-reducing immunoblot was captured and observed again to transition to the reduced state in both experiments.

5.3.3 Investigating the reduction of PKARIα with NTA-Ni-agarose and 6-AH-AMP-agarose

HEK 293 cells were incubated with Ni-NTA-agarose or 6-AH-AMP-agarose to determine whether the reduction of PKARIα to a monomer is specific to cAMP-agarose. The PKARIα disulfide dimer from HEK 293 cells treated with H_2O_2 was not captured when incubated with Ni-NTA- or 6-AH-AMP-agarose (Figure 5.7). Importantly the ratio of PKARIα monomer to dimer in the input was comparable to the ratio in the unbound fractions, indicating that the induced reduction of PKARIα is specific to cAMP-agarose.

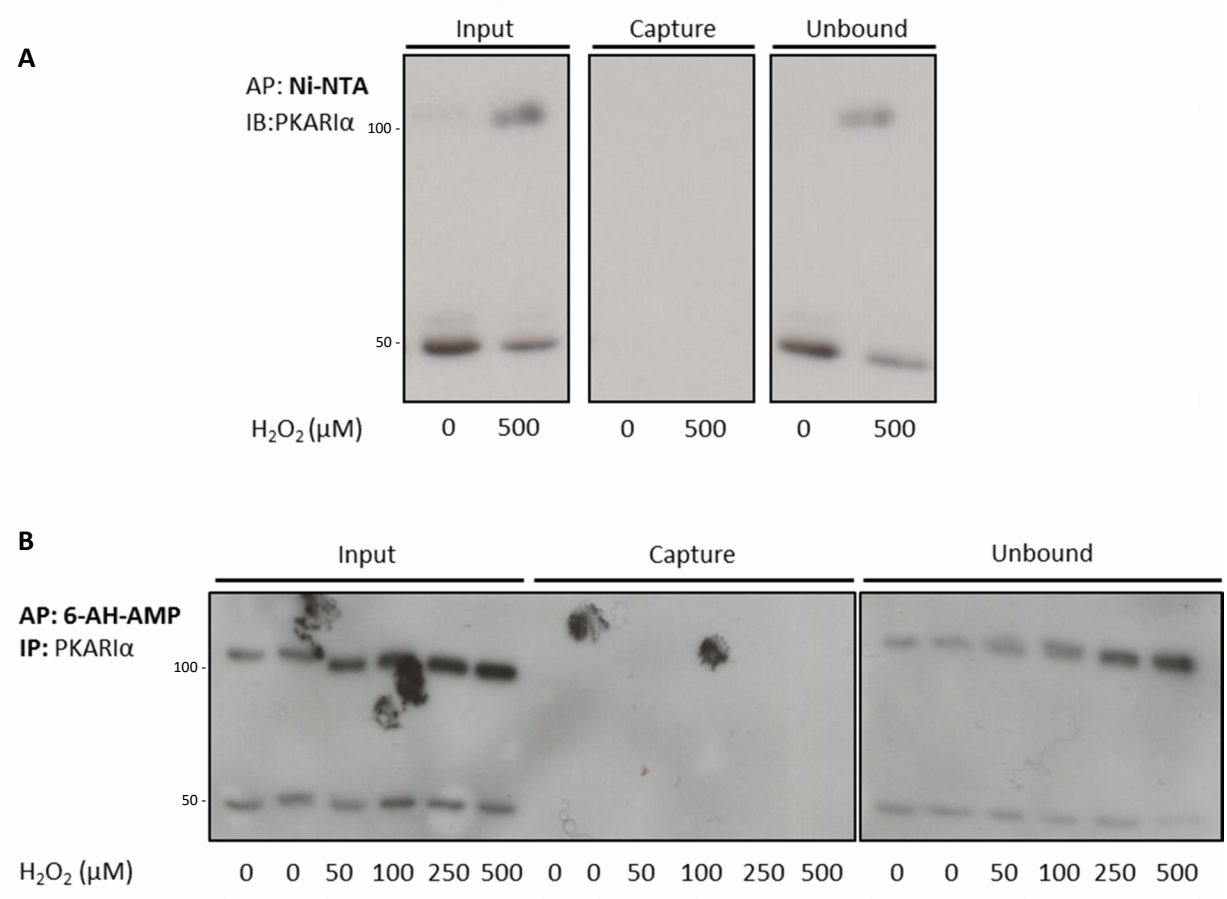

Figure 5.7 Neither Ni-NTA or 6-AH-AMP-agarose induce PKARIα disulfide dimer reduction. HEK 293 cells were treated with H_2O_2 (0-500 µM) and lysates were subsequently incubated with (**A**) Ni-NTA-agarose or (**B**) 6-AH-AMP-agarose. PKARIα was detected on a non-reducing immunoblot.

5.3.4 Investigating effects of cAMP on DTT-dependent reduction of disulfide PKARIα

To further assess whether cAMP could regulate PKARIα disulfide dimer reduction, the lysate of HEK 293 cells that had been challenged with H_2O_2 were incubated with cAMP (1mM) and various concentrations of the reducing agent dithiothreitol (DTT) (0- 100 mM). The incubation of lysate with DTT caused a dose-dependent decrease in PKARIα disulfide dimer. cAMP potentiated DTT-induced reduction of PKARIα disulfide dimer, which was significantly different at 75 mM compared to DTT alone (Figure 5.8A). To determine whether this cAMP potentiated reduction required a component from the cell lysate, purified recombinant PKARIα was incubated with DTT in the absence or presence of cAMP. Interestingly cAMP had no effect on DTT-dependent reduction of recombinant-PKARIα disulfide, suggesting that another component present in the cell lysate is necessary for cAMP to potentiate the reduction of PKARIα (Figure 5.8B).

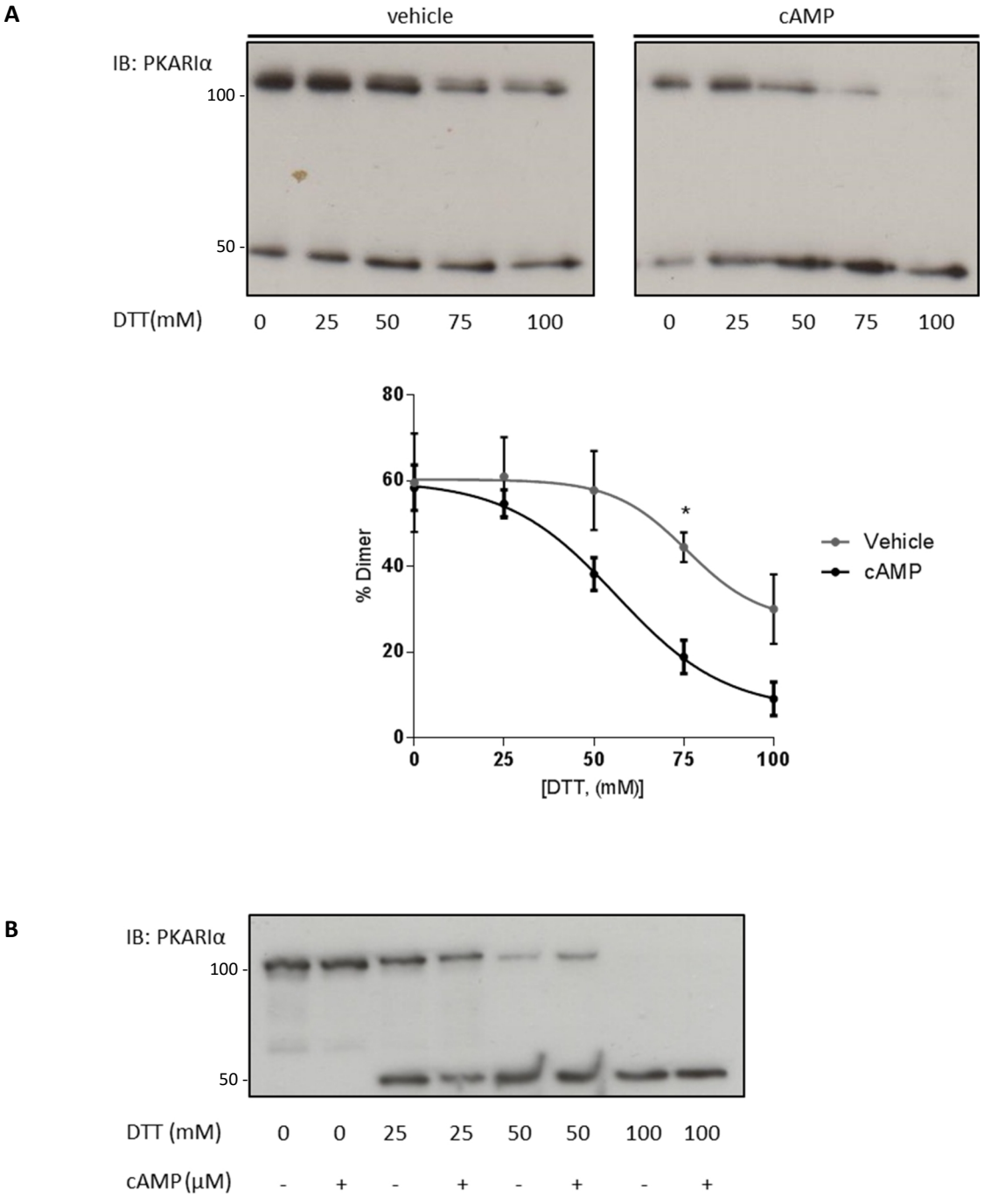

Figure 5.8 cAMP potentiates DTT-induced PKARIα reduction in HEK 293 cell lysate but not purified recombinant PKARIα. (**A**) HEK 293 cells were treated with H_2O_2 (500 µM) and lysates (containing 100 mM maleimide) were subsequently incubated with DTT (0-100 mM) in the absence or presence of cAMP (1 mM) for 30 min at room temperature. The percentage of PKARIα disulfide dimer was analysed after detection of PKARIα on a non-reducing immunoblot and is represented graphically (n=4 ± SEM). (**B**) Recombinant PKARIα was incubated with incubated with DTT (0-100 mM) in the absence or presence of cAMP (1mm) for 30 min at room temperature. PKARIα was detected on a non-reducing immunoblot.

5.3.5 Evidence for presence of free thiols during cAMP-agarose incubation

cAMP has no intrinsic capability to reduce PKARIα directly. However cAMP binding induces a conformational change in PKARIα. This structural change in PKARIα may conceivably allow a thiol containing protein or molecule to access and attack a sulphur atom in the disulfide bond to enable the reduction of PKARIα to the monomeric state observed. However, the presence of a free thiol during the capture phase is difficult to reconcile given that the HEK 293 cells are lysed in the presence of an excess of the alkylation reagent maleimide. Studies in this laboratory have demonstrated that efficient alkylation requires heating lysates containing maleimide to 50°C in the presence of SDS. Such harsh conditions are not compatible with cAMP-agarose experiments therefore it is possible that lysates may contain free thiols due to inefficient alkylation. To test this hypothesis, lysates for cAMP-agarose incubation were prepared as outlined above, but an aliquot was taken pre- and post-incubation, desalted to remove excess maleimide and then incubated with biotin-maleimide (0.5 mM) for 1 hour at room temperature to label any remaining free thiols. Immunoblotting using streptavidin-HRP revealed multiple bands that represented biotin-maleimide labelled proteins before and after cAMP-agarose incubation despite the lysis buffer contacting maleimide (Figure 5.9). Therefore it is reasonable to conclude that there are free thiols available during cAMP-agarose incubation that could potentially reduce disulfide PKARIα.

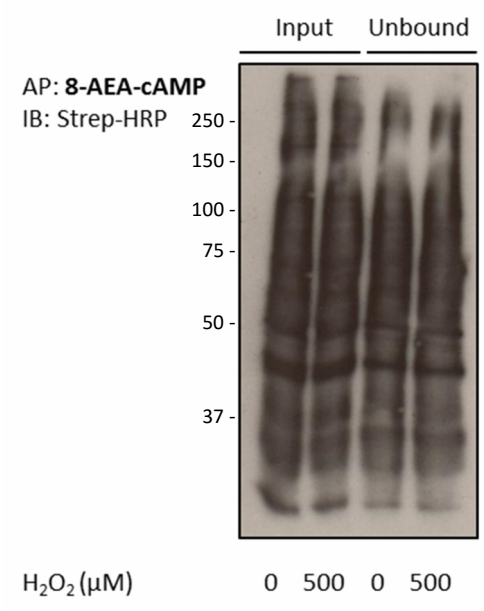

Figure 5.9 Free thiols are available during cAMP-agarose incubation. HEK 293 cells were treated with H_2O_2 (500 μM) and lysates were subsequently incubated with biotin-maleimide pre- and post-incubation with 8-AEA-cAMP-agarose. Biotin-maleimide labelled samples were detected by streptavidin-HRP antibody on a non-reducing immunoblot.

If cAMP-induced reduction of PKARIα does necessitate a free thiol in the lysate, high concentrations of H_2O_2 may lead to oxidation of this thiol and thus prevent disulfide PKARIα from becoming reduced to its monomeric form. With this in mind, HEK 293 cells were treated with high concentrations of H_2O_2 (0- 2 mM) and incubated with cAMP-agarose. In the input, PKARIα dimer formation increased with increased concentrations of H_2O_2 that is particularly striking at 1 or 2 mM H_2O_2. Despite this PKARIα was captured predominantly in the monomeric form at all H_2O_2 concentrations, showing again that cAMP somehow facilitated reduction of disulfide PKARIα (Figure 5.10). In cells treated with 1 mM or 2mM H_2O_2 there was increased captured PKARIα disulfide dimer compared to 0 and 500 µM H_2O_2. This could mean that some of the thiol(s) responsible for reduction of the PKARIα disulfide may become oxidised at this time.

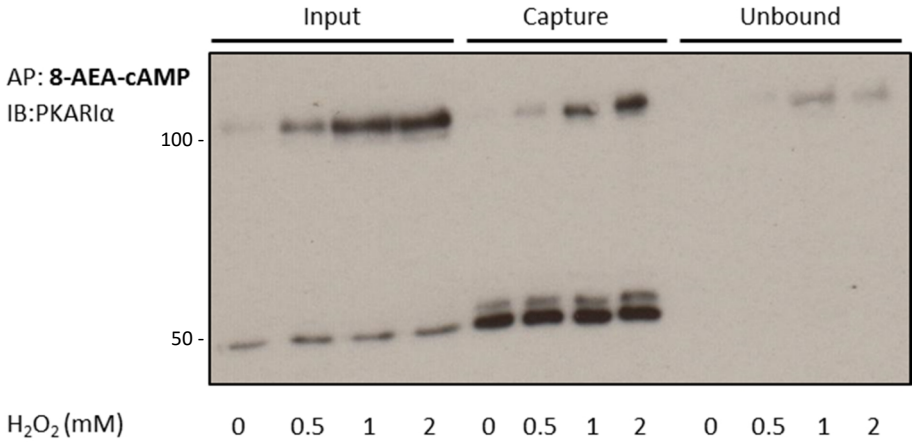

Figure 5.10 cAMP-agarose induced reduction of PKARIα is limited at high concentrations of H2O2. HEK 293 cells were treated with H_2O_2 (0-2 mM) and lysates were subsequently incubated with 8-AEA-cAMP-agarose. PKARIα was captured (concentrated) and detected on a non-reducing immunoblot.

5.3.6 Investigating cAMP-agarose induced reduction of PKARIα^{-cAMP}

To further investigate the role of cAMP on PKARIα disulfide reduction, a dominant negative PKARIα construct with a Gly200Glu mutation in the cAMP binding site that prevents cAMP binding (PKARIα^{-cAMP}) was generated. This construct was transfected into HEK 293 cells that were subsequently treated with H_2O_2 (0- 500 µM) and incubated with cAMP-agarose. In contrast to previous experiments the majority of PKARIα was detected in the unbound fraction (Figure 5.11A). The small amount of PKARIα that is captured can be attributed to endogenous PKARIα, whilst the inability for cAMP-agarose to capture PKARIα^{-cAMP} is verification that the mutations in the cAMP binding site were effective. Strikingly the ratio of PKARIα monomer and dimer in the input is similar to the ratio observed in the unbound fraction. This further demonstrates the requirement for cAMP to bind to PKARIα directly to induce reduction from dimer to monomer. Interestingly, when PKARIα^{-cAMP} cells were treated with H_2O_2 there was a dose-dependent formation of high molecular complexes above the weight of the dimer. It was hypothesised that these high molecular weight complexes could be PKARIα disulfide linked to proteins. To confirm this, a mutant form of PKARIα^{-cAMP} was engineered where Cys17, a critical cysteine necessary for disulfide formation, was mutated to a serine residue (C17SPKARIα^{-cAMP}). HEK 293 cells were transfected with C17SPKARIα^{-cAMP} which failed to dimerise upon H_2O_2 (0-500 µM) treatment, and notably the high molecular weight complexes that were previously observed were abrogated (Figure 5.11B). This suggests that PKARIα is capable of forming mixed disulfide complexes with target proteins, and that the formation of these complexes is contingent on the PKARIα disulfide dimer. Finally, in contrast to experiments undertaken with non-transfected HEK 293 cell lysate, cAMP did not potentiate DTT-induced PKARIα disulfide reduction in lysates from HEK 293 cell transfected with PKARIα^{-cAMP}. This provides further evidence that cAMP can regulate the redox state of PKARIα (Figure 5.11C).

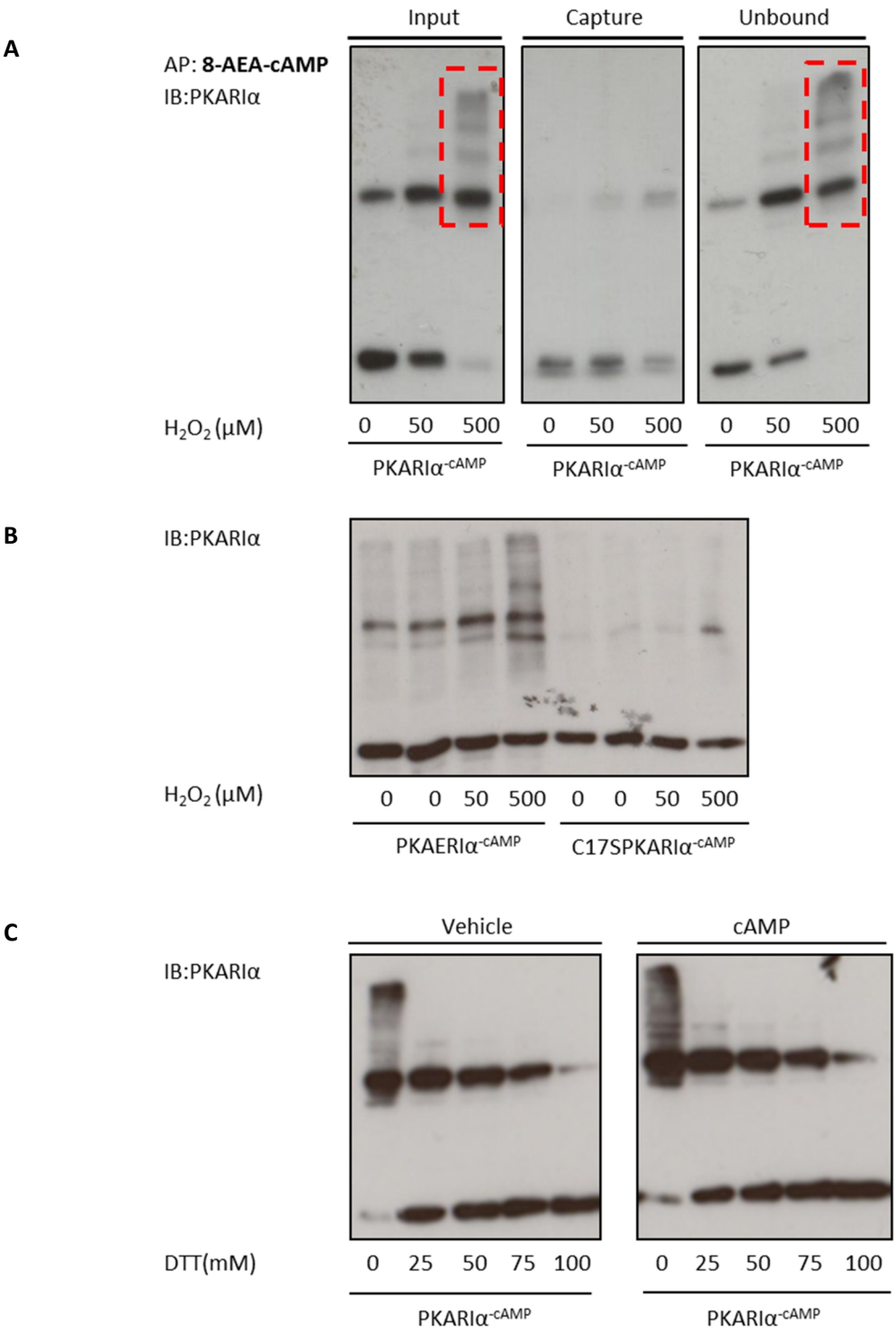

Figure 5.11 PKARIα^{-cAMP} forms high molecular weight complexes when oxidised which is not reduced by cAMP-agarose. (**A**) PKARIα^{-cAMP} transfected HEK 293 cells were treated with H_2O_2 (0-500 μM) and lysates were subsequently incubated with 8-AEA-cAMP-agarose. Red boxes indicate high molecular weight complexes (**B**) PKARIα^{-cAMP} or C17SPKARIα^{-cAMP} transfected HEK 293 cells were treated with H_2O_2 (0-500 μM). (**C**) PKARIα^{-cAMP} transfected HEK 293 cells were treated with H_2O_2 (500 μM) and lysates (with 100mM maleimide) and were subsequently incubated with DTT (0-100 mM) in the absence or presence of cAMP (1 mM) for 30 min at room temperature.

5.3.7 Identification of proteins present in PKARIα^{-cAMP} high molecular weight complexes

H_2O_2-treated HEK 293 cells transfected with PKARIα^{-cAMP} formed high molecular weight complexes. Biologically these high molecular weight complexes may represent AKAPs that PKARIα is targeted to under oxidative conditions. These complexes are observed only with a mutant form of PKARIα that cannot bind to cAMP. Therefore this may suggest that a transitory, intermediate mixed disulfide normally forms in WT PKARIα, but this interaction is stabilised in the mutant that cannot bind cAMP. cAMP may induce a conformational change that brings a free thiol into close proximity required to bring a necessary free thiol into close proximity to attack a sulphur atom in the mixed disulfide bond and result in cAMP-induced reduction of PKARIα via thiol disulfide exchange. Figure 5.12 illustrates a model of how H_2O_2 and cAMP may act co-operatively to regulate the PKARIα redox state, and consequently the PKARIα interaction with AKAPs.

As the high molecular weight complexes may represent potential PKARIα disulfide-dependent AKAPs, it was rational to identify them using mass spectrometry. This was achieved by first immunoprecipitating PKARIα^{-cAMP} from transfected HEK 293 cell lysate, and then performing two-dimensional sequential non-reducing-reducing diagonal gel electrophoresis[169]. Coomassie Blue staining allowed visualisation of spots that run off the diagonal and to the left of the slope which represented proteins that were disulfide-bound to PKARIα. These spots were excised and identified using liquid chromatography – mass spectrometry (LC-MS/MS).

Figure 5.13 shows the Coomassie Blue stained gels of two independent experiments that were carried out with vehicle- or H_2O_2-treated PKARIα^{-cAMP} transfected HEK 293 cells. Using immunoprecipitation rather than total cell lysate meant the diagonals and protein spots were faint, but were still visible with the naked eye for excision. LC-MS/MS analysis of tryptic digests identified 8 proteins as outlined in Table 5.2. To verify these targets as bona fide PKARIα oxidant-induced binding partners, immunoprecipitation of PKARIα^{-cAMP} from HEK 293 cell lysate followed by immunoblotting for the protein of interest was performed. It was expected that under control conditions these proteins would run at the expected weight, but in H_2O_2 treated samples a proportion of the protein would run 100 kDa higher due to the disulfide link with PKARIα disulfide.

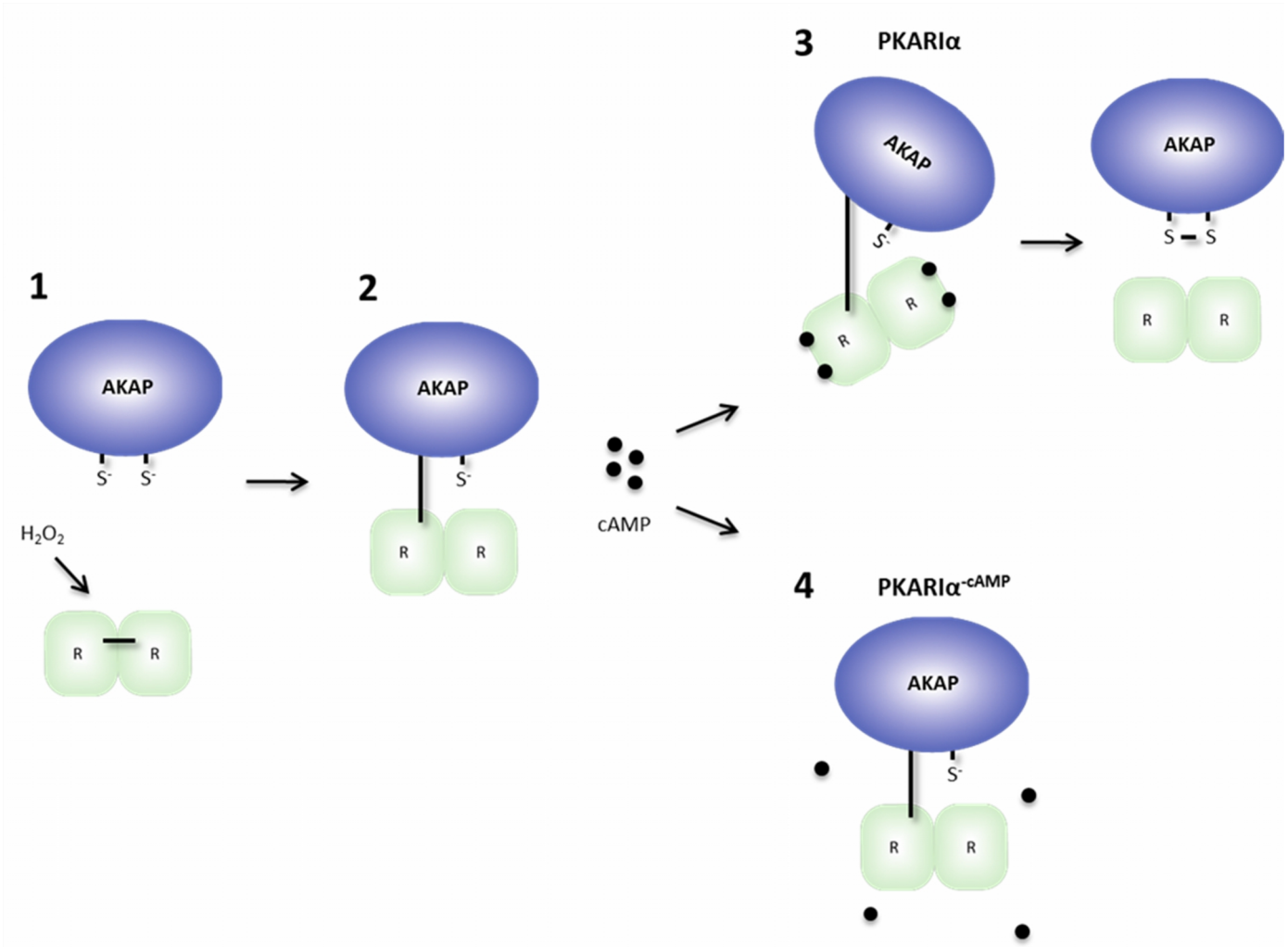

- H_2O_2 induces disulfide bond in PKARIα that increases its affinity for an AKAP
- Intermediate step in which disulfide PKARIα binds to an AKAP (observed in PKARIα^{-cAMP}) via inter-protein disulfide bond
- Endogenous PKARIα binds to cAMP which induces a conformational change that brings a thiolate into close proximity which attacks a sulphur atom in the mixed disulfide bond inducing thiol-disulfide exchange. PKARIα is reduced to a monomer and the AKAP now contains an intra-molecular disulfide bond.
- In PKARIα^{-cAMP}, cAMP cannot induce the conformational change and therefore the mixed disulfides can be observed after cAMP-agarose incubation.

Figure 5.12 A proposed model for cAMP-induced PKARIα reduction

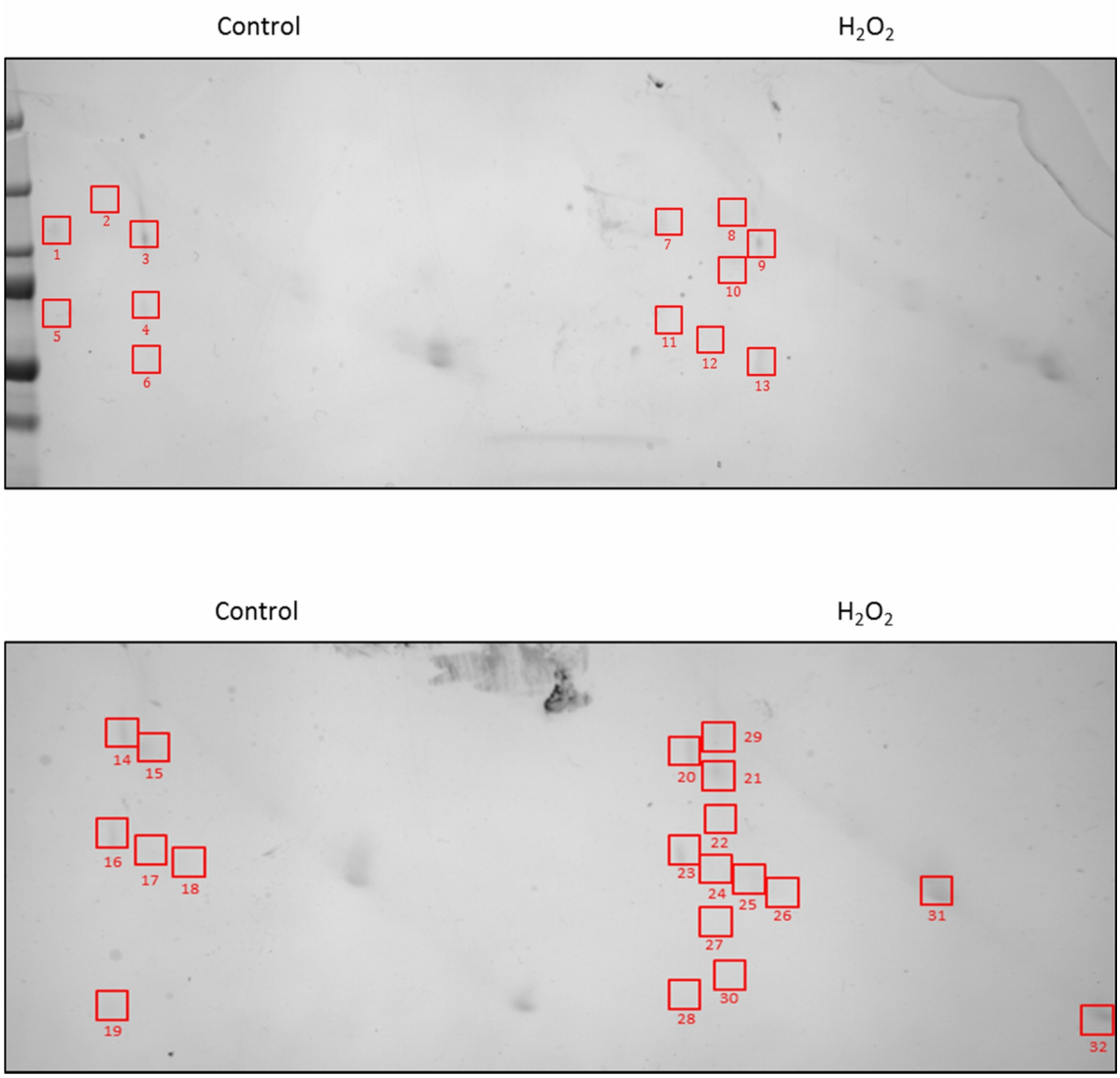

Figure 5.13 Coomassie Blue -stained diagonal gels of PKARIα^{-cAMP} immunoprecipitates. Shown here are examples of two stained gels from independent experiments. PKARIα^{-cAMP} transfected HEK 293 cells were treated with vehicle or H_2O_2 and then immunoprecipitated with anti-PKARIα. Samples were run under non-reducing conditions in the first dimension and under reducing conditions in the second (so called diagonal electrophoresis). Bands were subsequently excised after Coomassie staining and proteins present identified using LC-MS/MS.

Protein	MW	Spot Number (Total Spectral Counts)	Number of Peptides	Number of Cysteines	Vehicle	H_2O_2	Link to PKA?
GTPase-activating protein and VPS9 domain activating protein 1	156	20 (8), 29 (2)	7	26	No	Yes	✗
Caprin-1	78	9 (2)	2	3	No	Yes	✓
Tubulin 1A	50	16 (2), 17 (1), 23 (2), 25 (1), 26(1)	2	12	Yes	Yes	✓
Tubulin 4B	50	16 (1), 23 (1), 25 (2), 26 (2)	2	9	Yes	Yes	✓
Far Upstream Binding Protein 2	73	3 (9), 20 (1)	5	5	Yes	Yes	✗
Actin	42	29 (5)	3	7	No	Yes	✓
GAPDH	36	8 (3), 9 (4), 10 (2)	3	3	No	Yes	✗
Ubiquitin 40S ribosomal protein	18	3 (5), 8 (2), 9 (3), 14 (1), 15 (2), 20 (3), 21 (3), 22 (5), 29 (4)	3	5	Yes	Yes	✗

Table 5.2 Summary of proteins identified from excised spots that ran off the diagonal after gel electrophoresis.
Exclusion criteria: 2 unique peptides, 99% protein threshold, 90% peptide threshold

GTPase-activating protein and VPS9 domain activating protein 1 (GAPex-5) was assessed due to the relatively high number of spectral counts from the data set and because it has 26 cysteines in its primary sequence. Unfortunately the GAPex-5 antibody did not recognise a protein at the predicted molecular weight and therefore no conclusions could be drawn (Figure 5.14A). Caprin-1 has been identified as an AKAP350 binding partner thus making it an interesting candidate for further investigation[264]. The caprin-1 antibody detected a band at the correct weight in the input, and although a small amount was detected in the immunoprecipitate, there was no difference between vehicle- or H_2O_2-treated HEK293 cells (Figure 5.14B).

Tubulin has previously been suggested as a PKARIα AKAP[265]. Immunoblots for tubulin from the two PKARIα^{-cAMP} immunoprecipitates that were analysed by mass spectrometry, revealed tubulin running at its expected weight and also at approximately 150 kDa in samples that were treated with H_2O_2, consistent with a mixed disulfide complex with PKARIα (Figure 5.15AB). In support of this, the PEG-maleimide switch method revealed that tubulin was PEGylated after HEK 293 cells were treated with increasing concentrations of H_2O_2 (0- 500 µM) indicating that it is sensitive to reversible oxidative modifications (Figure 5.15C).

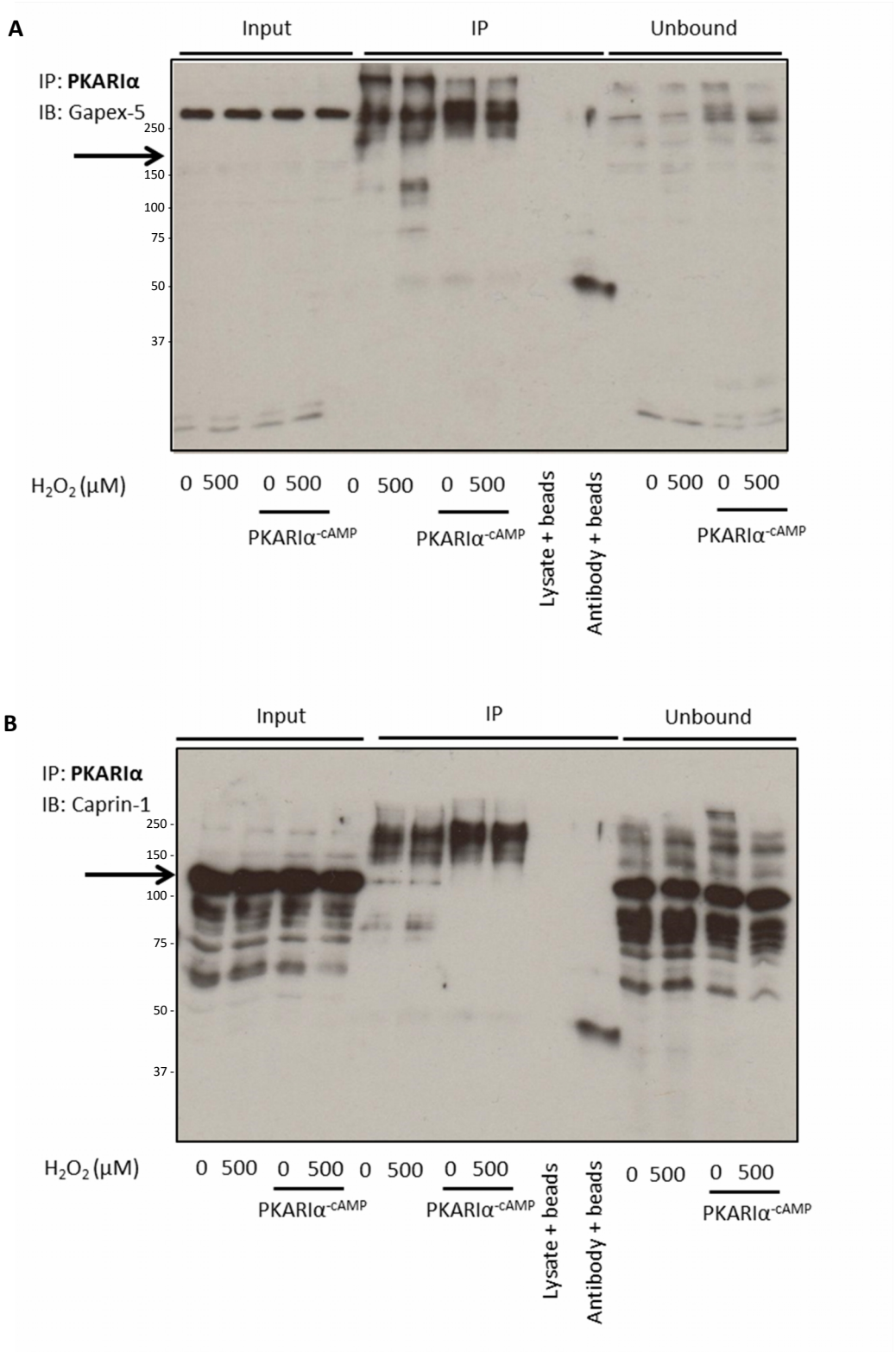

Figure 5.14 GAPex-5 and Caprin-1 are not redox state-dependent PKARIα binding partners. HEK 293 or PKARIα^{-cAMP} transfected HEK 293 cells were treated with vehicle or H_2O_2 were immunoprecipitated with anti-PKARIα. (**A**) GAPex-5 was not detected at the expected molecular weight on an immunoblot as indicated by the black arrow. (**B**) Caprin-1 was detected in immunoprecipitates as indicated by the black arrow.

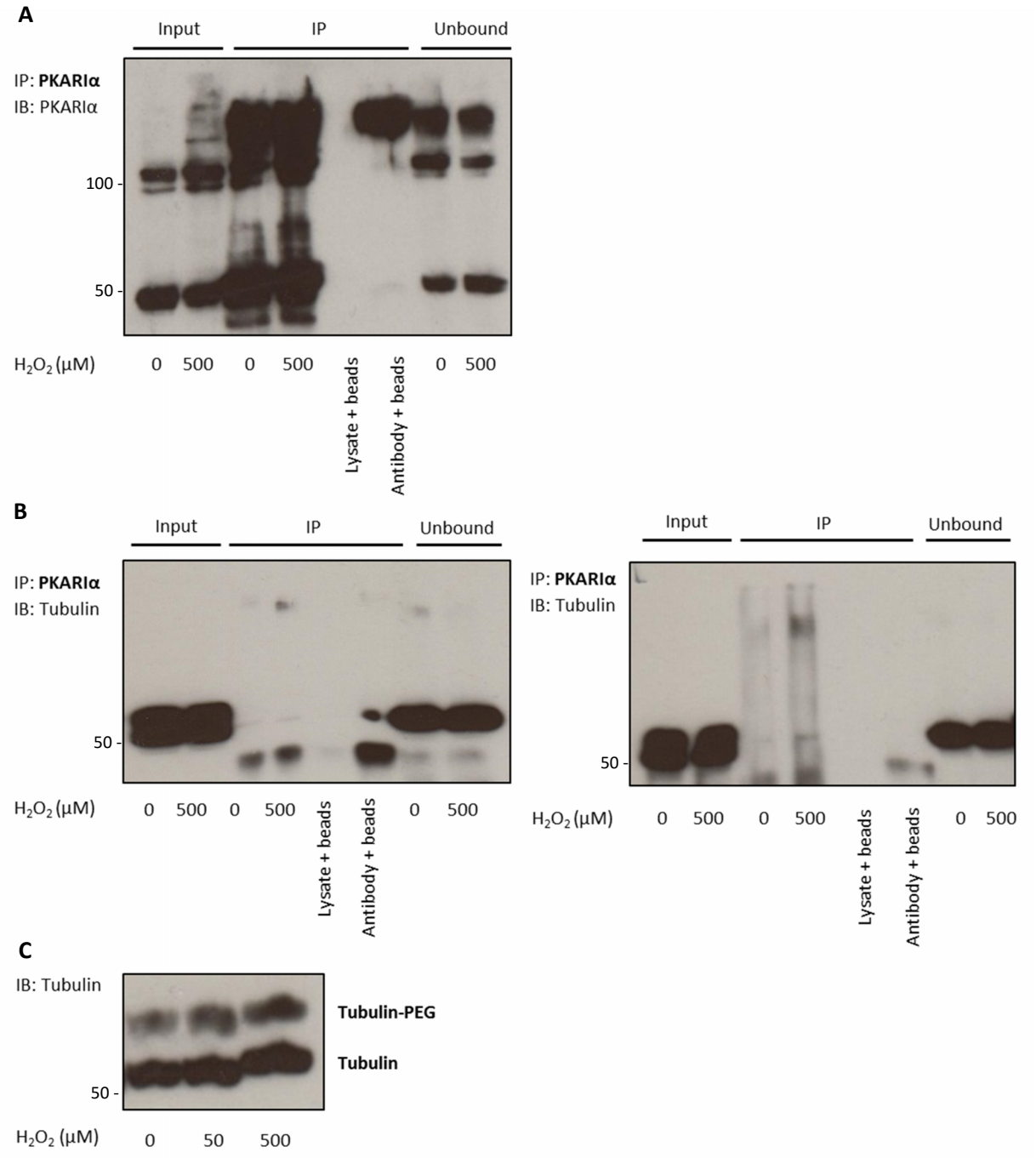

Figure 5.15 Tubulin forms a high molecular weight complex with PKARIα^{-cAMP} and is sensitive to reversible oxidative modifications. PKARIα^{-cAMP} transfected HEK 293 cells were treated with vehicle or H_2O_2 and the immunoprecipitated with anti-PKARIα. Immunoblots were probed with (**A**) anti-PKARIα or (**B**) anti-tubulin. (**C**) H_2O_2 treated (0-500 μM) HEK 293 cells underwent PEG-maleimide switch processing and tubulin was monitored in these samples by non-reducing immunoblotting.

5.3.8 Investigating the PKARIα and tubulin interaction

Further immunoprecipitation experiments were conducted in an attempt to verify the interaction between PKARIα and tubulin. HEK 293 cells were transfected with either PKARIα^{-cAMP} or C17SPKARIα^{-cAMP} and treated with H_2O_2 (500 μM). These experiments were performed using exactly the same protocol above whereby tubulin was co-captured or was identified by LC-MS/MS as part of a high molecular weight PKARIα complex. However quite inexplicably in these experiments, which were carried out at later date, tubulin was co-captured but was now observed at its expected molecular weight only (Figure 5.16). It is worth noting that only a small proportion of tubulin migrated at the higher weight complexes in the original experiments, and as explained above this is potentially only a transient, intermediate interaction. Despite the inability to detect a higher molecular weight complex, these immunoprecipitations still corroborated that PKARIα^{-cAMP} and tubulin exist in a complex, as tubulin was co-captured to a greater extent in cells where PKARIα^{-cAMP} was over-expressed. However, unlike the LC-MS/MS immunoprecipitations there did not appear to be a difference between in the PKARIα-tubulin interaction when cells were treated with H_2O_2. In immunoprecipitation experiments where HEK 293 cells were transfected with V5-PKARIα or V5-C17SPKARIα (these constructs had wild type cAMP binding sites), PKARIα was pulled down and tubulin was co-captured using a V5 antibody conjugated to agarose beads with no difference observed between vehicle or H_2O_2 treatment (Figure 5.17). Again, in non-transfected cells the amount of tubulin that was captured was significantly less than in transfected cells.

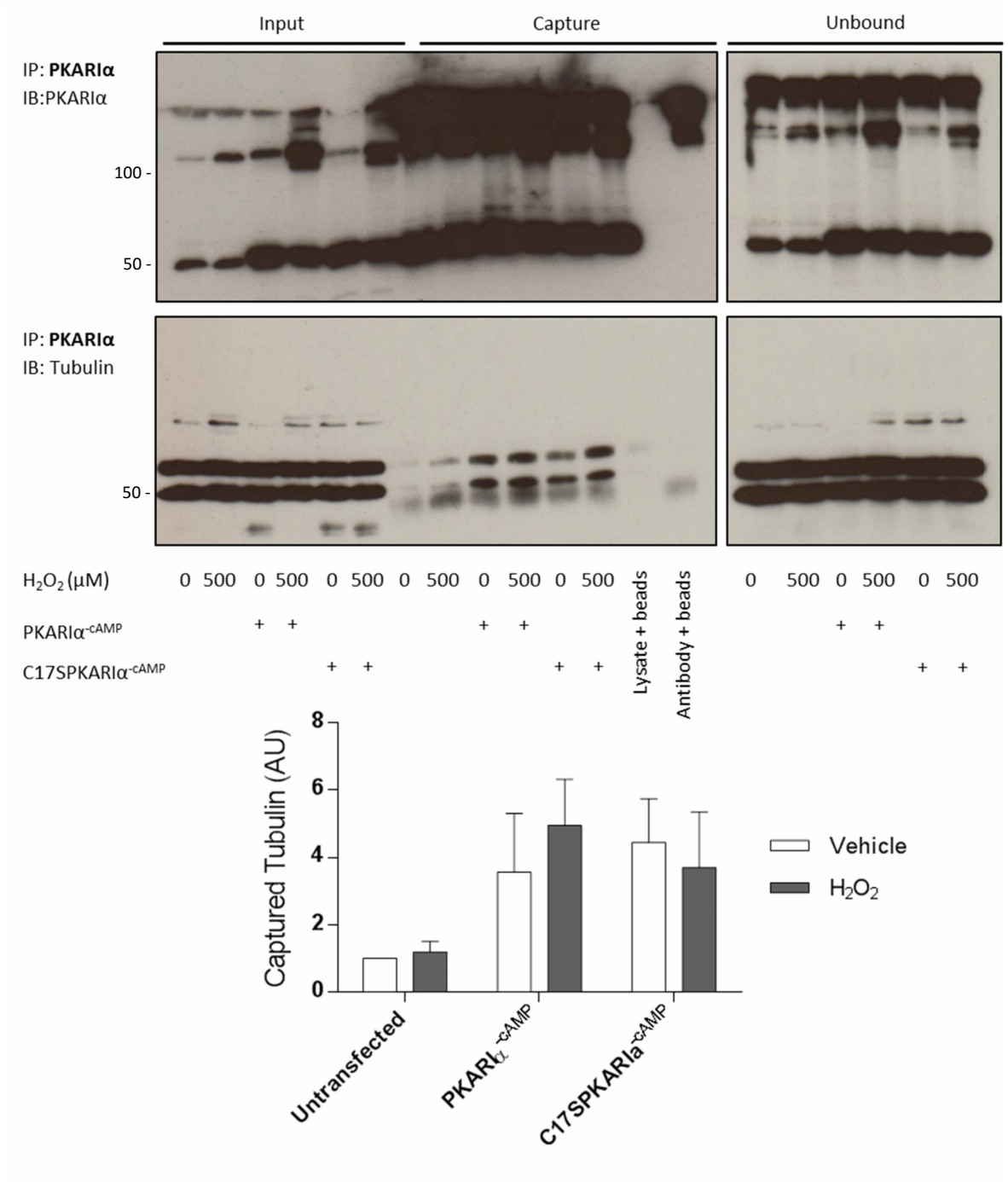

Figure 5.16 Tubulin is co-captured with PKARIα^{-cAMP} or C17SPKARIα^{-cAMP}. PKARIα^{-cAMP} or C17SPKARIα^{-cAMP} transfected HEK 293 cells were treated with vehicle or H_2O_2 and their lysates immunoprecipitated with anti-PKARIα. Immunoblots were probed with an antibody for either PKARIα or tubulin. The extent of co-captured tubulin is represented graphically (n=3 ± SEM)

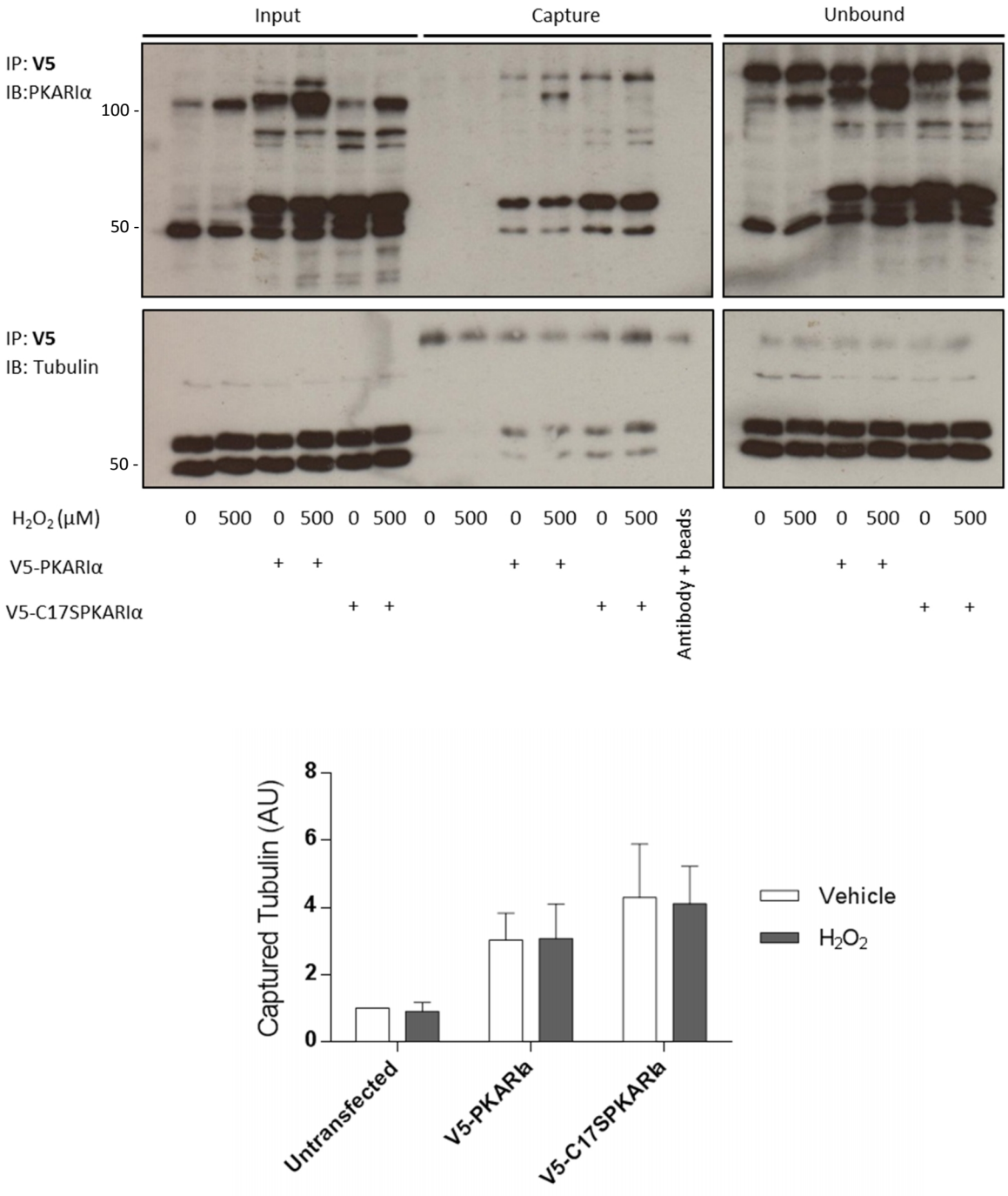

Figure 5.17 Tubulin is co-captured with V5-PKARIα or V5-C17SPKARIα. V5-PKARIα or V5-C17SPKARIα transfected HEK 293 cells were treated with vehicle or H_2O_2 and immunoprecipitated with a V5 antibody conjugated to agarose beads. Non-reducing immunoblots were probed with the antibody for either PKARIα or tubulin. The extent of co-captured tubulin is represented graphically (n=3 ± SEM)

The interaction between PKARIα and tubulin was further examined in vascular smooth muscle cells by co-immunostaining. Tubulin staining allowed visualisation of the microtubules. The pattern of PKARIα immunofluorescence was diffuse throughout the cell and overlapped with that of tubulin (Figure 15.18). However, there was no clear difference in co-localisation when cells were treated with vehicle or H_2O_2 (500 μM). Due to the ubiquitous nature of both of the proteins a more specific imaging technique was required to discern any differences between normal and oxidised conditions. Proximal ligation assay technology allows the detection of protein-protein (<40 nM apart) interactions of *in situ*. Figure 15.19 shows incubation with tubulin and PKARIα antibodies together generated staining in VSMCs following vehicle- or H_2O_2-treatment, whilst incubation of each antibody individually as negative controls generated negligible signals. H_2O_2 did not appear to increase the fluorescent signal which is consistent with the immunoprecipitation experiments. Taken together the immunoprecipitation and immunofluorescence experiments confirm tubulin as an AKAP.

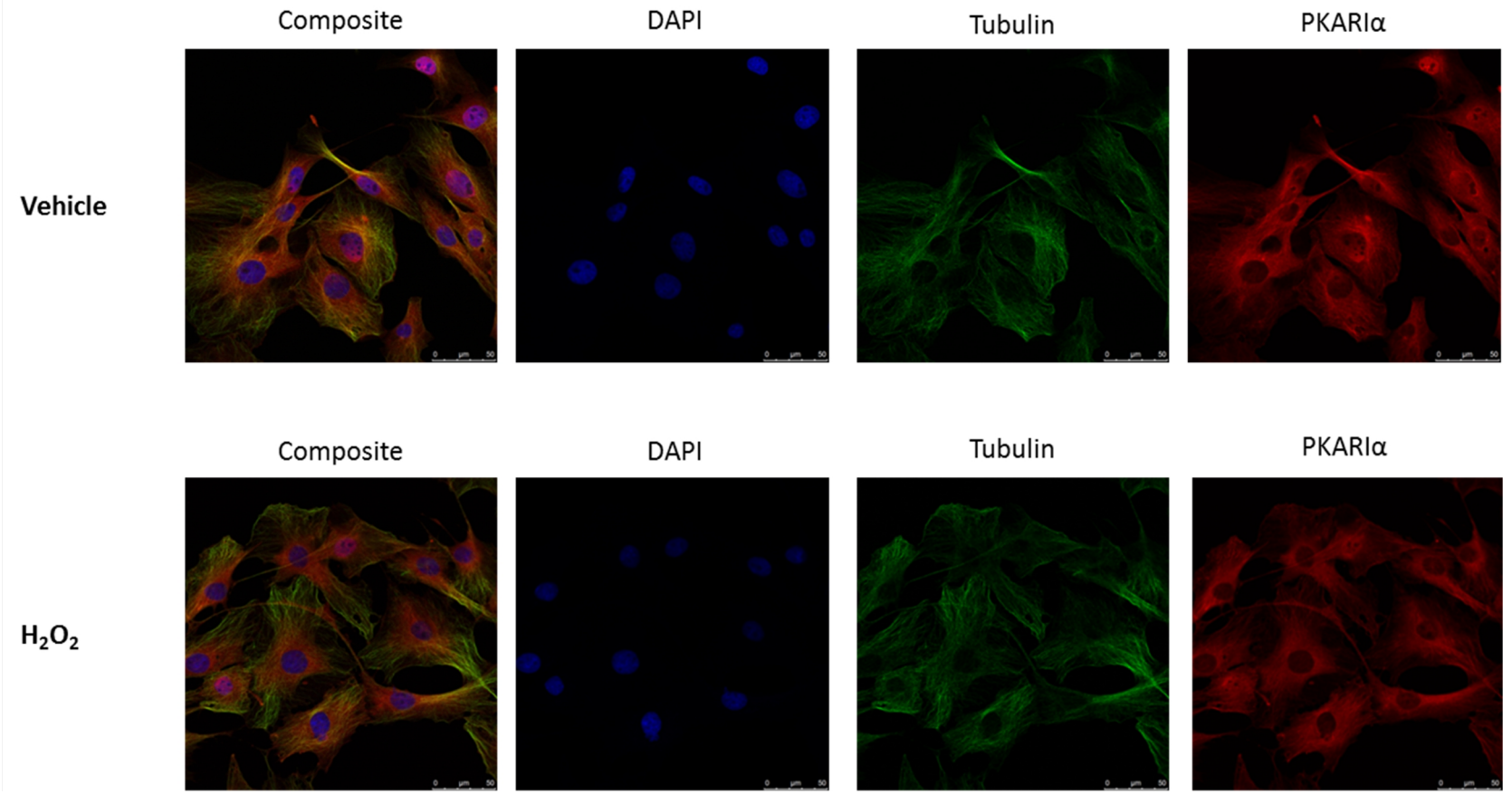

Figure 5.18 PKARIα is localised to tubulin in VSMCs. Representative immunofluorescent image. VSMCs were treated with vehicle or H_2O_2 (500 μM) and then stained with tubulin (green) and PKARIα (red) antibodies. The nucleus was stained with b4',6-diamidino-2-phenylindole (DAPI, blue).

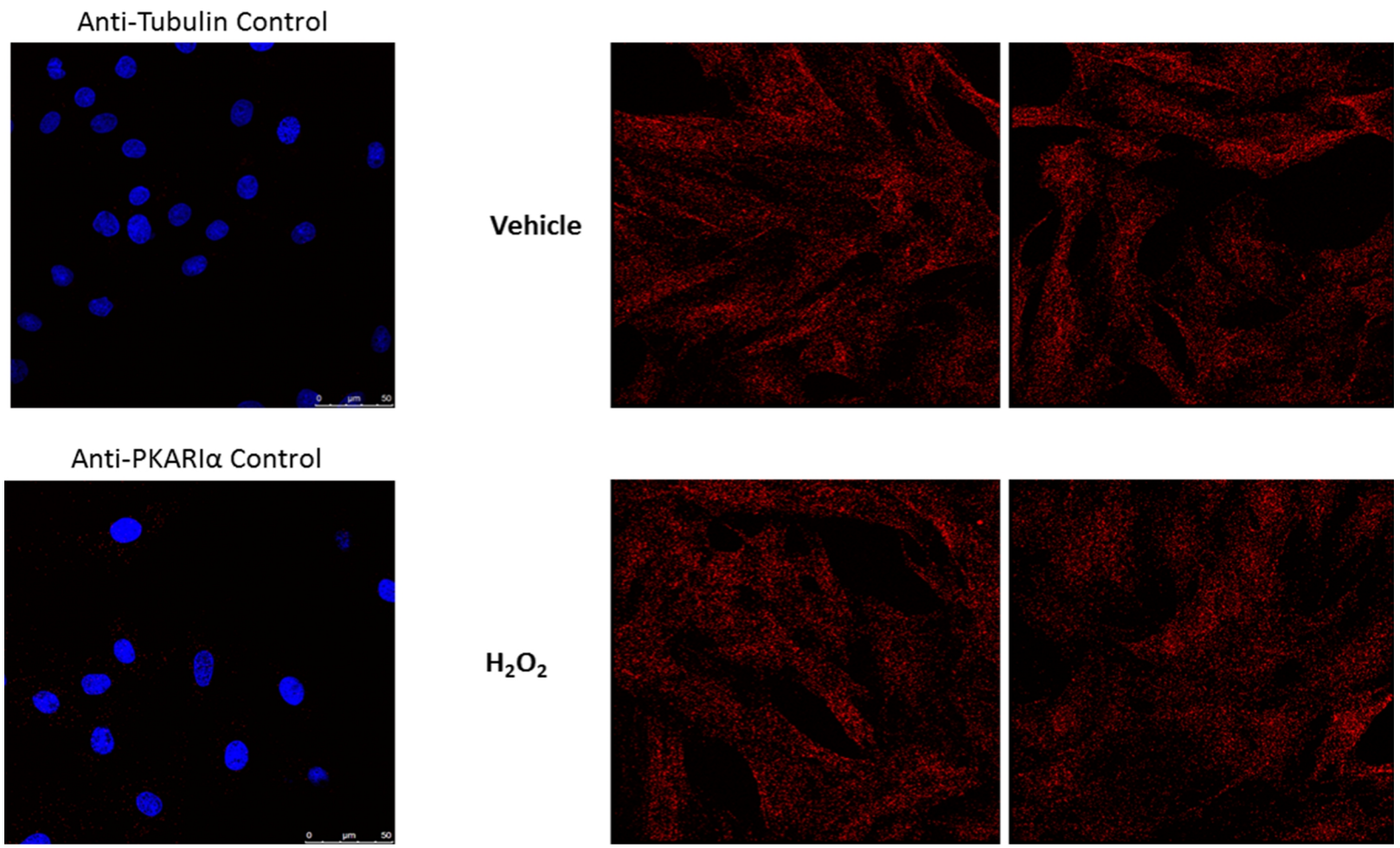

Figure 5.19 PKARIα is localised to tubulin in VSMCs. Representative image of Proximity Ligation Assay. VSMCs were treated with vehicle or H_2O_2 (500 µM) and then stained with tubulin and PKARIα antibodies. The nucleus was stained with b4',6-diamidino-2-phenylindole (DAPI, blue). Each red dot represents the detection of protein-protein complexes.

5.4 Discussion

cAMP activates PKARIα to induce substrate phosphorylation and here it is demonstrated that cAMP may also govern the localisation of PKARIα through its capacity to modulate the redox state of PKARIα. cAMP-agarose appears to induce the reduction of PKARIα from a disulfide dimer to a monomer, perhaps via allosteric modulation of a PKARIα-AKAP disulfide intermediate that leads to the reduction of the mixed disulfide complex and of PKARIα. Evidence of a cAMP- and redox-dependent transitory PKARIα-tubulin mixed disulfide complex was provided, as well as confirmation of tubulin as a bona-fide AKAP. Ultimately the redox-dependent interaction between tubulin and PKARIα may govern the phosphorylation of microtubule associated proteins which is explored in Chapter 6.

5.4.1 PKARIα reduction induced by cAMP-agarose

cAMP-agarose induced the reduction of PKARIα disulfide dimer in the presence of the alkylating agent maleimide, but failed to do so in the absence of maleimide. Figure 15.20 shows a model of what may be occurring under the two different conditions. As the redox state of PKARIα can be stabilised with maleimide-containing lysis buffer, and this is protective against artificial air oxidation, it is reasonable to assume that maleimide is capable of alkylating the disulfide PKARIα cysteines more rapidly than oxygen is able to induce disulfide formation. Therefore when cAMP induces the reduction of the PKARIα disulfide the free thiols rapidly react with maleimide, thus stabilising the monomer to allow detection of PKARIα in this form. Without maleimide, the free thiols simply re-oxidise in air after cAMP induced PKARIα disulfide reduction and therefore PKARIα is observed as a dimer on an immunoblot. To the best of my knowledge, there is no report of cAMP-agarose influencing the redox state of PKARIα. Typically alkylating agents such as maleimide are not included in the buffers used to prepare samples or during SDS-PAGE as it has been here, thus PKARIα would always be observed at 50 kDa under the standard reducing conditions that are widely used.

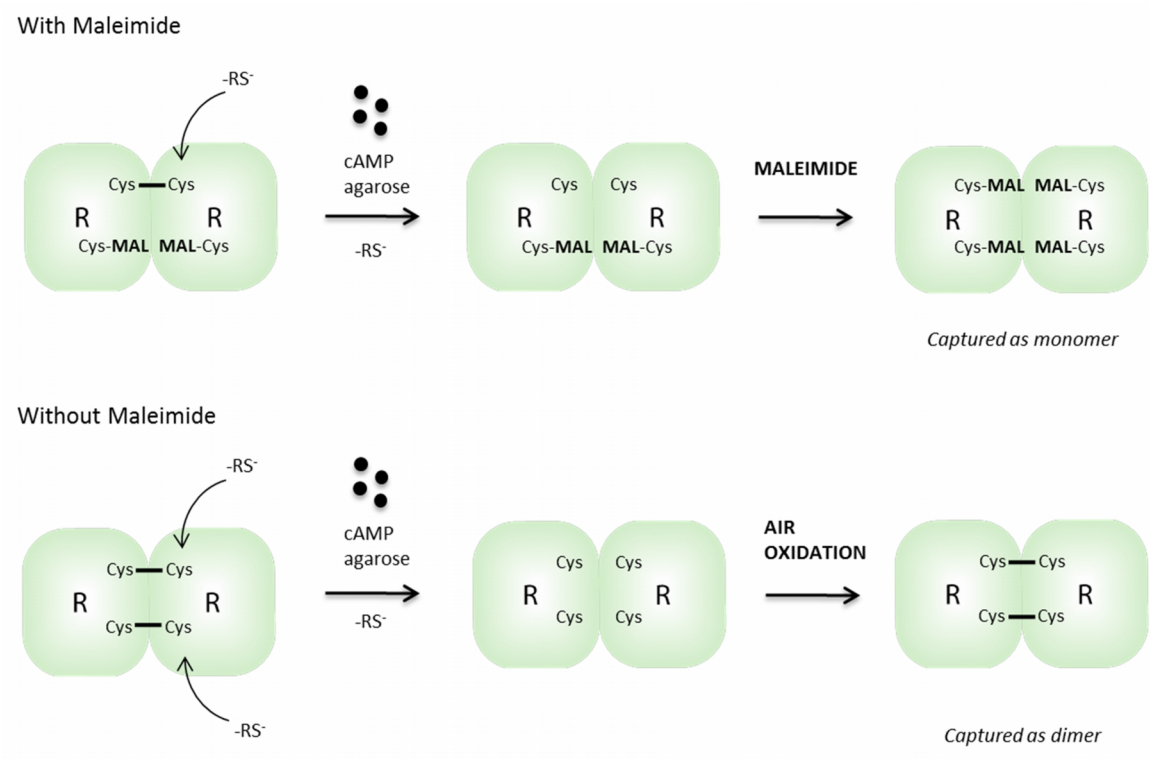

Figure 5.20 Model of disulfide PKARIα reduction during exposure to cAMP-agarose in the absence or presence of maleimide

The biotin-maleimide experiment demonstrates that there are free thiols in the lysate during cAMP-agarose incubation. 0.5 mM biotin-maleimide was able to label thiols even after lysate had been incubated with 100 mM maleimide, demonstrating the initial alkylation step is not fully efficient. The thiol(s) responsible for reducing PKARIα must be, at least partially, insensitive to air oxidation as well as resistant to maleimide alkylation (at the low temperature used for preparing lysate for homogenates). However it must be reactive enough to reduce a disulfide bond. This at first appears to be contradictory unless basally the thiol residue is concealed and therefore protected from oxidation and alkylation, and then upon cAMP binding, the structural conformation of the protein is altered thus revealing the free thiol which is now capable of attacking the cysteine on PKARIα. A mechanism whereby a conformational change can lead to the exposure of a reactive cysteine has previously been proposed in APE1[80].

One such thiol-containing candidate protein that may be involved in disulfide PKARIα reduction is thioredoxin (Trx). Members of this laboratory have used specially engineered mice where the resolving Cys35 in Trx has been mutated to a serine residue. Consequently Trx forms a mixed disulfide with target proteins and remains bound to them, enabling detection of these targets through immunoprecipitation of Trx and immunoblotting for suspected binding

partners. Using this method the known Trx target ASK1 was co-captured, as was the novel Trx target PKGIα[266]. However, PKARIα was not co-captured suggesting that it is not a target of Trx (data not shown). 1 mM or 2 mM concentrations of H_2O_2 led to increased capture of disulfide PKARIα which may indicate oxidation of the hypothesised resolving thiol (potentially in tubulin). To prove the existence of the resolving thiol systematic mutation of candidate cysteine residues to serines would lead to the stabilisation and accumulation of the PKARIα-AKAP intermediate post-H_2O_2 treatment.

In agreement with results presented above, it has previously described that high concentrations of DTT are necessary to reduce PKARIα which perhaps suggest that the thiols are reasonably inaccessible[198]. cAMP potentiated DTT-induced reduction of PKARIα but not PKARIα^{-cAMP}. This is consistent with the hypothesis that a cAMP-induced conformational change can alter the accessibility of PKARIα cysteines involved in dimer formation to DTT and other free thiols. DTT-inaccessible disulfides that become susceptible to reduction after allosteric modulation have been previously described in ionotropic glutamate receptors[198] and are also hypothesised to be present in titin[267].

5.4.2 LC-MS/MS identification of tubulin

The high molecular weight complexes observed after H_2O_2 with PKARIα^{-cAMP} potentially provides insight into PKARIα redox signalling as they may represent intermediates that arise from PKARIα targeting to AKAPs. MS analysis of tryptic digests excised from sequential non-reducing-reducing SDS-PAGE analysis of PKARIα^{-cAMP} immunoprecipitates identified tubulin as a component of a high molecular weight complex.

Kuruso *et al.* previously demonstrated that PKARI forms a high molecular weight complex with tubulin in both *Aplysia* and in mouse brain extract that was sensitive to the reducing agents DTT and β-ME[265]. Furthermore this high molecular weight complex was lost in *Aplysia* ganglia treated with serotonin, a neurotransmitter that elevates intracellular cAMP, an observation that compliments the cAMP-agarose data in this Chapter. The authors also suggest that the high molecular weight complex formation enriches PKARI at the synaptic end. In the context of redox signalling, the presence of PKARIα within disulfide complexes may be a mechanism by which oxidants intensify cAMP signals by concentrating the PKARIα holoenzyme in a specific location.

A quantitative replicative proteomic approach would have been a more comprehensive strategy for identifying PKARIα binding partners. Proteomics with replicates would have allowed the identification of interactions that were reproducible (i.e. statistically significant)

and so avoid false positive hits. This approach allows confidence that the identified protein are genuine interactors of PKARIα and would be considered as part of future work to identify other PKARIα binding partners that may interact via a similar redox mechanism to tubulin.

5.4.3 Tubulin as a redox sensitive protein

The α/β tubulin heterodimer contains up to 20 highly conserved cysteine residues[268]. Under basal conditions these are not disulfide-linked but have been shown to transiently form disulfides to aid correct folding[269]. 19 of the 20 cysteines are capable of reacting with disulfide reagents (such as ODNB, DTNB, 2-DTP) and the accessibility of these cysteines is greatly diminished when microtubules are intact[268]. Specifically, modification of Cys315, Cys316 or Cys376 in α-tubulin and Cys129, Cys131 Cys242 or Cys356 in β-tubulin have been putatively identified as redox sensitive cysteines. These cysteines are responsible for intra-protein disulfides or disulfide homodimers under favourable oxidative conditions which can then be reduced by the glutaredoxin reductase system[270,271]. Although it appears that no previous studies have demonstrated that PKARIα can disulfide hetero-dimerise with other proteins, tubulin has been shown to from such complexes. *in vitro* incubation of β-tubulin with glyceraldehyde-3-phosphate dehydrogenase (GAPDH) leads to the formation of high molecular weight complexes that are reducible with β-ME[272]. Interestingly GAPDH was also identified as a PKARIα disulfide binding protein from our proteomic screen and a potential redox interaction between the three proteins may be a rational subject of future investigation.

5.4.4 Analysis of the oxidant-dependent interaction between PKARIα and tubulin

PKA regulatory subunits classically bind to an amphipathic α-helix and α/β-tubulin both contain 12 α-helices. An examination of the X- ray crystal structure of the α/β- tubulin complex shows a few of these helices face externally and could potentially be PKARIα binding domains (Figure 5.21). Interestingly two cysteine residues (including the evolutionary conserved Cys128) separated by an aspartic acid lie adjacent to the outward facing helix 3 on the β subunit, and thus it is tempting to speculate that these cysteines may be involved in the redox interaction between PKARIα and tubulin, but this requires further investigation.

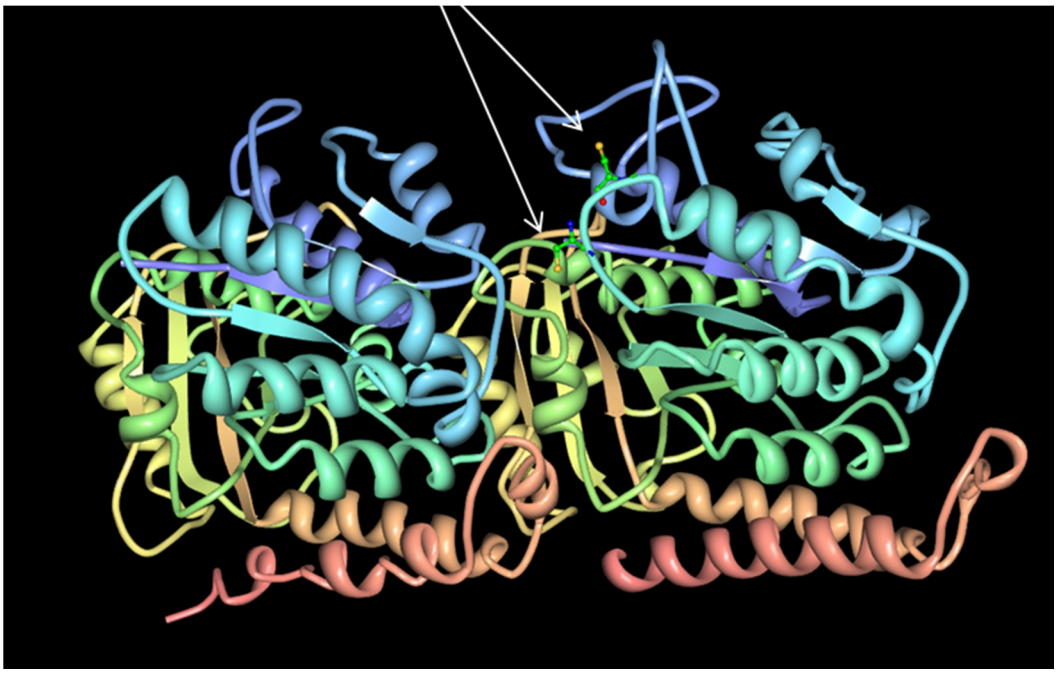

Figure 5.21 Crystal structure of α- and β-tubulin. The complex contains two proximal outward facing cysteines (Cys128 and Cys130, indicated with white arrows) residues adjacent to an α-helix

The tubulin antibody routinely used in the lab is a polyclonal antibody from Cell Signaling Technologies. Using this antibody I was initially able to detect tubulin running as a high molecular weight complex but subsequently this complex was no longer detected despite experimental conditions being the same. Due to the polyclonal nature of the antibody there may be slight batch-to-batch variation. This may mean that whilst one batch is able to detect the high molecular weight complex another batch may not. Still, in this study the interaction was established between tubulin and PKARIα via immunoprecipitations even if the oxidant-dependent higher molecular weight were not consistently observed. This can potentially be overcome by screening a number of other commercial tubulin antibodies from various companies that have been able to detect tubulin dimers[272,273]. Co-localisation of PKARIα and tubulin has previously been established. Immunofluorescent experiments show type I PKA is localised to interphase microtubules in epithelial cells[274]. PKARIα regulates meiotic arrest in oocytes mediated via co-localisation with tubulin[275] and PKA-Cα is associated with acetylated microtubules[276]. PLA is a useful tool to quantify such protein-protein interactions in their natural context at physiological expression levels. PLA detects interactions at <40 nm[277], and therefore likely detected a direct *in situ* cellular interaction between PKARIα and tubulin for the first time.

If PKARIα can be recruited to AKAPs such as tubulin via an inter-protein disulfide, and that cAMP may modulate this disulfide bond, then perhaps cAMP may regulate PKARIα activity by

more than just simply activating it. Figure 15.22 illustrates a proposed model whereby H_2O_2 targets PKARIα to tubulin, and once recruited, cAMP induces the reduction of the inter-protein disulfide whilst also activating the kinase to permit substrate phosphorylation. At this point the cycle continues whereby another PKARIα enzyme can be disulfide targeted to tubulin, reduced via cAMP and simultaneously activated to phosphorylate the tubulin associated substrate. ROS and cAMP work together to dictate the subcellular location of PKARIα, keeping the enzyme in close proximity to the substrate and in a region of high cAMP concentration to increase local responsiveness. The end result of this ROS and cAMP-dependent cycle is enhanced substrate phosphorylation compared to cAMP alone, as observed in Chapter 3. cAMP and ROS signalling are integral for correct cellular function and PKARIα is able to integrate these two inputs. The physiological or pathophysiological context would determine whether ROS-potentiated increase in PKA substrate phosphorylation would be beneficial or detrimental and such effects are explored further in Chapter 6.

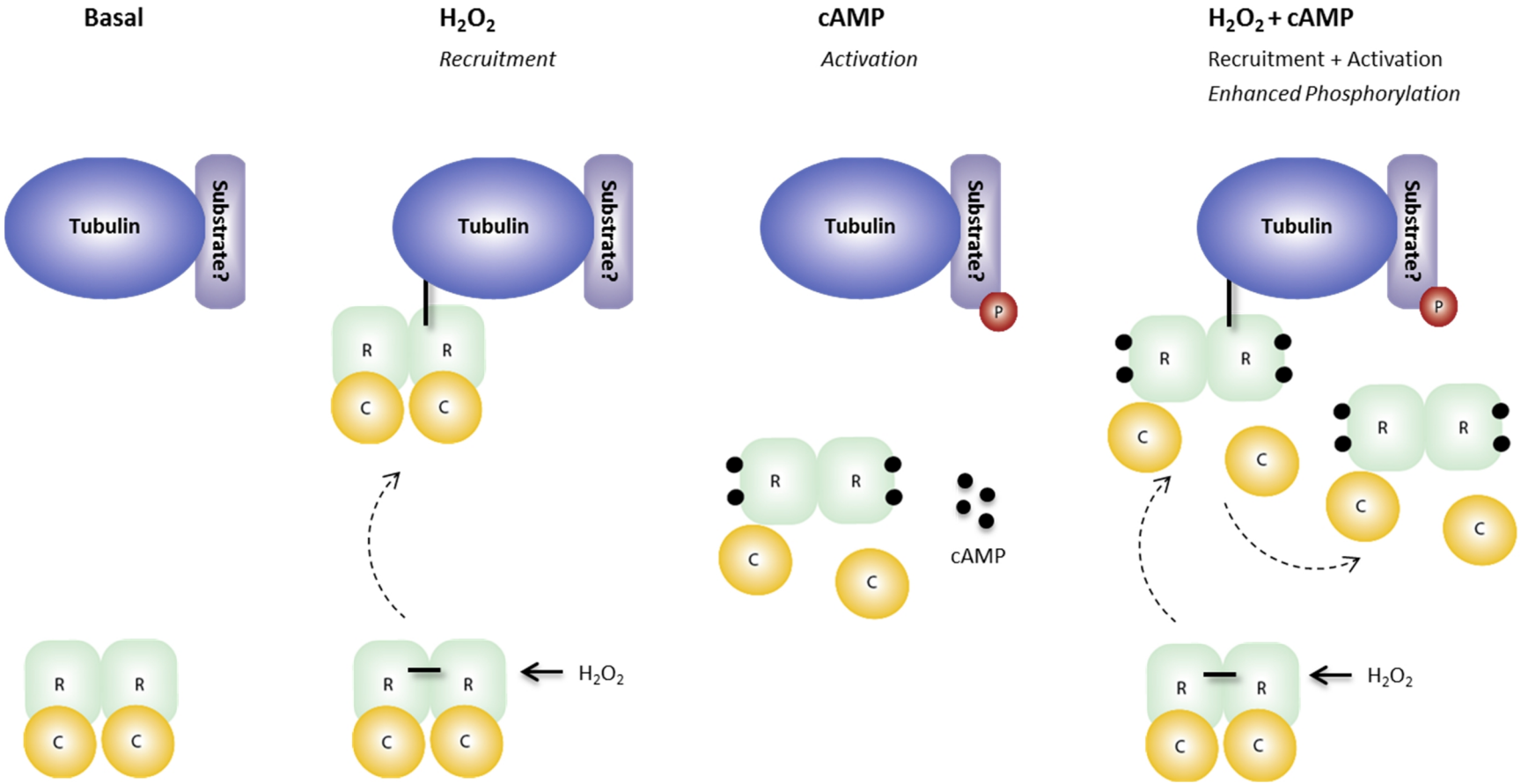

Figure 5.22 A proposed model for the co-operative action of cAMP and ROS on PKARIα and tubulin to facilitate substrate phosphorylation

6 Investigating the integration of cAMP and oxidant signals by PKARIα on GEF-H1 phosphorylation

6.1 Introduction

In the previous chapter tubulin was identified as a novel redox-dependent PKARIα AKAP. If tubulin is indeed an AKAP there will be substrates within the PKARIα-tubulin complex, and as such, tubulin would serve to localise the kinase with these specific targets. It is logical to predict that such substrates would be microtubule associated proteins (MAPs), a number of which have previously been described as targets of PKA phosphorylation as considered below in more detail. Therefore it is rational to suggest that the phosphorylation status of substrates within the PKARIα-tubulin complex will be dependent on both oxidant and cAMP signals. This chapter will aim to identify microtubule associated proteins (MAPs) that are differentially phosphorylated by PKARIα depending upon the concentrations of oxidants and cAMP.

6.1.1 Role of the microtubules

α- and β-tubulin are major components of the microtubules, filamentous structures that are an integral part of the eukaryotic cytoskeleton with many diverse roles including, organelle and protein trafficking, mitosis, and broadly maintenance of cell structure and shape[278]. α- and β-tubulin heterodimers bind head to tail to form protofilaments, 13 of which assemble laterally to form a hollow tubule to make up a microtubule (Figure 6.1A). Microtubules are highly dynamic polymers that are intrinsically polarised and switch between periods of slow growth and rapid shrinkage[279]. GTP must be bound to α- and β-heterodimers to allow association with other heterodimers, as such, the hydrolysis rate of tubulin bound GTP to GDP is thought to determine the rate of microtubule depolymerisation at the dynamic plus end. The minus end of the microtubules is usually stabilised by microtubule organising centres which in most cell types is the centrosome[280].

Broadly speaking there are three main classes of proteins that interact with the microtubules. One class are the motor proteins such as kinesin and dynein that drive organelle transport[281], another class being MAPs that bind to tubulin to destabilise or promote microtubule formation[278]. The phosphoregulation of MAP activity has been well documented[282-284]. Hyperphosphorylation of the MAP tau leads to detachment from tubulin and reduction in

microtubule stability, a hallmark of Alzheimer's disease[285]. Similarly phosphorylation of MAP2 inhibits its microtubule stabilising activity[286]. In contrast, stathmin forms a ternary complex with an α/β-tubulin heterodimer to prevent microtubule polymerisation, whilst stress-induced phosphorylation inhibits this action[287,288]. The third class of proteins is a heterogeneous group, including PKARIα, which bind to the microtubules as scaffolds or for other reasons that have not yet clearly been defined. The redox regulated PKARIα-tubulin interaction may play a role in microtubule dynamics but also in actin cytoskeleton dynamics through the phosphorylation of the MAP, and the established PKA substrate guanine nucleotide exchange factor H1 (GEF-H1).

6.1.2 RhoA and GEF-H1

Guanine nucleotide-binding proteins of the Ras homology family (Rho-GTPases) are intracellular signalling molecules that cycle between an active GTP bound and an inactive GDP bound conformation[289]. RhoA is a well-characterised GTPase that is best known for binding to and activating effector kinases Rho-associated protein kinase 1 and 2 (ROCK1/2) to induce local actin filament assembly[289]. For GTPase-dependent processes to proceed, guanine exchange factors (GEFs) are necessary to catalyse the dissociation of GDP and permit the binding of GTP to activate the protein. GEFs modify the nucleotide binding domain of GTPases to decrease its affinity for GDP thus facilitating release and replacement with GTP. The active GTP bound conformation of the G protein is favourable because the cytosolic concentration of GTP is 10 times greater than GDP[290].

GEF-H1 is a 100 kDa protein that contains the Dbl homology domain (DH) and an adjacent pleckstrin homology domain (PH) that underpins its exchange activity and characterises the RhoGEF family (Figure 6.1B). GEF-H1 activation of RhoA regulates actin cytoskeleton-dependent processes, promoting paracellular transport[291] and increasing endothelial barrier permeability[292-294]. GEF-H1 also has a role in cytokinesis[295], promotion of mitotic spindle assembly[296], enhancement of stress fibre formation[297]; therefore given this diverse number of cellular roles its exchange activity must be tightly regulated. Uniquely GEF-H1 activity is inhibited when bound to the microtubules. Mutations of key residues in the C-terminal zinc finger are sufficient to disrupt the interaction and increase GEF-H1 exchange activity[297]. Physiological or drug-induced depolarization of the microtubules releases GEF-H1, thus, it has emerged as a prominent effector of microtubule-dependent RhoA activation[294].

6.1.3 Phospho-regulation of GEF-H1

Phosphorylation of specific GEF-H1 residues can positively or negatively regulate its exchange activity. ERK1/2 phosphorylates Thr^{678} to enhance GEF-H1 activity and promote RhoA-dependent actin fibre assembly. In contrast, PKA phosphorylates GEF-H1 on Ser^{885} to promote its association with 14-3-3η and inhibit its exchange activity[298]. Meiri *et al.* demonstrated GEF-H1 phosphorylation was prevented by the PKA inhibitor H89. Furthermore, lysophosphatidic acid (LPA)-induced actin stress fibre formation in fibroblasts was suppressed by forskolin (an activator of AC) treatment directly due to the inability of GEF-H1 to activate RhoA (Figure 6.1C)[298].

The oxidant-dependent interaction between PKARIα and tubulin may regulate phosphorylation of MAPs such as GEF-H1. PKA-dependent phosphorylation of GEF-H1 represents a regulatory mechanism to prevent over-activity of GEF-H1 and consequent RhoA-dependent actin fibre formation that induces an increase in endothelial barrier permeability[292,294,299,300]. Exacerbated vascular permeability and consequent interstitial fluid accumulation is associated with the pathogenesis of sepsis[301]. As such, GEF-H1 phosphorylation may play a role in disease progression. A mechanism for PKA to fine-tune the extent of GEF-H1 phosphorylation would allow the cell to tightly co-ordinate downstream cellular responses. Here I present evidence that suggests PKARIα can integrate oxidant and cAMP signals to synergistically phosphorylate GEF-H1 to decrease RhoA activity and regulate endothelial barrier permeability.

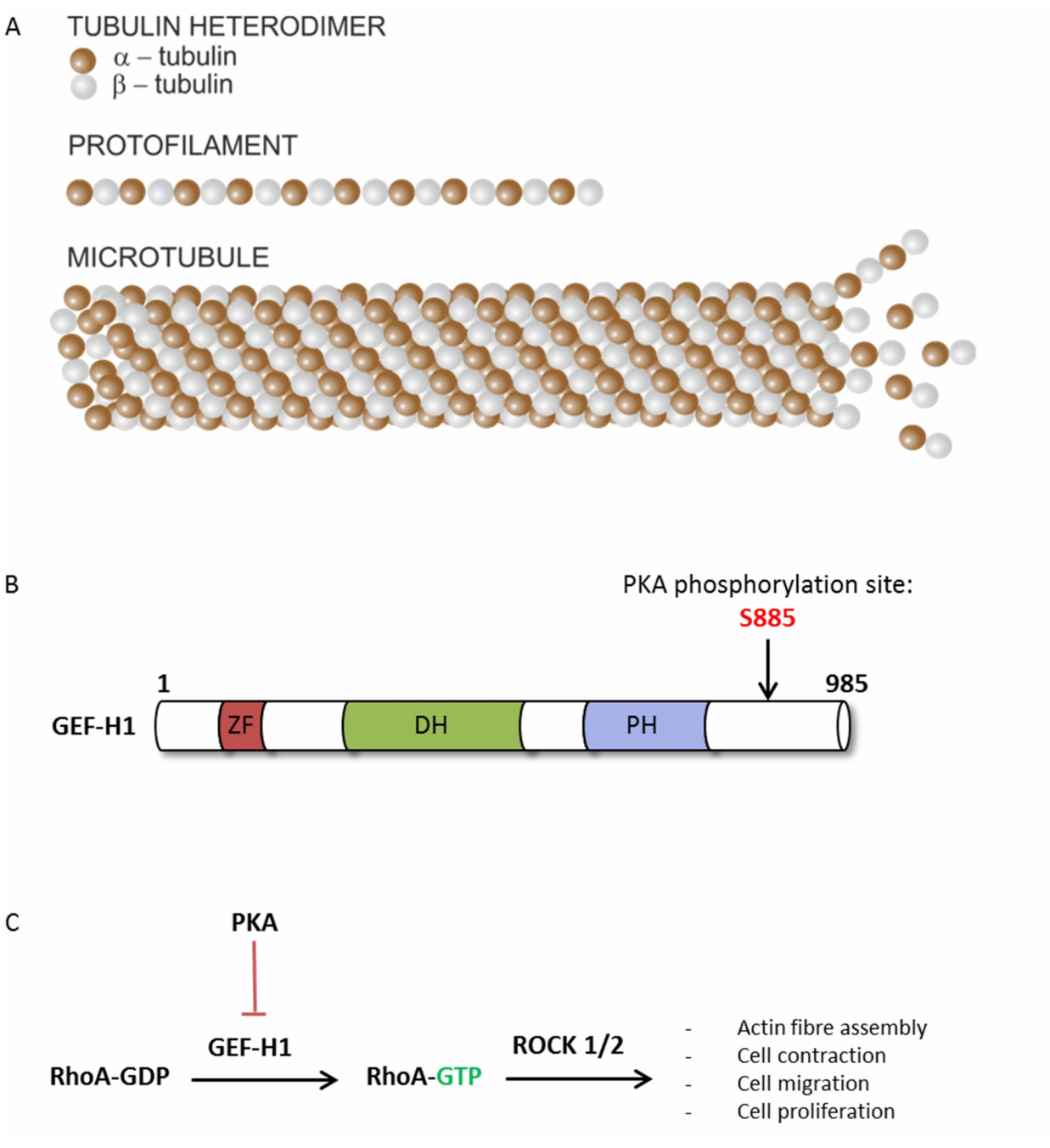

Figure 6.1 Overview of microtubules, GEF-H1 and RhoA. (**A**) Cartoon depicting the arrangement of α- and β-tubulin as components of the microtubules. (**B**) A schematic representing the domain structure of full length GEF-H1. Abbreviations: Zinc finger motif (ZF) Dbl-homologous domain (DH), Pleckstrin domain (PH). (**C**) The role of GEF-H1 and PKA in the classical RhoA signalling pathway. *Figure adapted from Vydra and Havelka 2012*[302].

6.2 Specific Methods

6.2.1 Antibodies

Antibody	Purchase Code	Company	Species	Dilution
anti-GEF-H1	4076	Cell Signaling Technology	Rabbit	1:500
anti-pGEH-H1	ab74156	Abcam	Rabbit	1:500

Table 6.1 Antibodies used in Chapter 6

6.2.2 Microtubule polymerisation assay

Cells were lysed in a microtubule stabilization buffer (100 mM PIPES (pH 6.9), 5 mM $MgCl_2$, 1 mM EGTA, 30% glycerol, 0.125% Nonidet-P40, 0.1% Triton X-100, 0.1% Tween 20, 100 µM GTP, 1 mM ATP, and 2 µM paclitaxel and protease inhibitors) which was maintained at 37°C. Lysates were centrifuged at 15,000 g for 30 min at 37°C. Soluble fractions were removed and added to x4 SDS-sample buffer and represented unpolymerised microtubules. Pellets were resuspended in microtubule stabilisation buffer, added to x4 SDS-PAGE sample buffer and boiled at 95°C for 5 min. This represented the polymerised microtubules.

6.2.3 PKARIα Cys17Ser knock-in mice

Mice constitutively expressing PKARIα Cys17Ser were generated for us on a pure C57BL/6 background by TaconicArtemis. A targeting vector was constructed for murine Prkar1a by introducing the Cys17Ser mutation into exon 1 by site-directed mutagenesis and inserting an FRT-flanked neomycin selection marker (to allow for selection of transfected embryonic stem cells) close to the mutation to favour homologous recombination. Then screening by Southern blot was carried out to identify if homologous recombination had occurred followed by validation of the positive clones. Embryonic stem cell transfection was then carried out followed by chimera generation. The chimeras were directly bred with an Flp deletor for the *in vivo* deletion of the selection marker. As the embryonic stem cells always go germline, chimeras can be directly bred to the deletor to obtain germline transmission and selection marker deletion at the same time.

6.2.4 Analysis of GEF-H1 phosphorylation in aortic rings

The thoracic aorta was isolated, excised and cleaned to remove fat, connective tissue and blood by Miss Alisa Kamynina. Aortas were cut into four equally sized ring and placed into 96

well plates with pre –heated x media and incubated overnight at 37°C. Aortic rings were treated with vehicle, 200 μM H_2O_2, 100 nM forskolin or co-treated with both on the subsequent day for 10 min. Rings were snap frozen in liquid nitrogen, crushed on with pre-cooled, small pestle and mortal and solubilised with x4 SDS-sample buffer prior to boiling at 95°C.

6.2.5 Induction of sepsis with cecal ligation and puncture

The cecal ligation and puncture (CLP) procedure was used as a model of sepsis and was performed as described[303]. 9-15 week-old C57BL/6J mice were anesthetised using 5% (vol/vol) isoflurane with oxygen (flow rate of 0.5 L/min) in an induction chamber and subsequently maintained with 2% isoflurane with oxygen (flow rate of 0.5 L/min) via a nose cone. Mice were placed on a heating pad to maintain body temperature and positioned in dorsal recumbency. A 10 mm laparotomy was performed, and the cecum was exteriorised. The distal half of the cecum was subjected to ligation with suture and subsequently punctured twice with a 19-gauge needle. The cecum was gently squeezed to exteriorise a 1-2 mm of cecum content and then replaced in the abdomen. Sham operated mice underwent an identical procedure without cecal ligation and puncture. The abdominal wall incision was subsequently sutured shut. After surgery, mice were injected with analgesia (Vetergesic, Alsoe Ltd, 0.1 mg/kg) intraperitoneally and resuscitated with 1 ml per 30 g body weight subcutaneous injection of pre-warmed physiological salt solution (Normasol, STERETS). Animals were left to recover for 30 min in an incubator at 26°C. Sham mice received 0.5 ml saline per 30g body weight subcutaneously instead of 1 ml. All surgical procedures were kindly performed by Miss Alisa Kamynina. After 24 h lungs were harvested, snap-frozen in liquid nitrogen and stored at -80°C. Lung homogenates (100 mM Tris pH 7.4, 100 mM maleimide, protease inhibitor, 10% w/v) were re-suspended in non-reducing SDS-PAGE sample buffer.

6.2.6 Sepsis score

The sepsis score, reflecting the severity of the disease, was assessed at 24 h immediately prior to culling and recorded for each mouse. The evaluated parameters were general appearance, eye appearance, activity, level of consciousness, response to stimuli, respiration rate and respiration quality. Mice were given a score from 0 to 5 for each parameter, with 5 indicating the most severe state. After the parameters were assessed the modal value was taken to be the sepsis score for each mouse. The sepsis scores were then averaged to give a sepsis score for each experimental group. Blinded observations and assessment was conducted by Miss Alisa Kamynina.

6.3 Results

6.3.1 Investigating the effect of PKA activation on microtubule dynamics

As demonstrated in the previous chapter PKARIα interacts with tubulin. To investigate whether the redox-dependent PKARIα-tubulin interaction has an effect on microtubule dynamics, a microtubule polymerisation assay was conducted in HEK 293 cells. The presence of tubulin in the detergent-soluble fraction represented the free tubulin at the time of cell lysis, whilst purification of tubulin in the pellet represented tubulin that was polymerised as microtubules. The percentage of tubulin in each fraction was subsequently determined by immunoblot analysis.

PKA activation did not significantly alter the percentage of free tubulin in the supernatant after 10 min (control: 37±2% vs. 8-CPT-cAMP: 32±7% vs. H_2O_2: 30±2% vs. cAMP + H_2O_2: 38±7%) or 120 min treatment (control: 37% ± 2% vs. 8-CPT-cAMP: 26% ± 4% vs. H_2O_2: 35% ± 9% vs. cAMP + H_2O_2: 33% ± 3%) (Figure 6.2). HEK 293 cells were also treated with the microtubule stabilising agent paclitaxel, or the microtubule depolymerising drug nocodazole as controls to ensure the assay was functioning as expected. The percentage of tubulin in the soluble fraction after paclitaxel treatment was significantly lower (5±1%) compared to control (37±2%), whilst the percentage of tubulin in the soluble fraction was significantly higher post nocodazole treatment (37±2% vs. 83±7%). These results substantiate that the assay was performing as intended, but also confirmed that activation of PKA has no effect on microtubule dynamics.

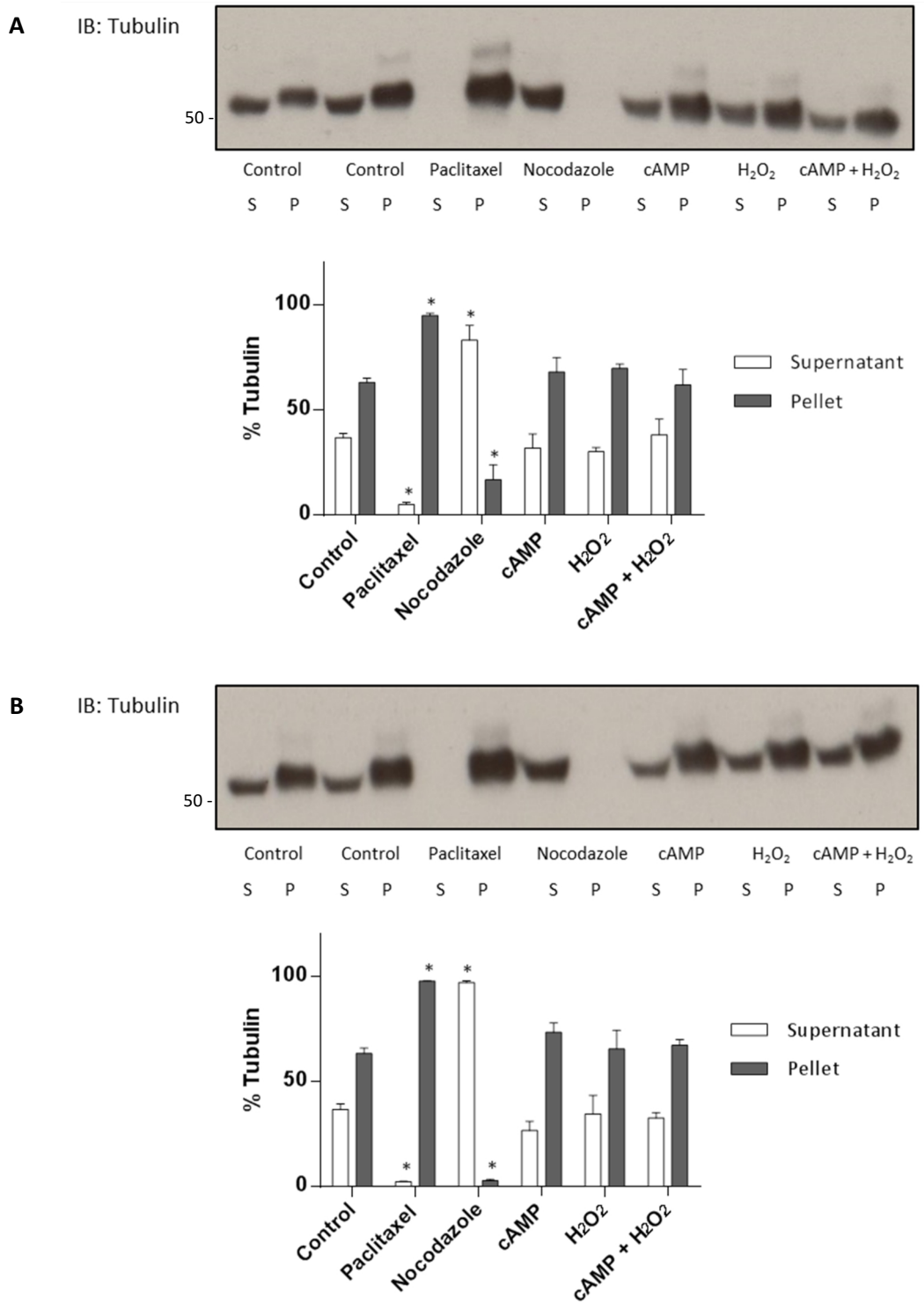

Figure 6.2 PKA activation does not alter microtubule dynamics in HEK 293 cells. HEK 293 cells were treated with 8-CPT-cAMP (100 µM), H_2O_2 (500 µM) or co-treated with both for (**A**) 10 or, (**B**) 120 min. Cells were also treated with paclitaxel (5 µM) or nocodazole (50 µM) for 30 min as positive controls. Lysates were processed with the centrifugation protocol where S= supernatant, representing free tubulin and P= Pellet, representing polymerised microtubules. Immunoblots were probed with anti-tubulin and the % tubulin in each fraction was summated and represented graphically (n= 4-8 ± SEM, * $p<0.05$ vs control).

6.3.2 Investigating redox-dependent GEF-H1 phosphorylation

The next logical step was to investigate potential substrates within the PKARIα-tubulin complex. As there is an oxidant-dependent interaction between the two proteins, the presence of oxidants together with cAMP may lead to enhanced phosphorylation of any associated substrates within the complex (Figure 6.3A). As previously discussed, the microtubules bind to MAPs, many of which are susceptible to phosphorylation and have been identified as targets of PKA. Some potential substrates could not be investigated as there were no commercial antibodies available to interrogate their phosphorylation status. The remaining proteins were separated into two categories according to whether their phosphorylation status was known to alter microtubule dynamics or not (Figure 6.3B).

To investigate whether oxidants could potentiate PKA-dependent phosphorylation of these substrates, HEK 293 cells were treated with 8-CPT-cAMP alone or co-treated with 8-CPT-cAMP and H_2O_2 to simultaneously induce the PKARIα-tubulin oxidant-dependent interaction. Stathmin, MAP4 and tau were each characterised as PKA substrates capable of regulating microtubule dynamics, but their phosphorylation was either not detected or not altered by the treatment interventions (Figure 6.3C). According to the literature GEF-H1 phosphorylation has not been shown to alter microtubule dynamics. Figure 6.4 demonstrates that GEF-H1 was present in HEK 293 cells, VSMCs, BAECs but not in ARVM. Treatment of HEK 293 cells with 8-CPT-cAMP increased Ser^{885} GEF-H1 phosphorylation and this was potentiated approximately 2-fold when HEK 293 cells were co-treated with 8-CPT-cAMP and H_2O_2 (Figure 6.4). This oxidant-induced potentiation of GEF-H1 phosphorylation was also observed in VSMCs and BAECs. Interestingly, longer immunoblot exposures demonstrated that GEF-H1 phosphorylation tended to decrease with H_2O_2 treatment alone, implying that induction of PKARIα disulfide dimer alone was not sufficient to activate PKARIα in this context. Furthermore, the H_2O_2 potentiation of GEF-H1 Ser^{885} phosphorylation was also clearly contingent on the presence of cAMP.

A

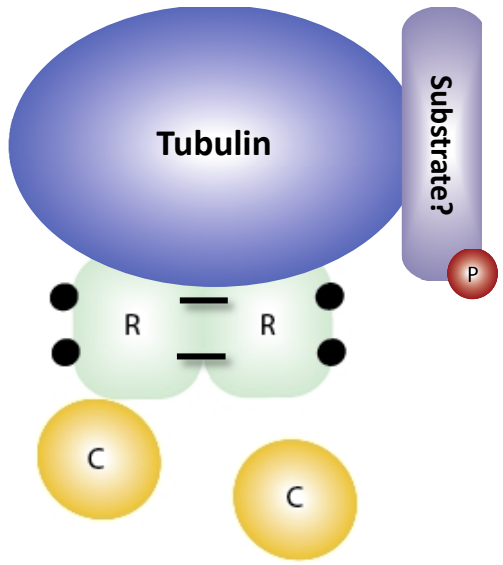

B

MAP	Phos. Site
Syntabulin	-
RASSF1A	Ser-203
BIG1	Ser-883
Stathmin	Ser-16
Stathmin	Ser-63
MAP4	Ser- 941
MAP4	Ser -1046
Tau	Ser-214
GEF-H1	Ser-885

C

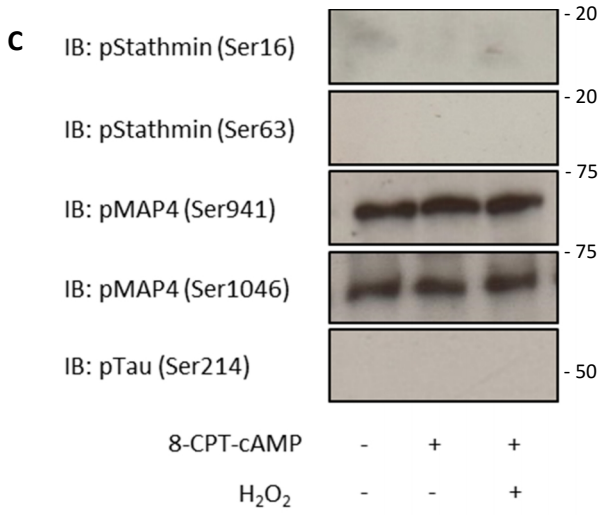

Figure 6.3 Stathmin, Tau and MAP4 are not phosphorylated as part of a PKARIα-tubulin redox-dependent complex. (**A**) Model of the redox-dependent PKARIα-tubulin interaction indicating phosphorylation of a potential substrate in the presence of oxidants and cAMP (black circles). (**B**) Table of MAPs and their phosphorylation sites that are established PKA substrates. Antibodies were not available for substrates in grey. Known effectors of microtubule dynamics are shown in black and do not effect dynamics are shown in green. (**C**) HEK 293 cells were treated with 8-CPT-cAMP (100 µM) or co-treated with 8-CPT-cAMP (100 µM) and H_2O_2 (500 µM). Immunoblots were probed with phospho- antibodies for stathmin (Ser16, Ser63), MAP4 (Ser941, Ser1046), tau (Ser214).

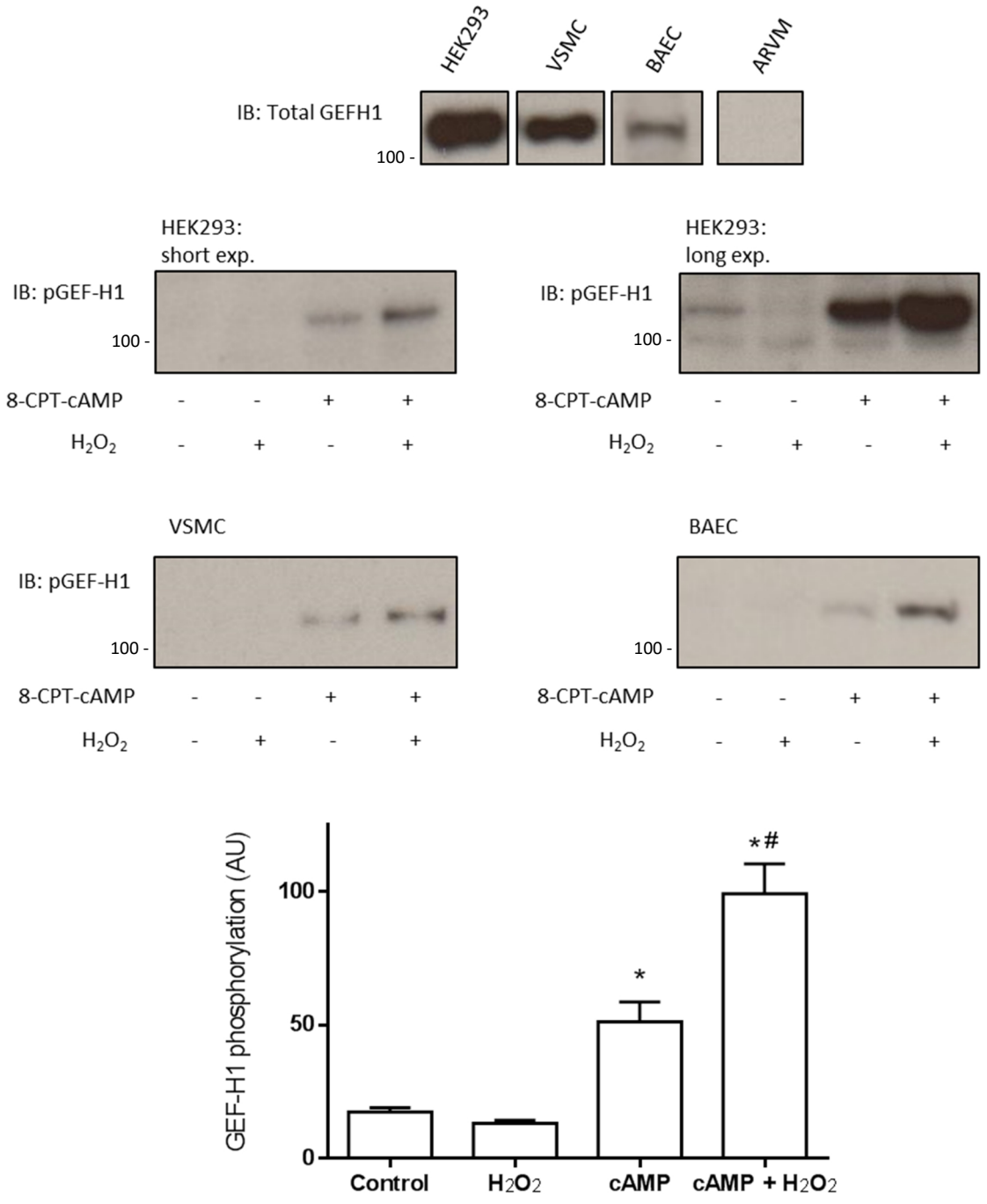

Figure 6.4 8-CPT-cAMP-dependent GEF-H1 phosphorylation is potentiated by H_2O_2. HEK 293 cells, VSMCs and BAECs were treated with 8-CPT-cAMP (100 µM), H_2O_2 (500 µM) or co-treated with both for 10 min. Immunoblots were probed with total or phospho-GEF-H1 antibodies. Phosphorylation events in HEK 293 cells were summated and represented graphically (n= 6-11 ± SEM,* $p<0.05$ vs control, # $p<0.05$ vs. cAMP)

To further investigate the effect of oxidants and cAMP on GEF-H1 Ser^{885} phosphorylation HEK 293 cells were treated with 8-CPT-cAMP (0–300 µM) in the absence or presence of H_2O_2. At concentrations of 3 µM 8-CPT-cAMP, GEF-H1 was phosphorylated but the effect of H_2O_2 was negligible. However GEF-H1 Ser^{885} phosphorylation was significantly increased in the presence of H_2O_2 at 30 µM or 300 µM 8-CPT-cAMP compared to 8-CPT-cAMP alone (Figure 6.5). This again confirmed that the effect of oxidant-potentiated Ser^{855} phosphorylation is contingent upon 8-CPT-cAMP concentration.

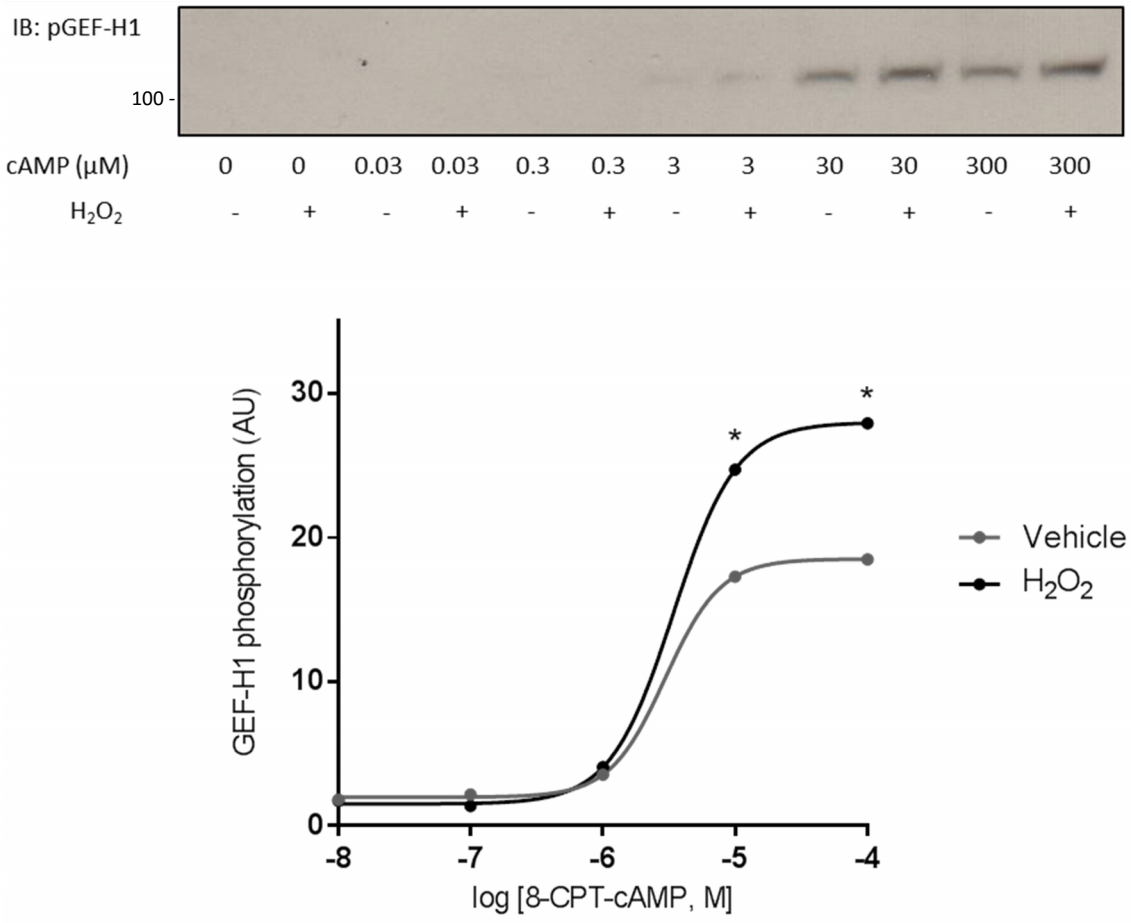

Figure 6.5 H_2O_2 potentiates GEF-H1 phosphorylation at higher 8-CPT-cAMP concentrations. HEK 293 cells were treated with 8-CPT-cAMP (0.3-300 µM) in the absence or presence of H_2O_2 (500 µM) for 10 min. Immunoblots were probed with the phospho-GEF-H1 antibody. Phosphorylation events were summated and represented graphically (n=3 ± SEM,* $p<0.05$ vs vehicle)

HEK 293 cells were treated with the PDE inhibitor IBMX (100 µM) to determine whether the oxidant-potentiated Ser^{885} phosphorylation was due to PDE inhibition. IBMX caused a small increase in Ser^{885} GEF-H1 phosphorylation whilst, as shown previously, H_2O_2 alone did not increase Ser^{885} phosphorylation (Figure 6.6). Furthermore Ser^{885} phosphorylation of HEK 293 cells treated with 8-CPT-cAMP and IBMX was significantly lower than in cells treated with 8-CPT-cAMP, IBMX and H_2O_2 together, again implying the H_2O_2 is potentiating phosphorylation via a mechanism other than PDE inhibition. Taken together, this precludes H_2O_2 mediated inhibition of PDEs as an explanation for oxidant-dependent potentiation of Ser^{885} phosphorylation.

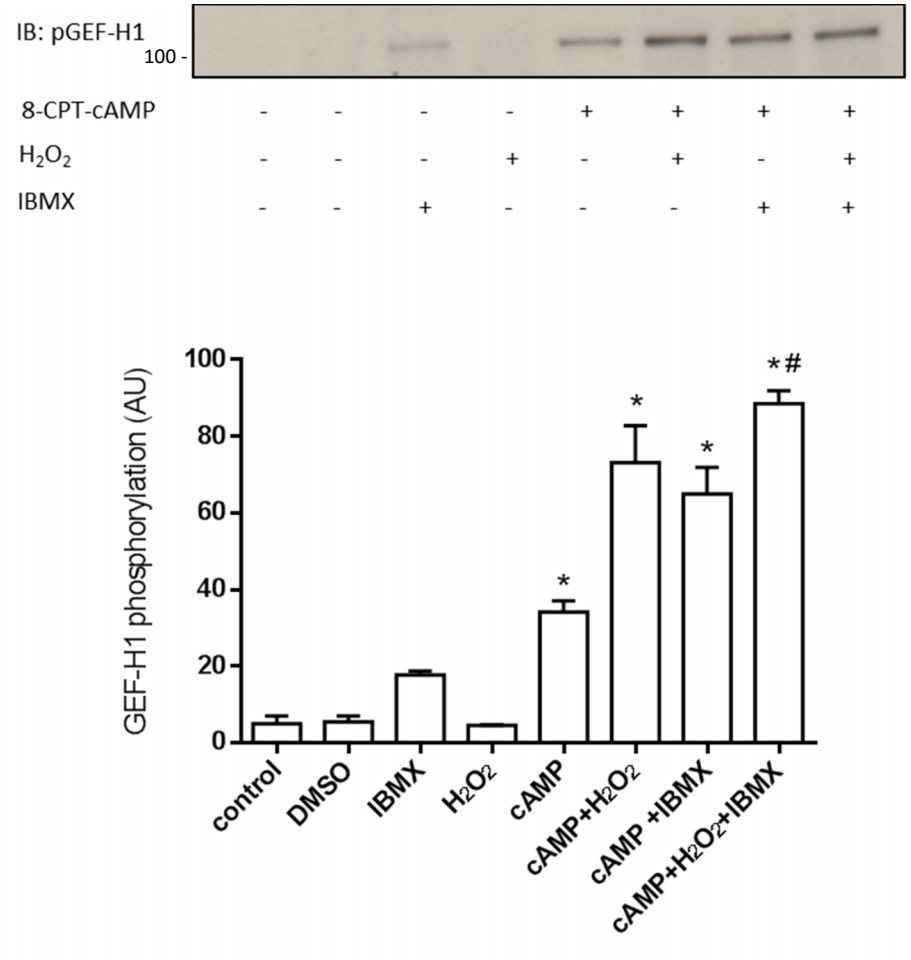

Figure 6.6 IBMX and H_2O_2 contribute to GEF-H1 phosphorylation via different mechanisms. HEK 293 cells were treated with a combination of 8-CPT-cAMP (100 µM), IBMX (100 µM) and/or H_2O_2 (500 µM) for 10 min. Immunoblots were probed with the phospho-GEF-H1 antibody. Phosphorylation events were summated and represented graphically (n=3 ± SEM,* $p<0.05$ vs control, # $p<0.05$ vs. cAMP + IBMX)

6.3.3 Investigating pharmacological inhibition of PKA on GEF-H1 phosphorylation

To determine if indeed Ser^{885} phosphorylation was a PKA-dependent process HEK 293 cells were pre-treated with pharmacological inhibitors of PKA. RP-8-cAMPS is an analogue of cAMP that reversibly competes for the cAMP binding site on the regulatory subunits of PKA but does not activate the kinase. RP-8-cAMPS (100 μM) pre-treatment for 30 min prior to 8-CPT-cAMP or 8-CPT-cAMP and H_2O_2 co-treatment reduced Ser^{885} phosphorylation by 52% and 60% respectively. The drug H89 inhibits the ATP binding site of the catalytic subunit of PKA. Pre-treatment with H89 (1 μM) for 30 min completely abolished GEF-H1 Ser^{885} phosphorylation in HEK 293 cells that had been challenged with 8-CPT-cAMP or 8-CPT-cAMP and H_2O_2 (Figure 6.7). Taken together this indicates that ROS-potentiated Ser^{885} phosphorylation is dependent on cAMP concentration and is likely to be PKA-dependent.

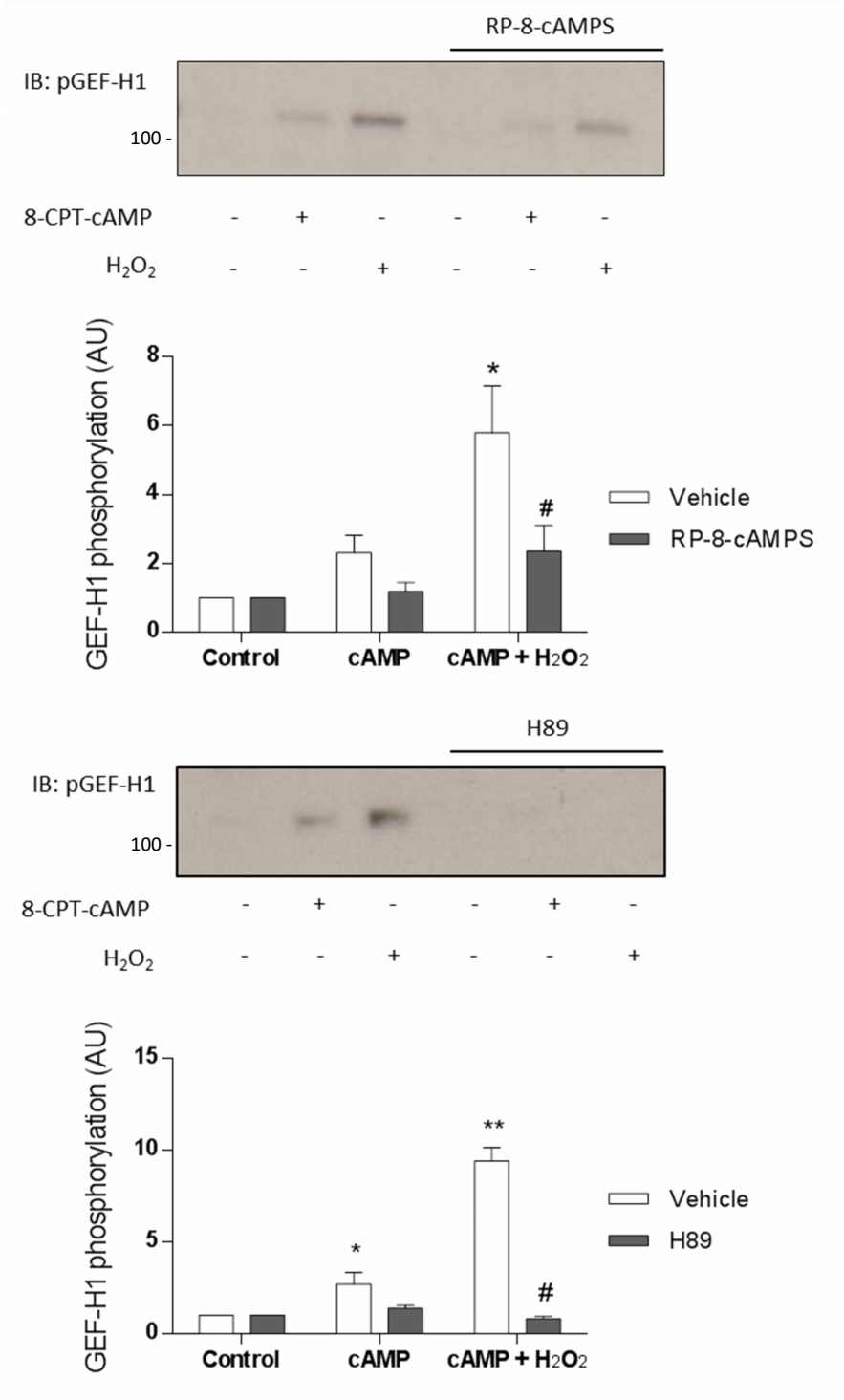

Figure 6.7 GEF-H1 phosphorylation is inhibited by RP-8-cAMPS and H89. HEK 293 cells were treated with 8-CPT-cAMP (100 µM), with or without H_2O_2 (500 µM), in the absence or presence of (**A**) RP-8-cAMPS or (**B**) H89 for 10 min. Immunoblots were probed with the phospho-GEF-H1 antibody. Phosphorylation events were summated and represented graphically (n=4-5 ± SEM,* $p<0.05$ vs control, ** $p<0.01$ vs control, # $p<0.05$ vs. vehicle)

6.3.4 Investigating PKARIα over-expression on GEF-H1 phosphorylation

The evidence thus far suggests that PKARIα disulfide dimer formation may contribute to potentiated GEF-H1 phosphorylation. The effect of PKARIα over-expression on Ser^{885} GEF-H1 was next investigated. HEK 293 cells transiently transfected with V5-PKARIα exhibited decreased Ser^{885} phosphorylation when treated with 8-CPT-cAMP or 8-CPT-cAMP and H_2O_2 together 24 hours post-transfection compared to untransfected cells, although this did not reach statistical significance (Figure 6.8). HEK 293 cells transfected with the V5-C17SPKARIα, a mutant form of PKARIα that cannot form the disulfide dimer, exhibited a further decrease in Ser^{885} phosphorylation after 8-CPT-cAMP and 8-CPT-cAMP and H_2O_2 co-treatment, the latter being significantly different compared to untransfected cells.

In separate experiments HEK 293 cells were transiently transfected for 72 hours with the dominant negative constructs PKARIα^{-cAMP} or C17SPKARIα^{-cAMP}. This time was chosen to allow maximum expression of these constructs, at which point cells were treated with 8-CPT-cAMP or 8-CPT-cAMP and H_2O_2 together. Ser^{885} GEF-H1 phosphorylation in cells that had been transfected with PKARIα^{-cAMP} or C17SPKARIα^{-cAMP} exhibited markedly reduced Ser^{885} phosphorylation to near baseline levels post treatment (% decrease in Ser^{885} phosphorylation: PKARIα^{-cAMP} 8-CPT-cAMP: 68%, cAMP + H_2O_2: 83%; C17SPKARIα^{-cAMP} 8-CPT-cAMP: 78%, cAMP + H_2O_2: 85%) (Figure 6.9). Finally, the expression of PKARIα^{-cAMP} or C17SPKARIα^{-cAMP} did not alter PKARIIα or PKACα expression. These data suggests that cAMP binding to PKARIα is a prerequisite for oxidant-potentiated PKA-dependent Ser^{885} GEF-H1 phosphorylation.

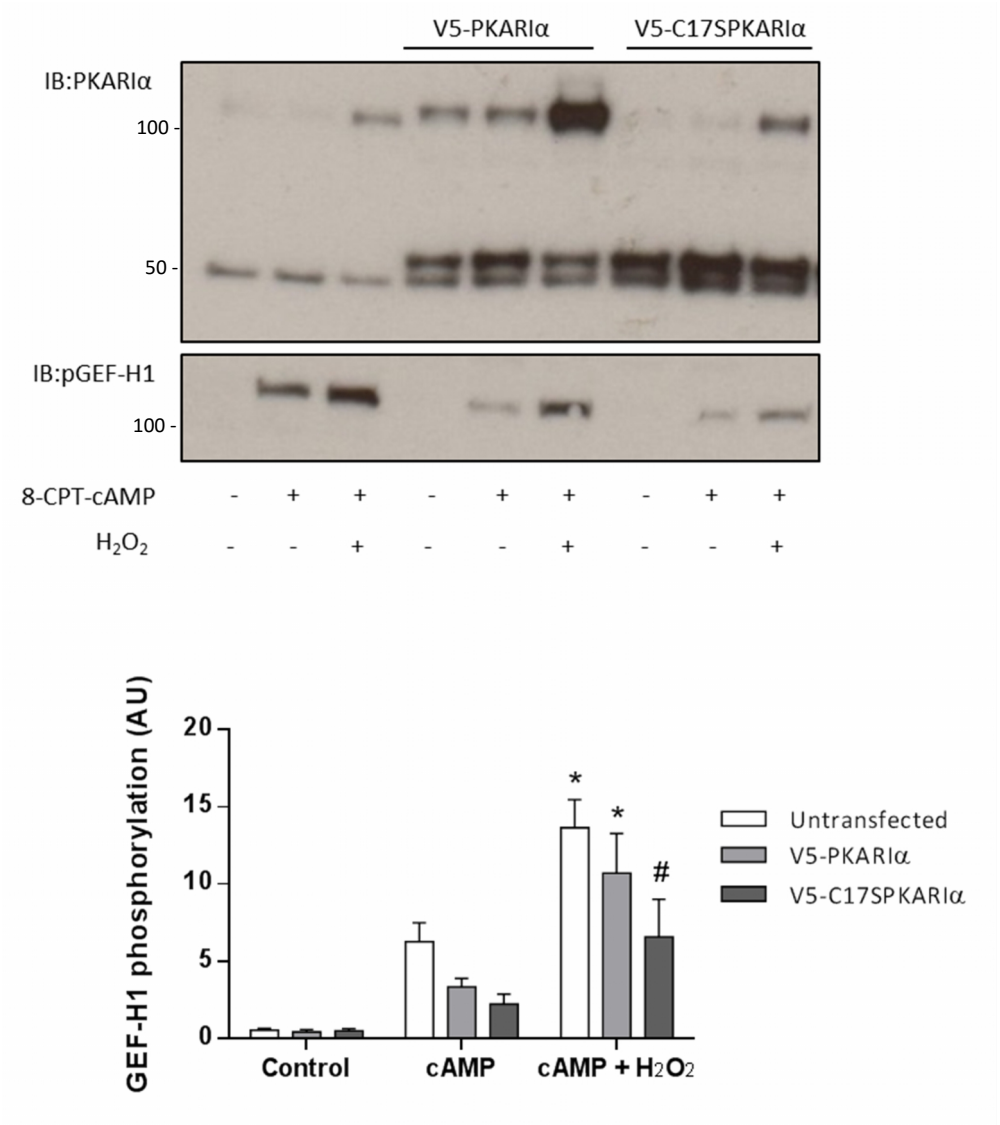

Figure 6.8 GEF-H1 phosphorylation is inhibited by PKARIα over-expression. HEK 293 cells were transiently transfected with V5-PKARIα or V5-C17SPKARIα, and after 24 hours were treated with 8-CPT-cAMP (100 µM), with and without H_2O_2 (500 µM) for 10 min. Immunoblots were probed with anti-PKARIα or the phospho-GEF-H1 antibody. Phosphorylation events were summated and represented graphically (n=4-6 ± SEM,* $p<0.05$ vs control, # $p<0.05$ vs. untransfected)

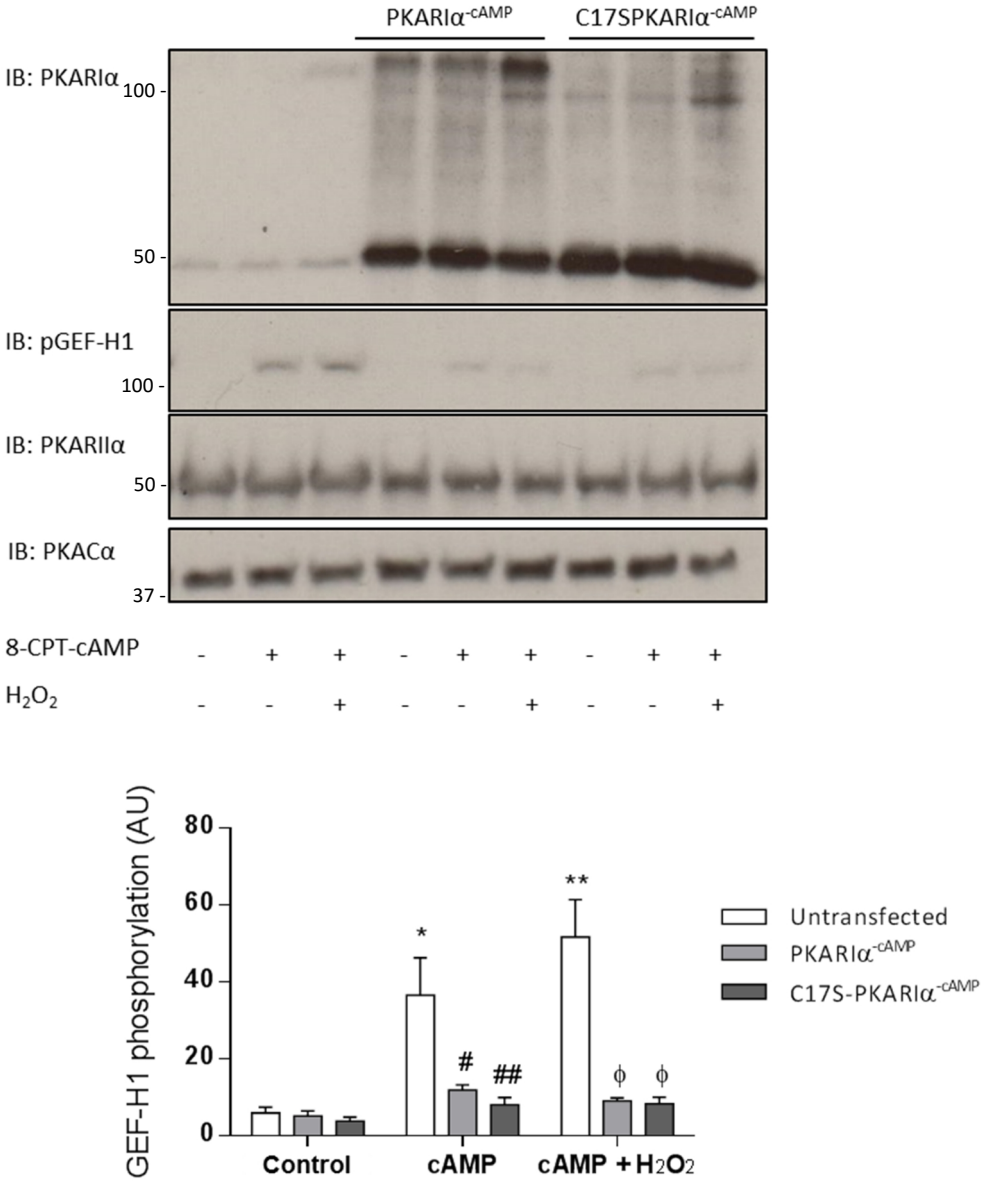

Figure 6.9 GEF-H1 phosphorylation is inhibited by PKARIα^{-cAMP} over-expression. HEK 293 cells were transiently transfected with PKARIα^{-cAMP} or C17SPKARIα^{-cAMP}, and after 72 hours were treated with 8-CPT-cAMP (100 µM), with and without H_2O_2 (500 µM) for 10 min. Immunoblots were probed with anti-PKARIα, anti-PKARIIα, anti-PKACα or the phospho-GEF-H1 antibody. Phosphorylation events were summated and represented graphically (n=4-5 ± SEM,* p<0.05 vs control, ** p<0.01 vs control, # p<0.05 vs. untransfected, ϕ p<0.05 vs. untransfected)

6.3.5 Investigating PKACα knock-down on GEF-H1 phosphorylation

To further investigate whether the PKA holoenzyme is necessary for cAMP/oxidant- induced GEF-H1 Ser ^{885} phosphorylation, HEK 293 cells were transfected with PKACα siRNA to delete the phospho-active component of the holoenzyme. Firstly, the extent of PKACα knockdown was assessed at various siRNA concentrations (10, 20 or 40 pmol) and different time points (24, 48 or 72 hours) to find the optimum conditions to conduct the experiment. Effective knockdown was achieved at all concentrations and at every time point (Figure 6.10A). Interestingly, this did not significantly alter basal global PKA substrate phosphorylation as determined by the phospho-PKA substrate antibody. To determine the effect of PKACα knockdown on Ser^{885} GEF-H1 phosphorylation HEK 293 cells were transfected with 20 pmol siRNA and subsequently treated with either 8-CPT-cAMP or 8-CPT-CAMP and H_2O_2 after 48 hours. There was a trend towards decreased Ser^{885} phosphorylation in HEK 293 cells transfected with siRNA-PKACα knockdown relative to control cells, but this was not significantly different (Figure 6.10B). Therefore, the α isoform of PKAC may be involved with PKA-dependent Ser^{885} GEF-H1 phosphorylation.

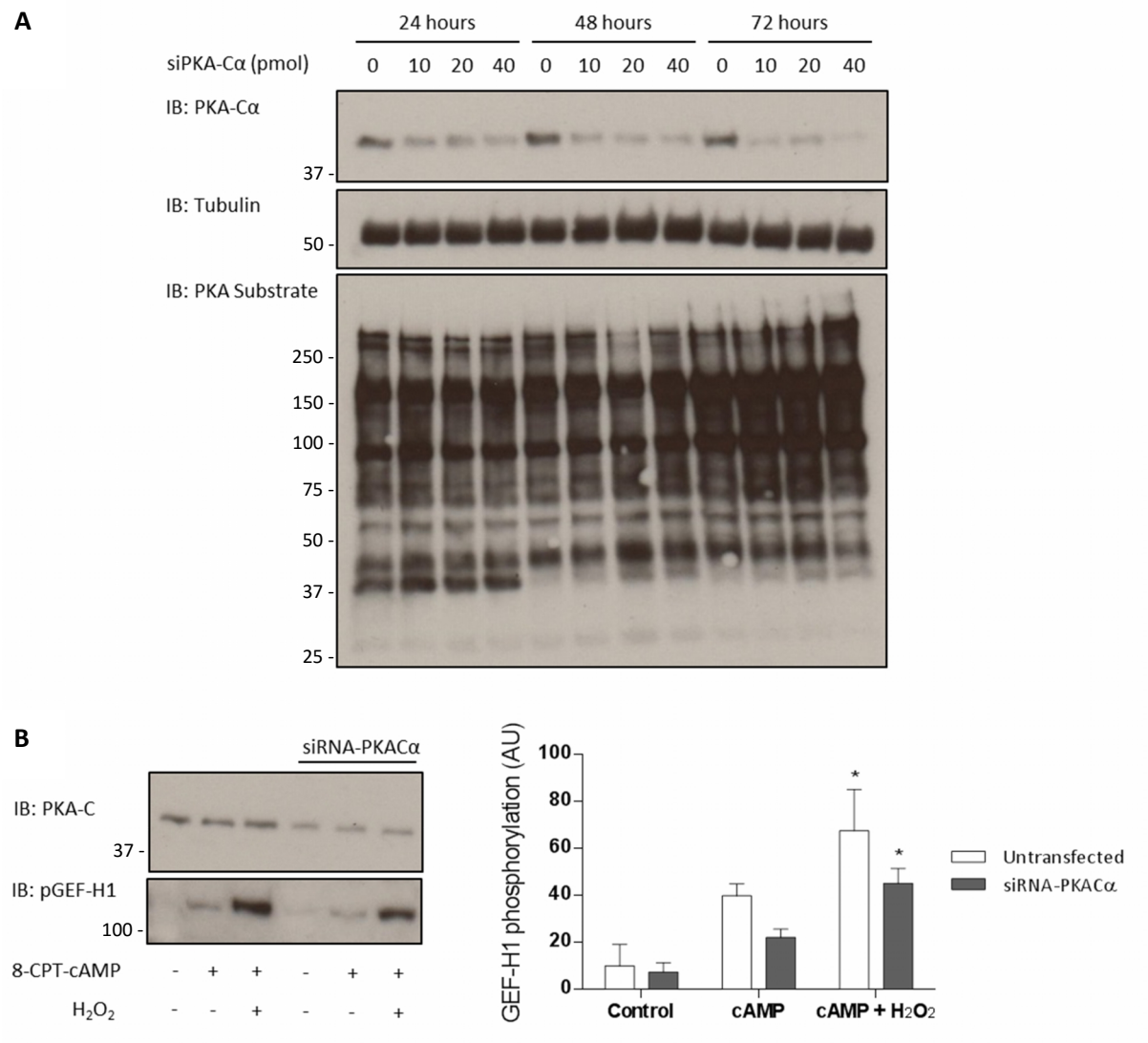

Figure 6.10 GEF-H1 phosphorylation is decreased with PKACα knockdown. (**A**) HEK 293 cells were transiently transfected with siRNA-PKACα (10-40 pmol) and harvested at 24, 48 or 72 hours (**B**) HEK 293 cells were transiently transfected with siRNA-PKACα (20 pmol) and after 48 hours were treated with 8-CPT-cAMP (100 µM), with and without H_2O_2 (500 µM) for 10 min. Immunoblots were probed with anti-PKACα, anti-tubulin, anti-phospho-PKA substrate and the phospho-GEF-H1 antibody. GEF-H1 Phosphorylation events were summated and represented graphically (n=4-6 ± SEM,* p<0.05 vs control)

6.3.6 Investigating the effect of microtubule stability on redox-dependent GEF-H1 phosphorylation

In the previous chapter it was suggested that PKARIα is capable of forming a disulfide bond with tubulin. Since GEF-H1 has been shown to be associated with the microtubules, the oxidant-dependent interaction between PKARIα and tubulin may explain the observed increase in Ser^{885} phosphorylation when cells are co-challenged with both 8-CPT-cAMP and H_2O_2. Therefore in this proposed model of oxidant-dependent GEF-H1 phosphorylation it is rational to characterise the role of the microtubule network. To this end HEK 293 cells were pre-treated with either nocodazole (50 µM) or paclitaxel (5µM) for 30 min and subsequently treated with H_2O_2, 8-CPT-cAMP or 8-CPT-cAMP and H_2O_2 together. The immunoblots reveal that simply challenging the cells with either paclitaxel or nocodazole increases Ser^{885} GEF-H1 phosphorylation, implying that disruption to the microtubules increases basal phosphorylation of Ser^{885}. Importantly, cells pre-treated with paclitaxel maintained their ability to potentiate Ser^{885} GEF-H1 phosphorylation in an oxidant-dependent manner although this was markedly reduced compared to control cells. However, H_2O_2 potentiated Ser^{885} GEF-H1 phosphorylation was abrogated in cells pre-treated with nocodazole (Figure 6.11). This data suggests that an intact microtubule network is necessary for oxidant-potentiated PKA-dependent Ser^{885} GEF-H1 phosphorylation.

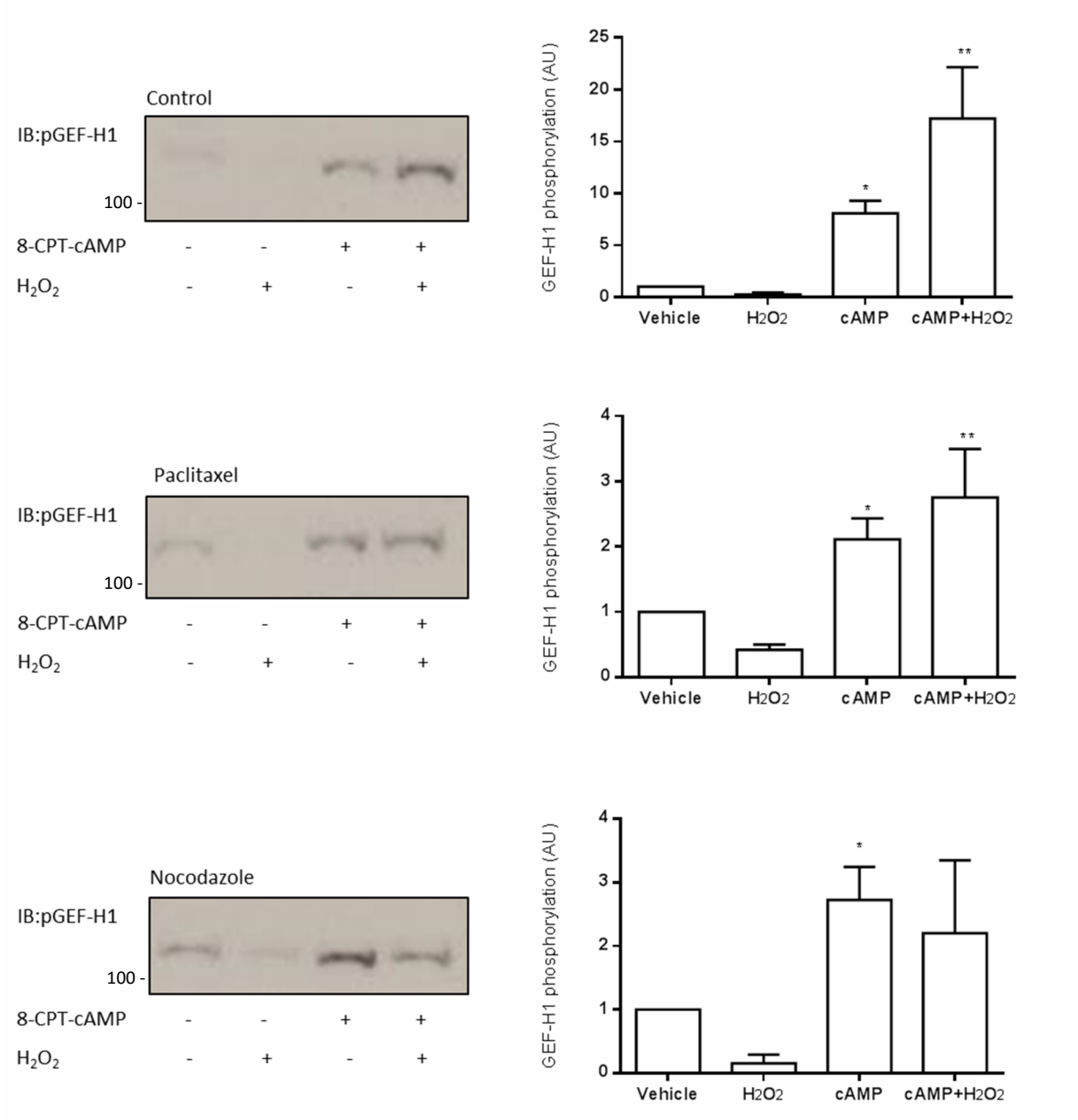

Figure 6.11 Microtubule dynamics alter H_2O_2-dependent potentiation of GEF-H1 phosphorylation. HEK 293 cells were pre-treated with paclitaxel (5 µM) or nocodazole (50 µM) for 30 min and subsequently treated with 8-CPT-cAMP (100 µM), H_2O_2 (500 µM) or co-treated with both for 10 min. Immunoblots were probed with the phospho-GEF-H1 antibody. Phosphorylation events were summated and represented graphically (n=3-4 ± SEM,* p<0.05 vs vehicle, ** p<0.01 vs vehicle)

6.3.7 Investigating the effect of oxidant potentiated GEF-H1 phosphorylation on stress fibre assembly

When dephosphorylated GEF-H1 activates RhoA, which is a critical mediator of actin fibre assembly. Phosphorylation of Ser^{885} on GEF-H1 has been shown to inhibit the capacity for GEF-H1 to activate RhoA and thus limit actin cytoskeleton fibre assembly. To further investigate whether ROS-potentiated PKA-dependent GEF-H1 phosphorylation exerted a functional effect, HEK 293 cells were co-treated with 8-CPT-cAMP and H_2O_2 for 10 min, fixed and stained with phalloidin to measure the extent of actin fibre assembly relative to control. Stress fibres were detected basally under control conditions, however cells co-challenged with 8-CPT-cAMP and H_2O_2 were unable to assemble stress fibres (Figure 6.12). The correlation between Ser^{885} GEF-H1 phosphorylation and stress fibre formation implies that the concerted action of cAMP and H_2O_2 together on PKARIα produces a functional response in this system.

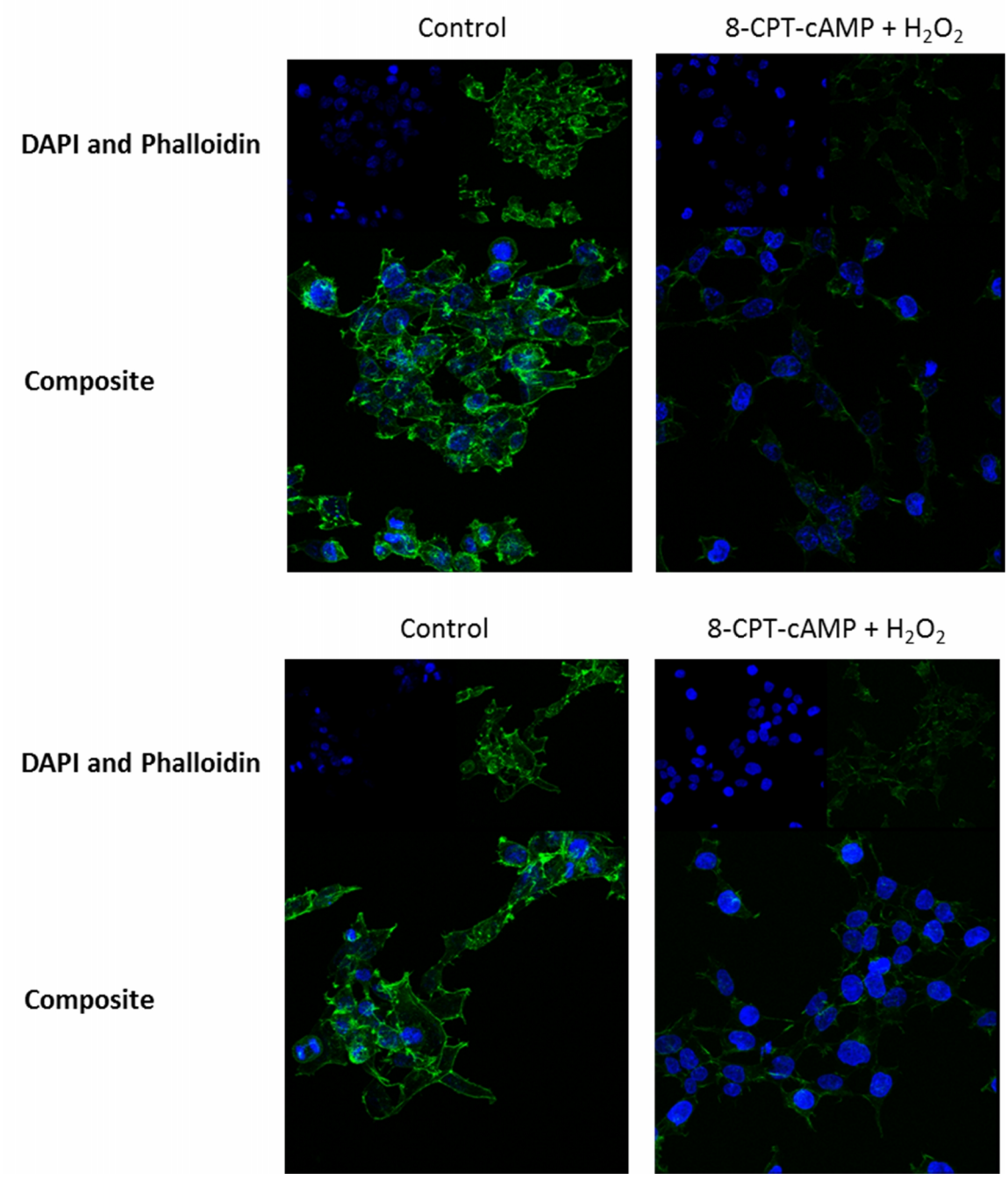

Figure 6.12 Co-treatment with 8-CPT-cAMP and H_2O_2 induced actin fibre loss in HEK 293 cells. Representative immunofluorescent images. HEK 293 cells were treated with vehicle or 8-CPT-cAMP (100 µM) and H_2O_2 (500 µM) together and then stained with phalloidin (green) to identify actin fibres. The nucleus was stained with b4',6-diamidino-2-phenylindole (DAPI, blue).

6.3.8 Investigating the effect of GEF-H1 phosphorylation in C17S PKARIα knock-in mice

Similar to the PKARIα constructs that have been used throughout this investigation, this laboratory has engineered a novel mouse that has had the PKARIα Cys17, a cysteine residue critical for the formation PKARIα disulfide, mutated to a serine. It has been termed the C17S PKARIα 'redox-dead' knock-in (KI). The RIα subunit in these mice are unable to form a disulfide bond between the two subunits and therefore is theoretically unable to transduce any oxidant signal that regulates PKARIα activity[91]. The data in this chapter thus far suggests a model in which H_2O_2 potentiates cAMP-induced Ser^{885} GEF-H1 phosphorylation and that this is mediated via the formation of the PKARIα disulfide dimer because it increases its interaction with tubulin. To investigate this hypothesis further, thoracic aorta were isolated from both WT or C17S PKARIα KI mice, cut into equal size strips, incubated overnight in media and subsequently treated with H_2O_2 (200 μM), forskolin (100 nM) or forskolin and H_2O_2 administered simultaneously. Forskolin directly activates adenylate cyclase to elevate intracellular cAMP, and was used instead of 8-CPT-cAMP in this model due to concerns about the permeability of 8-CPT-cAMP in tissue raised during preliminary experiments (data not shown). The pattern for Ser^{885} GEF-H1 phosphorylation in WT aortas was similar to the observed pattern in the cell models as H_2O_2 potentiated forskolin-induced phosphorylation. However, in the C17S PKARIα KI mice that cannot form the disulfide dimer, H_2O_2 failed to potentiate forskolin-induced Ser^{885} GEF-H1 phosphorylation, suggesting that the PKARIα disulfide dimer is necessary for this event (Figure 6.13).

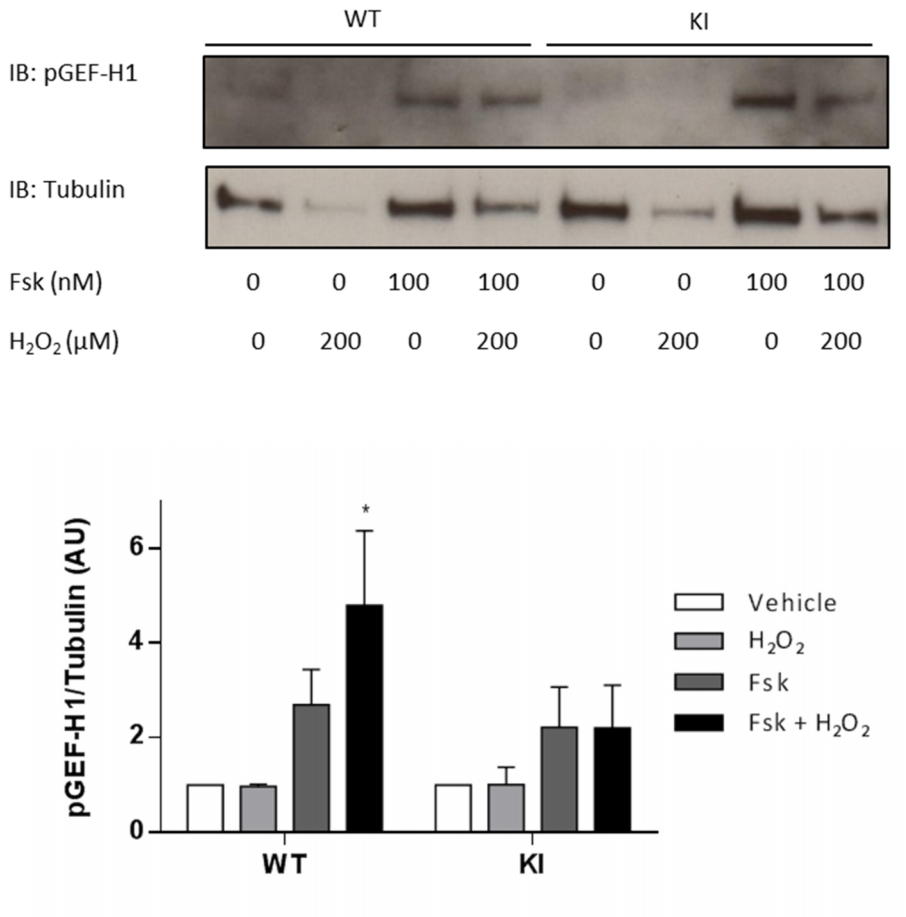

Figure 6.13 H_2O_2 does not potentiate GEF-H1 phosphorylation in aortic rings from PKARIα KI mice. Isolated aortic rings from WT and C17S PKARIα KI mice were treated with forskolin (100 nM), H_2O_2 (200 μM) or co-treated with both for 10 min. Immunoblots were probed with anti-tubulin and the phospho-GEF-H1 antibody. Phosphorylation events were normalised to tubulin as a measure of total protein, summated and represented graphically (n=3 ± SEM,* $p<0.05$ vs vehicle).

Having established GEF-H1 in PKARIα KI mice is not enhanced in the presence of cAMP and H_2O_2 compared to WT animals, it was rational to investigate whether this deficit contributed to (patho)physiology. Phosphorylation of GEF-H1 Ser^{885} inhibits its exchange activity to limit RhoA-dependent stress fibre formation and decrease endothelial permeability. Sepsis occurs when infection results in systemic inflammation accompanied by end-organ damage[304]. This is, in part, mediated by an increase in vascular permeability which compromises microvascular perfusion due to increased interstitial pressure[301]. Since GEF-H1 has been shown to regulate vascular permeability, and levels of oxidants are elevated during disease progression[305-307], a model of sepsis was deemed appropriate to investigate oxidant signal transduction via PKARIα disulfide dimer formation. I hypothesised that the C17S PKARIα KI animals will be more susceptible to sepsis due to hypophosphorylation of GEF-H1 relative to WT mice, leading to exacerbated endothelial permeability. Cecal ligation and puncture (CLP) is a widely used animal model exhibiting many clinical features of sepsis and has previously been validated in our laboratory[303].

Mice were allowed to recover from sham or CLP surgery for 24 h before they were sacrificed, and the lungs were harvested and homogenised for biochemical analysis. Immediately prior to culling, mice were observed and assessed based on numerous criteria, including their physical appearance and response to stimuli, and allocated a sepsis score out of 5 as a measure of injury. A higher sepsis score indicated more severe disease progression. Table 6.2 demonstrates that PKARIα KI mice had a higher sepsis score compared to WT mice implying more severe pathology 24 hours after CLP surgery. Furthermore there was a trend towards increased PKARIα oxidation in CLP mice compared to sham mice, whilst as expected, KI animals had no disulfide PKARIα. However there was no difference in GEF-H1 phosphorylation between WT and C17S PKARIα KI mice regardless of whether they had undergone sham or CLP surgery (Figure 6.14).

Animal	Sepsis Score	
	Sham	CLP
WT	0	2.3 ± 0.3
PKARIα KI	0	3.3 ± 0.3

Table 6.2 Sepsis score of WT and C17S PKARIα KI mice 24 hours after sham or CLP surgery

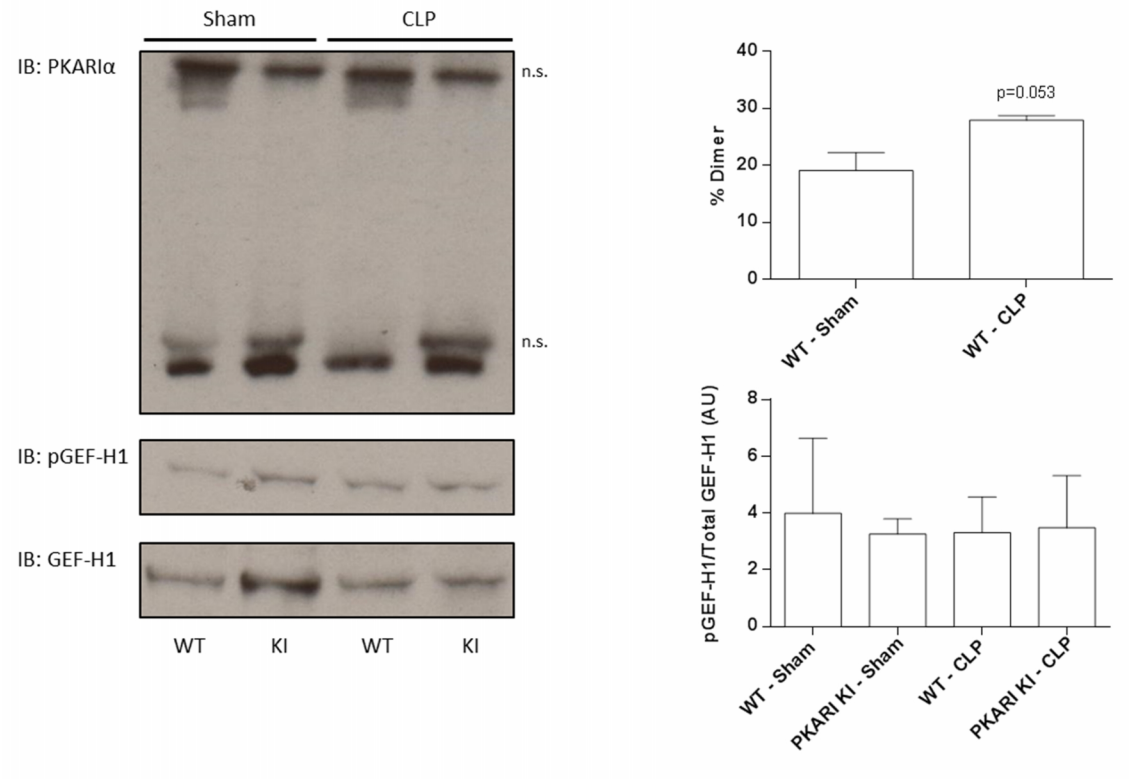

Figure 6.14 PKARIα oxidation, but not GEF-H1 phosphorylation, is elevated 24 hours after CLP surgery. C57BL/6J WT and C17S PKARIα KI mice underwent sham or CLP surgical procedure and allowed to recover for 24 hours. At this time lungs were excised and homogenised for analysis by immunoblotting using anti-PKARIα, anti-GEF-H1, anti-pGEF-H1. Phosphorylation events were normalised to total GEF-H1 protein summated and represented graphically (n=3, n.s. = non-specific band).

6.4 Discussion

In this chapter I examined the effect of PKARIα activation on microtubule dynamics. I also explored the phospho-status of various MAPs including the known PKA substrate GEF-H1. For the first time, I demonstrated that PKARIα and can integrate both H_2O_2 and cAMP signals to enhance GEF-H1 phosphorylation.

6.4.1 PKARIα mediates the oxidant potentiated GEF-H1 phosphorylation

PKA has been demonstrated to phosphorylate the MAPs stathmin[308], tau[309], syntabulin[310], RASSF1A[311], BIG1[312] which all regulate microtubule dynamics. Despite this cAMP or H_2O_2 failed to disrupt microtubule integrity in HEK 293 cells. Kratzer *et al.* demonstrated that pre-treatment with the antioxidant N-acetyl cysteine prevented lipopolysaccharide (LPS)-induced ROS-dependent disassembly of microtubules[293]. Furthermore 48 hour treatment of human osteosarcoma 143B cells with H_2O_2 resulted in depolymerised microtubules[313]. The divergence in results may be accounted for by differences in cell types or experimental protocols. To the best of my knowledge there are no reports of GEF-H1 phosphorylation altering microtubule dynamics and the findings discussed above are consistent with that.

H_2O_2 potentiated cAMP-dependent Ser^{885} GEF-H1 phosphorylation in a number of cell types. Interestingly, H_2O_2 alone decreased Ser^{885} GEF-H1 phosphorylation which is confounding because oxidants are broadly thought to inhibit phosphatases and consequently increase protein phosphorylation[314]. However because of this decrease in phosphorylation it allows phosphatase inhibition to be ruled out as the cause of H_2O_2 potentiated Ser^{885} phosphorylation. The decrease in phosphorylation observed when cells were treated with H_2O_2 alone also precludes the role of an unknown H_2O_2-activated kinase in oxidant potentiated Ser^{885} phosphorylation. Furthermore pre-treatment of cells with the phosphodiesterase inhibitor IBMX induced a slight increase in GEF-H1 phosphorylation, the opposite effect observed with H_2O_2, therefore it is possible to rule out phosphodiesterase inhibition as a cause of H_2O_2-potentiated GEF-H1 phosphorylation. Thus it is reasonable to suggest that the integration of the cAMP and oxidant signals must occur at the level of the PKA holoenzyme; furthermore it is likely that the disulfide PKARIα-tubulin interaction mediates this synergistic phosphorylation of GEF-H1.

Over-expression of WT-PKARIα significantly increased disulfide dimer upon H_2O_2 treatment but also decreased GEF-H1 phosphorylation. This is because the regulatory subunits inhibit PKA catalytic activity regardless of their redox state. The over-expression of WT-PKARIα would cause a rightward shift of the a concentration-response curve, meaning a greater concentration of cAMP would be required to overcome the inhibitory effect of the regulatory

subunits[315], whilst H_2O_2-dependent potentiation of GEF-H1 phosphorylation would remain intact as observed. In Chapter 3 the ability of cells to modulate cellular PKARIα concentrations was described, and therefore PKARIα expression may represent an additional mechanism whereby phosphorylation events are regulated in response to cAMP and oxidants. GEF-H1 phosphorylation was abrogated in cells over-expressing PKARIα^{-cAMP} therefore I can conclude that cAMP-dependent phosphorylation of GEF-H1 is primarily due to PKARIα activation. Furthermore it highlights that this H_2O_2-induced potentiation is directly via PKARIα, as this is also abrogated in PKARIα^{-cAMP} transfected cells. It reveals for the first time that co-ordinated oxidant and cAMP sensing at the PKARIα interface are both necessary for enhanced GEF-H1 phosphorylation.

siRNA experiments were designed to abolish GEF-H1 phosphorylation via knockdown of PKACα. There was a trend towards decreased GEF-H1 phosphorylation with siRNA PKACα but this was not significant. Furthermore global PKA phosphorylation remained unchanged despite PKACα knockdown. Therefore other PKAC isoforms are likely to have a more prominent role in the phospho-status of GEF-H1, at least in HEK 293 cells, an observation which merits further investigation.

According to a local hypothesis which follows from my initial observation, an increased interaction between tubulin and PKARIα is likely to be the mechanism underlying oxidant-induced potentiation of GEF-H1 phosphorylation. The loss of oxidant potentiated GEF-H1 phosphorylation after treatment with the microtubule depolymerising drug nocodazole highlights the necessity of an intact microtubule network for the phenomenon to occur, and reinforces the idea that the redox control of the PKARIα and tubulin interaction is critical to how oxidants potentiate GEF-H1 phosphorylation. Nocodazole disrupts the GEF-H1/tubulin complex potentially negating any effect of enhanced tubulin/PKARIα interaction, but this requires further investigation to better understand the mechanism.

6.4.2 Effect of GEF-H1 phosphorylation on actin fibres

Phosphorylation of Ser^{885} on GEF-H1 leads to inhibition of its guanine exchange activity and therefore decreased activity of RhoA[299]. Confocal imaging demonstrated a loss of actin fibres after co-treatment with cAMP and H_2O_2 indicative of a downstream physiological effect consistent with RhoA inhibition. The PKA catalytic subunit can directly phosphorylate Ser^{188} RhoA *in vitro*[316] and post-forskolin treatment *in vivo*[317] thus inhibiting the small GTPase. Ser^{188} on RhoA is a well-established PKG site, however the importance or extent of PKA-dependent Ser^{188} phosphorylation *in vivo* is unclear[317]. Furthermore cAMP influences actin cytoskeleton arrangement independent of GEF-H1 and RhoA. The small GTPases Rac1 and Cdc42 are activated by cAMP to oppose the actions of RhoA[96]. Therefore these factors cannot be

discounted with respect to the loss of actin stress fibres in the confocal studies. The relative contribution of each mechanism RhoA opposing mechanism is unknown; however forskolin fails to suppress stress fibre formation in cells expressing a non-phosphorylateable GEF-H1 mutant, suggesting that GEF-H1 is an important cAMP target in regulating actin structures[298].

Ser^{885} on GEF-H1 can also be phosphorylated by p21 activated kinase 1 (PAK1)[318] and the mitotic kinase aurora A/B[295]. Whilst there is no evidence that aurora A/B can be activated by cAMP or H_2O_2, PAK1 is activated downstream of Rac1 and Cdc4 and has also been shown to be directly phosphorylated by PKA[319,320]. Although unlikely, it is not possible to rule out the involvement of PAK1 on GEF-H1 phosphorylation in this model without pharmacological inhibition or knock-down. However over-expression experiments with $PKARI\alpha^{-cAMP}$ directly implicate the enzyme in oxidant-sensing and the H_2O_2-dependent potentiation of GEF-H1 phosphorylation. Furthermore, the importance of oxidant sensing by PKARIα was confirmed in experiments using aortas from PKARIα knock-in mice, which did not undergo H_2O_2-potentiated GEF-H1 phosphorylation compared to WT aortas. Thus disulfide bond formation in PKARIα is necessary for enhanced GEF-H1 phosphorylation, and can integrate cAMP and oxidant signals to fine-tune GEF-H1 phosphorylation.

6.4.3 Oxidant-dependent GEF-H1 phosphorylation in sepsis

GEF-H1 has many RhoA-dependent and -independent roles within the cell and has been implicated with numerous diseases. GEF-H1 contributes to excitotoxicity and neuronal plasticity[321]; acts as an adaptor protein during oncogenic RAS signalling[322]; and plays a role in viral nucleic acid sensing as part of the innate immune response[323]. Ultimately the effect of ROS-potentiated PKA Ser^{855} phosphorylation on these processes is unknown and would warrant further investigation. GEF-H1 has been well-characterised as a mediator of LPS-dependent endothelial barrier permeability via RhoA activation[292-294,324,325]. Interestingly LPS activation of TLR4 receptors induces NOX-dependent oxidant stress[326,327]. LPS also stimulates the release of the cytokines IL-1β and TNFα which also generates oxidants that can induce PKARIα dimerisation[173]. Therefore GEF-H1 phosphorylation may represent a novel feedback mechanism whereby PKA synergises the cAMP and oxidant signals to negatively regulate GEF-H1 activity and prevent excessive endothelial cell permeability. I hypothesised that this may be relevant during sepsis where LPS from gram negative bacteria contributes to the loss of endothelial barrier integrity, disrupting the physical barrier between the circulation and the interstitial space. Progressive subcutaneous and body-cavity oedema typically develops in patients with sepsis due to this increase in vascular permeability[301]. The accumulation of interstitial fluid increases the distance necessary for efficient diffusion of oxygen and

simultaneously compromises microvascular perfusion due to increased interstitial pressure; consequently elevated permeability is associated with the pathogenesis of sepsis[328].

A preliminary study was conducted in WT and C17S PKARI KI mice using the CLP model of sepsis. I hypothesised that the oxidant-dependent activation of PKARIα would lead to enhanced GEF-H1 phosphorylation in the WT mice thus preserving some endothelial barrier function compared to PKARIα KI. The lungs are an organ of particular interest because they highly vascularised, express GEF-H1 and are susceptible to oedema during sepsis[329,330]. There was a strong trend towards increased PKARIα disulfide dimer in the lungs of WT animals 24 hours post CLP implying an increase in cellular oxidants, and indicating that oxidant-dependent PKARIα activation may be relevant in this disease. Furthermore the sepsis score, a measure of sceptic injury that was visually determined by a blinded and independent investigator, revealed that the progression of the disease was worse in WT mice compared to C17S PKARIα KI mice. Despite this there was no difference in GEF-H1 phosphorylation between WT and C17S PKARIα KI mice regardless of whether they had undergone sham or CLP surgery. Crucially, it is not known how the concentration of cAMP may have been altered by the CLP intervention in my studies, and this would be important to eventually define how this changes temporally, as this is envisaged to significantly influence GEF-H1 phosphorylation. Wu *et al.* demonstrated that cAMP levels are elevated in early sepsis (9 hours) but drop below baseline levels during late sepsis (18 hours) in a rat CLP model[331]. If cAMP levels follow a similar pattern in our model of CLP then this may explain why no difference in GEF-H1 phosphorylation was observed between WT and KI animals. Speculatively, the higher sepsis score observed in the C17S PKARIα KI mice may be related to exacerbated vascular permeability at earlier time-points. Follow-up studies assessing a time course of sepsis to define if PKARIα serves as a coincidence detector of oxidant and cAMP signals, thereby contributing to the pathogenesis of sepsis, are clearly a logical way to proceed. Such studies would assess whether GEF-H1 phosphorylation and consequently vascular permeability is enhanced in C17S PKARIα KI mice compared to WT. Understanding the contribution of PKARIα at the interface of cAMP and oxidant signalling could provide novel physiological and pathophysiological insights that could potentially be exploited for therapeutic benefit during sepsis.

7 General Discussion

This thesis described studies investigating oxidant-dependent interprotein disulfide bond formation within PKARIα, interrogating whether these oxidation events modulates interactions with AKAPs and the phosphorylation of associated substrates. A particular focus of these studies was deciphering the impact of concomitant cAMP and oxidant signals on PKARIα activation and downstream signalling.

7.1 Analysis of experiments with cAMP-agarose

Treatment of cardiomyocytes with H_2O_2 induces disulfide-formation in PKARIα and simultaneously increases phosphorylation of PKA substrates[170]. However, the exact mechanism of oxidant-dependent PKARIα activation is unknown. Upon examination of the PKARIα structure it is evident that the disulfide bonds in PKARIα directly flank the α-helix binding domain in AKAPs. Therefore it was a logical possibility that the presence or absence of the disulfide bonds in PKARIα would modulate the affinity between the kinase and AKAPs due to their proximity to the AKAP α-helix. Binding affinity measurements have been made that are consistent with this hypothesis where mutation of the PKARIα cysteine residues necessary for disulfide formation resulted in decreased affinity for DAKAP2[103].

cAMP-agarose has been used extensively to co-capture AKAPs with PKAR subunits[246-249,252]. cAMP-agarose pull-downs had been identified as an useful method to investigate whether PKARIα bound to AKAPs with greater affinity under oxidising conditions as a disulfide dimer. I was successfully able to capture PKARIα, but unfortunately I was unable to co-capture any AKAPs using this method. This was despite numerous efforts to optimise the co-capture protocol as previously outlined in Chapter 4. Considering that the optimisations were carried out in accordance with various other published studies, it is difficult to reconcile why I was unable to co-capture AKAPs. In my experiments I used cAMP tethered to agarose beads by a 2 or 8 carbon linker lengths. Although such cAMP-agarose beads have been used in published studies[249,252,253], it is possible that steric hindrance upon PKARIα binding results in loss of a previously bound AKAP. As such a longer length linker between the agarose bead and cAMP may aid the likelihood of AKAP co-capture in future experiments.

I was able to capture DAKAP1 but this was found to be non-specific, as excess free cAMP did not reverse the association. Such negative controls appear not to have been used in published studies with solid phase-cAMP, meaning that there could be false positive identifications in the

literature. Furthermore AKAP antibodies have been known to produce non-specific bands which has purportedly led to false identification of AKAPs in PKARIα complexes[234]. Indeed, the unreliability of AKAP antibodies was a considerable issue during these investigations, exemplified by the AKAP7 antibodies detecting bands at unexpected molecular weights, or in some cases no detectable bands at all. Therefore use of immunoblotting to assess presence of candidate AKAPS may not be the most suitable methods for testing if oxidative conditions modulates their interaction with PKARIα. These issues with immunoblotting may be overcome by using LC-MS/MS, which potentially allows identification and quantification of changes in AKAPs-PKAR association during oxidative conditions; assuming that AKAPs are indeed present in the pull-downs. Ultimately use of cAMP-agarose to determine whether PKARIα disulfide dimer has greater affinity for AKAPs was perhaps unsuitable because it was unexpectedly found to induce the reduction PKARIα to its monomeric form, with a potential mechanism for how this occurs being presented. Yeast two-hybrid screening has also been used to identify AKAPs that bind PKAR[146], with surface plasmon resonance having been valuable in defining the affinity of such interactions[240].

Another method that was explored to co-capture PKARIα with AKAPs during these investigations was the Caprotec™ Capture Compound Assay (CCCA). The preliminary results obtained with the CCCA were promising, as numerous proteins were co-captured with PKARIα after H_2O_2 treatment. The CCCA allows covalently crosslinking a protein of interest, here RI, to potential binding partners. Covalent crosslinking potentially overcomes loss of reversibly bound interaction partners during co-capture experiments using cAMP-agarose. This is pertinent as identifying PKARIα-specific AKAPs is known to be challenging because of their transient interactions due the fast off-rate of binding[146]. Crosslinking would serve to stabilise the interaction between PKARIα and its binding partners, thus increasing the likelihood of detection by immunoblotting or MS. Unfortunately the manufacturers stopped providing support for this product and there were issues with the quality control of subsequent CCCA batches.

7.2 AKAP7

AKAP7 formed a major part of my investigations because of its potential redox-dependent interaction with PKARIα. Electrically stimulated isolated ventricular myocytes from PKARα KI mice exhibit delayed decay of their Ca^{2+} transients compared to WT myocytes (unpublished data from Wagner and Maier, Gottingen University). Unphosphorylated PLB inhibits SERCA2a to decrease the active transport of Ca^{2+} back into the SR. The delayed Ca^{2+} transient in PKARIα KI myocytes could potentially by explained by SERCA2a underactivity due to decreased PKA-

dependent phosphorylation of PLB. I hypothesised that this would be caused by deficient targeting of C17SPKARIα to AKAP7, the AKAP thought to be responsible for assembling the PKA/PLB/SERCA2a signalling complex at the SR[140].

Furthermore, examination of the AKAP7 crystal structure revealed the presence of a putative disulfide bond adjacent to AKB domain. I hypothesised that the formation of a disulfide bond in AKAP7 under oxidative conditions may modulate the AKAPs affinity for PKARIα due to its close proximity to the AKB domain. Unfortunately I was unable to co-capture AKAP7 with PKARIα using cAMP-agarose. I was able to co-purify with PKARIIα, but not PKARIα, with His-AKAP7δ using Ni-NTA-agarose, and this interaction appeared to increase after H_2O_2 treatment. AKAP7δ and PKARIIα regulate water reabsorption renal collecting duct principal cells[237], and the potential for this process to be modulated by oxidants could provide an interesting subject of future investigation.

7.3 PEG-maleimide switch assay

The PEG-maleimide switch assay was developed to identify proteins susceptible to reversible oxidative modifications. This method involved chemically reducing reversibly oxidised thiols, and then labelling them with the thiol alkylating agent PEG-maleimide. This reagent is essentially maleimide with a PEG tag of a specified mass that adducts to a modified protein. During these investigations PEG-maleimide that added 5 kDa to the molecular mass of the protein was utilised. Changes in mass were monitored by western immunoblotting using a specific antibody to the protein of interest, with an increase in mass in oxidant-treated samples compared to control indicating reversible oxidation. The PEG-maleimide switch assay successfully confirmed PKARIα and PKGIα were redox sensitive proteins thus validating the method. Furthermore the assay enabled me to conclude that tubulin and PKARIIα were susceptible to reversible thiol oxidation, but that AKAP7 is not susceptible to such modification. This novel method involves fewer steps than conventional thiol-labelling approaches such as the biotin-switch assay[256] or the AMS assay[332], thus there is less chance of losing protein during preparation, it is quicker and easier to perform and also is likely more quantitative.

7.4 Modulation of PKARIα disulfide dimer by cAMP

One of the primary findings of these investigations was the discovery that cAMP-agarose can induce the chemical reduction of disulfide PKARIα, despite the experiments occurring under oxidising conditions (in the air). Since cAMP has no intrinsic reducing properties, I hypothesised that the reduction of PKARIα was due to the conformational change in PKARIα

that occurs upon cAMP binding, perhaps allowing a free thiol on another proximal protein to access and reduce the disulfide in the kinase. PKARIα requires a surprisingly high concentration of DTT to reduce its disulfides[198]. In Chapter 5 I demonstrated that the concentration of DTT that is necessary to reduce PKARIα is decreased in the presence of cAMP, an effect that is lost with the PKARIα^{-cAMP} mutant. Therefore the idea that a cAMP-induced conformational change of PKARIα can increase the solvent accessibility of the disulfide is feasible. In Chapter 6 I presented a model whereby the free thiol responsible for the cAMP-induced reduction of disulfide PKARIα is present on a closely associated AKAP, such as tubulin. The physiological effect of the cAMP-induced reduction of disulfide PKARIα remains to be fully elucidated, but as previously suggested it may lead to enhanced local substrate phosphorylation. The cycle of oxidant-dependent PKARIα recruitment to AKAPs and cAMP-dependent reduction would keep multiple holoenzymes in close proximity to an associated substrate and in a region of high cAMP concentration to increase local responsiveness.

Curiously treatment of cells with 8-CPT-cAMP did not induce the reduction of PKARIα. This may suggest that whilst there is evidence supporting a role for cAMP in the modulation of PKARIα disulfide dimer, such results may be experimental artefacts that are not relevant in cells or *in vivo*. However, due to the compartmentalised nature of cAMP/PKA signalling it is tempting to suggest that cAMP-induced reduction of PKARIα occurs *in vivo*, but perhaps in very specific subcellular locations. As such, when monitoring global PKARIα levels via immunoblotting after cells are treated with 8-CPT-cAMP, subtle changes in disulfide dimer may not be detectable. Identifying cAMP-induced reduction of PKARIα in cell models requires further investigation, and may potentially be achieved by monitoring PKARIα disulfide in fractionated cell or tissues samples.

7.5 H_2O_2 potentiates PKA substrate phosphorylation

H_2O_2-induced phosphorylation of PKA substrates has previously been demonstrated in cardiomyocytes[170] and I was able to corroborate this during my investigations. Interestingly this effect was not as robust in VSMCs or HEK 293 cells. Cardiomyocytes have at least 10 times higher basal cAMP levels compared to HEK 293 cells[215], which has led me to hypothesise that H_2O_2-induced phosphorylation of PKA substrates is contingent upon the concentration of cAMP. This hypothesis may be examined in future experiments, for example, pre-treatment of cardiomyocytes with the adenylate cyclase inhibitor 2',3'-Dideoxyadenosine (ddA), to decrease intracellular cAMP levels, prior to treatment with H_2O_2. This could reveal the importance of cAMP in H_2O_2-induced phosphorylation of PKA substrates. Indeed, there was a trend towards increased PKA substrate phosphorylation when HEK 293 cells were co-treated with both cAMP

and H_2O_2 compared to cAMP or H_2O_2 alone. This suggests further that the presence of cAMP is necessary for H_2O_2-induced PKA substrate phosphorylation. This led to the postulation that PKARIα operates as a co-incidence detector, capable of integrating concomitant oxidant and cAMP signals to enhance substrate phosphorylation, a concept that was explored further with tubulin and GEF-H1.

7.6 Tubulin as a PKARIα redox-dependent AKAP

cAMP-agarose induced the reduction of PKARIα disulfide dimer. Furthermore the mutant PKARIα^{-cAMP} formed high molecular weight complexes in the presence of H_2O_2, which reinforced the idea that cAMP has a role in reversing PKARIα disulfide, perhaps through a mechanism that involves a thiol present on a proximal AKAP i.e. tubulin. To unify the two observations I hypothesised that these high molecular weight bands represented transitory intermediates of PKARIα complexed with AKAPs by an inter-protein disulfide bond; that these complexes formed upon H_2O_2-induced targeting of PKARIα to AKAPs; and because they were only evident with the PKARIα^{-cAMP} mutant, that cAMP binding was required to catalyse the full resolution of the complex resulting in PKARIα being reduced to its monomeric form.

LC-MS/MS analysis of samples resolved using diagonal gel electrophoresis identified tubulin as one of the high molecular weight complexes formed when cells expressing the mutant PKARIα^{-cAMP} were exposed to H_2O_2. This was validated in anti-PKARIα immunoprecipitates where tubulin was observed to run above its normal weight after H_2O_2 treatment, potentially in a disulfide linked complex with PKARIα. Many redox modifications, such as short-lived intermediates involved in thiol-disulfide exchange reactions, can often be difficult to detect due to their labile nature and low stoichiometry at any given time. This may explain why it is not possible to observe disulfide linked complexes with WT PKARIα because they are quickly resolved. Mutation of the cAMP binding site slows the reduction of the intermediate disulfide complex (hypothetically due to the lack of conformational change in PKARIα), thus permitting detection of PKARIα disulfide-bound to tubulin. The stoichiometry of the PKARIα-tubulin high molecular weight complex was fairly low, as may be anticipated in reactions that can redox cycle. This is a potential reason why no differences were observed between control and H_2O_2 treated cells in the immunofluorescence experiments.

As previously suggested an oxidant-dependent interaction between PKARIα and an AKAP would serve to localise the kinase to specific substrates during oxidative signalling. Evidence suggests that a significant proportion of the PKA holoenzyme remains intact at physiological and even supraphysiological concentrations of cAMP[189]. The PKARIα holoenzyme undergoes

partial dissociation in the presence of cAMP but full dissociation in the presence of cAMP and substrate, a feature that is unique to the RIα isoform[189,193]. It is reasonable to suggest that full dissociation of the PKARIα holoenzyme complex would translate into enhanced substrate phosphorylation compared to partial dissociation. Therefore the increased interaction between PKARIα and tubulin in the presence of oxidants would rationally lead to enhanced phosphorylation of substrates associated with this complex, as was the case with GEF-H1. The integration of oxidant and cAMP signals may allow the cell to dynamically regulate phosphorylation events to fine-tune functional responses to several stimuli simultaneously. It has been suggested that there is differentiation between type I and type II PKA signalling downstream of specific GPCR activation, although I saw no evidence of this[181]. Perhaps the ability of PKARIα to integrate concomitant oxidant signals extends this paradigm to ensure further selectivity and specificity of cAMP signal transduction.

The exact mechanism of the redox-dependent PKARIα-tubulin interaction remains to be elucidated and may be the subject of future investigations. Systematic mutation of candidate cysteine residues on tubulin and subsequently monitoring for loss of high molecular weight complexes *in vitro* or in cells may help define which cysteines were important for the PKARIα redox interaction. Complex formation between PKARIα and tubulin has previously been described[265], consistent with my findings documented here. To the best of my knowledge it is the only example of a novel disulfide-linked PKARIα interaction with an AKAP, and it remains to be determined if tubulin contributes an α-helix to the interaction. The cytoplasmic tail of the AKAP α4-integrin binds to a C-terminal region of PKARIα, but this not via an amphipathic helix[150]. Likewise, pericentrin sequesters PKA to the centrosome through a 100 amino-acid domain that interacts with a leucine rich region of RIIα[333]. Furthermore, RI binding to dual-specificity AKAPs can be enhanced through an additional sequence outside of the amphipathic helix, termed the RI specifier region (RISR)[334]. As such an interaction between PKA and an AKAP that does not involve a classical AKAP helix, in this case an inter-protein disulfide between PKARIα and tubulin, is not without precedence. I observed numerous high molecular weight complexes with anti-PKARIα after H_2O_2 treatment, and therefore there may be other AKAPs that also interact with PKARIα via an inter-protein disulfide bond. Identifying these putative redox-dependent PKARIα AKAPs is worth considering as part of future investigations.

7.7 Oxidant-potentiated GEF-H1 phosphorylation

It was reasonable to suggest that an increased interaction between tubulin and PKARIα under oxidative conditions would lead to enhanced phosphorylation of substrates associated with the complex. Indeed the phosphorylation of GEF-H1, a MAP, and known PKA substrate, was

enhanced when cells were co-treated with both cAMP and H_2O_2 compared to cells treated with cAMP or H_2O_2 alone. Furthermore GEF-H1 phosphorylation was abrogated when cells were transfected with PKARIα^{-cAMP}, highlighting the importance of cAMP sensing at the level of PKARIα for GEF-H1 phosphorylation. The ability of PKARIα to sense oxidant concentration via the formation of the disulfide dimer was found to be necessary for oxidant-potentiated GEF-H1 phosphorylation, as evidenced by the loss of this effect in the aortas of C17S PKARIα KI mice. Taken together PKARIα detects both cAMP and oxidant signals to enhance GEF-H1 phosphorylation. PKA-dependent phosphorylation of GEF-H1 Ser^{885} inhibits its GTP exchange activity and therefore decreases RhoA-dependent actin cytoskeleton assembly, thus maintaining endothelial cell barrier integrity and limiting vascular permeability[96,294]. Here, I was able to demonstrate that co-treatment of cells with cAMP and H_2O_2 lead to a decrease of actin fibres in HEK 293 cells.

Although the results from the aortas from C17S PKARIα KI mice is promising, in the context of vascular permeability it is still necessary to determine whether cAMP combines with H_2O_2 to enhance GEF-H1 phosphorylation in endothelial cells isolated from WT mice. Subsequently it will also be necessary to interrogate whether the H_2O_2-potentiated GEF-H1 phosphorylation is lost in endothelial cells from C17S PKARIα KI mice. If as expected there is a difference in the GEF-H1 phospho-status between the WT and KI mice an endothelial monolayer permeability assay could be used to determine if there is a difference in endothelial barrier integrity between WT and C17S-PKARIα KI mice. Measurement of the flux of fluorescent labelled dextran (FITC-dextran) across an endothelial cell monolayer[335] can be used to quantify the degree of endothelial permeability after treatment with cAMP, H_2O_2 or co-treatment with both cAMP and H_2O_2. I anticipate that the endothelial cells from PKARIα KI mice will be more permeable to FITC-dextran as they cannot sense cellular oxidants to enhance GEF-H1 phosphorylation, leading to more RhoA-dependent actin fibres and thus greater endothelial permeability.

7.8 PKARIα oxidant-dependent GEF-H1 phosphorylation in sepsis

Inflammatory mediators such as TNFα and IL-1β that are upregulated during sepsis contribute to oxidant production during this time, and may contribute to the associated increase in vascular permeability. I hypothesised that PKARIα can synergise cAMP and oxidant signals to limit vascular permeability via the phosphorylation of GEF-H1 (Figure 7.1).

As of at the time of writing, I was able to conduct a small preliminary *in vivo* experiment to evaluate the development of sepsis in WT and C17S PKARIα KI mice. PKARIα oxidation was

elevated in WT mice, but contrary to my hypothesis GEF-H1 phosphorylation appeared to decrease. Reasonably this could be because intracellular cAMP levels are low 24 hour post sepsis induction. My studies in cells suggest oxidant-dependent phosphorylation of GEF-H1 is contingent upon the presence of cAMP. Although these initial findings do not categorically disprove my hypothesis, further studies assessing a time course of sepsis, and in which cAMP concentration, PKARIα oxidation, GEF-H1 phosphorylation are monitored, is required. Future work may also focus on measuring vascular permeability *in vivo*, comparing WT and C17S PKARIα KI mice basally or after sepsis. This can be achieved using Evans Blue, a dye that conjugates to serum albumin and can subsequently be detected and quantified in organs as a measure of endothelial permeability. I anticipate that the PKARIα KI mice will have a greater amount of blue dye in their organs, indicating increased vascular leak, especially at earlier time points of the CLP model. GEF-H1 activity regulates numerous cellular processes, including epithelial and endothelial permeability[294,336], inflammation[330], oncogenic signalling[322] and neuroplasticity[321]. How PKARIα oxidant-dependent GEF-H1 Ser[885] phosphorylation may impact on these various functions seems important to define in future studies.

The importance of oxidant-dependent PKARIα activation was recently demonstrated in models of angiogenesis/vascular growth[91]. C17S PKARIα KI mice suffered an impairment of vessel growth highlighting the oxidant-sensing ability of PKARIα for adequate physiological responses. I was able to demonstrate that PKARIα forms an oxidant-dependent disulfide-linked complex with tubulin, thereby regulating the phosphorylation of the associated substrate within the complex. Indeed PKARIα serves as a co-incidence detector that is able to integrate cAMP and oxidant signals to synergistically activate PKARIα, leading to the phosphorylation of GEF-H1.

7.9 Other Experimental Limitations

As previously discussed the concentration of H_2O_2 used in experimental studies is the subject of controversy. 500 μM H_2O_2 was routinely used throughout this thesis to induce PKARIα oxidation however some may consider this concentration to only be relevant to pathological conditions rather than homeostatic oxidative signalling. Whilst the evidence for ROS-potentiated GEF-H1 phosphorylation presented in this thesis is robust, it should be cautiously interpreted, as with all results obtained with exogenously applied oxidants.

Throughout this thesis 8-CPT-cAMP was used to activate PKA. The reasons for this are two-fold: cAMP is not cell-permeable; and the use of beta-adrenergic receptor agonists or forskolin may only produce cAMP in specific subcellular compartments. The membrane permeable 8-CPT-cAMP (and other cell-permeable cAMP analogues) is routinely used at a concentration of

100 µM and above[337-340], as was the case in these studies too. However, the permeability of these analogues has not been well characterised. An important question becomes: what is the final intracellular concentration of the cAMP analogue? If these molecules are specifically designed to be membrane permeable, it is reasonable to suggest that the intracellular concentrations approach the applied concentration. This would put the intracellular concentration of cAMP at 100-1000 times greater than the basal cAMP concentration in the cell types I used throughout this thesis. This is potentially further exacerbated because cAMP analogues tend to be more resistant to degradation by PDE's. As such, the results obtained here and throughout the established literature with cAMP analogues should be approached with caution when relating them to physiology/pathology. Furthermore, I routinely used different cell types to investigate the biochemistry related to PKARIα signalling. These cells were grown on plastic 6-well or 12-well plates; however there is now a greater appreciation that results obtained from cells grown on plastic without the context of extra-hormonal signals/physical interactions that are present in normal physiology can have a profound effect on downstream cellular signalling.

7.10 Future Research

Primarily I will continue to investigate the role of GEF-H1 in sepsis pathogenesis in mice, with particular focus on determining at what time-point post sepsis induction GEF-H1 phosphorylation is maximal. From there I intend to continue to investigate PKARIα as a co-incidence detector of oxidant and cAMP signals, and its role on GEF-H1 phosphorylation in the context of sepsis. This will be achieved using PKARIα KI mice which I anticipate will have a deficiency in their GEF-H1 phosphorylation due to their inability to transduce the oxidant signal. I predict that GEF-H1 phosphorylation during sepsis would be beneficial and therefore I would expect the PKARIα KI mice to have a more severe sepsis phenotype as a consequence. Furthermore I will continue to evaluate the redox-dependent interaction between PKARIα and tubulin whilst continuing investigations concerning the mechanism of cAMP-induced reduction of PKARIα, and whether this phenomenon can be observed *in vivo.* Finally, I would like to explore alternative methods of co-capturing PKARIα with AKAPs, to establish whether to oxidation state of the kinase alters the affinity to proteins other than tubulin.

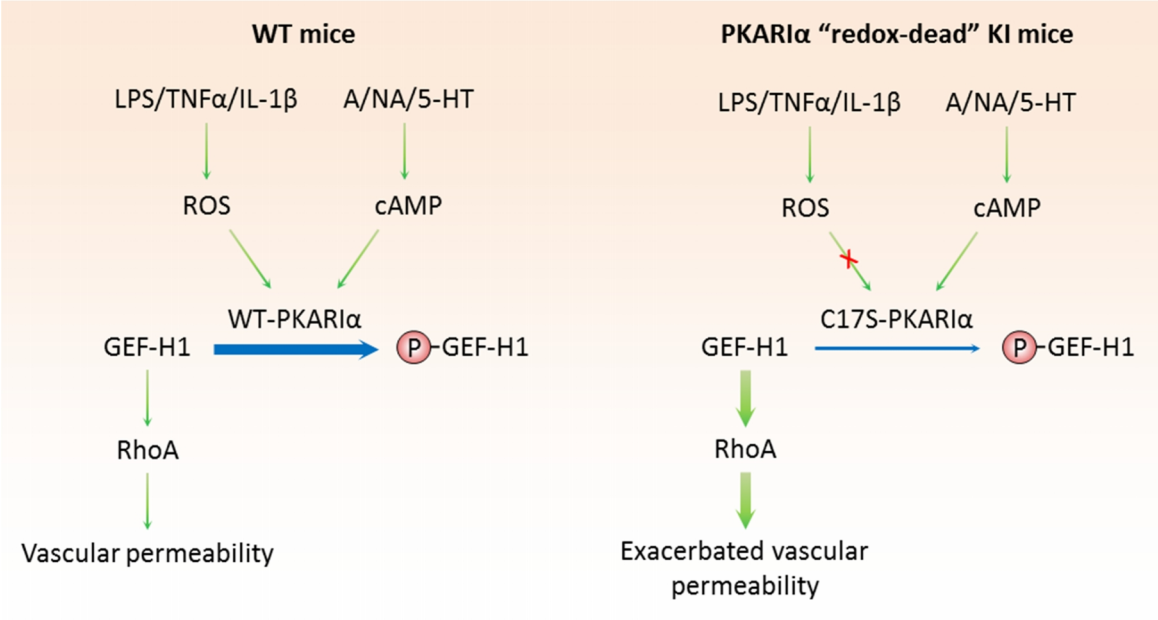

Figure 7.1 Working model of oxidant-dependent activation of PKARIα during sepsis. One mechanism that lipopolysaccharide (LPS), tumour necrosis factor α (TNFα) and interleukin-1β (IL-1β) contribute to the pathogenesis of sepsis is via increasing vascular permeability. Furthermore LPS, TNFα and IL-1β have all been shown to induce ROS production during disease progression. Adrenaline (A), noradrenaline (NA) and serotonin (5-HT) activate GPCRs to stimulate cAMP production. PKARIα in WT mice synergises both ROS and cAMP signals to enhance GEF-H1 phosphorylation in comparison to C17SPKARIα in KI mice that can only be activated by cAMP. Phosphorylation of GEF-H1 decreases its nucleotide exchange activity and consequently limits RhoA-dependent vascular permeability. As C17SPKARIα cannot sense the oxidant signal, GEF-H1 will be hypophosphorylated in KI mice compared to WT mice. Therefore in C17S PKARIα KI mice, the exchange activity of GEF-H1 will be elevated thus enhancing RhoA activation and consequently exacerbating vascular permeability. (Thicker arrows = enhanced activation).

8 References

1 Sawyer, D. B. *et al.* Role of oxidative stress in myocardial hypertrophy and failure. *J Mol Cell Cardiol* **34**, 379-388, (2002).

2 Duthie, G. G., Wahle, K. W. & James, W. P. Oxidants, antioxidants and cardiovascular disease. *Nutr Res Rev* **2**, 51-62, (1989).

3 Reuter, S., Gupta, S. C., Chaturvedi, M. M. & Aggarwal, B. B. Oxidative stress, inflammation, and cancer: how are they linked? *Free Radic Biol Med* **49**, 1603-1616, (2010).

4 Madamanchi, N. R., Vendrov, A. & Runge, M. S. Oxidative stress and vascular disease. *Arterioscler Thromb Vasc Biol* **25**, 29-38, (2005).

5 Uttara, B., Singh, A. V., Zamboni, P. & Mahajan, R. T. Oxidative stress and neurodegenerative diseases: a review of upstream and downstream antioxidant therapeutic options. *Curr Neuropharmacol* **7**, 65-74, (2009).

6 Holmstrom, K. M. & Finkel, T. Cellular mechanisms and physiological consequences of redox-dependent signalling. *Nat Rev Mol Cell Biol* **15**, 411-421, (2014).

7 Maxwell, S. R. Prospects for the use of antioxidant therapies. *Drugs* **49**, 345-361, (1995).

8 Andersen, J. K. Oxidative stress in neurodegeneration: cause or consequence? *Nat Med* **10 Suppl**, S18-25, (2004).

9 Griendling, K. K. & FitzGerald, G. A. Oxidative stress and cardiovascular injury: Part II: animal and human studies. *Circulation* **108**, 2034-2040, (2003).

10 Melov, S. Animal models of oxidative stress, aging, and therapeutic antioxidant interventions. *Int J Biochem Cell Biol* **34**, 1395-1400, (2002).

11 Hennekens, C. H. *et al.* Lack of effect of long-term supplementation with beta carotene on the incidence of malignant neoplasms and cardiovascular disease. *N Engl J Med* **334**, 1145-1149, (1996).

12 Bjelakovic, G., Nikolova, D., Gluud, L. L., Simonetti, R. G. & Gluud, C. Mortality in randomized trials of antioxidant supplements for primary and secondary prevention: systematic review and meta-analysis. *JAMA* **297**, 842-857, (2007).

13 Ray, P. D., Huang, B. W. & Tsuji, Y. Reactive oxygen species (ROS) homeostasis and redox regulation in cellular signaling. *Cell Signal* **24**, 981-990, (2012).

14 Burgoyne, J. R., Mongue-Din, H., Eaton, P. & Shah, A. M. Redox signaling in cardiac physiology and pathology. *Circ Res* **111**, 1091-1106, (2012).

15 Pham-Huy, L. A., He, H. & Pham-Huy, C. Free radicals, antioxidants in disease and health. *Int J Biomed Sci* **4**, 89-96, (2008).

16 Poole, L. B. & Nelson, K. J. Discovering mechanisms of signaling-mediated cysteine oxidation. *Curr Opin Chem Biol* **12**, 18-24, (2008).

17 Shao, D. *et al.* Redox modification of cell signaling in the cardiovascular system. *J Mol Cell Cardiol* **52**, 550-558, (2012).

18 Pacher, P., Beckman, J. S. & Liaudet, L. Nitric oxide and peroxynitrite in health and disease. *Physiol Rev* **87**, 315-424, (2007).

19 Forman, H. J., Fukuto, J. M. & Torres, M. Redox signaling: thiol chemistry defines which reactive oxygen and nitrogen species can act as second messengers. *Am J Physiol Cell Physiol* **287**, C246-256, (2004).

20 Chung, H. S., Wang, S. B., Venkatraman, V., Murray, C. I. & Van Eyk, J. E. Cysteine oxidative posttranslational modifications: emerging regulation in the cardiovascular system. *Circ Res* **112**, 382-392, (2013).

21 Witt, A. C. *et al.* Cysteine pKa depression by a protonated glutamic acid in human DJ-1. *Biochemistry* **47**, 7430-7440, (2008).

22 Jastroch, M., Divakaruni, A. S., Mookerjee, S., Treberg, J. R. & Brand, M. D. Mitochondrial proton and electron leaks. *Essays Biochem* **47**, 53-67, (2010).

23 Tipton, K. F., Boyce, S., O'Sullivan, J., Davey, G. P. & Healy, J. Monoamine oxidases: certainties and uncertainties. *Curr Med Chem* **11**, 1965-1982, (2004).

24 Pena-Silva, R. A., Miller, J. D., Chu, Y. & Heistad, D. D. Serotonin produces monoamine oxidase-dependent oxidative stress in human heart valves. *Am J Physiol Heart Circ Physiol* **297**, H1354-1360, (2009).

25 Kaludercic, N., Carpi, A., Menabo, R., Di Lisa, F. & Paolocci, N. Monoamine oxidases (MAO) in the pathogenesis of heart failure and ischemia/reperfusion injury. *Biochim Biophys Acta* **1813**, 1323-1332, (2011).

26 Ago, T. *et al.* Nox4 as the major catalytic component of an endothelial NAD(P)H oxidase. *Circulation* **109**, 227-233, (2004).

27 Rada, B. & Leto, T. L. Oxidative innate immune defenses by Nox/Duox family NADPH oxidases. *Contrib Microbiol* **15**, 164-187, (2008).

28 Stasia, M. J. & Li, X. J. Genetics and immunopathology of chronic granulomatous disease. *Semin Immunopathol* **30**, 209-235, (2008).

29 Dupre-Crochet, S., Erard, M. & Nubetae, O. ROS production in phagocytes: why, when, and where? *J Leukoc Biol* **94**, 657-670, (2013).

30 Jiang, F., Zhang, Y. & Dusting, G. J. NADPH oxidase-mediated redox signaling: roles in cellular stress response, stress tolerance, and tissue repair. *Pharmacol Rev* **63**, 218-242, (2011).

31 Nauseef, W. M. Biological roles for the NOX family NADPH oxidases. *J Biol Chem* **283**, 16961-16965, (2008).

32 Lassegue, B., San Martin, A. & Griendling, K. K. Biochemistry, physiology, and pathophysiology of NADPH oxidases in the cardiovascular system. *Circ Res* **110**, 1364-1390, (2012).

33 Santos, C. X., Anilkumar, N., Zhang, M., Brewer, A. C. & Shah, A. M. Redox signaling in cardiac myocytes. *Free Radic Biol Med* **50**, 777-793, (2011).

34 Faraci, F. M. & Didion, S. P. Vascular protection: superoxide dismutase isoforms in the vessel wall. *Arterioscler Thromb Vasc Biol* **24**, 1367-1373, (2004).

35 Valacchi, G. (Springer Science & Business Media, 2008).

36 Bedard, K. & Krause, K. H. The NOX family of ROS-generating NADPH oxidases: physiology and pathophysiology. *Physiol Rev* **87**, 245-313, (2007).

37 Santillo, M., Colantuoni, A., Mondola, P., Guida, B. & Damiano, S. NOX signaling in molecular cardiovascular mechanisms involved in the blood pressure homeostasis. *Front Physiol* **6**, 194, (2015).

38 Panday, A., Sahoo, M. K., Osorio, D. & Batra, S. NADPH oxidases: an overview from structure to innate immunity-associated pathologies. *Cell Mol Immunol* **12**, 5-23, (2015).

39 Rahal, A. *et al.* Oxidative stress, prooxidants, and antioxidants: the interplay. *Biomed Res Int* **2014**, 761264, (2014).

40 Chow, C. K., Ibrahim, W., Wei, Z. & Chan, A. C. Vitamin E regulates mitochondrial hydrogen peroxide generation. *Free Radic Biol Med* **27**, 580-587, (1999).

41 Padayatty, S. J. *et al.* Vitamin C as an antioxidant: evaluation of its role in disease prevention. *J Am Coll Nutr* **22**, 18-35, (2003).

42 Mari, M., Morales, A., Colell, A., Garcia-Ruiz, C. & Fernandez-Checa, J. C. Mitochondrial glutathione, a key survival antioxidant. *Antioxid Redox Signal* **11**, 2685-2700, (2009).

43 Montero, D., Tachibana, C., Rahr Winther, J. & Appenzeller-Herzog, C. Intracellular glutathione pools are heterogeneously concentrated. *Redox Biol* **1**, 508-513, (2013).

44 Lu, S. C. Glutathione synthesis. *Biochim Biophys Acta* **1830**, 3143-3153, (2013).

45 Higgins, L. G. *et al.* Transcription factor Nrf2 mediates an adaptive response to sulforaphane that protects fibroblasts in vitro against the cytotoxic effects of

electrophiles, peroxides and redox-cycling agents. *Toxicol Appl Pharmacol* **237**, 267-280, (2009).

46 Wood, Z. A., Schroder, E., Robin Harris, J. & Poole, L. B. Structure, mechanism and regulation of peroxiredoxins. *Trends Biochem Sci* **28**, 32-40, (2003).

47 Day, A. M. *et al.* Inactivation of a peroxiredoxin by hydrogen peroxide is critical for thioredoxin-mediated repair of oxidized proteins and cell survival. *Mol Cell* **45**, 398-408, (2012).

48 Holmgren, A. Thioredoxin structure and mechanism: conformational changes on oxidation of the active-site sulfhydryls to a disulfide. *Structure* **3**, 239-243, (1995).

49 Wood, Z. A., Poole, L. B. & Karplus, P. A. Peroxiredoxin evolution and the regulation of hydrogen peroxide signaling. *Science* **300**, 650-653, (2003).

50 Rhee, S. G., Woo, H. A., Kil, I. S. & Bae, S. H. Peroxiredoxin functions as a peroxidase and a regulator and sensor of local peroxides. *J Biol Chem* **287**, 4403-4410, (2012).

51 Tavender, T. J., Springate, J. J. & Bulleid, N. J. Recycling of peroxiredoxin IV provides a novel pathway for disulphide formation in the endoplasmic reticulum. *EMBO J* **29**, 4185-4197, (2010).

52 Remondino, A. *et al.* Beta-adrenergic receptor-stimulated apoptosis in cardiac myocytes is mediated by reactive oxygen species/c-Jun NH2-terminal kinase-dependent activation of the mitochondrial pathway. *Circ Res* **92**, 136-138, (2003).

53 Hayakawa, R., Hayakawa, T., Takeda, K. & Ichijo, H. Therapeutic targets in the ASK1-dependent stress signaling pathways. *Proc Jpn Acad Ser B Phys Biol Sci* **88**, 434-453, (2012).

54 Yamaguchi, O. *et al.* Targeted deletion of apoptosis signal-regulating kinase 1 attenuates left ventricular remodeling. *Proc Natl Acad Sci U S A* **100**, 15883-15888, (2003).

55 Johnston, A. S., Lehnart, S. E. & Burgoyne, J. R. Ca(2+) signaling in the myocardium by (redox) regulation of PKA/CaMKII. *Front Pharmacol* **6**, 166, (2015).

56 Rosenberg, O. S., Deindl, S., Sung, R. J., Nairn, A. C. & Kuriyan, J. Structure of the autoinhibited kinase domain of CaMKII and SAXS analysis of the holoenzyme. *Cell* **123**, 849-860, (2005).

57 Erickson, J. R. *et al.* A dynamic pathway for calcium-independent activation of CaMKII by methionine oxidation. *Cell* **133**, 462-474, (2008).

58 Wagner, S. *et al.* Reactive oxygen species-activated Ca/calmodulin kinase IIdelta is required for late I(Na) augmentation leading to cellular Na and Ca overload. *Circ Res* **108**, 555-565, (2011).

59 Libby, P., Ridker, P. M. & Hansson, G. K. Progress and challenges in translating the biology of atherosclerosis. *Nature* **473**, 317-325, (2011).

60 Shah, P. K. *et al.* Human monocyte-derived macrophages induce collagen breakdown in fibrous caps of atherosclerotic plaques. Potential role of matrix-degrading metalloproteinases and implications for plaque rupture. *Circulation* **92**, 1565-1569, (1995).

61 Fabrizio Rodella, L. *et al.* Atherosclerosis and the protective role played by different proteins in apolipoprotein E-deficient mice. *Acta Histochem* **109**, 45-51, (2007).

62 Lusis, A. J. Atherosclerosis. *Nature* **407**, 233-241, (2000).

63 Lu, Y. & Wahl, L. M. Oxidative stress augments the production of matrix metalloproteinase-1, cyclooxygenase-2, and prostaglandin E2 through enhancement of NF-kappa B activity in lipopolysaccharide-activated human primary monocytes. *J Immunol* **175**, 5423-5429, (2005).

64 Yang, H. *et al.* Retardation of atherosclerosis by overexpression of catalase or both Cu/Zn-superoxide dismutase and catalase in mice lacking apolipoprotein E. *Circ Res* **95**, 1075-1081, (2004).

65 Lum, H. & Roebuck, K. A. Oxidant stress and endothelial cell dysfunction. *Am J Physiol Cell Physiol* **280**, C719-741, (2001).

66 Aghajanian, A., Wittchen, E. S., Allingham, M. J., Garrett, T. A. & Burridge, K. Endothelial cell junctions and the regulation of vascular permeability and leukocyte transmigration. *J Thromb Haemost* **6**, 1453-1460, (2008).

67 Ochoa, L., Waypa, G., Mahoney, J. R., Jr., Rodriguez, L. & Minnear, F. L. Contrasting effects of hypochlorous acid and hydrogen peroxide on endothelial permeability: prevention with cAMP drugs. *Am J Respir Crit Care Med* **156**, 1247-1255, (1997).

68 Lee, K. S. *et al.* Hydrogen peroxide induces vascular permeability via regulation of vascular endothelial growth factor. *Am J Respir Cell Mol Biol* **35**, 190-197, (2006).

69 Moldovan, L., Moldovan, N. I., Sohn, R. H., Parikh, S. A. & Goldschmidt-Clermont, P. J. Redox changes of cultured endothelial cells and actin dynamics. *Circ Res* **86**, 549-557, (2000).

70 Sprague, A. H. & Khalil, R. A. Inflammatory cytokines in vascular dysfunction and vascular disease. *Biochem Pharmacol* **78**, 539-552, (2009).

71 Zheng, M., Aslund, F. & Storz, G. Activation of the OxyR transcription factor by reversible disulfide bond formation. *Science* **279**, 1718-1721, (1998).

72 Wei, Q. *et al.* Global regulation of gene expression by OxyR in an important human opportunistic pathogen. *Nucleic Acids Res* **40**, 4320-4333, (2012).

73 Hansen, J. M., Go, Y. M. & Jones, D. P. Nuclear and mitochondrial compartmentation of oxidative stress and redox signaling. *Annu Rev Pharmacol Toxicol* **46**, 215-234, (2006).

74 Suzuki, T. & Yamamoto, M. Molecular basis of the Keap1-Nrf2 system. *Free Radic Biol Med* **88**, 93-100, (2015).

75 Gorrini, C., Harris, I. S. & Mak, T. W. Modulation of oxidative stress as an anticancer strategy. *Nat Rev Drug Discov* **12**, 931-947, (2013).

76 Soriano, F. X. *et al.* Transcriptional regulation of the AP-1 and Nrf2 target gene sulfiredoxin. *Mol Cells* **27**, 279-282, (2009).

77 Tell, G., Quadrifoglio, F., Tiribelli, C. & Kelley, M. R. The many functions of APE1/Ref-1: not only a DNA repair enzyme. *Antioxid Redox Signal* **11**, 601-620, (2009).

78 Kelley, M. R., Georgiadis, M. M. & Fishel, M. L. APE1/Ref-1 role in redox signaling: translational applications of targeting the redox function of the DNA repair/redox protein APE1/Ref-1. *Curr Mol Pharmacol* **5**, 36-53, (2012).

79 Walker, L. J., Robson, C. N., Black, E., Gillespie, D. & Hickson, I. D. Identification of residues in the human DNA repair enzyme HAP1 (Ref-1) that are essential for redox regulation of Jun DNA binding. *Mol Cell Biol* **13**, 5370-5376, (1993).

80 Georgiadis, M. M. *et al.* Evolution of the redox function in mammalian apurinic/apyrimidinic endonuclease. *Mutat Res* **643**, 54-63, (2008).

81 Burgoyne, J. R. *et al.* Cysteine redox sensor in PKGIa enables oxidant-induced activation. *Science* **317**, 1393-1397, (2007).

82 Dulce, R. A., Schulman, I. H. & Hare, J. M. S-glutathionylation: a redox-sensitive switch participating in nitroso-redox balance. *Circ Res* **108**, 531-533, (2011).

83 Deanfield, J. *et al.* Endothelial function and dysfunction. Part I: Methodological issues for assessment in the different vascular beds: a statement by the Working Group on Endothelin and Endothelial Factors of the European Society of Hypertension. *J Hypertens* **23**, 7-17, (2005).

84 Chen, C. A. *et al.* S-glutathionylation uncouples eNOS and regulates its cellular and vascular function. *Nature* **468**, 1115-1118, (2010).

85 Burgoyne, J. R. & Eaton, P. Transnitrosylating nitric oxide species directly activate type I protein kinase A, providing a novel adenylate cyclase-independent cross-talk to beta-adrenergic-like signaling. *J Biol Chem* **284**, 29260-29268, (2009).

86 Wang, Y. T., Piyankarage, S. C., Williams, D. L. & Thatcher, G. R. Proteomic profiling of nitrosative stress: protein S-oxidation accompanies S-nitrosylation. *ACS Chem Biol* **9**, 821-830, (2014).

87 Prysyazhna, O., Rudyk, O. & Eaton, P. Single atom substitution in mouse protein kinase G eliminates oxidant sensing to cause hypertension. *Nat Med* **18**, 286-290, (2012).

88 Meng, T. C., Fukada, T. & Tonks, N. K. Reversible oxidation and inactivation of protein tyrosine phosphatases in vivo. *Mol Cell* **9**, 387-399, (2002).

89 Denu, J. M. & Tanner, K. G. Specific and reversible inactivation of protein tyrosine phosphatases by hydrogen peroxide: evidence for a sulfenic acid intermediate and implications for redox regulation. *Biochemistry* **37**, 5633-5642, (1998).

90 Ushio-Fukai, M. Redox signaling in angiogenesis: role of NADPH oxidase. *Cardiovasc Res* **71**, 226-235, (2006).

91 Burgoyne, J. R. *et al.* Deficient angiogenesis in redox-dead Cys17Ser PKARIalpha knock-in mice. *Nat Commun* **6**, 7920, (2015).

92 Bers, D. M. Calcium cycling and signaling in cardiac myocytes. *Annu Rev Physiol* **70**, 23-49, (2008).

93 Bers, D. M., Eisner, D. A. & Valdivia, H. H. Sarcoplasmic reticulum Ca2+ and heart failure: roles of diastolic leak and Ca2+ transport. *Circ Res* **93**, 487-490, (2003).

94 Goldberg, N. D. *et al.* Biologic regulation through opposing influences of cyclic GMP and cyclic AMP: the Yin Yang hypothesis. *Adv Cyclic Nucleotide Res* **5**, 307-330, (1975).

95 Haynes, J., Jr., Robinson, J., Saunders, L., Taylor, A. E. & Strada, S. J. Role of cAMP-dependent protein kinase in cAMP-mediated vasodilation. *Am J Physiol* **262**, H511-516, (1992).

96 Spindler, V., Schlegel, N. & Waschke, J. Role of GTPases in control of microvascular permeability. *Cardiovasc Res* **87**, 243-253, (2010).

97 Adamson, R. H., Liu, B., Fry, G. N., Rubin, L. L. & Curry, F. E. Microvascular permeability and number of tight junctions are modulated by cAMP. *Am J Physiol* **274**, H1885-1894, (1998).

98 Mayr, B. & Montminy, M. Transcriptional regulation by the phosphorylation-dependent factor CREB. *Nat Rev Mol Cell Biol* **2**, 599-609, (2001).

99 Delghandi, M. P., Johannessen, M. & Moens, U. The cAMP signalling pathway activates CREB through PKA, p38 and MSK1 in NIH 3T3 cells. *Cell Signal* **17**, 1343-1351, (2005).

100 Bacallao, K. & Monje, P. V. Opposing roles of PKA and EPAC in the cAMP-dependent regulation of schwann cell proliferation and differentiation [corrected]. *PLoS One* **8**, e82354, (2013).

101 Hewer, R. C., Sala-Newby, G. B., Wu, Y. J., Newby, A. C. & Bond, M. PKA and Epac synergistically inhibit smooth muscle cell proliferation. *J Mol Cell Cardiol* **50**, 87-98, (2011).

102 Zaccolo, M. *et al.* Restricted diffusion of a freely diffusible second messenger: mechanisms underlying compartmentalized cAMP signalling. *Biochem Soc Trans* **34**, 495-497, (2006).

103 Sarma, G. N. *et al.* Structure of D-AKAP2:PKA RI complex: insights into AKAP specificity and selectivity. *Structure* **18**, 155-166, (2010).

104 Gao, X., Chaturvedi, D. & Patel, T. B. p90 ribosomal S6 kinase 1 (RSK1) and the catalytic subunit of protein kinase A (PKA) compete for binding the pseudosubstrate region of PKAR1alpha: role in the regulation of PKA and RSK1 activities. *J Biol Chem* **285**, 6970-6979, (2010).

105 Taylor, S. S., Buechler, J. A. & Yonemoto, W. cAMP-dependent protein kinase: framework for a diverse family of regulatory enzymes. *Annu Rev Biochem* **59**, 971-1005, (1990).

106 Kim, C., Xuong, N. H. & Taylor, S. S. Crystal structure of a complex between the catalytic and regulatory (RIalpha) subunits of PKA. *Science* **307**, 690-696, (2005).

107 de Pina, M. Z. *et al.* Signaling the signal, cyclic AMP-dependent protein kinase inhibition by insulin-formed H2O2 and reactivation by thioredoxin. *J Biol Chem* **283**, 12373-12386, (2008).

108 Cadd, G. & McKnight, G. S. Distinct patterns of cAMP-dependent protein kinase gene expression in mouse brain. *Neuron* **3**, 71-79, (1989).

109 Amieux, P. S. *et al.* Compensatory regulation of RIalpha protein levels in protein kinase A mutant mice. *J Biol Chem* **272**, 3993-3998, (1997).

110 Wang, Y. *et al.* PKA-Type I Selective Constrained Peptide Disruptors of AKAP Complexes. *ACS Chem Biol* **10**, 1502-1510, (2015).

111 Casey, M. *et al.* Mutations in the protein kinase A R1alpha regulatory subunit cause familial cardiac myxomas and Carney complex. *J Clin Invest* **106**, R31-38, (2000).

112 Taylor, S. S., Ilouz, R., Zhang, P. & Kornev, A. P. Assembly of allosteric macromolecular switches: lessons from PKA. *Nat Rev Mol Cell Biol* **13**, 646-658, (2012).

113 Beavo, J. A. & Brunton, L. L. Cyclic nucleotide research -- still expanding after half a century. *Nat Rev Mol Cell Biol* **3**, 710-718, (2002).

114 Newlon, M. G. *et al.* A novel mechanism of PKA anchoring revealed by solution structures of anchoring complexes. *EMBO J* **20**, 1651-1662, (2001).

115 Kinderman, F. S. *et al.* A dynamic mechanism for AKAP binding to RII isoforms of cAMP-dependent protein kinase. *Mol Cell* **24**, 397-408, (2006).

116 Burgers, P. P. *et al.* A Small Novel A-Kinase Anchoring Protein (AKAP) That Localizes Specifically Protein Kinase A-Regulatory Subunit I (PKA-RI) to the Plasma Membrane. *J Biol Chem* **287**, 43789-43797, (2012).

117 Poteet-Smith, C. E., Shabb, J. B., Francis, S. H. & Corbin, J. D. Identification of critical determinants for autoinhibition in the pseudosubstrate region of type I alpha cAMP-dependent protein kinase. *J Biol Chem* **272**, 379-388, (1997).

118 Seino, S. & Shibasaki, T. PKA-dependent and PKA-independent pathways for cAMP-regulated exocytosis. *Physiol Rev* **85**, 1303-1342, (2005).

119 Houslay, M. D. Underpinning compartmentalised cAMP signalling through targeted cAMP breakdown. *Trends Biochem Sci* **35**, 91-100, (2010).

120 Xiang, Y. K. Compartmentalization of beta-adrenergic signals in cardiomyocytes. *Circ Res* **109**, 231-244, (2011).

121 Aye, T. T. *et al.* Selectivity in enrichment of cAMP-dependent protein kinase regulatory subunits type I and type II and their interactors using modified cAMP affinity resins. *Mol Cell Proteomics* **8**, 1016-1028, (2009).

122 Kaupp, U. B. & Seifert, R. Molecular diversity of pacemaker ion channels. *Annu Rev Physiol* **63**, 235-257, (2001).

123 Gloerich, M. & Bos, J. L. Epac: defining a new mechanism for cAMP action. *Annu Rev Pharmacol Toxicol* **50**, 355-375, (2010).

124 Sugden, P. H. & Bogoyevitch, M. A. Intracellular signalling through protein kinases in the heart. *Cardiovasc Res* **30**, 478-492, (1995).

125 Lissandron, V. & Zaccolo, M. Compartmentalized cAMP/PKA signalling regulates cardiac excitation-contraction coupling. *J Muscle Res Cell Motil* **27**, 399-403, (2006).

126 Bunemann, M., Gerhardstein, B. L., Gao, T. & Hosey, M. M. Functional regulation of L-type calcium channels via protein kinase A-mediated phosphorylation of the beta(2) subunit. *J Biol Chem* **274**, 33851-33854, (1999).

127 Bers, D. M. Cardiac excitation-contraction coupling. *Nature* **415**, 198-205, (2002).

128 Pidoux, G. & Tasken, K. Specificity and spatial dynamics of protein kinase A signaling organized by A-kinase-anchoring proteins. *J Mol Endocrinol* **44**, 271-284, (2010).

129 Parker, D. *et al.* Phosphorylation of CREB at Ser-133 induces complex formation with CREB-binding protein via a direct mechanism. *Mol Cell Biol* **16**, 694-703, (1996).

130 Ichiki, T. Role of cAMP response element binding protein in cardiovascular remodeling: good, bad, or both? *Arterioscler Thromb Vasc Biol* **26**, 449-455, (2006).

131 Miller, C. An overview of the potassium channel family. *Genome Biol* **1**, REVIEWS0004, (2000).

132 Ledoux, J., Werner, M. E., Brayden, J. E. & Nelson, M. T. Calcium-activated potassium channels and the regulation of vascular tone. *Physiology (Bethesda)* **21**, 69-78, (2006).

133 Hai, C. M. & Murphy, R. A. Ca2+, crossbridge phosphorylation, and contraction. *Annu Rev Physiol* **51**, 285-298, (1989).

134 Morgado, M., Cairrao, E., Santos-Silva, A. J. & Verde, I. Cyclic nucleotide-dependent relaxation pathways in vascular smooth muscle. *Cell Mol Life Sci* **69**, 247-266, (2012).

135 Diviani, D., Dodge-Kafka, K. L., Li, J. & Kapiloff, M. S. A-kinase anchoring proteins: scaffolding proteins in the heart. *Am J Physiol Heart Circ Physiol* **301**, H1742-1753, (2011).

136 Lygren, B. & Tasken, K. The potential use of AKAP18delta as a drug target in heart failure patients. *Expert Opin Biol Ther* **8**, 1099-1108, (2008).

137 Theurkauf, W. E. & Vallee, R. B. Molecular characterization of the cAMP-dependent protein kinase bound to microtubule-associated protein 2. *J Biol Chem* **257**, 3284-3290, (1982).

138 Welch, E. J., Jones, B. W. & Scott, J. D. Networking with AKAPs: context-dependent regulation of anchored enzymes. *Mol Interv* **10**, 86-97, (2010).

139 Scott, J. D., Dessauer, C. W. & Tasken, K. Creating order from chaos: cellular regulation by kinase anchoring. *Annu Rev Pharmacol Toxicol* **53**, 187-210, (2013).

140 Lygren, B. *et al.* AKAP complex regulates Ca2+ re-uptake into heart sarcoplasmic reticulum. *EMBO Rep* **8**, 1061-1067, (2007).

141 Banky, P. *et al.* Isoform-specific differences between the type Ialpha and IIalpha cyclic AMP-dependent protein kinase anchoring domains revealed by solution NMR. *J Biol Chem* **275**, 35146-35152, (2000).

142 Wong, W. & Scott, J. D. AKAP signalling complexes: focal points in space and time. *Nat Rev Mol Cell Biol* **5**, 959-970, (2004).

143 Skalhegg, B. S. *et al.* Location of cAMP-dependent protein kinase type I with the TCR-CD3 complex. *Science* **263**, 84-87, (1994).

144 Miki, K. & Eddy, E. M. Single amino acids determine specificity of binding of protein kinase A regulatory subunits by protein kinase A anchoring proteins. *J Biol Chem* **274**, 29057-29062, (1999).

145 Hausken, Z. E., Coghlan, V. M., Hastings, C. A., Reimann, E. M. & Scott, J. D. Type II regulatory subunit (RII) of the cAMP-dependent protein kinase interaction with A-kinase anchor proteins requires isoleucines 3 and 5. *J Biol Chem* **269**, 24245-24251, (1994).

146 Herberg, F. W., Maleszka, A., Eide, T., Vossebein, L. & Tasken, K. Analysis of A-kinase anchoring protein (AKAP) interaction with protein kinase A (PKA) regulatory subunits: PKA isoform specificity in AKAP binding. *J Mol Biol* **298**, 329-339, (2000).

147 Gold, M. G. *et al.* Molecular basis of AKAP specificity for PKA regulatory subunits. *Mol Cell* **24**, 383-395, (2006).

148 Carr, D. W., Stofko-Hahn, R. E., Fraser, I. D., Cone, R. D. & Scott, J. D. Localization of the cAMP-dependent protein kinase to the postsynaptic densities by A-kinase anchoring proteins. Characterization of AKAP 79. *J Biol Chem* **267**, 16816-16823, (1992).

149 Trotter, K. W. *et al.* Alternative splicing regulates the subcellular localization of A-kinase anchoring protein 18 isoforms. *J Cell Biol* **147**, 1481-1492, (1999).

150 Lim, C. J. *et al.* Alpha4 integrins are type I cAMP-dependent protein kinase-anchoring proteins. *Nat Cell Biol* **9**, 415-421, (2007).

151 Dransfield, D. T. *et al.* Ezrin is a cyclic AMP-dependent protein kinase anchoring protein. *EMBO J* **16**, 35-43, (1997).

152 Ruppelt, A. *et al.* Inhibition of T cell activation by cyclic adenosine 5'-monophosphate requires lipid raft targeting of protein kinase A type I by the A-kinase anchoring protein ezrin. *J Immunol* **179**, 5159-5168, (2007).

153 Takenawa, T. & Suetsugu, S. The WASP-WAVE protein network: connecting the membrane to the cytoskeleton. *Nat Rev Mol Cell Biol* **8**, 37-48, (2007).

154 Fink, M. A. *et al.* AKAP-mediated targeting of protein kinase a regulates contractility in cardiac myocytes. *Circ Res* **88**, 291-297, (2001).

155 Smith, F. D. *et al.* AKAP-Lbc enhances cyclic AMP control of the ERK1/2 cascade. *Nat Cell Biol* **12**, 1242-1249, (2010).

156 Appert-Collin, A., Cotecchia, S., Nenniger-Tosato, M., Pedrazzini, T. & Diviani, D. The A-kinase anchoring protein (AKAP)-Lbc-signaling complex mediates alpha1 adrenergic receptor-induced cardiomyocyte hypertrophy. *Proc Natl Acad Sci U S A* **104**, 10140-10145, (2007).

157 Smith, F. D., Langeberg, L. K. & Scott, J. D. The where's and when's of kinase anchoring. *Trends Biochem Sci* **31**, 316-323, (2006).

158 Osteen, J. D., Sampson, K. J. & Kass, R. S. The cardiac IKs channel, complex indeed. *Proc Natl Acad Sci U S A* **107**, 18751-18752, (2010).

159 Navedo, M. F. *et al.* AKAP150 is required for stuttering persistent Ca2+ sparklets and angiotensin II-induced hypertension. *Circ Res* **102**, e1-e11, (2008).

160 Nichols, C. B. *et al.* Sympathetic stimulation of adult cardiomyocytes requires association of AKAP5 with a subpopulation of L-type calcium channels. *Circ Res* **107**, 747-756, (2010).

161 Means, C. K. *et al.* An entirely specific type I A-kinase anchoring protein that can sequester two molecules of protein kinase A at mitochondria. *Proc Natl Acad Sci U S A* **108**, E1227-1235, (2011).

162 Affaitati, A. *et al.* Essential role of A-kinase anchor protein 121 for cAMP signaling to mitochondria. *J Biol Chem* **278**, 4286-4294, (2003).

163 Cribbs, J. T. & Strack, S. Reversible phosphorylation of Drp1 by cyclic AMP-dependent protein kinase and calcineurin regulates mitochondrial fission and cell death. *EMBO Rep* **8**, 939-944, (2007).

164 Merrill, R. A. *et al.* Mechanism of neuroprotective mitochondrial remodeling by PKA/AKAP1. *PLoS Biol* **9**, e1000612, (2011).

165 Tingley, W. G. *et al.* Gene-trapped mouse embryonic stem cell-derived cardiac myocytes and human genetics implicate AKAP10 in heart rhythm regulation. *Proc Natl Acad Sci U S A* **104**, 8461-8466, (2007).

166 Mayers, C. M. *et al.* The Rho guanine nucleotide exchange factor AKAP13 (BRX) is essential for cardiac development in mice. *J Biol Chem* **285**, 12344-12354, (2010).

167 Dodge-Kafka, K. L. *et al.* The protein kinase A anchoring protein mAKAP coordinates two integrated cAMP effector pathways. *Nature* **437**, 574-578, (2005).

168 Chen, L. *et al.* Mutation of an A-kinase-anchoring protein causes long-QT syndrome. *Proc Natl Acad Sci U S A* **104**, 20990-20995, (2007).

169 Brennan, J. P. *et al.* Detection and mapping of widespread intermolecular protein disulfide formation during cardiac oxidative stress using proteomics with diagonal electrophoresis. *J Biol Chem* **279**, 41352-41360, (2004).

170 Brennan, J. P. *et al.* Oxidant-induced activation of type I protein kinase A is mediated by RI subunit interprotein disulfide bond formation. *J Biol Chem* **281**, 21827-21836, (2006).

171 Hathaway, N. *Redox Regulation of Type Ia PKA in the Heart*, King's College London, (2013).

172 Eisel, F. *et al.* Platelet-derived growth factor triggers PKA-mediated signalling by a redox-dependent mechanism in rat renal mesangial cells. *Biochem Pharmacol* **85**, 101-108, (2013).

173 Beck, K. F. *et al.* Cytokines induce protein kinase A-mediated signalling by a redox-dependent mechanism in rat renal mesangial cells. *Biochem Pharmacol* **93**, 362-369, (2015).

174 Sambrook, J. F. F., Fritsch E.F., Manaitis T. . *Molecular Cloning: A Laboratory Manual* (Cold Spring Harbor Laboratory, 1989).

175 Snabaitis, A. K., Muntendorf, A., Wieland, T. & Avkiran, M. Regulation of the extracellular signal-regulated kinase pathway in adult myocardium: differential roles of G(q/11), Gi and G(12/13) proteins in signalling by alpha1-adrenergic, endothelin-1 and thrombin-sensitive protease-activated receptors. *Cell Signal* **17**, 655-664, (2005).

176 Burgoyne, J. R., Oviosu, O. & Eaton, P. The PEG-switch assay: a fast semi-quantitative method to determine protein reversible cysteine oxidation. *J Pharmacol Toxicol Methods* **68**, 297-301, (2013).
177 Willoughby, D. & Cooper, D. M. Organization and Ca2+ regulation of adenylyl cyclases in cAMP microdomains. *Physiol Rev* **87**, 965-1010, (2007).
178 Hayes, J. S., Brunton, L. L. & Mayer, S. E. Selective activation of particulate cAMP-dependent protein kinase by isoproterenol and prostaglandin E1. *J Biol Chem* **255**, 5113-5119, (1980).
179 Buxton, I. L. & Brunton, L. L. Compartments of cyclic AMP and protein kinase in mammalian cardiomyocytes. *J Biol Chem* **258**, 10233-10239, (1983).
180 Evellin, S., Mongillo, M., Terrin, A., Lissandron, V. & Zaccolo, M. Measuring dynamic changes in cAMP using fluorescence resonance energy transfer. *Methods Mol Biol* **284**, 259-270, (2004).
181 Terrin, A. *et al.* PGE(1) stimulation of HEK293 cells generates multiple contiguous domains with different [cAMP]: role of compartmentalized phosphodiesterases. *J Cell Biol* **175**, 441-451, (2006).
182 Zaccolo, M. & Pozzan, T. Discrete microdomains with high concentration of cAMP in stimulated rat neonatal cardiac myocytes. *Science* **295**, 1711-1715, (2002).
183 DiPilato, L. M., Cheng, X. & Zhang, J. Fluorescent indicators of cAMP and Epac activation reveal differential dynamics of cAMP signaling within discrete subcellular compartments. *Proc Natl Acad Sci U S A* **101**, 16513-16518, (2004).
184 Houslay, M. D. & Adams, D. R. PDE4 cAMP phosphodiesterases: modular enzymes that orchestrate signalling cross-talk, desensitization and compartmentalization. *Biochem J* **370**, 1-18, (2003).
185 Rochais, F. *et al.* A specific pattern of phosphodiesterases controls the cAMP signals generated by different Gs-coupled receptors in adult rat ventricular myocytes. *Circ Res* **98**, 1081-1088, (2006).
186 Baillie, G. S. Compartmentalized signalling: spatial regulation of cAMP by the action of compartmentalized phosphodiesterases. *FEBS J* **276**, 1790-1799, (2009).
187 Brunton, L. L., Hayes, J. S. & Mayer, S. E. Functional compartmentation of cyclic AMP and protein kinase in heart. *Adv Cyclic Nucleotide Res* **14**, 391-397, (1981).
188 Di Benedetto, G. *et al.* Protein kinase A type I and type II define distinct intracellular signaling compartments. *Circ Res* **103**, 836-844, (2008).
189 Vigil, D., Blumenthal, D. K., Brown, S., Taylor, S. S. & Trewhella, J. Differential effects of substrate on type I and type II PKA holoenzyme dissociation. *Biochemistry* **43**, 5629-5636, (2004).
190 Yang, S., Fletcher, W. H. & Johnson, D. A. Regulation of cAMP-dependent protein kinase: enzyme activation without dissociation. *Biochemistry* **34**, 6267-6271, (1995).
191 Smith, F. D. *et al.* Intrinsic disorder within an AKAP-protein kinase A complex guides local substrate phosphorylation. *Elife* **2**, e01319, (2013).
192 Kopperud, R. *et al.* Formation of inactive cAMP-saturated holoenzyme of cAMP-dependent protein kinase under physiological conditions. *J Biol Chem* **277**, 13443-13448, (2002).
193 Viste, K., Kopperud, R. K., Christensen, A. E. & Doskeland, S. O. Substrate enhances the sensitivity of type I protein kinase a to cAMP. *J Biol Chem* **280**, 13279-13284, (2005).
194 Burgoyne, J. R., Prysyazhna, O., Rudyk, O. & Eaton, P. cGMP-dependent activation of protein kinase G precludes disulfide activation: implications for blood pressure control. *Hypertension* **60**, 1301-1308, (2012).
195 Boguslavskyi, A. *et al.* Cardiac hypertrophy in mice expressing unphosphorylatable phospholemman. *Cardiovasc Res* **104**, 72-82, (2014).
196 Brede, M. *et al.* Feedback inhibition of catecholamine release by two different alpha2-adrenoceptor subtypes prevents progression of heart failure. *Circulation* **106**, 2491-2496, (2002).

197 Banky, P., Huang, L. J. & Taylor, S. S. Dimerization/docking domain of the type Ialpha regulatory subunit of cAMP-dependent protein kinase. Requirements for dimerization and docking are distinct but overlapping. *J Biol Chem* **273**, 35048-35055, (1998).

198 Leon, D. A., Herberg, F. W., Banky, P. & Taylor, S. S. A stable alpha-helical domain at the N terminus of the RIalpha subunits of cAMP-dependent protein kinase is a novel dimerization/docking motif. *J Biol Chem* **272**, 28431-28437, (1997).

199 Lange-Carter, C. A., Fossli, T., Jahnsen, T. & Malkinson, A. M. Decreased expression of the type I isozyme of cAMP-dependent protein kinase in tumor cell lines of lung epithelial origin. *J Biol Chem* **265**, 7814-7818, (1990).

200 Samuelsen, J. T. *et al.* Regulation of rat alveolar type 2 cell proliferation in vitro involves type II cAMP-dependent protein kinase. *Am J Physiol Lung Cell Mol Physiol* **292**, L232-239, (2007).

201 Parisiadou, L. *et al.* LRRK2 regulates synaptogenesis and dopamine receptor activation through modulation of PKA activity. *Nat Neurosci* **17**, 367-376, (2014).

202 Bianchi, P. *et al.* Oxidative stress by monoamine oxidase mediates receptor-independent cardiomyocyte apoptosis by serotonin and postischemic myocardial injury. *Circulation* **112**, 3297-3305, (2005).

203 Vindis, C., Seguelas, M. H., Lanier, S., Parini, A. & Cambon, C. Dopamine induces ERK activation in renal epithelial cells through H2O2 produced by monoamine oxidase. *Kidney Int* **59**, 76-86, (2001).

204 Eisensamer, B. *et al.* Antidepressants are functional antagonists at the serotonin type 3 (5-HT3) receptor. *Mol Psychiatry* **8**, 994-1007, (2003).

205 Li, J. M. & Shah, A. M. Intracellular localization and preassembly of the NADPH oxidase complex in cultured endothelial cells. *J Biol Chem* **277**, 19952-19960, (2002).

206 Mahadev, K. *et al.* The NAD(P)H oxidase homolog Nox4 modulates insulin-stimulated generation of H2O2 and plays an integral role in insulin signal transduction. *Mol Cell Biol* **24**, 1844-1854, (2004).

207 Echeverria, V., Clerman, A. & Dore, S. Stimulation of PGE receptors EP2 and EP4 protects cultured neurons against oxidative stress and cell death following beta-amyloid exposure. *Eur J Neurosci* **22**, 2199-2206, (2005).

208 He, W. *et al.* Sirt1 activation protects the mouse renal medulla from oxidative injury. *J Clin Invest* **120**, 1056-1068, (2010).

209 Liu, S. *et al.* Phosphodiesterases coordinate cAMP propagation induced by two stimulatory G protein-coupled receptors in hearts. *Proc Natl Acad Sci U S A* **109**, 6578-6583, (2012).

210 Warrier, S. *et al.* cAMP microdomains and L-type Ca2+ channel regulation in guinea-pig ventricular myocytes. *J Physiol* **580**, 765-776, (2007).

211 Saucerman, J. J. *et al.* Systems analysis of PKA-mediated phosphorylation gradients in live cardiac myocytes. *Proc Natl Acad Sci U S A* **103**, 12923-12928, (2006).

212 Humphries, K. M., Pennypacker, J. K. & Taylor, S. S. Redox regulation of cAMP-dependent protein kinase signaling: kinase versus phosphatase inactivation. *J Biol Chem* **282**, 22072-22079, (2007).

213 Fischmeister, R. *et al.* Compartmentation of cyclic nucleotide signaling in the heart: the role of cyclic nucleotide phosphodiesterases. *Circ Res* **99**, 816-828, (2006).

214 Conti, M., Mika, D. & Richter, W. Cyclic AMP compartments and signaling specificity: role of cyclic nucleotide phosphodiesterases. *J Gen Physiol* **143**, 29-38, (2014).

215 Borner, S. *et al.* FRET measurements of intracellular cAMP concentrations and cAMP analog permeability in intact cells. *Nat Protoc* **6**, 427-438, (2011).

216 Perrino, C. *et al.* Intermittent pressure overload triggers hypertrophy-independent cardiac dysfunction and vascular rarefaction. *J Clin Invest* **116**, 1547-1560, (2006).

217 Morel, E. *et al.* cAMP-binding protein Epac induces cardiomyocyte hypertrophy. *Circ Res* **97**, 1296-1304, (2005).

218 Han, Y. S., Arroyo, J. & Ogut, O. Human heart failure is accompanied by altered protein kinase A subunit expression and post-translational state. *Arch Biochem Biophys* **538**, 25-33, (2013).

219 Akazawa, H. & Komuro, I. Roles of cardiac transcription factors in cardiac hypertrophy. *Circ Res* **92**, 1079-1088, (2003).

220 Inserte, J., Taimor, G., Hofstaetter, B., Garcia-Dorado, D. & Piper, H. M. Influence of simulated ischemia on apoptosis induction by oxidative stress in adult cardiomyocytes of rats. *Am J Physiol Heart Circ Physiol* **278**, H94-99, (2000).

221 Hopper-Borge, E., Chen, Z. S., Shchaveleva, I., Belinsky, M. G. & Kruh, G. D. Analysis of the drug resistance profile of multidrug resistance protein 7 (ABCC10): resistance to docetaxel. *Cancer Res* **64**, 4927-4930, (2004).

222 Selak, M. A. *et al.* Succinate links TCA cycle dysfunction to oncogenesis by inhibiting HIF-alpha prolyl hydroxylase. *Cancer Cell* **7**, 77-85, (2005).

223 Martin, S. F., Sawai, H., Villalba, J. M. & Hannun, Y. A. Redox regulation of neutral sphingomyelinase-1 activity in HEK293 cells through a GSH-dependent mechanism. *Arch Biochem Biophys* **459**, 295-300, (2007).

224 Malinouski, M., Zhou, Y., Belousov, V. V., Hatfield, D. L. & Gladyshev, V. N. Hydrogen peroxide probes directed to different cellular compartments. *PLoS One* **6**, e14564, (2011).

225 Ermakova, Y. G. *et al.* Red fluorescent genetically encoded indicator for intracellular hydrogen peroxide. *Nat Commun* **5**, 5222, (2014).

226 Sena, L. A. & Chandel, N. S. Physiological roles of mitochondrial reactive oxygen species. *Mol Cell* **48**, 158-167, (2012).

227 Burgoyne, J. R., Oka, S., Ale-Agha, N. & Eaton, P. Hydrogen peroxide sensing and signaling by protein kinases in the cardiovascular system. *Antioxid Redox Signal* **18**, 1042-1052, (2013).

228 Schroder, E. & Eaton, P. Hydrogen peroxide as an endogenous mediator and exogenous tool in cardiovascular research: issues and considerations. *Curr Opin Pharmacol* **8**, 153-159, (2008).

229 Gold, M. G., Smith, F. D., Scott, J. D. & Barford, D. AKAP18 contains a phosphoesterase domain that binds AMP. *J Mol Biol* **375**, 1329-1343, (2008).

230 Josefsen, K., Lee, Y. C., Thams, P., Efendic, S. & Nielsen, J. H. AKAP 18 alpha and gamma have opposing effects on insulin release in INS-1E cells. *FEBS Lett* **584**, 81-85, (2010).

231 Fraser, I. D. *et al.* A novel lipid-anchored A-kinase Anchoring Protein facilitates cAMP-responsive membrane events. *EMBO J* **17**, 2261-2272, (1998).

232 Hulme, J. T., Lin, T. W., Westenbroek, R. E., Scheuer, T. & Catterall, W. A. Beta-adrenergic regulation requires direct anchoring of PKA to cardiac CaV1.2 channels via a leucine zipper interaction with A kinase-anchoring protein 15. *Proc Natl Acad Sci U S A* **100**, 13093-13098, (2003).

233 Hulme, J. T., Ahn, M., Hauschka, S. D., Scheuer, T. & Catterall, W. A. A novel leucine zipper targets AKAP15 and cyclic AMP-dependent protein kinase to the C terminus of the skeletal muscle Ca2+ channel and modulates its function. *J Biol Chem* **277**, 4079-4087, (2002).

234 Jones, B. W. *et al.* Cardiomyocytes from AKAP7 knockout mice respond normally to adrenergic stimulation. *Proc Natl Acad Sci U S A* **109**, 17099-17104, (2012).

235 Rigatti, M., Le, A. V., Gerber, C., Moraru, II & Dodge-Kafka, K. L. Phosphorylation state-dependent interaction between AKAP7delta/gamma and phospholamban increases phospholamban phosphorylation. *Cell Signal* **27**, 1807-1815, (2015).

236 Henn, V. *et al.* Identification of a novel A-kinase anchoring protein 18 isoform and evidence for its role in the vasopressin-induced aquaporin-2 shuttle in renal principal cells. *J Biol Chem* **279**, 26654-26665, (2004).

237 McSorley, T. *et al.* Spatial organisation of AKAP18 and PDE4 isoforms in renal collecting duct principal cells. *Eur J Cell Biol* **85**, 673-678, (2006).

238 Nauert, J. B., Klauck, T. M., Langeberg, L. K. & Scott, J. D. Gravin, an autoantigen recognized by serum from myasthenia gravis patients, is a kinase scaffold protein. *Curr Biol* **7**, 52-62, (1997).

239 Redden, J. M. *et al.* Spatiotemporal Regulation of PKC via Interactions with AKAP7 Isoforms. *Biochem J*, (2012).

240 Brown, R. L., August, S. L., Williams, C. J. & Moss, S. B. AKAP7gamma is a nuclear RI-binding AKAP. *Biochem Biophys Res Commun* **306**, 394-401, (2003).

241 Singh, A., Redden, J. M., Kapiloff, M. S. & Dodge-Kafka, K. L. The large isoforms of A-kinase anchoring protein 18 mediate the phosphorylation of inhibitor-1 by protein kinase A and the inhibition of protein phosphatase 1 activity. *Mol Pharmacol* **79**, 533-540, (2011).

242 Ahmad, F. *et al.* Regulation of sarcoplasmic reticulum Ca2+ ATPase 2 (SERCA2) activity by phosphodiesterase 3A (PDE3A) in human myocardium: phosphorylation-dependent interaction of PDE3A1 with SERCA2. *J Biol Chem* **290**, 6763-6776, (2015).

243 Luo, Y. *et al.* The cAMP capture compound mass spectrometry as a novel tool for targeting cAMP-binding proteins: from protein kinase A to potassium/sodium hyperpolarization-activated cyclic nucleotide-gated channels. *Mol Cell Proteomics* **8**, 2843-2856, (2009).

244 Sanchez, R., Riddle, M., Woo, J. & Momand, J. Prediction of reversibly oxidized protein cysteine thiols using protein structure properties. *Protein Sci* **17**, 473-481, (2008).

245 Kwon, J. *et al.* Reversible oxidation and inactivation of the tumor suppressor PTEN in cells stimulated with peptide growth factors. *Proc Natl Acad Sci U S A* **101**, 16419-16424, (2004).

246 Jarnaess, E. *et al.* Splicing factor arginine/serine-rich 17A (SFRS17A) is an A-kinase anchoring protein that targets protein kinase A to splicing factor compartments. *J Biol Chem* **284**, 35154-35164, (2009).

247 Lignitto, L. *et al.* Control of PKA stability and signalling by the RING ligase praja2. *Nat Cell Biol* **13**, 412-422, (2011).

248 Hanke, S. E. *et al.* Cyclic nucleotides as affinity tools: phosphorothioate cAMP analogues address specific PKA subproteomes. *N Biotechnol* **28**, 294-301, (2011).

249 Bertinetti, D. *et al.* Chemical tools selectively target components of the PKA system. *BMC Chem Biol* **9**, 3, (2009).

250 Horner, A., Goetz, F., Tampe, R., Klussmann, E. & Pohl, P. Mechanism for targeting the A-kinase anchoring protein AKAP18delta to the membrane. *J Biol Chem* **287**, 42495-42501, (2012).

251 Beca, S. *et al.* Phosphodiesterase type 3A regulates basal myocardial contractility through interacting with sarcoplasmic reticulum calcium ATPase type 2a signaling complexes in mouse heart. *Circ Res* **112**, 289-297, (2013).

252 Scholten, A., van Veen, T. A., Vos, M. A. & Heck, A. J. Diversity of cAMP-dependent protein kinase isoforms and their anchoring proteins in mouse ventricular tissue. *J Proteome Res* **6**, 1705-1717, (2007).

253 Scholten, A. *et al.* Analysis of the cGMP/cAMP interactome using a chemical proteomics approach in mammalian heart tissue validates sphingosine kinase type 1-interacting protein as a genuine and highly abundant AKAP. *J Proteome Res* **5**, 1435-1447, (2006).

254 Day, M. E. *et al.* Isoform-specific targeting of PKA to multivesicular bodies. *J Cell Biol* **193**, 347-363, (2011).

255 Hundsrucker, C. *et al.* High-affinity AKAP7delta-protein kinase A interaction yields novel protein kinase A-anchoring disruptor peptides. *Biochem J* **396**, 297-306, (2006).

256 Jaffrey, S. R. & Snyder, S. H. The biotin switch method for the detection of S-nitrosylated proteins. *Sci STKE* **2001**, pl1, (2001).

257 Paige, J. S., Xu, G., Stancevic, B. & Jaffrey, S. R. Nitrosothiol reactivity profiling identifies S-nitrosylated proteins with unexpected stability. *Chem Biol* **15**, 1307-1316, (2008).

258 Fischer, J. J. *et al.* Improvement of capture compound mass spectrometry technology (CCMS) for the profiling of human kinases by combination with 2D LC-MS/MS. *J Biomed Biotechnol* **2011**, 850589, (2011).

259 Brown, L. J. *et al.* Using S-adenosyl-L-homocysteine capture compounds to characterize S-adenosyl-L-methionine and S-adenosyl-L-homocysteine binding proteins. *Anal Biochem* **467**, 14-21, (2014).

260 Kim, C., Cheng, C. Y., Saldanha, S. A. & Taylor, S. S. PKA-I holoenzyme structure reveals a mechanism for cAMP-dependent activation. *Cell* **130**, 1032-1043, (2007).

261 Hamuro, Y. *et al.* Mapping intersubunit interactions of the regulatory subunit (RIalpha) in the type I holoenzyme of protein kinase A by amide hydrogen/deuterium exchange mass spectrometry (DXMS). *J Mol Biol* **340**, 1185-1196, (2004).

262 Berman, H. M. *et al.* The Protein Data Bank. *Nucleic Acids Res* **28**, 235-242, (2000).

263 Ungar, A. R. & Moon, R. T. Inhibition of protein kinase A phenocopies ectopic expression of hedgehog in the CNS of wild-type and cyclops mutant embryos. *Dev Biol* **178**, 186-191, (1996).

264 Kolobova, E. *et al.* Microtubule-dependent association of AKAP350A and CCAR1 with RNA stress granules. *Exp Cell Res* **315**, 542-555, (2009).

265 Kurosu, T., Hernandez, A. I., Wolk, J., Liu, J. & Schwartz, J. H. Alpha/beta-tubulin are A kinase anchor proteins for type I PKA in neurons. *Brain Res* **1251**, 53-64, (2009).

266 Stubbart, D. *Defining the molecular basis of H_2S-mediated sensing and signalling*, King's College London, (2014).

267 Alegre-Cebollada, J. *et al.* S-glutathionylation of cryptic cysteines enhances titin elasticity by blocking protein folding. *Cell* **156**, 1235-1246, (2014).

268 Britto, P. J., Knipling, L., McPhie, P. & Wolff, J. Thiol-disulphide interchange in tubulin: kinetics and the effect on polymerization. *Biochem J* **389**, 549-558, (2005).

269 Chaudhuri, A. R., Khan, I. A. & Luduena, R. F. Detection of disulfide bonds in bovine brain tubulin and their role in protein folding and microtubule assembly in vitro: a novel disulfide detection approach. *Biochemistry* **40**, 8834-8841, (2001).

270 Landino, L. M., Moynihan, K. L., Todd, J. V. & Kennett, K. L. Modulation of the redox state of tubulin by the glutathione/glutaredoxin reductase system. *Biochem Biophys Res Commun* **314**, 555-560, (2004).

271 Lind, C. *et al.* Identification of S-glutathionylated cellular proteins during oxidative stress and constitutive metabolism by affinity purification and proteomic analysis. *Arch Biochem Biophys* **406**, 229-240, (2002).

272 Landino, L. M., Hagedorn, T. D. & Kennett, K. L. Evidence for thiol/disulfide exchange reactions between tubulin and glyceraldehyde-3-phosphate dehydrogenase. *Cytoskeleton (Hoboken)* **71**, 707-718, (2014).

273 Mackenzie, G. G., Salvador, G. A., Romero, C., Keen, C. L. & Oteiza, P. I. A deficit in zinc availability can cause alterations in tubulin thiol redox status in cultured neurons and in the developing fetal rat brain. *Free Radic Biol Med* **51**, 480-489, (2011).

274 Imaizumi-Scherrer, T., Faust, D. M., Barradeau, S., Hellio, R. & Weiss, M. C. Type I protein kinase a is localized to interphase microtubules and strongly associated with the mitotic spindle. *Exp Cell Res* **264**, 250-265, (2001).

275 Duncan, F. E., Moss, S. B. & Williams, C. J. Knockdown of the cAMP-dependent protein kinase (PKA) Type Ialpha regulatory subunit in mouse oocytes disrupts meiotic arrest and results in meiotic spindle defects. *Dev Dyn* **235**, 2961-2968, (2006).

276 Barzi, M., Berenguer, J., Menendez, A., Alvarez-Rodriguez, R. & Pons, S. Sonic-hedgehog-mediated proliferation requires the localization of PKA to the cilium base. *J Cell Sci* **123**, 62-69, (2010).

277 Radu, M. & Chernoff, J. An in vivo assay to test blood vessel permeability. *J Vis Exp*, e50062, (2013).

278 Mandelkow, E. & Mandelkow, E. M. Microtubules and microtubule-associated proteins. *Curr Opin Cell Biol* **7**, 72-81, (1995).

279 Bowne-Anderson, H., Zanic, M., Kauer, M. & Howard, J. Microtubule dynamic instability: a new model with coupled GTP hydrolysis and multistep catastrophe. *Bioessays* **35**, 452-461, (2013).
280 Kaverina, I. & Straube, A. Regulation of cell migration by dynamic microtubules. *Semin Cell Dev Biol* **22**, 968-974, (2011).
281 Burkhardt, J. K. The role of microtubule-based motor proteins in maintaining the structure and function of the Golgi complex. *Biochim Biophys Acta* **1404**, 113-126, (1998).
282 Illenberger, S. *et al.* Phosphorylation of microtubule-associated proteins MAP2 and MAP4 by the protein kinase p110mark. Phosphorylation sites and regulation of microtubule dynamics. *J Biol Chem* **271**, 10834-10843, (1996).
283 Goedert, M. *et al.* Phosphorylation of microtubule-associated protein tau by stress-activated protein kinases. *FEBS Lett* **409**, 57-62, (1997).
284 Etienne-Manneville, S. From signaling pathways to microtubule dynamics: the key players. *Curr Opin Cell Biol* **22**, 104-111, (2010).
285 Johnson, G. V. & Stoothoff, W. H. Tau phosphorylation in neuronal cell function and dysfunction. *J Cell Sci* **117**, 5721-5729, (2004).
286 Itoh, T. J., Hisanaga, S., Hosoi, T., Kishimoto, T. & Hotani, H. Phosphorylation states of microtubule-associated protein 2 (MAP2) determine the regulatory role of MAP2 in microtubule dynamics. *Biochemistry* **36**, 12574-12582, (1997).
287 Jourdain, L., Curmi, P., Sobel, A., Pantaloni, D. & Carlier, M. F. Stathmin: a tubulin-sequestering protein which forms a ternary T2S complex with two tubulin molecules. *Biochemistry* **36**, 10817-10821, (1997).
288 Yip, Y. Y., Yeap, Y. Y., Bogoyevitch, M. A. & Ng, D. C. cAMP-dependent protein kinase and c-Jun N-terminal kinase mediate stathmin phosphorylation for the maintenance of interphase microtubules during osmotic stress. *J Biol Chem* **289**, 2157-2169, (2014).
289 Heasman, S. J. & Ridley, A. J. Mammalian Rho GTPases: new insights into their functions from in vivo studies. *Nat Rev Mol Cell Biol* **9**, 690-701, (2008).
290 Bos, J. L., Rehmann, H. & Wittinghofer, A. GEFs and GAPs: critical elements in the control of small G proteins. *Cell* **129**, 865-877, (2007).
291 Benais-Pont, G. *et al.* Identification of a tight junction-associated guanine nucleotide exchange factor that activates Rho and regulates paracellular permeability. *J Cell Biol* **160**, 729-740, (2003).
292 Tian, X. *et al.* Control of vascular permeability by atrial natriuretic peptide via a GEF-H1-dependent mechanism. *J Biol Chem* **289**, 5168-5183, (2014).
293 Kratzer, E. *et al.* Oxidative stress contributes to lung injury and barrier dysfunction via microtubule destabilization. *Am J Respir Cell Mol Biol* **47**, 688-697, (2012).
294 Birukova, A. A. *et al.* GEF-H1 is involved in agonist-induced human pulmonary endothelial barrier dysfunction. *Am J Physiol Lung Cell Mol Physiol* **290**, L540-548, (2006).
295 Birkenfeld, J. *et al.* GEF-H1 modulates localized RhoA activation during cytokinesis under the control of mitotic kinases. *Dev Cell* **12**, 699-712, (2007).
296 Bakal, C. J. *et al.* The Rho GTP exchange factor Lfc promotes spindle assembly in early mitosis. *Proc Natl Acad Sci U S A* **102**, 9529-9534, (2005).
297 Krendel, M., Zenke, F. T. & Bokoch, G. M. Nucleotide exchange factor GEF-H1 mediates cross-talk between microtubules and the actin cytoskeleton. *Nat Cell Biol* **4**, 294-301, (2002).
298 Meiri, D. *et al.* Modulation of Rho guanine exchange factor Lfc activity by protein kinase A-mediated phosphorylation. *Mol Cell Biol* **29**, 5963-5973, (2009).
299 Meiri, D. *et al.* Mechanistic insight into GPCR-mediated activation of the microtubule-associated RhoA exchange factor GEF-H1. *Nat Commun* **5**, 4857, (2014).

300 Zhou, Z., Guo, F., Dou, Y., Tang, J. & Huan, J. Guanine nucleotide exchange factor-H1 signaling is involved in lipopolysaccharide-induced endothelial barrier dysfunction. *Surgery* **154**, 621-631, (2013).

301 Lee, W. L. & Slutsky, A. S. Sepsis and endothelial permeability. *N Engl J Med* **363**, 689-691, (2010).

302 Vydra, T. & Havelka, D. *MATLAB - A Fundamental Tool for Scientific Computing and Engineering Applications*. Vol. 1 (InTech, 2012).

303 Rudyk, O. *et al.* Protein kinase G oxidation is a major cause of injury during sepsis. *Proc Natl Acad Sci U S A* **110**, 9909-9913, (2013).

304 Rittirsch, D., Flierl, M. A. & Ward, P. A. Harmful molecular mechanisms in sepsis. *Nat Rev Immunol* **8**, 776-787, (2008).

305 Phillipson, M. & Kubes, P. The neutrophil in vascular inflammation. *Nat Med* **17**, 1381-1390, (2011).

306 Galley, H. F. Oxidative stress and mitochondrial dysfunction in sepsis. *Br J Anaesth* **107**, 57-64, (2011).

307 Berg, R. M., Moller, K. & Bailey, D. M. Neuro-oxidative-nitrosative stress in sepsis. *J Cereb Blood Flow Metab* **31**, 1532-1544, (2011).

308 Di Paolo, G., Antonsson, B., Kassel, D., Riederer, B. M. & Grenningloh, G. Phosphorylation regulates the microtubule-destabilizing activity of stathmin and its interaction with tubulin. *FEBS Lett* **416**, 149-152, (1997).

309 Jicha, G. A. *et al.* cAMP-dependent protein kinase phosphorylations on tau in Alzheimer's disease. *J Neurosci* **19**, 7486-7494, (1999).

310 Ying, Y. *et al.* The microtubule associated protein syntabulin is required for glucose-stimulated and cAMP-potentiated insulin secretion. *FEBS Lett* **586**, 3674-3680, (2012).

311 Richter, A. M., Schagdarsurengin, U., Rastetter, M., Steinmann, K. & Dammann, R. H. Protein kinase A-mediated phosphorylation of the RASSF1A tumour suppressor at Serine 203 and regulation of RASSF1A function. *Eur J Cancer* **46**, 2986-2995, (2010).

312 Kuroda, F., Moss, J. & Vaughan, M. Regulation of brefeldin A-inhibited guanine nucleotide-exchange protein 1 (BIG1) and BIG2 activity via PKA and protein phosphatase 1gamma. *Proc Natl Acad Sci U S A* **104**, 3201-3206, (2007).

313 Lee, C. F., Liu, C. Y., Hsieh, R. H. & Wei, Y. H. Oxidative stress-induced depolymerization of microtubules and alteration of mitochondrial mass in human cells. *Ann N Y Acad Sci* **1042**, 246-254, (2005).

314 Wright, V. P., Reiser, P. J. & Clanton, T. L. Redox modulation of global phosphatase activity and protein phosphorylation in intact skeletal muscle. *J Physiol* **587**, 5767-5781, (2009).

315 Clegg, C. H., Correll, L. A., Cadd, G. G. & McKnight, G. S. Inhibition of intracellular cAMP-dependent protein kinase using mutant genes of the regulatory type I subunit. *J Biol Chem* **262**, 13111-13119, (1987).

316 Lang, P. *et al.* Protein kinase A phosphorylation of RhoA mediates the morphological and functional effects of cyclic AMP in cytotoxic lymphocytes. *EMBO J* **15**, 510-519, (1996).

317 Ellerbroek, S. M., Wennerberg, K. & Burridge, K. Serine phosphorylation negatively regulates RhoA in vivo. *J Biol Chem* **278**, 19023-19031, (2003).

318 Zenke, F. T. *et al.* p21-activated kinase 1 phosphorylates and regulates 14-3-3 binding to GEF-H1, a microtubule-localized Rho exchange factor. *J Biol Chem* **279**, 18392-18400, (2004).

319 Howe, A. K. & Juliano, R. L. Regulation of anchorage-dependent signal transduction by protein kinase A and p21-activated kinase. *Nat Cell Biol* **2**, 593-600, (2000).

320 Fryer, B. H. *et al.* cGMP-dependent protein kinase phosphorylates p21-activated kinase (Pak) 1, inhibiting Pak/Nck binding and stimulating Pak/vasodilator-stimulated phosphoprotein association. *J Biol Chem* **281**, 11487-11495, (2006).

321 Luo, T. *et al.* Upregulation of the GEF-H1 pathway after transient cerebral ischemia. *Exp Neurol* **263**, 306-313, (2015).

322 Cullis, J. *et al.* The RhoGEF GEF-H1 is required for oncogenic RAS signaling via KSR-1. *Cancer Cell* **25**, 181-195, (2014).

323 Chiang, H. S. *et al.* GEF-H1 controls microtubule-dependent sensing of nucleic acids for antiviral host defenses. *Nat Immunol* **15**, 63-71, (2014).

324 Tian, Y., Mambetsariev, I., Sarich, N., Meng, F. & Birukova, A. A. Role of microtubules in attenuation of PepG-induced vascular endothelial dysfunction by atrial natriuretic peptide. *Biochim Biophys Acta* **1852**, 104-119, (2015).

325 Gawlak, G. *et al.* Paxillin mediates stretch-induced Rho signaling and endothelial permeability via assembly of paxillin-p42/44MAPK-GEF-H1 complex. *FASEB J* **28**, 3249-3260, (2014).

326 Simon, F. & Fernandez, R. Early lipopolysaccharide-induced reactive oxygen species production evokes necrotic cell death in human umbilical vein endothelial cells. *J Hypertens* **27**, 1202-1216, (2009).

327 Wu, F., Tyml, K. & Wilson, J. X. iNOS expression requires NADPH oxidase-dependent redox signaling in microvascular endothelial cells. *J Cell Physiol* **217**, 207-214, (2008).

328 London, N. R. *et al.* Targeting Robo4-dependent Slit signaling to survive the cytokine storm in sepsis and influenza. *Sci Transl Med* **2**, 23ra19, (2010).

329 Yin, K., Wilmanski, J., Wang, C., Qiu, G. & Tahamont, M. Lung compartmentalization of inflammatory cells in sepsis. *Inflammation* **24**, 547-557, (2000).

330 Mambetsariev, I. *et al.* Stiffness-activated GEF-H1 expression exacerbates LPS-induced lung inflammation. *PLoS One* **9**, e92670, (2014).

331 Wu, L. L., Tang, C. & Liu, M. S. Altered phosphorylation and calcium sensitivity of cardiac myofibrillar proteins during sepsis. *Am J Physiol Regul Integr Comp Physiol* **281**, R408-416, (2001).

332 Lee, C. *et al.* Redox regulation of OxyR requires specific disulfide bond formation involving a rapid kinetic reaction path. *Nat Struct Mol Biol* **11**, 1179-1185, (2004).

333 Diviani, D., Langeberg, L. K., Doxsey, S. J. & Scott, J. D. Pericentrin anchors protein kinase A at the centrosome through a newly identified RII-binding domain. *Curr Biol* **10**, 417-420, (2000).

334 Jarnaess, E. *et al.* Dual specificity A-kinase anchoring proteins (AKAPs) contain an additional binding region that enhances targeting of protein kinase A type I. *J Biol Chem* **283**, 33708-33718, (2008).

335 Lal, B. K., Varma, S., Pappas, P. J., Hobson, R. W., 2nd & Duran, W. N. VEGF increases permeability of the endothelial cell monolayer by activation of PKB/akt, endothelial nitric-oxide synthase, and MAP kinase pathways. *Microvasc Res* **62**, 252-262, (2001).

336 Mouawad, F., Aoudjit, L., Jiang, R., Szaszi, K. & Takano, T. Role of guanine nucleotide exchange factor-H1 in complement-mediated RhoA activation in glomerular epithelial cells. *J Biol Chem* **289**, 4206-4218, (2014).

337 Naderi, E. H., Findley, H. W., Ruud, E., Blomhoff, H. K. & Naderi, S. Activation of cAMP signaling inhibits DNA damage-induced apoptosis in BCP-ALL cells through abrogation of p53 accumulation. *Blood* **114**, 608-618, (2009).

338 Jiao, B. *et al.* 8-CPT-cAMP/all-trans retinoic acid targets t(11;17) acute promyelocytic leukemia through enhanced cell differentiation and PLZF/RARalpha degradation. *Proc Natl Acad Sci U S A* **110**, 3495-3500, (2013).

339 Chen, J. *et al.* Cardiac sodium channel mutation associated with epinephrine-induced QT prolongation and sinus node dysfunction. *Heart Rhythm* **13**, 289-298, (2016).

340 Nguyen, E. *et al.* Activation of both protein kinase A (PKA) type I and PKA type II isozymes is required for retinoid-induced maturation of acute promyelocytic leukemia cells. *Mol Pharmacol* **83**, 1057-1065, (2013).